Supplementary Information

Antiferroelectric Fluids with Hierarchical Polar Organization

Hiroya Nishikawa, Hina Saito, Tetsu Katayama, Atsuko Nihonyanagi, Dennis Kwaria, Hiroyuki Inuzuka, Junxi Liu, Go Watanabe and Fumito Araoka**

*To whom correspondence should be addressed.

E-mail: hiroya.nishikawa@riken.jp (H.N.), fumito.araoka@riken.jp (F.A.)

Table of contents

Methods

1. General and materials S2

2. Synthesis and characterization S6

Supplementary Notes (Notes 1–5) S15

Supplementary Figures (Figs. 1–105) S22

Supplementary Tables (Tables 1–11) S127

Supplementary References S140

Methods

1. General and materials

Nuclear magnetic resonance (NMR) spectroscopy: ^{1}H, ^{13}C, and ^{19}F NMR spectra were recorded on JNM-ECZ500 (JEOL) operating at 500 MHz, 126 MHz, and 471 MHz for ^{1}H [$^{1}H\{^{19}F\}$], $^{13}C\{^{1}H\}$ [$^{13}C\{^{1}H,^{19}F\}$] and ^{19}F [$^{19}F\{^{1}H\}$] NMR, respectively, using the TMS (trimethylsilane) as an internal standard for ^{1}H NMR and the deuterated solvent for ^{13}C NMR. The absolute values of the coupling constants are given in Hz, regardless of their signs. Signal multiplicities were abbreviated by s (singlet), d (doublet), t (triplet), q (quartet), quint (quintet), sext (sextet), and dd (double–doublet), respectively.

High-resolution mass (HRMS) spectroscopy: HR-ESI-TOF-MS spectra were recorded on a Waters Cyclic IMS system using flow injection analysis with a Waters UPC^2 system. The mobile phase was liquid CO_2/MeOH (6:4, v/v).

Density Functional Theory (DFT) Calculation: DFT calculations were performed using the Gaussian 09 revision E01 package at the B3LYP/6-31G(d,p) level of theory.[S^1] The calculation method is as follows: opt b3lyp /6-31g(d,p) SCF=tight pop=MK iop(6/33=2,6/42=6).

Information of used liquid crystalline (LC) cells:

ITO glass cell (EHC):

- ITO-coated type, electrode area: 5 × 10 mm
- Experiments: POM (thickness: 5.0 μm) and BDS (thickness: 10.0 μm)

ITO glass cell (homemade):

- Experiments: PRC studies (thickness: 4.6 μm)

ITO glass cell (homemade):

- Experiments: SHG studies (thickness: 22 μm)
- The ITO glass plates were baked at 400 °C for 1 h before fabrication.

Antiparallel-rubbed (AP)and Synparallel-rubbed (SP) cell (EHC):

- PI-coated type, thickness: 5.0 μm
- Alignment layer: LX-1400
- Experiments: POM studies

2. Synthesis of Compounds.

2.1. Synthetic route

All compounds were synthesized according to the protocols described below (Scheme S1). NMR and MS spectra for final target ***n*-012-CN** (n = 1–20) are shown in Supplementary Figs. 66–105.

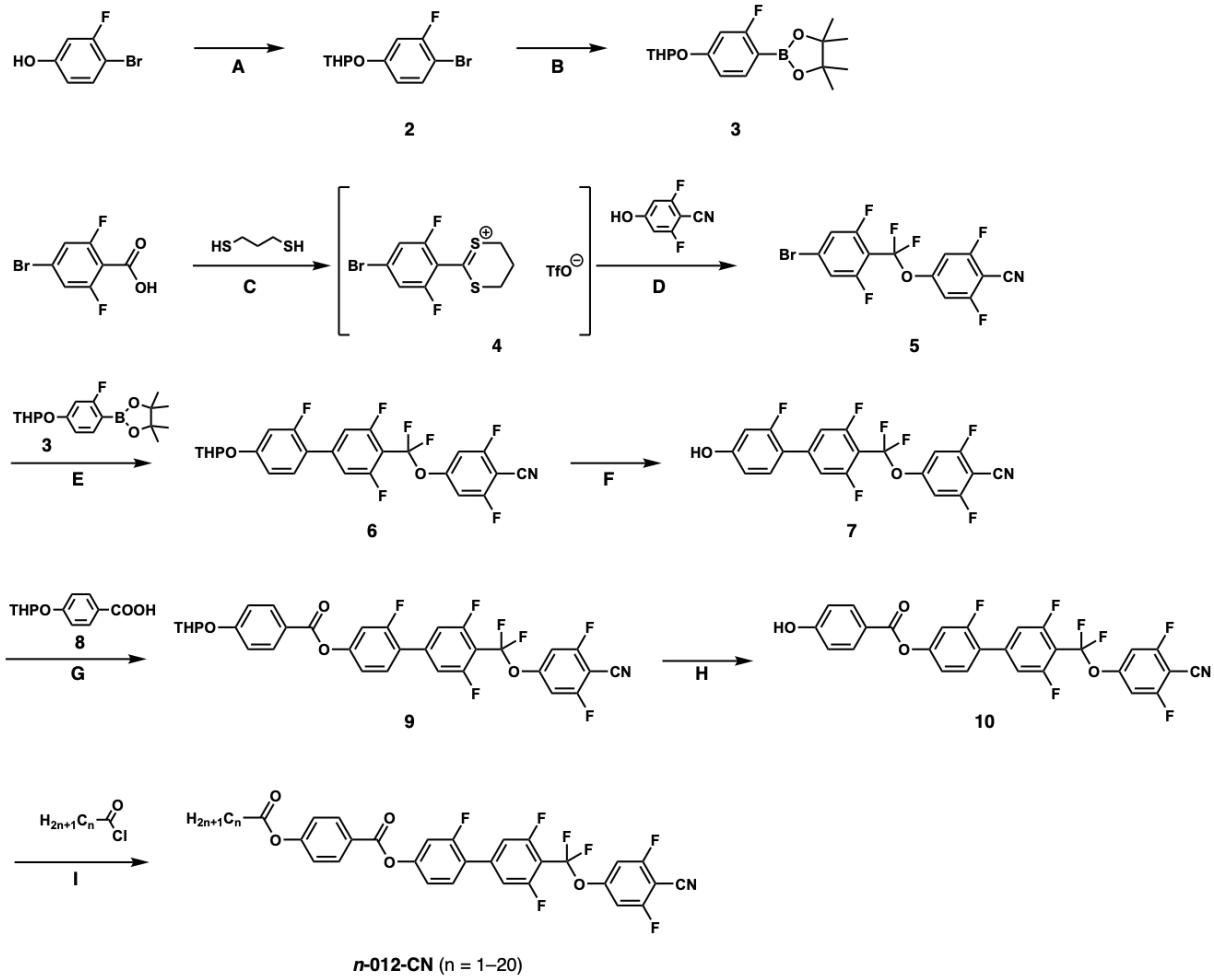

Supplementary Scheme 1 Synthetic pathway of ***n*-012-CN** (*n* = 1–20). (A) 3,4-dihydro-2H-pyran, PPTS, CH_2Cl_2, r.t., 4.5 h, (B) B_2pin_2, Pd(dppf)Cl_2-CH_2Cl_2, KOAc, 1,4-dioxane, 80 °C 2 h; 100 °C 8 h, (C) 1,3-propanedithiol, trifluoromethanesulfonic acid, isooctane, *tert*-butyl methyl ether, toluene, 60 °C 0.5 h; 110 °C 2 h; 0 °C 0.5 h, (D) 2,6-Difluoro-4-hydroxybenzonitrile, Et_3N, Et_3N-3HF, Br_2, −78 °C 0.5 h; 0 °C 2 h, (E) 3, Pd(dppf)Cl_2-CH_2Cl_2, K_2CO_3, 1,4-dioxane/H_2O, 80 °C 7 h, (F) *p*-TsOH, CH_2Cl_2/MeOH, 40 °C, 2.5 h, (G) WSCI, DMAP, CH_2Cl_2, 0 °C, 1 h; r.t., 14 h, (H) *p*-TsOH, CH_2Cl_2/MeOH, 40 °C, 2 h, (I) RCO_2Cl, Et_3N, CH_2Cl_2, 0 °C, or RCO_2H, WSCI, DMAP, CH_2Cl_2, 0 °C; r.t., overnight.

2.2.1. ***Synthesis of 2-(4-bromo-3-fluorophenoxy)tetrahydro-2H-pyran*** **(2)**

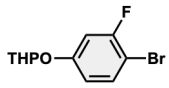

This compound was synthesized according to the procedure described in the literature.[S2]

$^{1}H\{^{19}F\}$-NMR (500 MHz, $CDCl_3$): δ 7.40 (d, *J* = 8.9 Hz, 1H), 6.88 (d, *J* = 2.7 Hz, 1H), 6.75 (dd, *J* = 8.9, 2.7 Hz, 1H), 5.37 (t, *J* = 3.0 Hz, 1H), 3.86–3.82 (m, 1H), 3.63–3.59 (m, 1H), 2.00–1.93 (m, 1H), 1.87–1.84 (m, 2H), 1.74–1.65 (m, 2H), 1.62–1.58 (m, 1H);

$^{19}F\{^{1}H\}$-NMR (471 MHz, $CDCl_3$): δ −105.4 (s, 1F)

2.2.2. ***Synthesis of 2-(2-fluoro-4-((tetrahydro-2H-pyran-2-yl)oxy)phenyl)-4,4,5,5-tetramethyl-1,3,2-dioxaborolane*** **(3)**

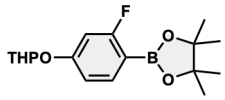

This compound was synthesized according to the procedure described in the literature.[S2]

$^{1}H\{^{19}F\}$-NMR (500 MHz, $CDCl_3$): δ 7.64 (d, *J* = 8.3 Hz, 1H), 6.82 (dd, *J* = 8.3, 2.3 Hz, 1H), 6.75 (d, *J* = 2.1 Hz, 1H), 5.45 (t, *J* = 3.0 Hz, 1H), 3.87-3.82 (m, 1H), 3.63-3.59 (m, 1H), 2.02–1.94 (m, 1H), 1.87–1.84 (m, 2H), 1.73–1.63 (m, 2H), 1.62–1.58 (m, 1H), 1.34 (s, 12H);

$^{19}F\{^{1}H\}$-NMR (471 MHz, $CDCl_3$): δ −100.5 (s, 1F)

2.2.3. ***Synthesis of 2-(4-bromo-2,6-difluorophenyl)-5,6-dihydro-4H-1,3-dithiyn-1-ylium triflate*** **(4)**

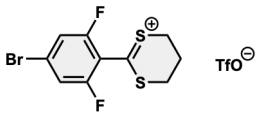

This compound was synthesized according to the procedure described in the literature.[S3] This compound was used in next step without purification.

2.2.4. ***Synthesis of 4-((4-bromo-2,6-difluorophenyl)difluoromethoxy)-2,6-difluorobenzonitrile*** **(5)**

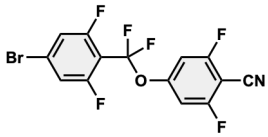

This compound was synthesized according to the procedure described in the literature. [S3]

$^{1}H\{^{19}F\}$-NMR (500 MHz, $CDCl_3$): δ 7.24 (s, 2H), 7.00 (s, 2H);

$^{19}F\{^{1}H\}$-NMR (471 MHz, $CDCl_3$): δ −62.0 (t, *J* = 25.7 Hz, 2F), −101.1 (s, 2F), −108.6 (t, *J* = 27.5 Hz, 2F)

2.2.5. ***Synthesis of 4-(difluoro(2',3,5-trifluoro-4'-((tetrahydro-2H-pyran-2-yl)oxy)-[1,1'-biphenyl]-4-yl)methoxy)-2,6-difluorobenzonitrile*** **(6)**

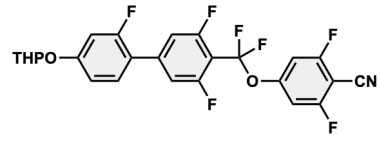

To a solution of **3** (1.22 g, 3.77 mmol) and 5 (1.36 g, 3.43 mmol) in 1,4-dioxane/H_2O (15 mL/1.5 mL) were added Pd(dppf)Cl_2-CH_2Cl_2 (154 mg, 0.189 mmol) and K_2CO_3 (1.42 g, 10.3 mmol) at room temperature. The reaction mixture was stirred at 80 °C under Ar for 2 h. After cooling to room temperature, the mixture was filtered through a Celite pad and washed with AcOEt. The filtrate was concentrated under reduced pressure, and the residue was purified by flash column chromatography on silica gel (CH_2Cl_2/hexane, 25:70–50:50) to afford **6** (1.36 g, 2.65 mmol, 77.3 %) as a white solid.

$^1H\{^{19}F\}$-NMR (500 MHz, $CDCl_3$): δ 7.34 (d, J = 8.6 Hz, 1H), 7.20 (s, 2H), 7.02 (s, 2H), 6.96–6.93 (m, 2H), 5.47 (t, J = 3.0 Hz, 1H), 3.87 (td, J = 10.7, 2.9 Hz, 1H), 3.67-3.63 (m, 1H), 2.05–1.96 (m, 1H), 1.91–1.88 (m, 2H), 1.76–1.68 (m, 2H), 1.64-1.61 (m, 1H);

$^{19}F\{^1H\}$-NMR (471 MHz, $CDCl_3$): δ −61.7 (t, J = 25.7 Hz, 2F), -101.3 (s, 2F), −110.8 (t, J = 25.7 Hz, 2F), −114.4 (s, 1F).

2.2.6. *Synthesis of 4-(difluoro(2',3,5-trifluoro-4'-hydroxy-[1,1'-biphenyl]-4-yl)methoxy)-2,6-difluorobenzonitrile* (7)

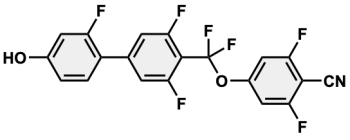

To a solution of **6** (1.24 g, 2.42 mmol) in CH_2Cl_2/MeOH (5 mL/5 mL) was added *p*-TsOH-H_2O (23.0 mg, 0.121 mmol) at room temperature and the reaction mixture was stirred at 40 °C under Ar for 2 h. After cooling to room temperature, the solvent was removed under reduced pressure, and the resulting residue was purified by flash column chromatography on silica gel (AcOEt/hexane, 40:60–80:20) to afford **7** (1.04 g, 2.42 mmol) as a white solid.

$^1H\{^{19}F\}$-NMR (500 MHz, $CDCl_3$): δ 7.31 (d, J = 8.6 Hz, 1H), 7.19 (s, 2H), 7.02 (s, 2H), 6.75–6.71 (m, 2H), 5.47 (s, 1H);

$^{19}F\{^1H\}$-NMR (471 MHz, $CDCl_3$): δ −61.7 (t, J = 27.5 Hz, 2F), -101.3 (s, 2F), −110.8 (t, J = 25.7 Hz, 2F), −114.3 (s, 1F).

2.2.7. *Synthesis of 4-((tetrahydro-2H-pyran-2-yl)oxy)benzoic acid* (8)

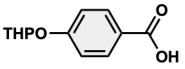

This compound was previously synthesized in our laboratory.[S2]

2.2.8. *Synthesis of 4'-((4-cyano-3,5-difluorophenoxy)difluoromethyl)-2,3',5'-trifluoro-[1,1'-biphenyl]-4-yl 4-((tetrahydro-2H-pyran-2-yl)oxy)benzoate* (9)

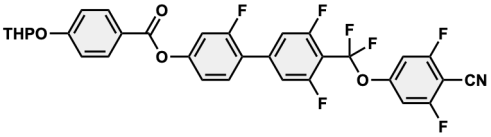

A solution of **7** (1.28 g, 3.00 mmol) and 8 (0.80 g, 3.60 mmol) in CH_2Cl_2 (20 mL) was treated with WSCI (690

mg, 3.60 mmol) and DMAP (36.7 mg, 0.300 mmol) at 0 °C. After stirring for 1 h at 0 °C under Ar atmosphere, the reaction mixture was warmed to room temperature and stirred for 16 h. The solvent was removed under reduced pressure, and the residue was purified by flash column chromatography on silica gel (CH_2Cl_2/hexane, 40:60–70:30) to give **9** (1.71 g, 2.71 mmol, 90.4%) as a white solid.

$^1H\{^{19}F\}$-NMR (500 MHz, $CDCl_3$): δ 8.14 (dd, *J* = 6.9, 2.1 Hz, 2H), 7.48 (dd, *J* = 8.0, 0.9 Hz, 1H), 7.25 (m, 2H), 7.18–7.15 (m, 4H), 7.04 (s, 2H), 5.57 (t, *J* = 3.0 Hz, 1H), 3.89–3.85 (m, 1H), 3.67–3.63 (m, 1H), 2.06–1.99 (m, 1H), 1.93-1.90 (m, 2H), 1.77–1.68 (m, 2H), 1.66-1.62 (m, 1H);

$^{19}F\{^1H\}$-NMR (471 MHz, $CDCl_3$): δ −61.8 (t, *J* = 27.5 Hz, 2F), −101.2 (s, 2F), −110.2 (t, *J* = 25.7 Hz, 2F), −113.9 (s, 1F).

2.2.9. *Synthesis of 4'-((4-cyano-3,5-difluorophenoxy)difluoromethyl)-2,3',5'-trifluoro-[1,1'-biphenyl]-4-yl 4-hydroxybenzoate* (10)

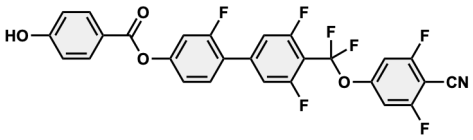

To a solution of **9** (2.70 g, 4.28 mmol) in CH_2Cl_2/MeOH (10 mL/10 mL) was added *p*-TsOH-H_2O (40.7 mg, 0.214 mmol) at room temperature. The resulting mixture was stirred at 40 °C under Ar atmosphere for 3 h. After cooling to room temperature, the solvent was removed under reduced pressure, and the resulting residue was purified by flash column chromatography on silica gel (EtOAc/hexane, 40:60–90:10) to afford **10** (1.04 g, 2.42 mmol) as a white solid.

$^1H\{^{19}F\}$-NMR (500 MHz, $CDCl_3$): δ 8.12 (d, *J* = 8.7 Hz, 2H), 7.49 (d, *J* = 8.2 Hz, 1H), 7.24 (s, 2H), 7.18–7.16 (m, 2H), 7.04 (s, 2H), 6.95 (d, *J* = 8.6 Hz, 2H), 5.78 (s, 1H);

$^{19}F\{^1H\}$-NMR (471 MHz, $CDCl_3$): δ -61.8 (t, *J* = 27.5 Hz, 2F), −101.2 (s, 2F), −110.2 (t, *J* = 25.7 Hz, 2F), −113.9 (s, 1F).

2.2.10. *Synthesis of 4'-((4-cyano-3,5-difluorophenoxy)difluoromethyl)-2,3',5'-trifluoro-[1,1'-biphenyl]-4-yl 4-acetoxybenzoate* (*1-012-CN*)

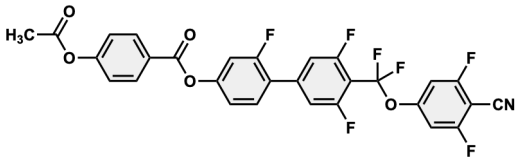

$^1H\{^{19}F\}$-NMR (500 MHz, $CDCl_3$): δ 8.24 (d, *J* = 8.6 Hz, 2H), 7.51–7.49 (d, *J* = 7.9 Hz, 1H), 7.29–7.25 (m, 4H), 7.19–7.17 (m, 2H), 7.04 (s, 2H), 2.36 (s, 3H);

$^{19}F\{^1H\}$-NMR (471 MHz, $CDCl_3$): δ −61.8 (t, *J* = 27.5 Hz, 2F), −101.2 (s, 2F), −110.1 (t, *J* = 25.7 Hz, 2F), −113.6 (s, 1F);

$^{13}C\{^{1}H,^{19}F\}$-NMR (126 MHz, $CDCl_3$): δ 168.7, 163.8, 163.6, 159.9, 159.5, 155.2, 152.4, 141.3, 131.9, 130.5, 126.2, 123.1, 122.1, 120.3 (t, *J* = 265.6 Hz), 118.5, 113.2, 110.9, 108.6, 108.2 (t, *J* = 31.4 Hz), 105.7, 89.9, 21.1;

ESI-HRMS (m/z): $[M-H]^-$ calc for 588.0682; found, 588.0680.

2.2.11. *Synthesis of 4'-((4-cyano-3,5-difluorophenoxy)difluoromethyl)-2,3',5'-trifluoro-[1,1'-biphenyl]-4-yl 4-(propionyloxy)benzoate* (*2-012-CN*)

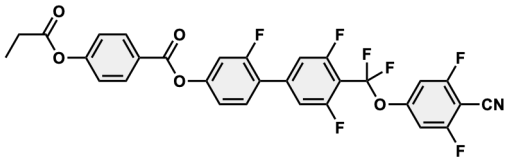

$^{1}H\{^{19}F\}$-NMR (500 MHz, $CDCl_3$): δ 8.24 (d, *J* = 8.5 Hz, 2H), 7.50 (d, *J* = 7.9 Hz, 1H), 7.29–7.25 (m, 4H), 7.19–7.17 (m, 2H), 7.04 (s, 2H), 2.65 (q, J = 7.5 Hz, 2H), 1.30 (t, *J* = 7.52 Hz, 3H);

$^{19}F\{^{1}H\}$-NMR (471 MHz, $CDCl_3$): δ −61.8 (t, *J* = 25.7 Hz, 2F), −101.2 (s, 2F), −110.1 (t, *J* = 25.7 Hz, 2F), −113.6 (s, 1F);

$^{13}C\{^{1}H,^{19}F\}$-NMR (126 MHz, $CDCl_3$): δ 172.3, 163.8, 163.6, 159.9, 159.5, 155.4, 155.2, 152.4, 141.3, 131.9, 130.5, 126.0, 123.1, 122.0, 120.3 (t, *J* = 265.6 Hz), 118.5, 113.2, 110.9, 108.6, 108.2 (t, *J* = 31.4 Hz), 105.7, 89.9, 27.8, 8.90;

ESI-HRMS (m/z): $[M-H]^-$ calc for 602.0839; found, 602.0836.

2.2.12. *Synthesis of 4'-((4-cyano-3,5-difluorophenoxy)difluoromethyl)-2,3',5'-trifluoro-[1,1'-biphenyl]-4-yl 4-(butyryloxy)benzoate* (*3-012-CN*)

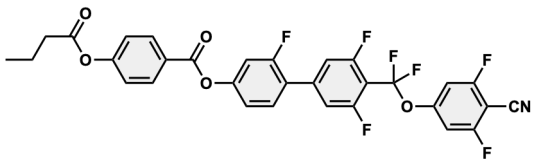

$^{1}H\{^{19}F\}$-NMR (500 MHz, $CDCl_3$): δ 8.24 (d, *J* = 8.6 Hz, 2H), 7.50 (d, *J* = 7.9 Hz, 1H), 7.29–7.25 (m, 4H), 7.19–7.17 (m, 2H), 7.04 (s, 2H), 2.60 (t, *J* = 7.4 Hz, 2H), 1.86-1.78 (m, 2H), 1.07 (t, *J* = 7.3 Hz, 3H);

$^{19}F\{^{1}H\}$-NMR (471 MHz, $CDCl_3$): δ −61.8 (t, *J* = 25.7 Hz, 2F), −101.2 (s, 2F), −110.1 (t, *J* = 25.7 Hz, 2F), −113.7 (s, 1F);

$^{13}C\{^{1}H,^{19}F\}$-NMR (126 MHz, $CDCl_3$): δ 171.5, 163.8, 163.6, 159.9, 159.5, 155.3, 155.2, 152.4, 141.3, 131.9, 130.5, 126.0, 123.1, 122.1, 120.3 (t, *J* = 265.6 Hz) , 118.5, 113.2, 111.0, 108.6, 108.2 (t, *J* = 31.4 Hz), 105.7, 89.9, 36.2, 18.3, 13.6;

ESI-HRMS (m/z): $[M-H]^-$ calc for 616.0995; found, 616.0999.

2.2.13. *Synthesis of 4'-((4-cyano-3,5-difluorophenoxy)difluoromethyl)-2,3',5'-trifluoro-[1,1'-biphenyl]-4-yl 4-(pentanoyloxy)benzoate* (*4-012-CN*)

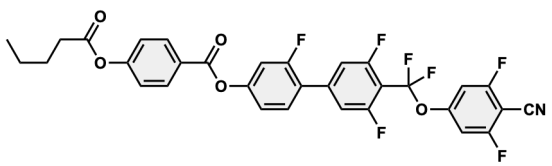

$^{1}H\{^{19}F\}$-NMR (500 MHz, $CDCl_3$): δ 8.24 (d, *J* = 8.6 Hz, 2H), 7.50 (d, *J* = 7.9 Hz, 1H), 7.28–7.25

(m, 4H), 7.19–7.17 (m, 2H), 7.04 (s, 2H), 2.62 (t, *J* = 7.5 Hz, 2H), 1.80–1.74 (m, 2H), 1.47 (td, *J* = 14.9, 7.4 Hz, 2H), 0.99 (t, *J* = 7.3 Hz, 3H);

$^{19}F\{^{1}H\}$-NMR (471 MHz, $CDCl_3$): δ −61.8 (t, *J* = 25.7 Hz, 2F), −101.2 (s, 2F), −110.1 (t, *J* = 25.7 Hz, 2F), −113.7 (s, 1F);

$^{13}C\{^{1}H,^{19}F\}$-NMR (126 MHz, $CDCl_3$): δ 171.6, 163.8, 163.6, 159.9, 159.5, 155.4, 155.2, 152.4, 141.3, 131.9, 130.5, 126.0, 123.1, 122.1, 120.3 (t, *J* = 265.6 Hz), 118.5, 113.2, 110.9, 108.6, 108.2 (t, *J* = 31.4 Hz), 105.7, 89.9, 34.1, 26.8, 22.2, 13.7;

ESI-HRMS (m/z): $[M-H]^-$ calc for 630.1152; found, 630.1150.

2.2.14. *Synthesis of 4'-((4-cyano-3,5-difluorophenoxy)difluoromethyl)-2,3',5'-trifluoro-[1,1'-biphenyl]-4-yl 4-(hexanoyloxy)benzoate* (*5-012-CN*)

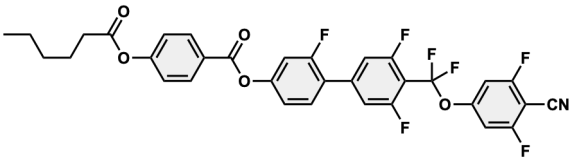

$^{1}H\{^{19}F\}$-NMR (500 MHz, $CDCl_3$): δ 8.24 (m, 2H), 7.50 (d, *J* = 7.9 Hz, 1H), 7.28–7.25 (m, 4H), 7.19–7.17 (m, 2H), 7.04 (s, 2H), 2.61 (t, *J* = 7.5 Hz, 2H), 1.82–1.76 (m, 2H), 1.46–1.36 (m, 4H), 0.95 (t, *J* = 7.0 Hz, 3H);

$^{19}F\{^{1}H\}$-NMR (471 MHz, $CDCl_3$): δ -61.8 (t, *J* = 25.7 Hz, 2F), −101.2 (s, 2F), −110.1 (t, *J* = 25.7 Hz, 2F), −113.7 (s, 1F);

$^{13}C\{^{1}H,^{19}F\}$-NMR (126 MHz, $CDCl_3$): δ 171.6, 163.8, 163.6, 159.9, 159.5, 155.4, 155.2, 152.4, 141.3, 131.9, 130.5, 126.0, 123.1, 122.4, 122.1, 120.3 (t, *J* = 265.6 Hz), 118.5, 118.2, 113.2, 111.0, 108.6, 108.5, 108.2 (t, *J* = 31.4 Hz), 108.0, 105.7, 89.9, 34.3, 31.2, 24.5, 22.3, 13.9;

ESI-HRMS (m/z): $[M-H]^-$ calc for 644.1308; found, 644.1306.

2.2.15. *Synthesis of 4'-((4-cyano-3,5-difluorophenoxy)difluoromethyl)-2,3',5'-trifluoro-[1,1'-biphenyl]-4-yl 4-(heptanoyloxy)benzoate* (*6-012-CN*)

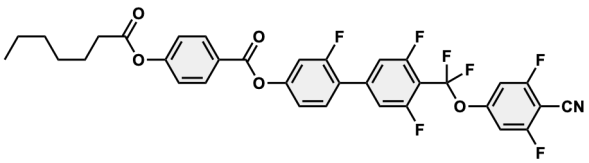

$^{1}H\{^{19}F\}$-NMR (500 MHz, $CDCl_3$): δ 8.25–8.22 (m, 2H), 7.50 (d, *J* = 8.7 Hz, 1H), 7.28–7.25 (m, 4H), 7.19–7.17 (m, 2H), 7.04 (s, 2H), 2.61 (t, *J* = 7.5 Hz, 2H), 1.81-1.75 (m, 2H), 1.45–1.41 (m, 2H), 1.38–1.34 (m, 4H), 0.92 (t, *J* = 6.9 Hz, 3H);

$^{19}F\{^{1}H\}$-NMR (471 MHz, $CDCl_3$): δ −61.8 (t, *J* = 25.7 Hz, 2F), −101.2 (s, 2F), −110.1 (t, *J* = 25.7 Hz, 2F), −113.7 (s, 1F);

$^{13}C\{^{1}H,^{19}F\}$-NMR (126 MHz, $CDCl_3$): δ 171.6, 163.8, 163.6, 159.9, 159.5, 155.4, 155.2, 152.4, 141.3, 131.9, 130.5, 126.0, 123.1, 122.1, 120.3 (t, *J* = 265.6 Hz), 118.5, 113.2, 110.9, 108.6, 108.2 (t, *J* = 31.4 Hz), 105.7, 89.9, 34.4, 31.4, 28.7, 24.8, 22.5, 14.0;

ESI-HRMS (m/z): $[M-H]^-$ calc for 658.1464; found, 658.1463.

2.2.16. ***Synthesis of 4'-((4-cyano-3,5-difluorophenoxy)difluoromethyl)-2,3',5'-trifluoro-[1,1'-biphenyl]-4-yl 4-(octanoyloxy)benzoate* (*7-012-CN*)**

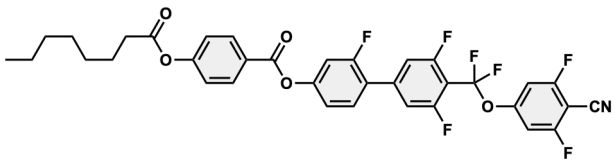

$^{1}H\{^{19}F\}$-NMR (500 MHz, $CDCl_3$): δ 8.24 (d, *J* = 8.6 Hz, 2H), 7.50 (d, *J* = 8.3 Hz, 1H), 7.28–7.25 (m, 4H), 7.19–7.17 (m, 2H), 7.04 (s, 2H), 2.61 (t, J = 7.5 Hz, 2H), 1.81–1.75 (m, 2H), 1.46–1.31 (m, 8H), 0.91 (t, *J* = 6.8 Hz, 3H);

$^{19}F\{^{1}H\}$-NMR (471 MHz, $CDCl_3$): δ −61.8 (t, *J* = 25.7 Hz, 2F), −101.2 (s, 2F), −110.1 (t, *J* = 25.7 Hz, 2F), −113.7 (s, 1F);

$^{13}C\{^{1}H,^{19}F\}$-NMR (126 MHz, $CDCl_3$): δ 171.6, 163.8, 163.6, 159.9, 159.5, 155.4, 155.2, 152.4, 141.3, 131.9, 130.5, 126.0, 123.1, 122.1, 120.3 (t, *J* = 265.6 Hz), 118.5, 113.2, 110.9, 108.6, 108.2 (t, *J* = 31.4 Hz), 105.7, 89.9, 34.4, 31.6, 29.0, 28.9, 24.8, 22.6, 14.0;

ESI-HRMS (m/z): $[M-H]^-$ calc for 672.1621; found, 672.1619.

2.2.17. ***Synthesis of 4'-((4-cyano-3,5-difluorophenoxy)difluoromethyl)-2,3',5'-trifluoro-[1,1'-biphenyl]-4-yl 4-(nonanoyloxy)benzoate* (*8-012-CN*)**

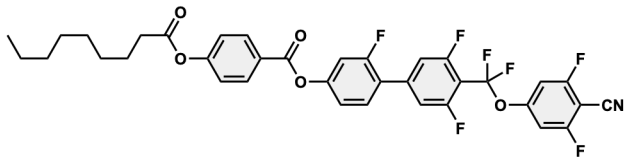

$^{1}H\{^{19}F\}$-NMR (500 MHz, $CDCl_3$): δ 8.24 (d, *J* = 8.9 Hz, 2H), 7.50 (d, *J* = 8.0 Hz, 1H), 7.28–7.25 (m, 4H), 7.19–7.17 (m, 2H), 7.04 (s, 2H), 2.61 (t, *J* = 7.6 Hz, 2H), 1.81–1.75 (m, 2H), 1.46–1.30 (m, 10H), 0.90 (t, *J* = 6.7 Hz, 3H);

$^{19}F\{^{1}H\}$-NMR (471 MHz, $CDCl_3$): δ −61.8 (t, *J* = 25.7 Hz, 2F), -101.2 (s, 2F), −110.1 (t, *J* = 25.7 Hz, 2F), −113.7 (s, 1F);

$^{13}C\{^{1}H,^{19}F\}$-NMR (126 MHz, $CDCl_3$): δ 171.6, 163.8, 163.6, 159.9, 159.5, 155.4, 155.2, 152.4, 141.3, 131.9, 130.5, 126.0, 123.1, 122.1, 120.3 (t, *J* = 264.4 Hz), 118.5, 113.2, 110.9, 108.6, 108.2 (t, *J* = 31.4 Hz), 105.7, 89.9, 34.4, 31.8, 29.2, 29.1, 29.1, 24.8, 22.6, 14.1;

ESI-HRMS (m/z): $[M-H]^-$ calc for 686.1777; found, 686.1773.

2.2.18. ***Synthesis of 4'-((4-cyano-3,5-difluorophenoxy)difluoromethyl)-2,3',5'-trifluoro-[1,1'-biphenyl]-4-yl 4-(decanoyloxy)benzoate* (*9-012-CN*)**

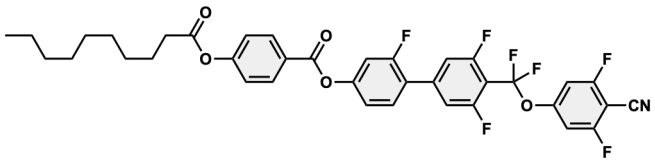

$^{1}H\{^{19}F\}$-NMR (500 MHz, $CDCl_3$): δ 8.24 (m, 2H), 7.50 (d, *J* = 8.0 Hz, 1H), 7.28–7.25 (m, 4H), 7.19–7.17 (m, 2H), 7.04 (s, 2H), 2.61 (t, *J* = 7.5 Hz, 2H), 1.81–1.75 (m, 2H), 1.46–1.30 (m, 12H), 0.89 (t, *J* = 6.3 Hz, 3H);

$^{19}F\{^{1}H\}$-NMR (471 MHz, $CDCl_3$): δ −61.8 (t, *J* = 25.7 Hz, 2F), −101.2 (s, 2F), −110.1 (t, *J* = 27.5 Hz, 2F), −113.7 (s, 1F);

$^{13}C\{^{1}H,^{19}F\}$-NMR (126 MHz, $CDCl_3$): δ 171.6, 163.8, 163.6, 159.9, 159.5, 155.4, 155.2, 152.4, 141.3, 131.9, 130.5, 126.0, 123.1, 122.1, 120.3 (t, *J* = 264.4 Hz), 118.5, 113.2, 111.0, 108.6, 108.5, 108.2 (t, *J* = 31.4 Hz), 108.0, 105.8, 89.9, 34.4, 31.8, 29.4, 29.2, 29.1, 24.8, 22.7, 14.1;
ESI-HRMS (m/z): $[M-H]^-$ calc for 700.1934; found, 700.1931.

2.2.19. ***Synthesis of 4'-((4-cyano-3,5-difluorophenoxy)difluoromethyl)-2,3',5'-trifluoro-[1,1'-biphenyl]-4-yl 4-(undecanoyloxy)benzoate* (*10-012-CN*)**

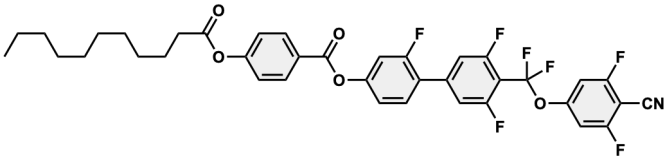

$^{1}H\{^{19}F\}$-NMR (500 MHz, $CDCl_3$): δ 8.24 (d, *J* = 8.7 Hz, 2H), 7.50 (d, *J* = 8.6 Hz, 1H), 7.28–7.25 (m, 4H), 7.19–7.17 (m, 2H), 7.04 (s, 2H), 2.61 (t, *J* = 7.6 Hz, 2H), 1.81-1.75 (m, 2H), 1.46–1.28 (m, 14H), 0.89 (t, *J* = 6.9 Hz, 3H);
$^{19}F\{^{1}H\}$-NMR (471 MHz, $CDCl_3$): δ −61.8 (t, *J* = 25.7 Hz, 2F), −101.2 (s, 2F), −110.1 (t, *J* = 25.7 Hz, 2F), −113.7 (s, 1F);
$^{13}C\{^{1}H,^{19}F\}$-NMR (126 MHz, $CDCl_3$): δ 171.6, 163.8, 163.6, 159.9, 159.5, 155.4, 155.2, 152.4, 141.3, 131.9, 130.5, 126.0, 123.1, 122.1, 120.3 (t, *J* = 264.4 Hz), 118.5, 113.2, 111.0, 108.6, 108.5, 108.2 (t, *J* = 30.8 Hz), 108.0, 105.8, 89.9, 34.4, 31.9, 29.5, 29.4, 29.3, 29.2, 29.1, 24.8, 22.7, 14.1;
ESI-HRMS (m/z): $[M-H]^-$ calc for 714.2090; found, 714.2086.

2.2.20. ***Synthesis of 4'-((4-cyano-3,5-difluorophenoxy)difluoromethyl)-2,3',5'-trifluoro-[1,1'-biphenyl]-4-yl 4-(dodecanoyloxy)benzoate* (*11-012-CN*)**

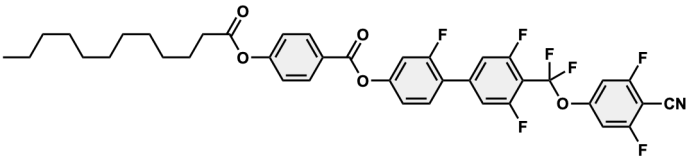

$^{1}H\{^{19}F\}$-NMR (500 MHz, $CDCl_3$): δ 8.25–8.22 (m, 2H), 7.50 (d, *J* = 8.2 Hz, 1H), 7.28–7.25 (m, 6H), 7.19–7.17 (m, 2H), 7.04 (s, 2H), 2.61 (t, *J* = 7.5 Hz, 2H), 1.81–1.75 (m, 2H), 1.46-1.41 (m, 2H), 1.37–1.27 (m, 16H), 0.89 (t, *J* = 6.9 Hz, 3H);
$^{19}F\{^{1}H\}$-NMR (471 MHz, $CDCl_3$): δ −61.8 (t, *J* = 27.5 Hz, 2F), −101.2 (s, 2F), −110.1 (t, *J* = 25.7 Hz, 2F), −113.7 (s, 1F);
$^{13}C\{^{1}H,^{19}F\}$-NMR (126 MHz, $CDCl_3$): δ 171.6, 163.8, 163.6, 159.9, 159.6, 155.4, 155.2, 152.4, 141.3, 131.9, 130.5, 126.0, 123.1, 122.1, 120.3 (t, *J* = 268.0 Hz), 118.5, 113.2, 111.0, 108.6, 108.5, 108.2 (t, *J* = 31.4 Hz), 108.0, 105.7, 89.9, 34.4, 31.9, 29.6, 29.4, 29.3, 29.2, 29.1, 24.8, 22.7, 14.1;
ESI-HRMS (m/z): $[M-H]^-$ calc for 728.2247; found, 728.2249.

2.2.21. ***Synthesis of 4'-((4-cyano-3,5-difluorophenoxy)difluoromethyl)-2,3',5'-trifluoro-[1,1'-biphenyl]-4-yl 4-(tridecanoyloxy)benzoate* (*12-012-CN*)**

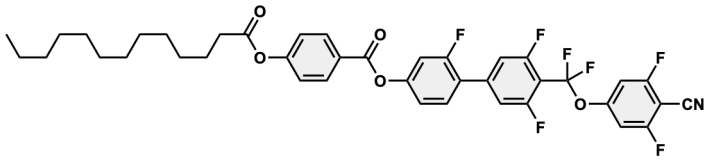

$^{1}H\{^{19}F\}$-NMR (500 MHz, $CDCl_3$): δ 8.24 (d, J = 8.4 Hz, 2H), 7.50 (d, J = 7.9 Hz, 1H), 7.28–7.25 (m, 4H), 7.19–7.17 (m, 2H), 7.04 (s, 2H), 2.60 (t, J = 7.5 Hz, 2H), 1.81–1.75 (m, 2H), 1.46–1.27 (m, 18H), 0.88 (t, *J* = 6.9 Hz, 3H);

$^{19}F\{^{1}H\}$-NMR (471 MHz, $CDCl_3$): δ −61.8 (t, J = 27.5 Hz, 2F), −101.2 (s, 2F), −110.1 (t, *J* = 25.7 Hz, 2F), −113.7 (s, 1F);

$^{13}C\{^{1}H,^{19}F\}$-NMR (126 MHz, $CDCl_3$): δ 171.6, 163.8, 163.6, 159.9, 159.5, 155.4, 155.2, 152.4, 141.3, 131.9, 130.5, 126.0, 123.1, 122.1, 120.3 (t, *J* = 265 Hz), 118.5, 113.2, 111.0, 108.6, 108.5, 108.2 (t, *J* = 31.4 Hz), 108.0, 105.8, 89.9, 34.4, 31.9, 29.6, 29.6, 29.4, 29.3, 29.2, 29.1, 24.8, 22.7, 14.1;

ESI-HRMS (m/z): $[M-H]^-$ calc for 742.2404; found, 742.2408.

2.2.22. ***Synthesis of 4'-((4-cyano-3,5-difluorophenoxy)difluoromethyl)-2,3',5'-trifluoro-[1,1'-biphenyl]-4-yl 4-(tetradecanoyloxy)benzoate* (*13-012-CN*)**

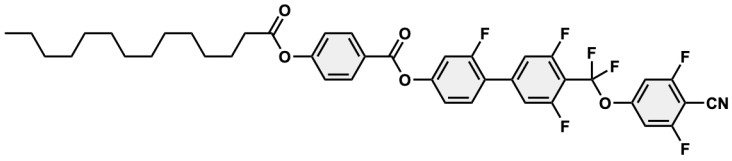

$^{1}H\{^{19}F\}$-NMR (500 MHz, $CDCl_3$): δ 8.24 (d, *J* = 8.9 Hz, 2H), 7.50 (d, *J* = 7.9 Hz, 1H), 7.28–7.25 (m, 4H), 7.19–7.17 (m, 2H), 7.04 (s, 2H), 2.61 (t, *J* = 7.5 Hz, 2H), 1.81-1.75 (m, 2H), 1.45–1.27 (m, 20H), 0.88 (t, *J* = 6.9 Hz, 3H);

$^{19}F\{^{1}H\}$-NMR (471 MHz, $CDCl_3$): δ −61.8 (t, *J* = 27.5 Hz, 2F), −101.2 (s, 2F), −110.1 (t, *J* = 25.7 Hz, 2F), −113.7 (s, 1F);

$^{13}C\{^{1}H,^{19}F\}$-NMR (126 MHz, $CDCl_3$): δ 171.7, 163.8, 163.6, 159.9, 159.5, 155.4, 155.2, 152.4, 141.2, 131.9, 130.5, 126.0, 123.1, 122.1, 120.3 (t, *J* = 264.4 Hz), 118.5, 113.2, 111.0, 108.6, 108.2 (t, *J* = 30.8 Hz), 105.7, 89.9, 34.4, 31.9, 29.7, 29.6, 29.6, 29.4, 29.4, 29.2, 29.1, 24.8, 22.7, 14.1;

ESI-HRMS (m/z): $[M-H]^-$ calc for 756.2560; found, 756.2552.

2.2.23. ***Synthesis of 4'-((4-cyano-3,5-difluorophenoxy)difluoromethyl)-2,3',5'-trifluoro-[1,1'-biphenyl]-4-yl 4-(pentadecanoyloxy)benzoate* (*14-012-CN*)**

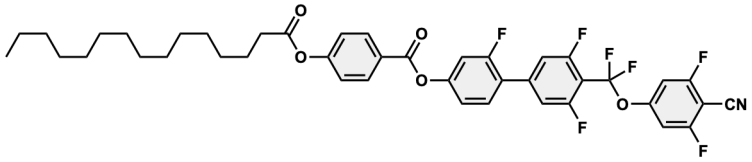

$^{1}H\{^{19}F\}$-NMR (500 MHz, $CDCl_3$): δ 8.24 (d, *J* = 8.4 Hz, 2H), 7.50 (d, *J* = 8.0 Hz, 1H), 7.28–7.25

(m, 4H), 7.19–7.17 (m, 2H), 7.04 (s, 2H), 2.61 (t, *J* = 7.4 Hz, 2H), 1.81-1.75 (m, 2H), 1.46–1.27 (m, 22H), 0.88 (t, J = 6.8 Hz, 3H);

$^{19}F\{^{1}H\}$-NMR (471 MHz, $CDCl_3$): δ −61.8 (t, *J* = 25.7 Hz, 2F), −101.2 (s, 2F), −110.1 (t, *J* = 25.7 Hz, 2F), −113.7 (s, 1F);

$^{13}C\{^{1}H,^{19}F\}$-NMR (126 MHz, $CDCl_3$): δ 171.6, 163.8, 163.6, 159.9, 159.5, 155.4, 155.2, 152.4, 141.3, 131.9, 130.5, 126.0, 123.1, 122.1, 120.3 (t, *J* = 264.4 Hz), 118.5, 113.2, 111.0, 108.6, 108.2 (t, *J* = 31.4 Hz), 105.8, 89.9, 34.4, 31.9, 29.7, 29.7, 29.6, 29.6, 29.4, 29.3, 29.2, 29.1, 24.8, 22.7, 14.1;

ESI-HRMS (m/z): $[M-H]^-$ calc for 770.2717; found, 770.2715.

2.2.24. *Synthesis of 4'-((4-cyano-3,5-difluorophenoxy)difluoromethyl)-2,3',5'-trifluoro-[1,1'-biphenyl]-4-yl 4-(palmitoyloxy)benzoate* (*15-012-CN*)

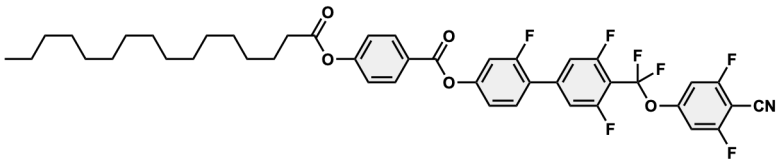

$^{1}H\{^{19}F\}$-NMR (500 MHz, $CDCl_3$): δ 8.24 (d, *J* = 8.6 Hz, 2H), 7.50 (d, *J* = 8.0 Hz, 1H), 7.29–7.25 (m, 4H), 7.19–7.17 (m, 2H), 7.04 (s, 2H), 2.60 (t, *J* = 7.5 Hz, 2H), 1.81–1.75 (m, 2H), 1.46–1.26 (m, 24H), 0.88 (t, *J* = 6.8 Hz, 3H);

$^{19}F\{^{1}H\}$-NMR (471 MHz, $CDCl_3$): δ −61.8 (t, *J* = 25.7 Hz, 2F), −101.2 (s, 2F), −110.1 (t, *J* = 25.7 Hz, 2F), −113.7 (s, 1F);

$^{13}C\{^{1}H,^{19}F\}$-NMR (126 MHz, $CDCl_3$): δ 171.7, 163.8, 163.6, 159.9, 159.5, 155.4, 155.2, 152.4, 141.2, 131.9, 130.5, 126.0, 123.1, 122.1, 120.3 (t, J = 265 Hz), 118.5, 113.2, 111.0, 108.6, 108.2 (t, *J* = 30.8 Hz), 105.7, 89.9, 34.4, 31.9, 29.7, 29.6, 29.6, 29.4, 29.4, 29.2, 29.1, 24.8, 22.7, 14.1;

ESI-HRMS (m/z): $[M-H]^-$ calc for 784.2873; found, 784.2877.

2.2.25. *Synthesis of 4'-((4-cyano-3,5-difluorophenoxy)difluoromethyl)-2,3',5'-trifluoro-[1,1'-biphenyl]-4-yl 4-(heptadecanoyloxy)benzoate* (*16-012-CN*)

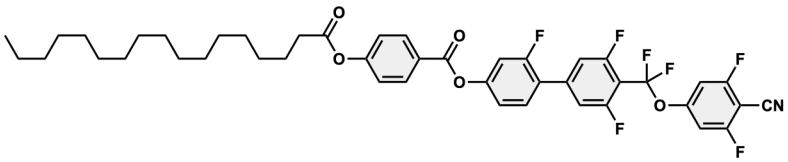

$^{1}H\{^{19}F\}$-NMR (500 MHz, $CDCl_3$): δ 8.24 (d, *J* = 8.6 Hz, 2H), 7.50 (d, *J* = 7.9 Hz, 1H), 7.28–7.25 (m, 4H), 7.18 (d, *J* = 8.0 Hz, 2H), 7.04 (s, 2H), 2.61 (t, *J* = 7.5 Hz, 2H), 1.81–1.75 (m, 2H), 1.44–1.26 (m, 26H), 0.88 (t, *J* = 6.7 Hz, 3H);

$^{19}F\{^{1}H\}$-NMR (471 MHz, $CDCl_3$): δ −61.8 (t, *J* = 25.7 Hz, 2F), −101.2 (s, 2F), −110.1 (t, *J* = 25.7 Hz, 2F), −113.7 (s, 1F);

$^{13}C\{^{1}H,^{19}F\}$-NMR (126 MHz, $CDCl_3$): δ 171.6, 163.8, 163.6, 159.9, 159.5, 155.4, 155.2, 152.4, 141.3, 131.9, 130.5, 126.0, 123.1, 122.1, 120.3 (t, *J* = 268 Hz), 118.5, 113.2, 111.0, 108.6, 108.2 (t, *J* = 31.4 Hz), 105.8, 89.9, 34.4, 31.9, 29.7, 29.6, 29.6, 29.4, 29.4, 29.2, 29.1, 24.8, 22.7, 14.1;
ESI-HRMS (m/z): $[M-H]^-$ calc for 798.3029; found, 798.3032.

2.2.26. ***Synthesis of 4'-((4-cyano-3,5-difluorophenoxy)difluoromethyl)-2,3',5'-trifluoro-[1,1'-biphenyl]-4-yl 4-(stearoyloxy)benzoate* (*17-012-CN*)**

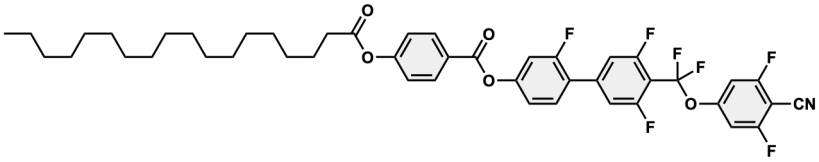

$^{1}H\{^{19}F\}$-NMR (500 MHz, $CDCl_3$): δ 8.24 (d, *J* = 8.7 Hz, 2H), 7.50 (d, *J* = 8.0 Hz, 1H), 7.28–7.25 (m, 4H), 7.19–7.17 (m, 2H), 7.04 (s, 2H), 2.61 (t, *J* = 7.5 Hz, 2H), 1.81-1.75 (m, 2H), 1.46–1.26 (m, 28H), 0.88 (t, *J* = 6.9 Hz, 3H);
$^{19}F\{^{1}H\}$-NMR (471 MHz, $CDCl_3$): δ −61.8 (t, *J* = 25.7 Hz, 2F), −101.2 (s, 2F), −110.1 (t, *J* = 25.7 Hz, 2F), −113.7 (s, 1F);
$^{13}C\{^{1}H,^{19}F\}$-NMR (126 MHz, $CDCl_3$): δ 171.7, 163.8, 163.6, 159.9, 159.5, 155.3, 155.2, 152.4, 141.2, 131.9, 130.5, 126.0, 123.1, 122.1, 120.3 (t, *J* = 265 Hz), 118.5, 113.2, 111.0, 108.6, 108.2 (t, *J* = 30.8 Hz), 105.7, 89.9, 34.4, 31.9, 29.7, 29.6, 29.6, 29.4, 29.4, 29.2, 29.1, 24.8, 22.7, 14.1;
ESI-HRMS (m/z): $[M-H]^{--}$ calc for 812.3186; found, 812.3186.

2.2.27. ***Synthesis of 4'-((4-cyano-3,5-difluorophenoxy)difluoromethyl)-2,3',5'-trifluoro-[1,1'-biphenyl]-4-yl 4-(nonadecanoyloxy)benzoate* (*18-012-CN*)**

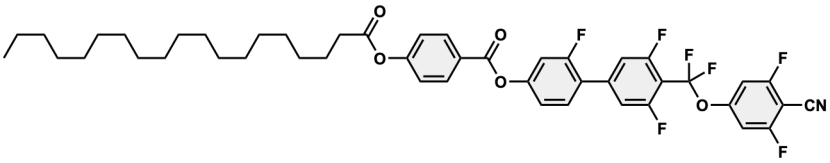

$^{1}H\{^{19}F\}$-NMR (500 MHz, $CDCl_3$): δ 8.24 (d, *J* = 8.6 Hz, 2H), 7.50 (d, *J* = 8.0 Hz, 1H), 7.28–7.25 (m, 4H), 7.19–7.17 (m, 2H), 7.04 (s, 2H), 2.61 (t, *J* = 7.5 Hz, 2H), 1.81–1.75 (m, 2H), 1.46–1.26 (m, 30H), 0.88 (t, *J* = 6.7 Hz, 3H);
$^{19}F\{^{1}H\}$-NMR (471 MHz, $CDCl_3$): δ −61.8 (t, *J* = 27.5 Hz, 2F), −101.2 (s, 2F), −110.1 (t, *J* = 25.7 Hz, 2F), −113.7 (s, 1F);
$^{13}C\{^{1}H,^{19}F\}$-NMR (126 MHz, $CDCl_3$): δ 171.6, 163.8, 163.6, 159.9, 159.5, 155.4, 155.2, 152.4, 141.3, 131.9, 130.5, 126.0, 123.1, 122.1, 120.3 (t, *J* = 264.4 Hz), 118.5, 113.2, 111.0, 108.6, 108.2 (t, *J* = 30.8 Hz), 105.8, 89.9, 34.4, 31.9, 29.7, 29.6, 29.4, 29.4, 29.2, 29.1, 24.8, 22.7, 14.1;
ESI-HRMS (m/z): $[M-H]^-$ calc for 826.3342; found, 826.3338.

2.2.28. ***Synthesis of 4'-((4-cyano-3,5-difluorophenoxy)difluoromethyl)-2,3',5'-trifluoro-[1,1'-biphenyl]-4-yl 4-(icosanoyloxy)benzoate* (*19-012-CN*)**

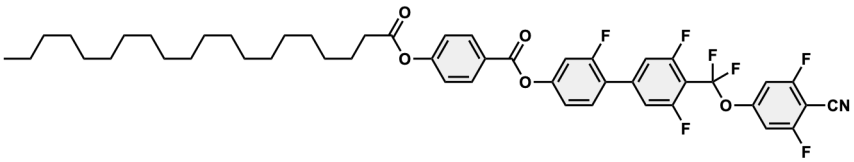

$^{1}H\{^{19}F\}$-NMR (500 MHz, $CDCl_3$): δ 8.23 (d, *J* = 8.7 Hz, 2H), 7.50 (d, *J* = 8.4 Hz, 1H), 7.28–7.25 (m, 4H), 7.19–7.17 (m, 2H), 7.04 (s, 2H), 2.60 (t, *J* = 7.5 Hz, 2H), 1.81-1.75 (m, 2H), 1.45–1.26 (m, 32H), 0.88 (t, *J* = 6.9 Hz, 3H);

$^{19}F\{^{1}H\}$-NMR (471 MHz, $CDCl_3$): δ −61.8 (t, J = 27.5 Hz, 2F), −101.2 (s, 2F), −110.1 (t, *J* = 25.7 Hz, 2F), −113.6 (s, 1F);

$^{13}C\{^{1}H,^{19}F\}$-NMR (126 MHz, $CDCl_3$): δ 171.6, 163.8, 163.6, 159.9, 159.5, 155.4, 155.2, 152.4, 147.8, 141.3, 131.9, 130.5, 126.0, 123.1, 122.1, 120.3 (t, *J* = 263.2 Hz), 118.5, 113.2, 111.0, 108.6, 108.2 (t, *J* = 31.4 Hz), 105.8, 89.9, 34.4, 31.9, 29.7, 29.6, 29.6, 29.4, 29.3, 29.2, 29.1, 24.8, 22.7, 14.1;

ESI-HRMS (m/z): $[M-H]^-$ calc for 840.3499; found, 840.3502.

2.2.29. *Synthesis of 4'-((4-cyano-3,5-difluorophenoxy)difluoromethyl)-2,3',5'-trifluoro-[1,1'-biphenyl]-4-yl 4-(henicosanoyloxy)benzoate* (*20-012-CN*)

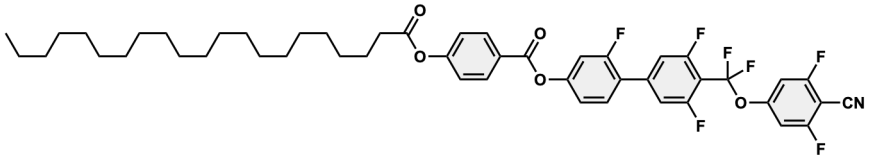

$^{1}H\{^{19}F\}$-NMR (500 MHz, $CDCl_3$): δ 8.24 (d, *J* = 8.6 Hz, 2H), 7.50 (d, *J* = 8.1 Hz, 1H), 7.28–7.25 (m, 4H), 7.19–7.17 (m, 2H), 7.04 (s, 2H), 2.60 (t, *J* = 7.6 Hz, 2H), 1.81–1.75 (m, 2H), 1.44–1.22 (m, 34H), 0.88 (t, J = 6.58 Hz, 3H);

$^{19}F\{^{1}H\}$-NMR (471 MHz, $CDCl_3$): δ −61.8 (t, *J* = 25.7 Hz, 2F), −101.2 (s, 2F), −110.1 (t, *J* = 25.7 Hz, 2F), −113.6 (s, 1F);

$^{13}C\{^{1}H,^{19}F\}$-NMR (126 MHz, $CDCl_3$): δ 171.6, 163.8, 163.6, 159.9, 159.5, 155.4, 155.2, 152.4, 141.3, 131.9, 130.5, 126.0, 123.1, 122.4, 122.1, 120.3 (t, *J* = 264.4 Hz), 118.5, 118.2, 113.2, 111.0, 108.6, 108.2 (t, *J* = 30.8 Hz), 105.8, 89.9, 34.4, 31.9, 29.7, 29.6, 29.4, 29.3, 29.2, 29.1, 24.8, 22.7, 14.1;

ESI-HRMS (m/z): $[M-H]^-$ calc for 854.3655; found, 854.3657.

Supplementary Note (Notes 1–4)

Supplementary Note 1 | XRD Analysis: Indexing of 2D lattices and determination of lattice parameters.

For each diffraction spot in the 2D X-ray scattering pattern, the magnitude of the scattering vector, q, and the azimuthal position were determined. The corresponding d-spacing was calculated as

$$d = \frac{2\pi}{q}.$$

The 2D lattices were indexed from the relationships between the experimental d-spacings, Miller indices, and lattice parameters, following standard procedures used for LC 2D lattices [S5]. Candidate indices were assigned to independent reflections, the lattice parameters were obtained from their experimental d-spacings, and the remaining reflections were used to test the assignment.

Rectangular lattice

For a rectangular lattice, $\gamma = 90°$ and

$$\frac{1}{d_{hk}^2} = \frac{h^2}{a^2} + \frac{k^2}{b^2}.$$

Independent $h0$ and $0k$ reflections were used to obtain a and b. For the representative indexing shown in Fig. 6a,d (main text), the (20) and (02) reflections give

$$\frac{1}{d_{20}^2} = \frac{4}{a^2}, \qquad \frac{1}{d_{02}^2} = \frac{4}{b^2},$$

and therefore

$$a = 2d_{20}, \qquad b = 2d_{02}.$$

The calculated spacing of any assigned (hk) reflection was then obtained from

$$d_{hk,\mathrm{cal}} = \left(\frac{h^2}{a^2} + \frac{k^2}{b^2}\right)^{-1/2}.$$

The resulting values were compared with the experimental spacings of the remaining reflections, such as (11) and (12). A single pair of a and b was required to reproduce the full set of indexed reflections.

Oblique lattice

For an oblique lattice, the unit cell is defined by a, b, and γ, and

$$\frac{1}{d_{hk}^2} = \frac{1}{\sin^2\gamma}\left(\frac{h^2}{a^2} + \frac{k^2}{b^2} - \frac{2hk\cos\gamma}{ab}\right).$$

For convenience, we define

$$A = \frac{1}{a\sin\gamma}, \qquad B = \frac{1}{b\sin\gamma},$$

so that

$$\frac{1}{d_{hk}^2} = h^2A^2 + k^2B^2 - 2hkAB\cos\gamma.$$

Independent $h0$, $0k$, and mixed-index reflections were used to determine the three unknown lattice parameters. For the representative oblique pattern shown in Fig. 7h (main text), the (30), (02), and (11) reflections were used. From (30) and (02),

$$A = \frac{1}{3d_{30}}, \qquad B = \frac{1}{2d_{02}}.$$

The lattice angle was then obtained from the (11) reflection as

$$\cos\gamma = \frac{A^2 + B^2 - 1/d_{11}^2}{2AB}.$$

The real-space lattice constants follow from

$$a = \frac{1}{A\sin\gamma}, \qquad b = \frac{1}{B\sin\gamma}.$$

The derived a, b, and γ were used to calculate the remaining reflections, including (31) and (40). For reflections containing negative indices, the signs of h and k were retained because the cross-term changes sign when one index is negative.

The n = 9–15 homologues were analyzed as rectangular lattices, whereas n = 16 and 17 were analyzed as oblique lattices.

Supplementary Note 2 | Pseudo-rectangular representations of the oblique 2D lattices

The two-dimensional (2D) oblique lattices of ***16*-012-CN** and ***17*-012-CN** were re-examined using alternative unit-cell settings to compare their relative positions of the columns on the lattice (Supplementary Fig. 62). The original lattice parameters were taken from Supplementary Tables 9 (***16*-012-CN**, 64 °C) and Supplementary Tables 10 (***17*-012-CN**, 59 °C). These transformations change the lattice basis without introducing additional reflections or new periodicities.

For the original real-space lattice vectors **a** and **b**, separated by an angle γ, the transformed vectors **A** and **B** were defined in terms of an integer m:

$$\mathbf{A} = m\mathbf{a} + \mathbf{b},$$

$$\mathbf{B} = \mathbf{b}$$

The transformed lattice parameters were calculated from the scalar products:

$$A^2 = m^2a^2 + b^2 + 2mabcos\gamma,$$

$$B = b,$$

$$cos\Gamma = \frac{macos\gamma + b}{A}$$

For ***16*-012-CN** (a = 14.17 nm, b = 5.78 nm, γ = 114.0°), m = 1 gives A = 12.949 nm, B = 5.780 nm, and $\Gamma \approx 90°$. The cell area is unchanged, yielding a nearly orthogonal primitive setting, here termed pseudo-simple (primitive) rectangular. For ***17*-012-CN** (a = 11.27 nm, b = 5.77 nm, γ = 104.8°), m = 2 gives A = 21.789 nm, B = 5.770 nm, and $\Gamma \approx 90°$. The transformed cell has twice the area of the original primitive cell. Because $a = (A-B)/2$, it contains an additional lattice point equivalent to fractional coordinates (1/2, 1/2), giving a pseudo-centered rectangular representation.

The original reflection indices (h, k) and transformed indices (H, K) are related by

$$H = mh + k, K = k$$

For m = 2, $H + K = 2(h + k)$, so only reflections with even $H + K$ occur in the doubled-cell representation.

Supplementary Note 3 | 3D ESP mapping.

The ESP mapped molecular surfaces were created using DFT calculations with the GAUSSIAN 09 program. The conditions for DFT calculation are the same as those for determining the RESP charge. The 3D ESP surface is displayed at an electron density iso-surface of 0.0004. The ESP was averaged as a function of the long molecular axis according to the previous study. [S6] The 3D electron density and ESP cube data were converted to 1D by slicing along the z-axis, aligned with the molecule's long axis. For each *z*-plane, an electron-density iso-contour (isovalue 0.0004) was traced to represent the 3D surface, and the corresponding ESP values on that contour were extracted. The ESP values were averaged over the contour and subsequently multiplied by the contour length (loop length) to compensate for the varying molecular cross section along the molecular axis

Supplementary Note 4 | All-atom molecular dynamics (MD) simulations.

All-atom MD simulations of ***12*-012-CN** and ***16*-012-CN** used the generalized Amber force field (GAFF)[S7], following our previous studies[S8]. Initial molecular geometries were generated using Winmostar. Atomic charges were obtained using the restrained electrostatic potential (RESP) method[S9] following geometry optimization at the B3LYP/6-31G(d,p) level in Gaussian 09[S1].

Initial assemblies were constructed using structural models informed by XRD analysis (Figs. 6a,i and 7h,l, main text). Each system comprised eight polar columns, with molecular arrays in the *xz* plane repeated ten times along the y axis. For ***12*-012-CN**, each array contained seven molecules, giving 560 molecules in total. The initial SmC-like configuration incorporated a molecular tilt of 38° and a longitudinal offset estimated from XRD. For ***16*-012-CN**, neither the local molecular tilt nor the longitudinal offset could be independently determined by XRD; both were therefore treated as model parameters. Two initial configurations with fourteen molecules per layer (1,120 molecules in total) were first examined, using SmA-like (β = 0°) and SmC-like (β = 19°) packing. Both relaxed toward similar tilted arrangements of polar columns at 335 K. Supplementary Fig. 65 shows the initial and relaxed configurations of both models.

The relaxed fourteen-molecule model initialized with SmC-like packing yielded lattice parameters of a = 12.30 nm and b = 5.40 nm. These were smaller than the experimental values of a = 14.09 nm and b = 5.77 nm at 62 °C. A model with sixteen molecules per layer (1,280 molecules in total) was therefore constructed using modified SmC-like initial packing. Its relaxed lattice parameters, a = 13.86 nm and b = 5.67 nm, were closer to experiment. This model was used for the structural analyses in Fig. 8d–f (main text). Supplementary Fig. 64a,b shows the initial configurations of the seven-molecule ***12*-012-CN** and sixteen-molecule ***16*-012-CN** models, respectively. The rationale for the molecular populations is provided in Supplementary Note 5, and the total molecule counts and simulation-box dimensions are listed in Supplementary Table 11.

Following steepest-descent energy minimization, each system was pre-equilibrated for 5 ns at 250 K, followed by 5 ns of pre-equilibration and 100 ns of equilibration at 300 K. Further equilibration was performed at 340 K for ***12*-012-CN** and 335 K for ***16*-012-CN**. All runs were conducted at 1 bar. During pre-equilibration, a Berendsen barostat[S10] and stochastic velocity-rescaling thermostat[S11] were used with coupling times of 2.0 and 0.2 ps, respectively. During equilibration, a Parrinello–Rahman barostat[S12] and Nosé–Hoover thermostat[S13–15] were used with coupling times of 5.0 and 1.0 ps, respectively. Long-range electrostatic interactions

were calculated using the smooth particle-mesh Ewald (PME) method[S16] with a grid spacing of 0.30 nm. Real-space cutoffs for Coulomb and van der Waals interactions were both 1.4 nm. The time step was 2 fs, and covalent bonds involving hydrogen atoms were constrained using LINCS[S4].

To examine layer-like positional organization, electron-density profiles were calculated along the local density-modulation direction, denoted by d and treated as the putative local layer normal[S17,S18]. For ***16*-012-CN**, these profiles describe the simulated local structure rather than an independently established experimental layer periodicity. Intermolecular positional correlations were characterized using cylindrical distribution functions (CDFs), following the previously reported method[S19].

Supplementary Note 5 | Estimation of the number of molecules per polar column segment. Conventional columnar LC phases typically comprise stacked disc-like molecules.[S20] Alternatively, rod-like molecules can assemble into multimolecular units that form columns, as previously described for phasmidic and polycatenar mesogens.[S21] The Col_{r_AF} and Col_{ob_AF} phases of the ***n*-012-CN** series are interpreted using the latter structural model. The number of molecules, N in a columnar unit-cell slice is related to its density and volume by

$$N = \frac{\rho V N_A}{M}, \tag{1}$$

where ρ is the density, V is the slice volume, N_A is the Avogadro constant, and M is the molar mass.[S5] For a two-dimensional lattice with parameters a, b, and γ, the cross-sectional area is $ab\sin\gamma$. The slice volume is therefore $V = abc\sin\gamma$, where c is the effective thickness along the column axis. Here, c was assumed to be 0.4 nm, corresponding to the assumed nearest-neighbor intermolecular separation within a polar bundle. For a unit-cell slice containing Z_b bundles, each comprising n_b molecules, $N = Z_b n_b$, giving

$$n_b = \frac{\rho abc\sin\gamma\, N_A}{Z_b M}. \tag{2}$$

Candidate molecular populations were evaluated for ***12*-012-CN** in the Col_{r_AF} phase at 68 °C and ***16*-012-CN** in the Col_{ob_AF} phase at 62 °C. Assuming two columns per unit cell ($Z_b = 2$), the density corresponding to each candidate population was calculated by rearranging Eq. (2).

For ***12*-012-CN**, the rectangular lattice parameters $a = 5.91$ nm and $b = 4.63$ nm give a cross-sectional area of 27.36 nm^2. 7 molecules per column segment correspond to a calculated density of 1.58 g cm^{-3}. For ***16*-012-CN**, the oblique lattice parameters $a = 14.09$ nm, $b = 5.77$ nm, and $\gamma = 114.02°$ give a cross-sectional area of 74.26 nm^2. Populations of 16–17 molecules per column segment correspond to calculated densities of 1.43–1.52 g cm^{-3}.

For comparison, highly densities of ca. 1.3–1.54 g cm^{-3} have been reported for materials exhibiting the N_F phase incorporating the offset alignment.[S22, S23] On this basis, initial MD models containing 7 and 16 molecules per polar bundle were adopted for ***12*-012-CN** and ***16*-012-CN**, respectively. These populations are model-building choices consistent with the assumed geometry and density range, rather than independently determined structural parameters. They depend on the assumed density, effective axial thickness, and number of columns per unit cell.

Supplementary Figures (Figs. 1–105)

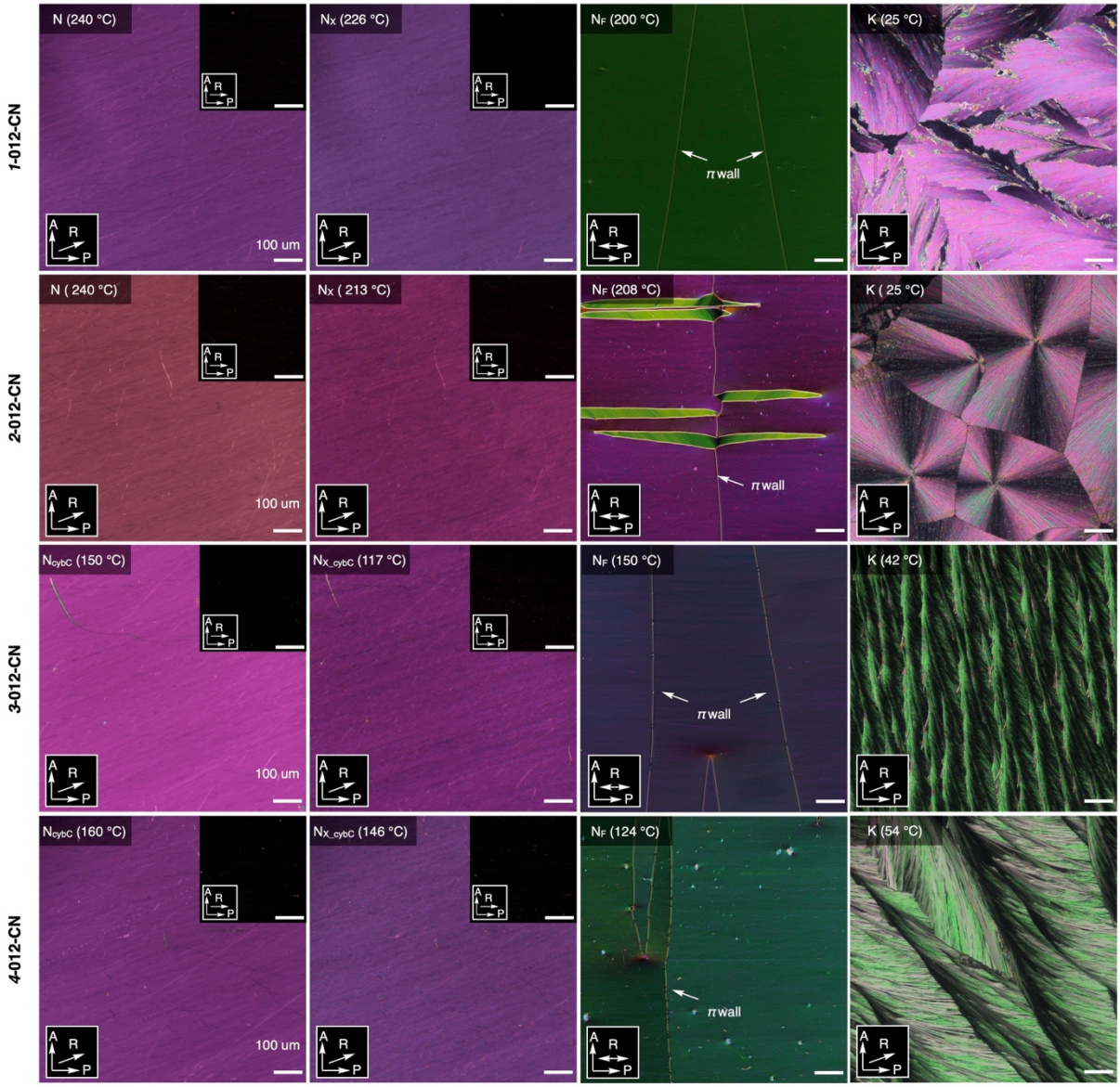

Supplementary Fig. 1 | POM images taken under cross polarizers in SP and AP cells for ***n*-012-CN** (n = 1–4). Abbrev.: A, P and R denote analyzer, polarizer and rubbing direction, respectively. For R, single and double arrows indicate unidirectional and antiparallel rubbing, respectively.

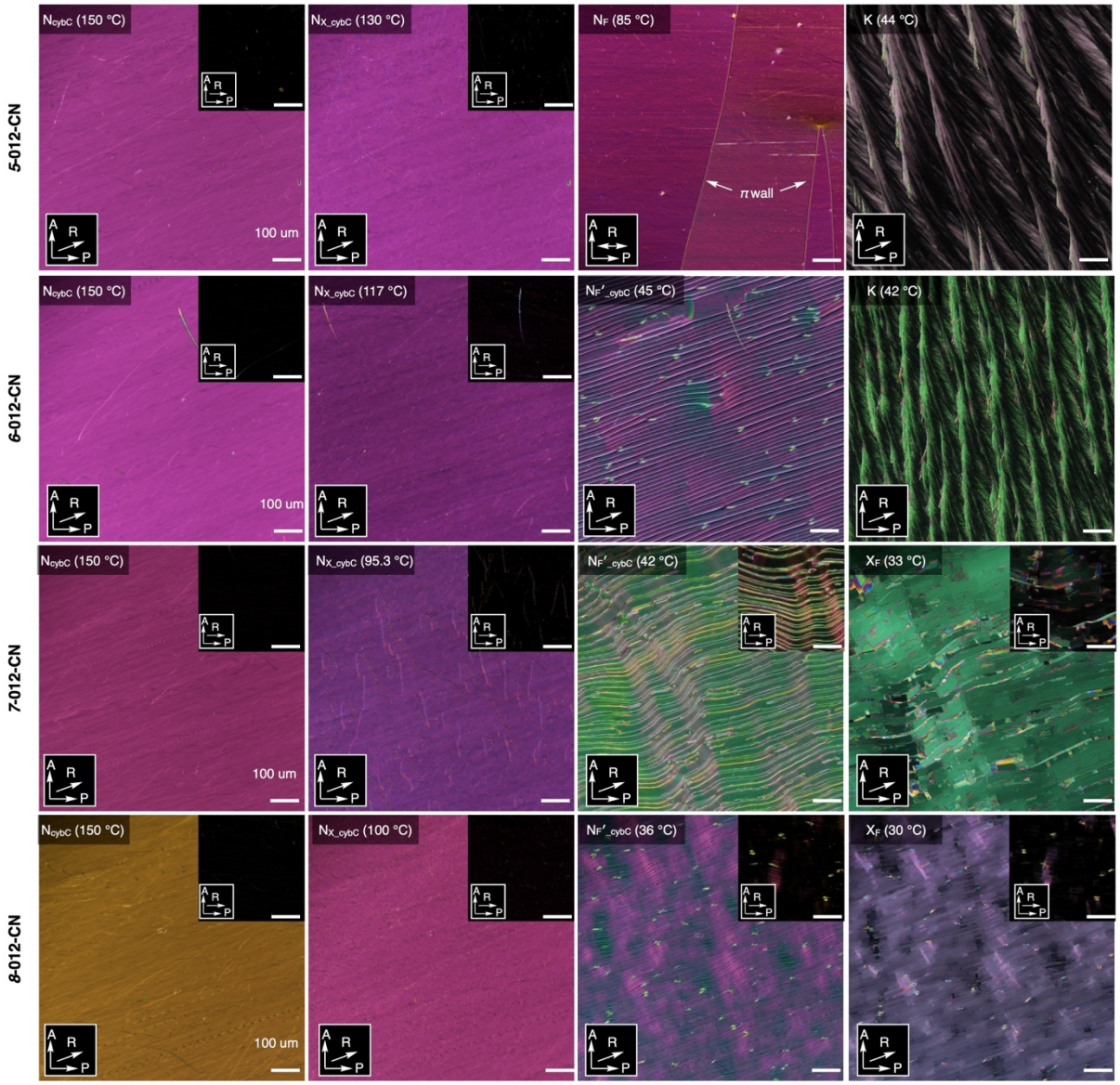

Supplementary Fig. 2 | POM images taken under cross polarizers in SP and AP cells for ***n*-012-CN** (n = 5–8). Abbrev.: A, P and R denote analyzer, polarizer and rubbing direction, respectively. For R, single and double arrows indicate unidirectional and antiparallel rubbing, respectively.

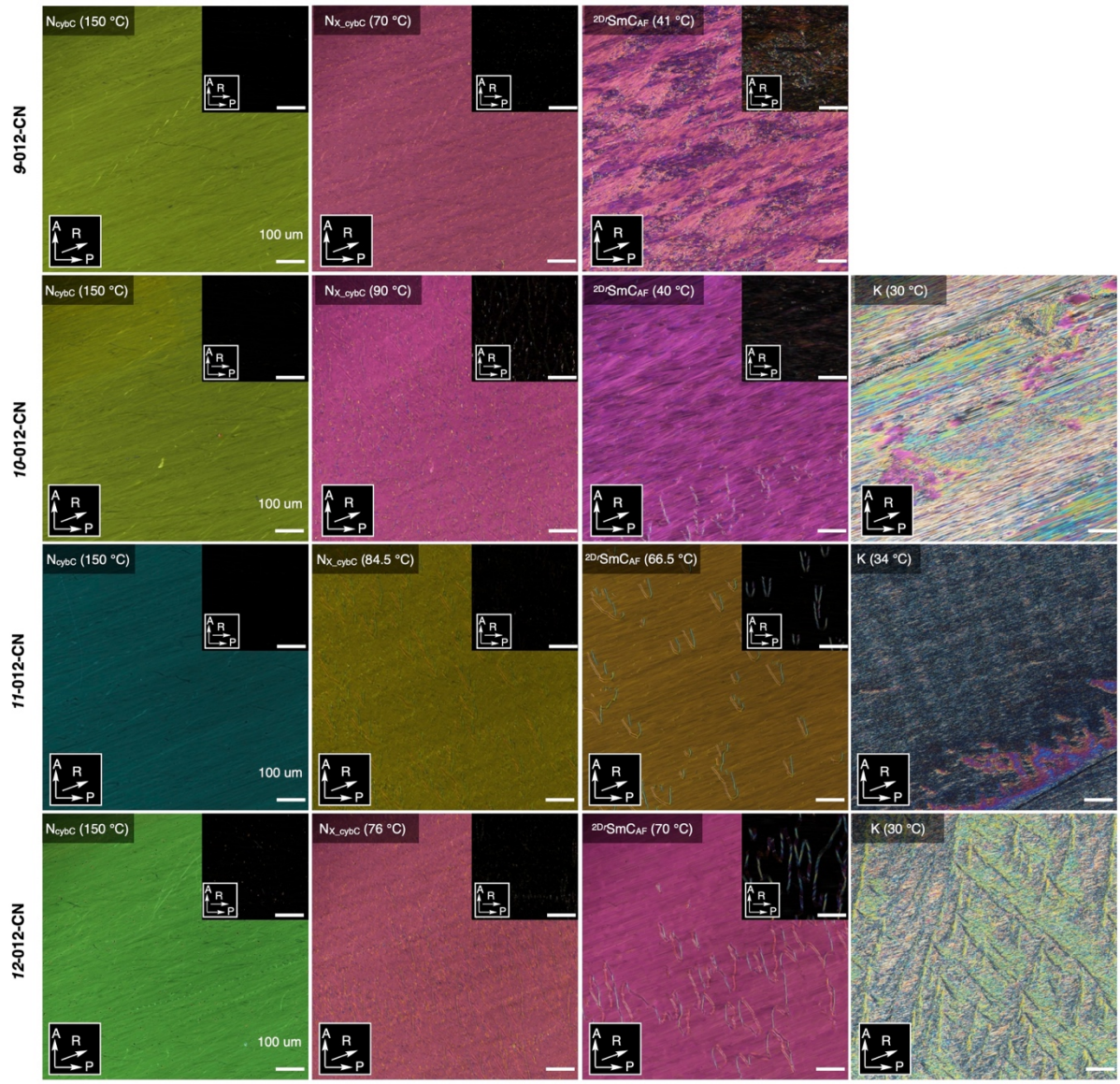

Supplementary Fig. 3 | POM images taken under cross polarizers in SP and AP cells for ***n*-012-CN** (n = 9–12). Abbrev.: A, P and R denote analyzer, polarizer and rubbing direction, respectively. For R, single and double arrows indicate unidirectional and antiparallel rubbing, respectively.

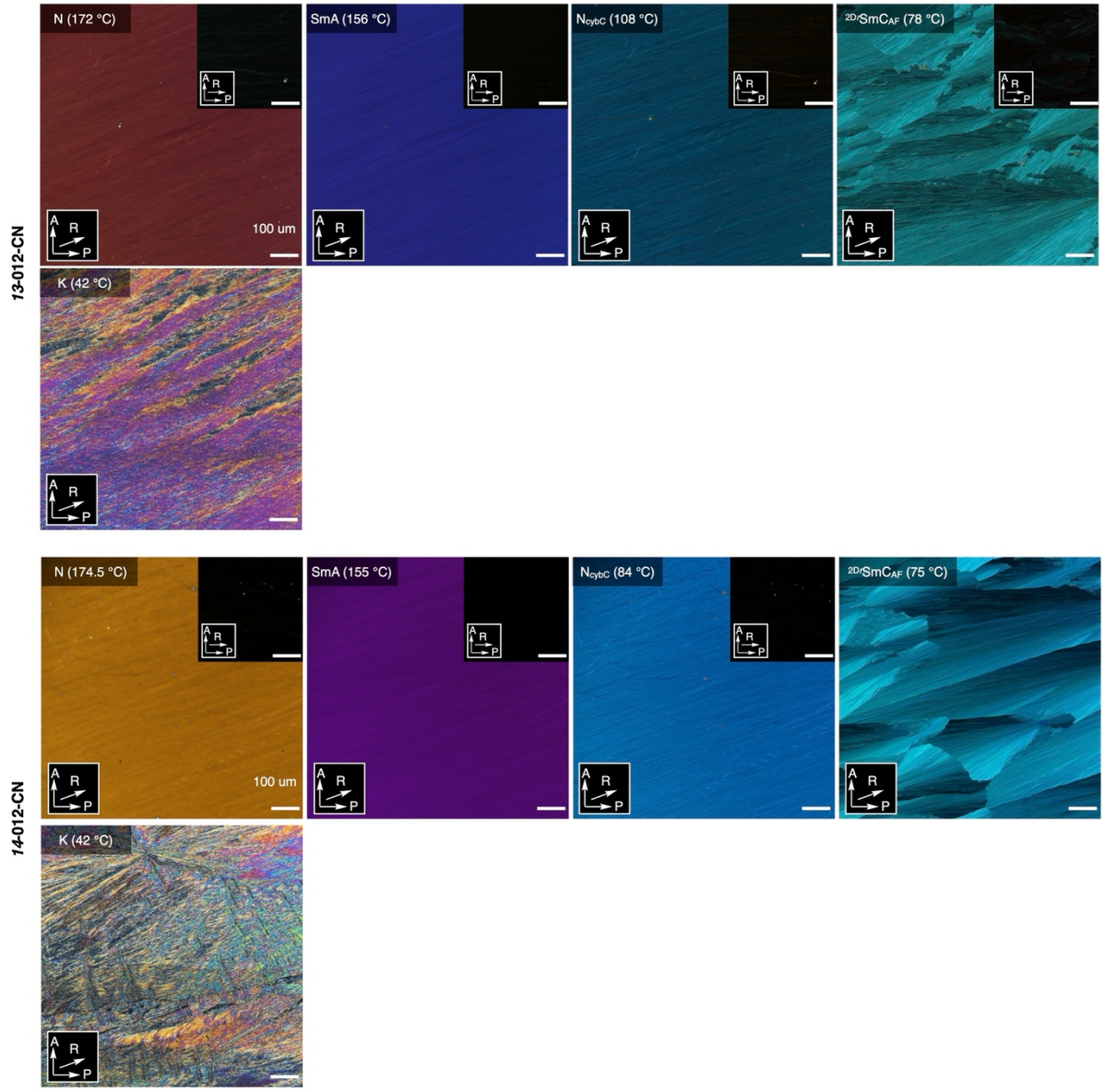

Supplementary Fig. 4 | POM images taken under cross polarizers in SP and AP cells for ***n*-012-CN** (n = 13–14). Abbrev.: A, P and R denote analyzer, polarizer and rubbing direction, respectively. For R, single and double arrows indicate unidirectional and antiparallel rubbing, respectively.

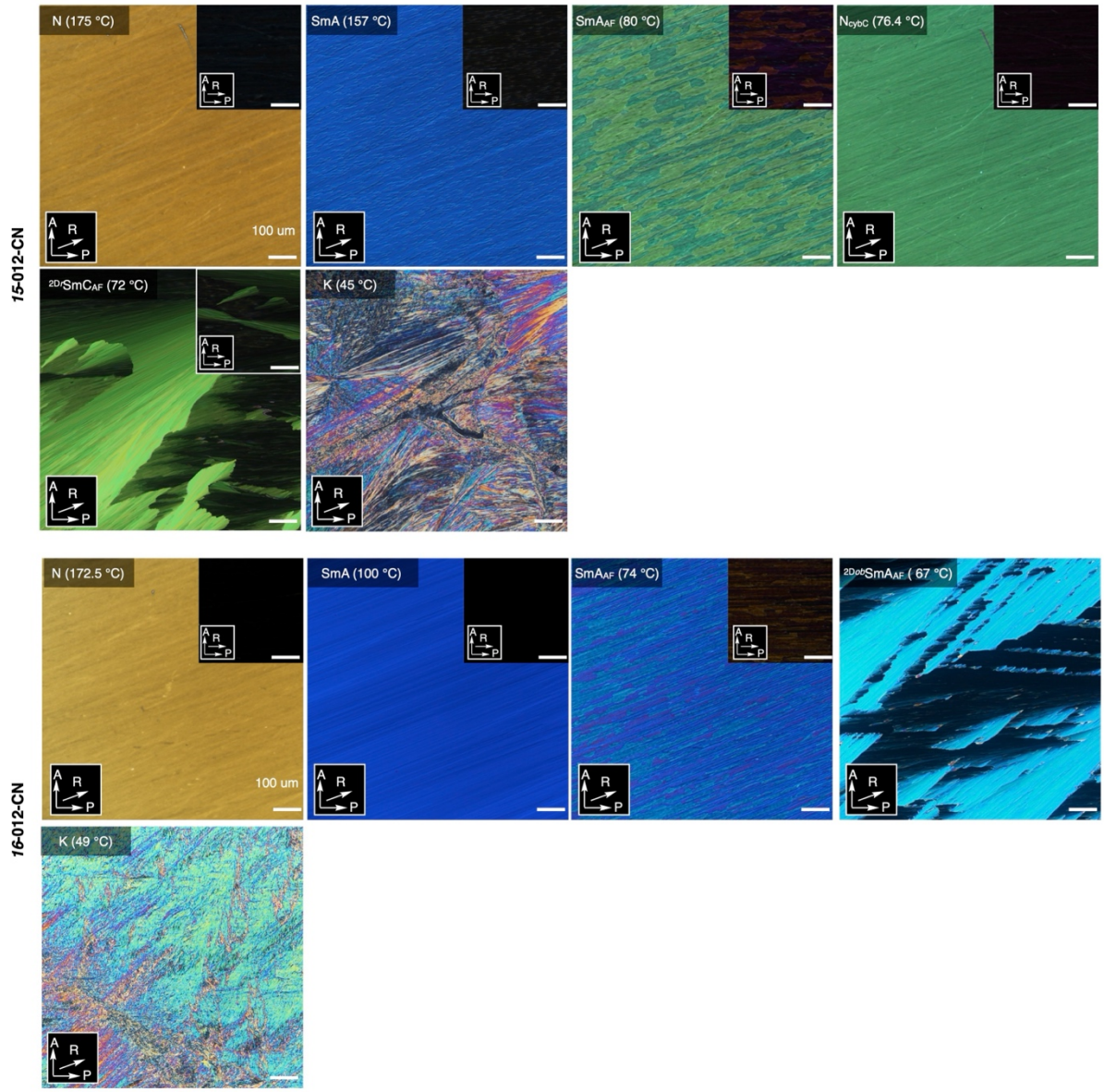

Supplementary Fig. 5 | POM images taken under cross polarizers in SP and AP cells for ***n*-012-CN** (n = 15–16). Abbrev.: A, P and R denote analyzer, polarizer and rubbing direction, respectively. For R, single and double arrows indicate unidirectional and antiparallel rubbing, respectively.

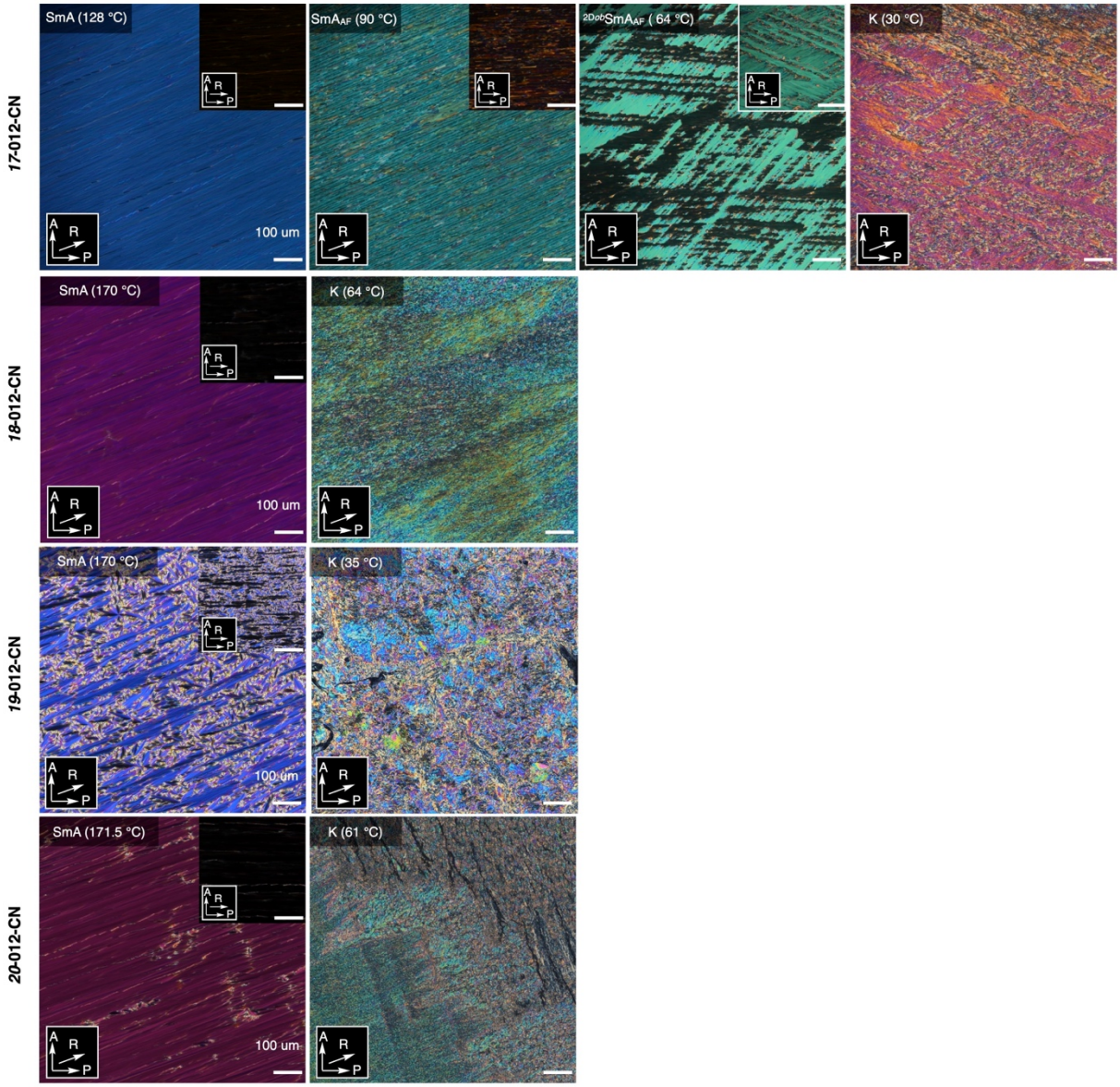

Supplementary Fig. 6 | POM images taken under cross polarizers in SP and AP cells for ***n*-012-CN** (n = 17–20). Abbrev.: A, P and R denote analyzer, polarizer and rubbing direction, respectively. For R, single and double arrows indicate unidirectional and antiparallel rubbing, respectively.

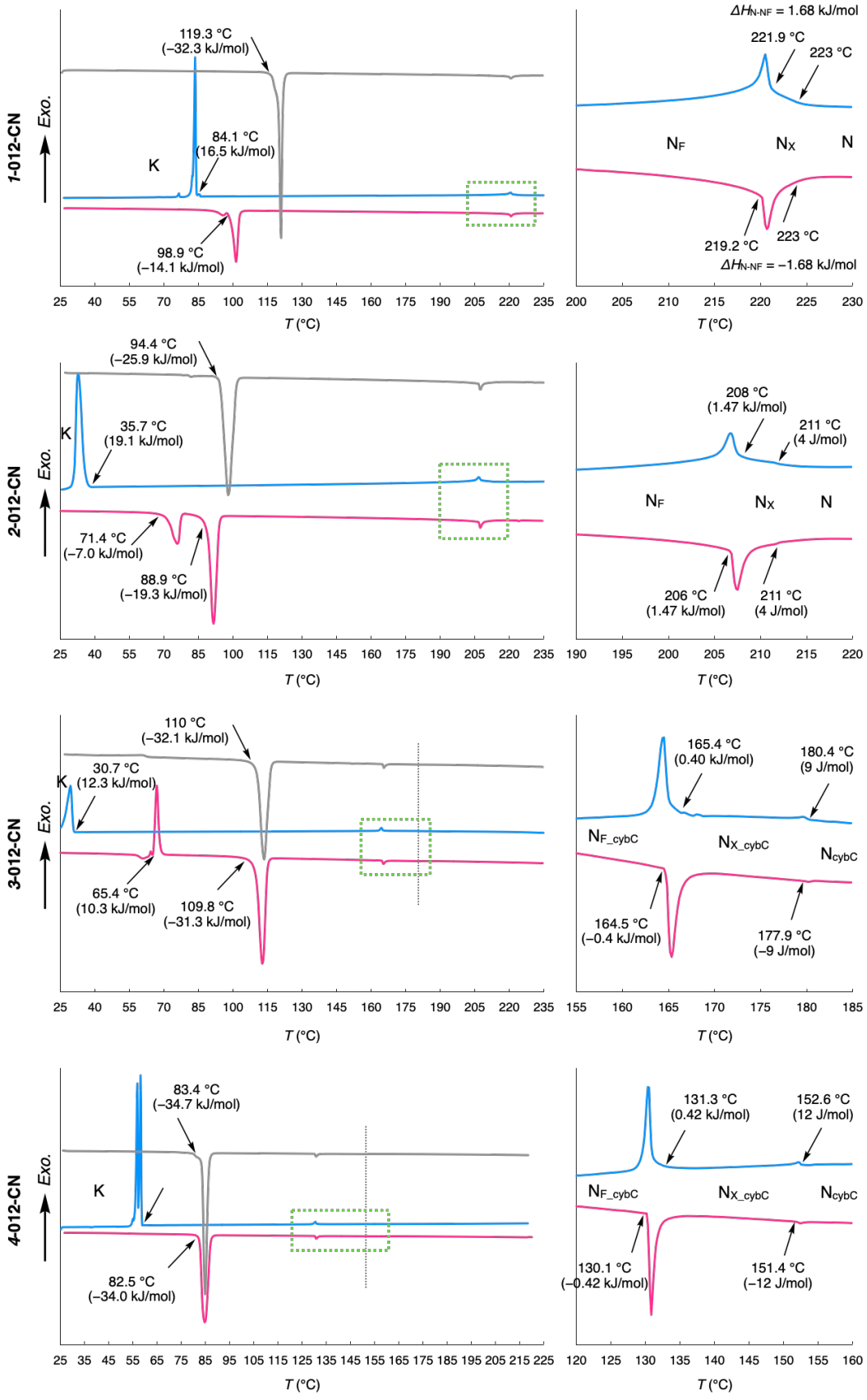

Supplementary Fig. 7 | DSC curves for ***n*-012-CN** (n = 1–4). The values in parentheses indicate the phase-transition enthalpies. The gray, blue, and magenta curves denote the first heating, first cooling, and second heating scans, respectively. Scan rate: 10 K min^{-1}.

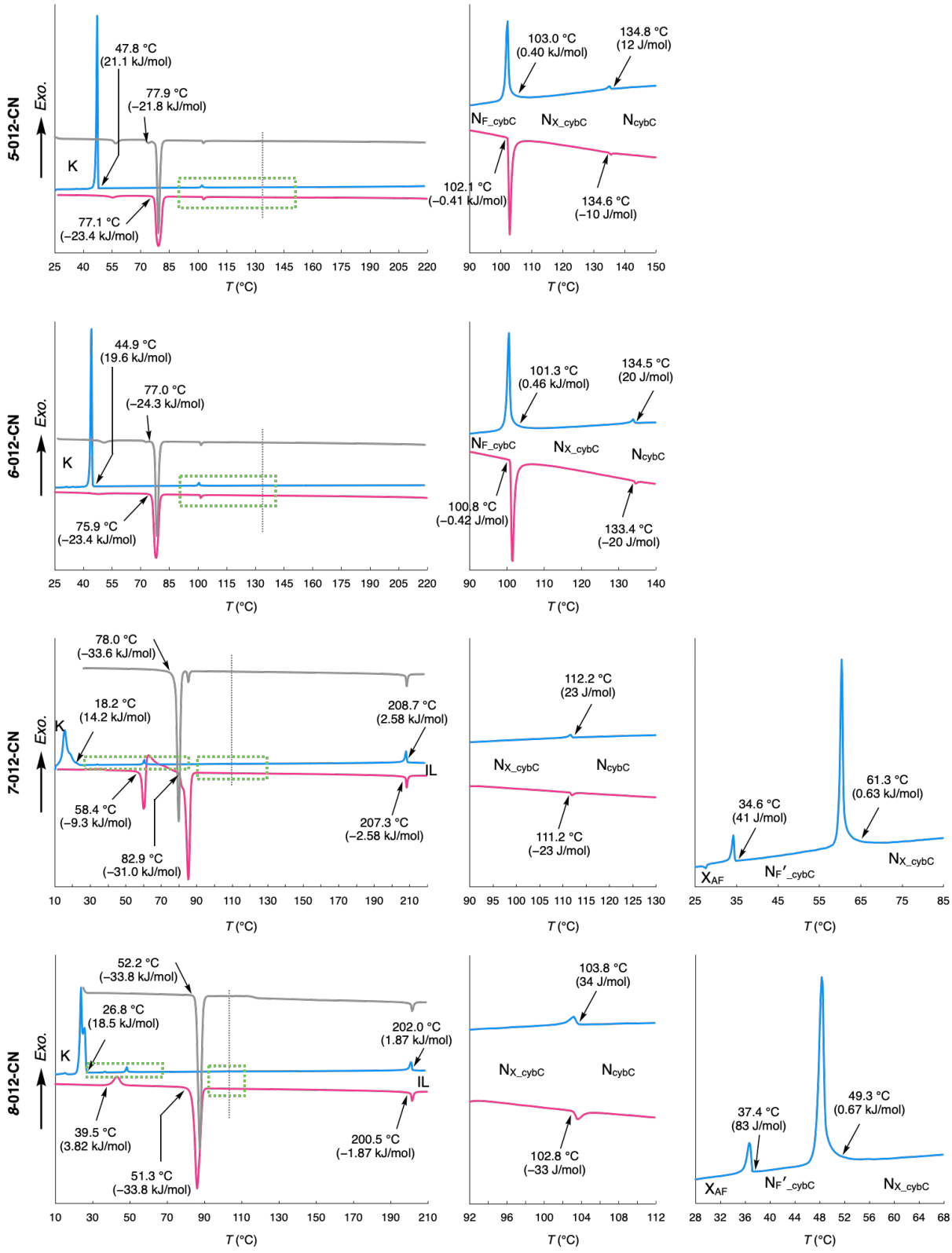

Supplementary Fig. 8 | DSC curves for ***n*-012-CN** (n = 5–8). The values in parentheses indicate the phase-transition enthalpies. The gray, blue, and magenta curves denote the first heating, first cooling, and second heating scans, respectively. Scan rate: 10 K min^{-1}.

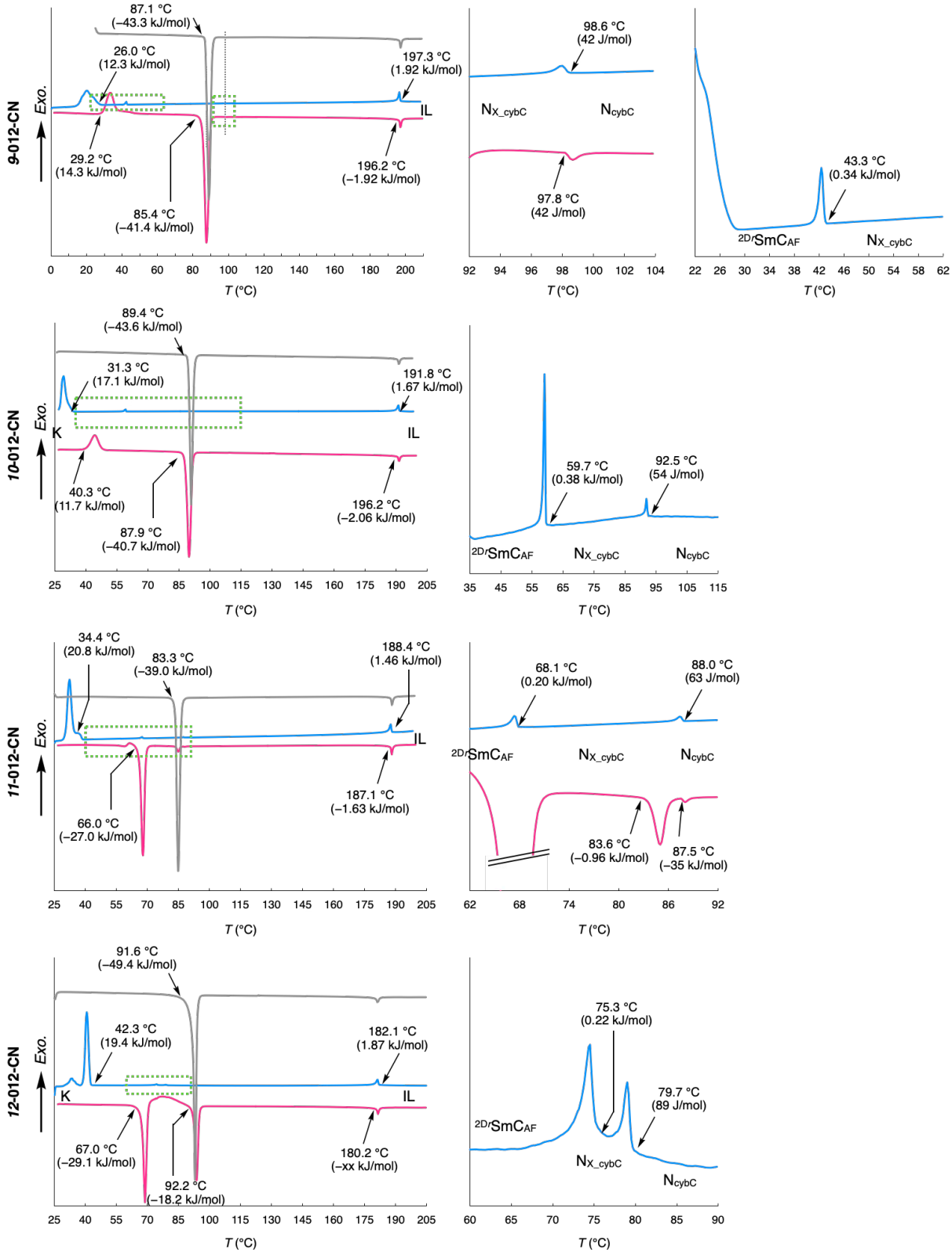

Supplementary Fig. 9 | DSC curves for ***n*-012-CN** (n = 9–12). The values in parentheses indicate the phase-transition enthalpies. The gray, blue, and magenta curves denote the first heating, first cooling, and second heating scans, respectively. Scan rate: 10 K min^{-1}.

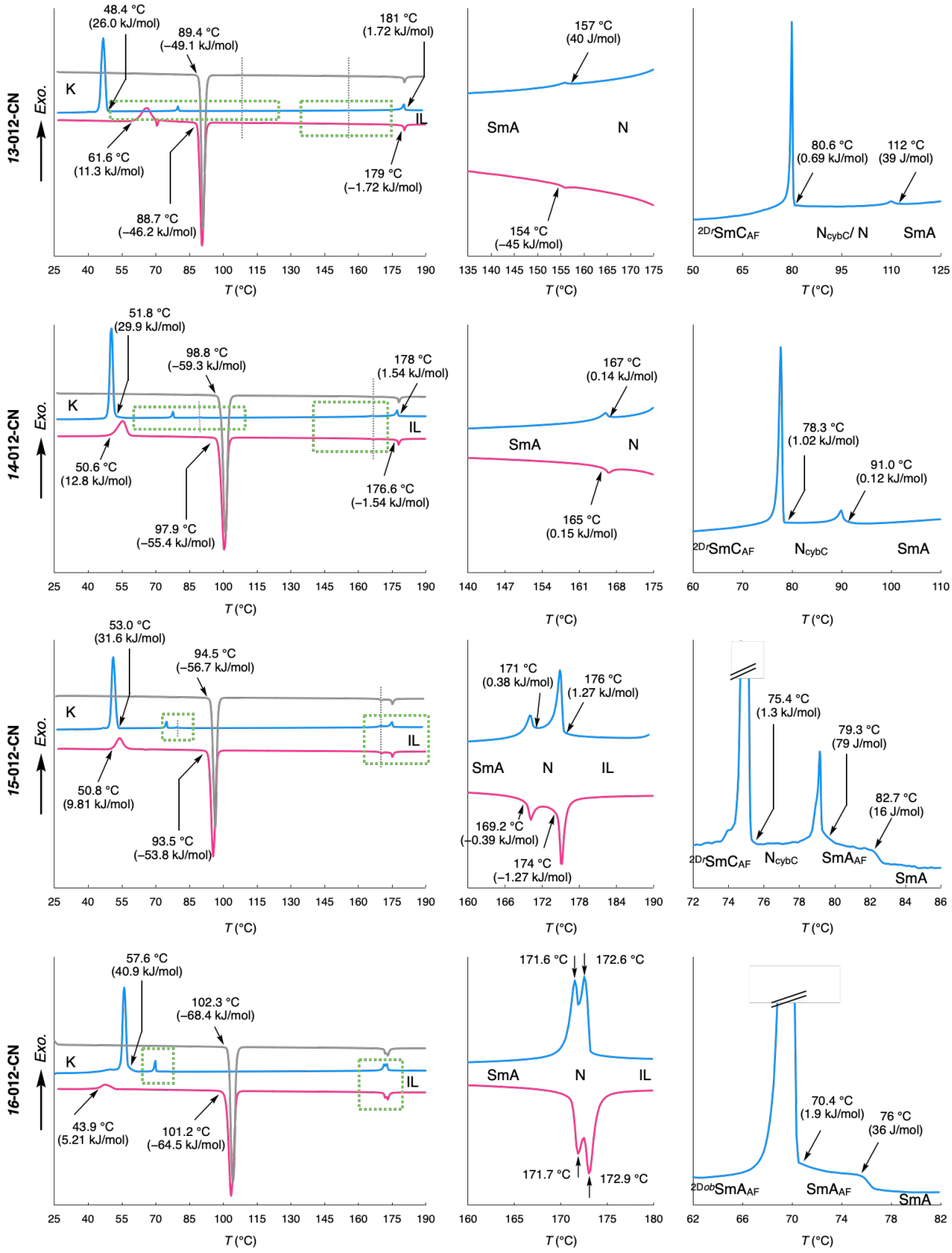

Supplementary Fig. 10 | DSC curves for ***n*-012-CN** (n = 13–16). The values in parentheses indicate the phase-transition enthalpies. The gray, blue, and magenta curves denote the first heating, first cooling, and second heating scans, respectively. Scan rate: 10 K min^{-1}.

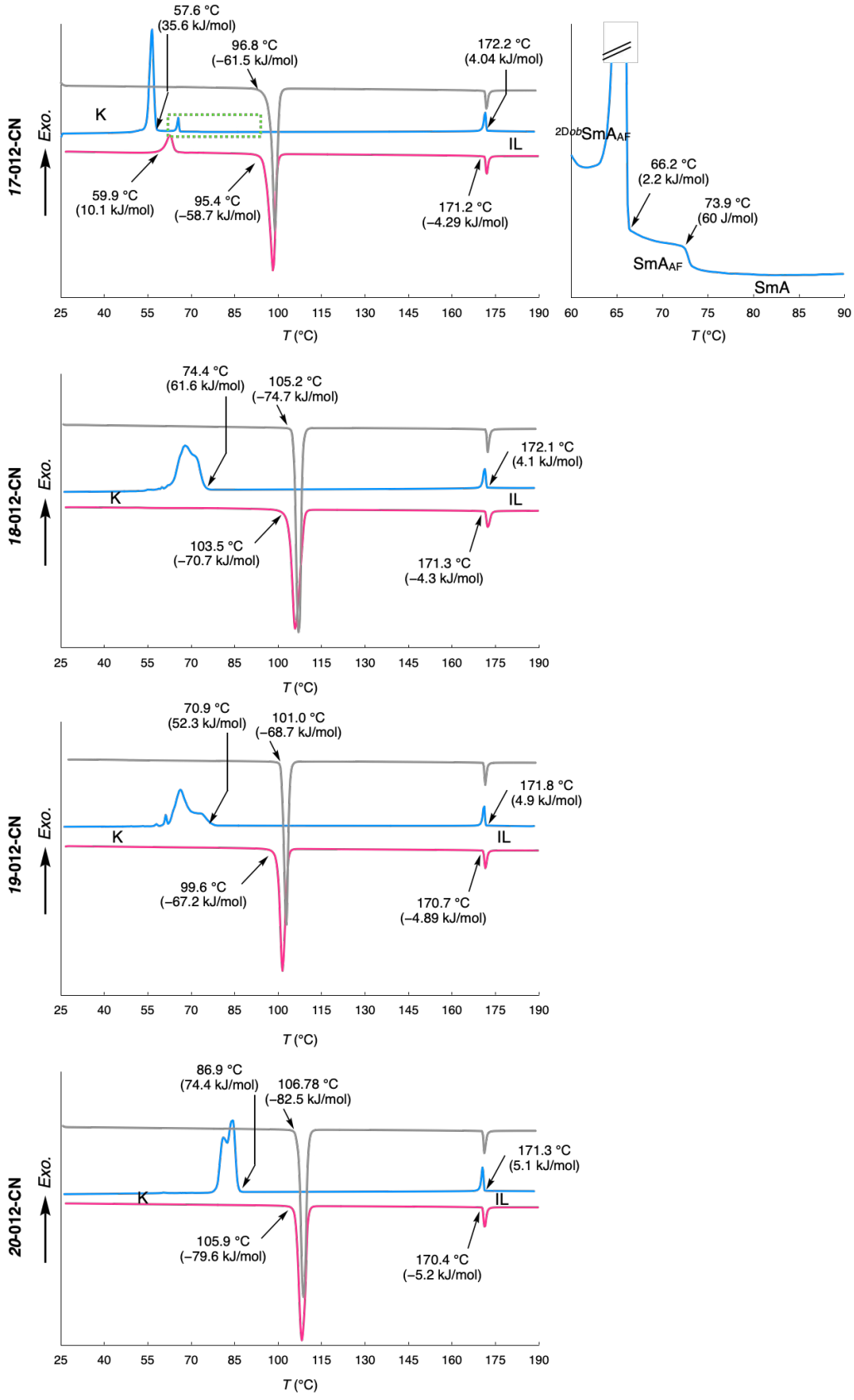

Supplementary Fig. 11 | DSC curves for ***n*-012-CN** (n = 17–20). The values in parentheses indicate the phase-transition enthalpies. The gray, blue, and magenta curves denote the first heating, first cooling, and second heating scans, respectively. Scan rate: 10 K min^{-1}.

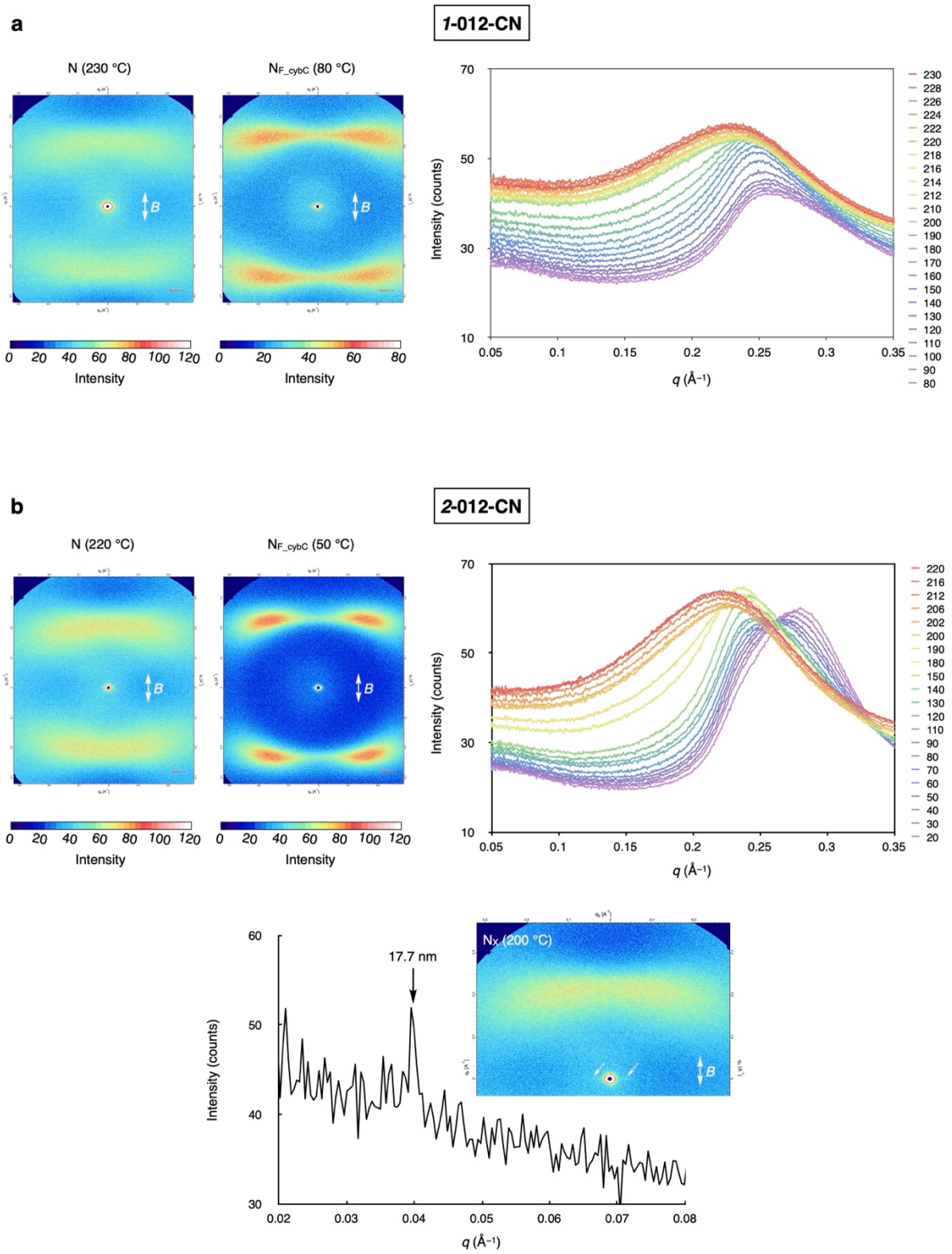

Supplementary Fig. 12 | 2D and corresponding 1D X-ray diffraction patterns at various temperatures under the magnetic field (~1 T, **B ‖ n**) for ***1*-012-CN** (a) and ***2*-012-CN** (b).

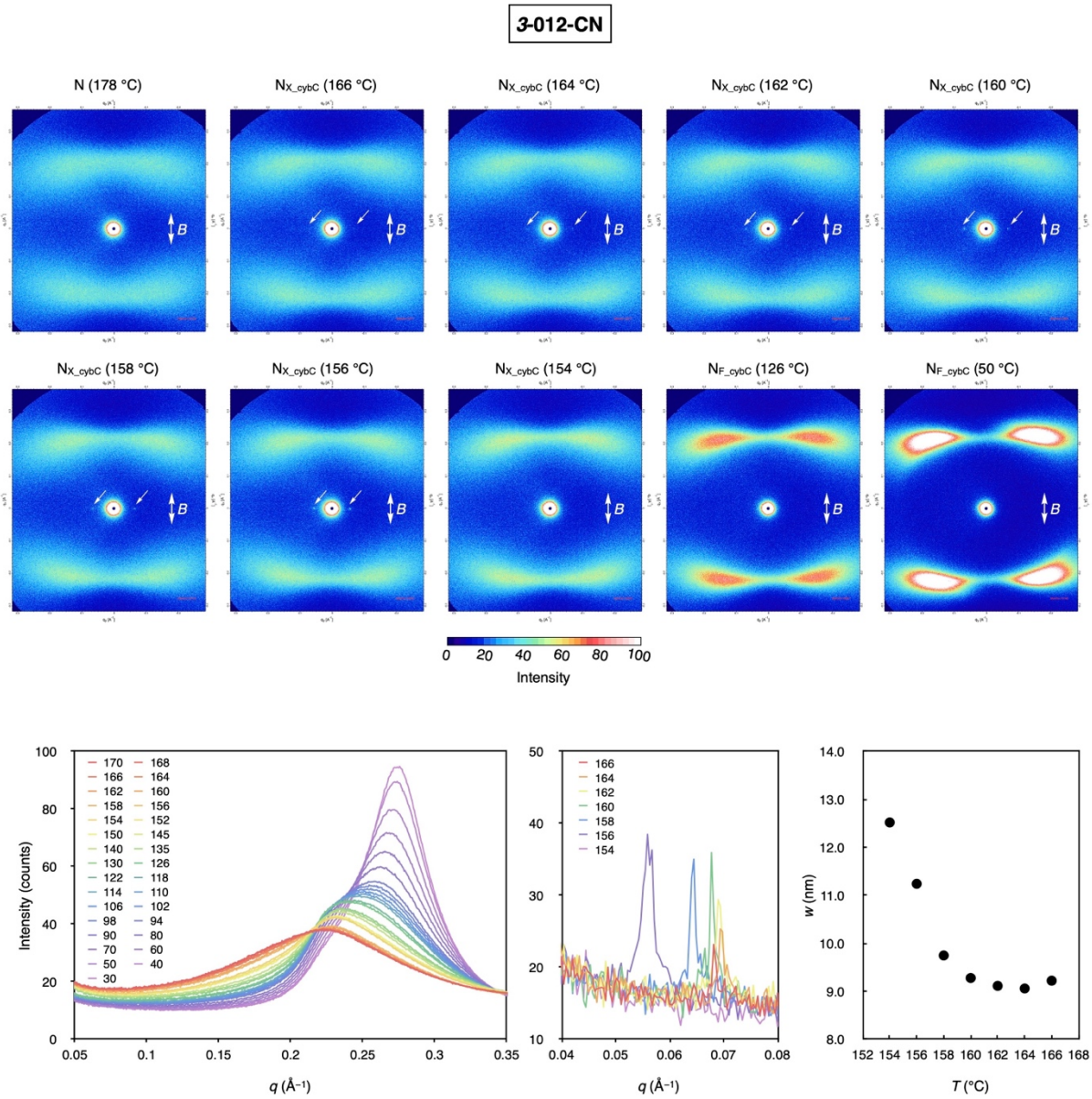

Supplementary Fig. 13 | 2D, corresponding 1D X-ray diffraction patterns and analyzed data at various temperatures under the magnetic field (~1 T, **B ∥ n**) for ***3*-012-CN**.

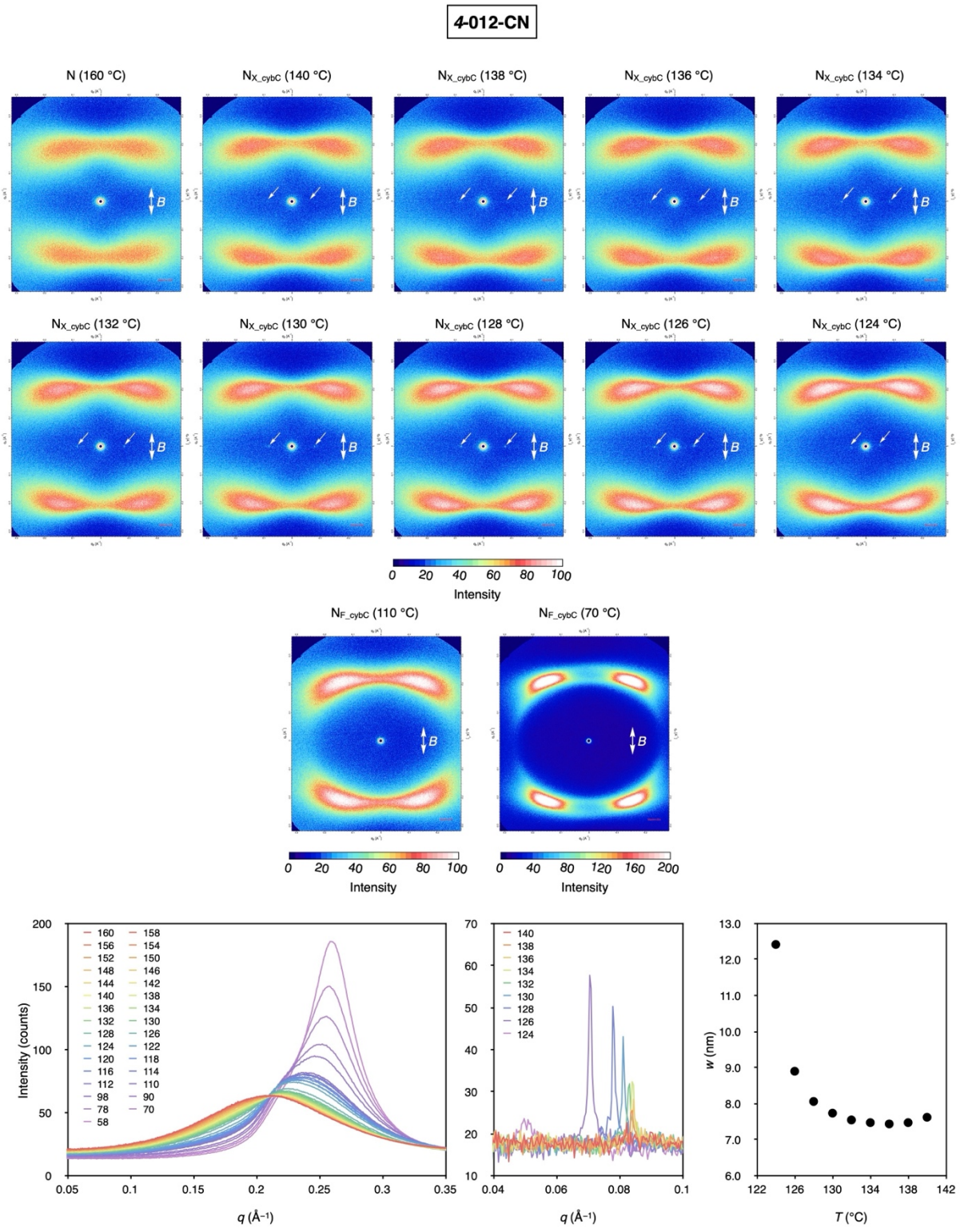

Supplementary Fig. 14 | 2D, corresponding 1D X-ray diffraction patterns and analyzed data at various temperatures under the magnetic field (~1 T, **B** ‖ **n**) for ***4*-012-CN**.

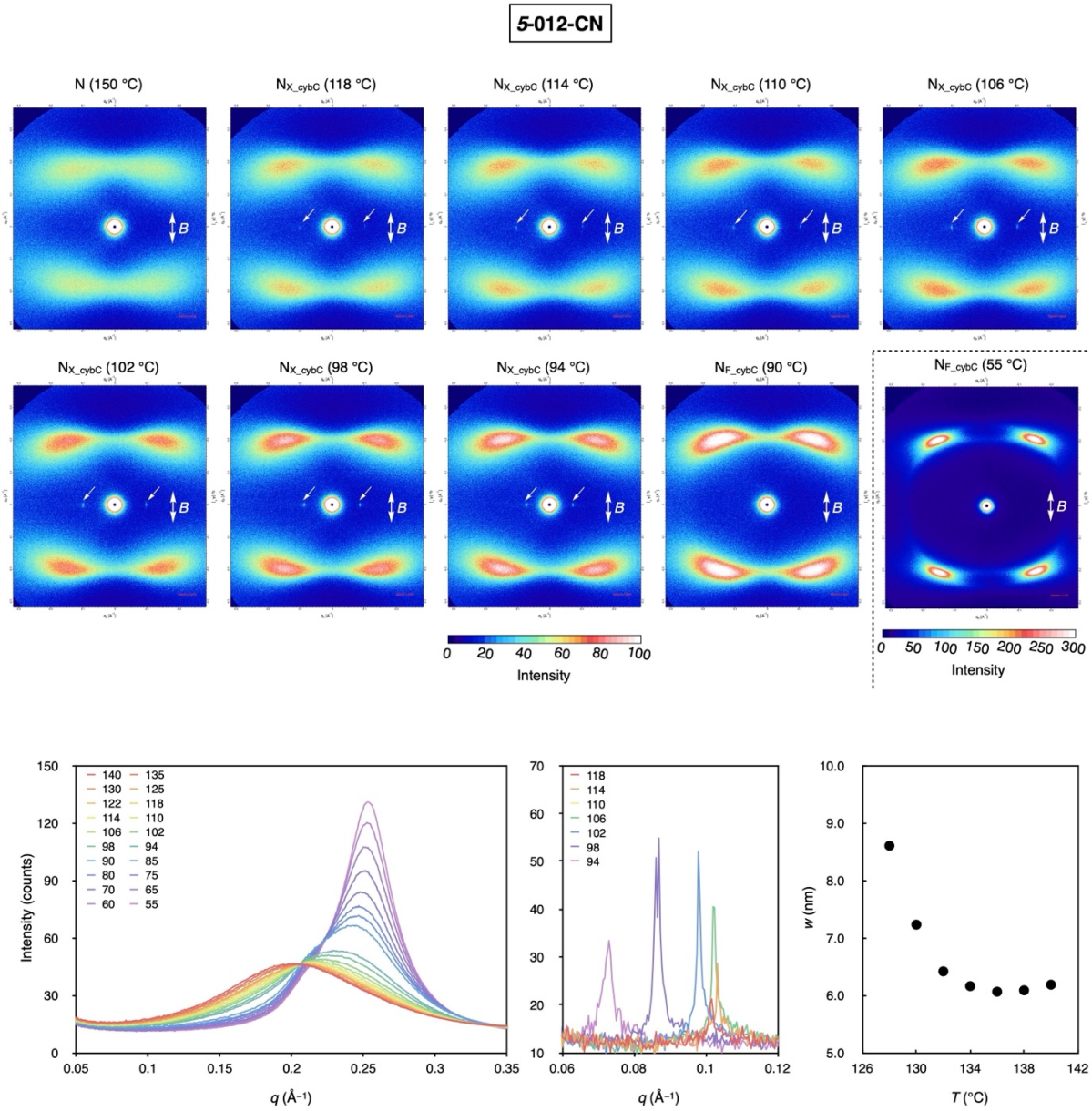

Supplementary Fig. 15 | 2D, corresponding 1D X-ray diffraction patterns and analyzed data at various temperatures under the magnetic field (~1 T, **B ∥ n**) for ***5*-012-CN**.

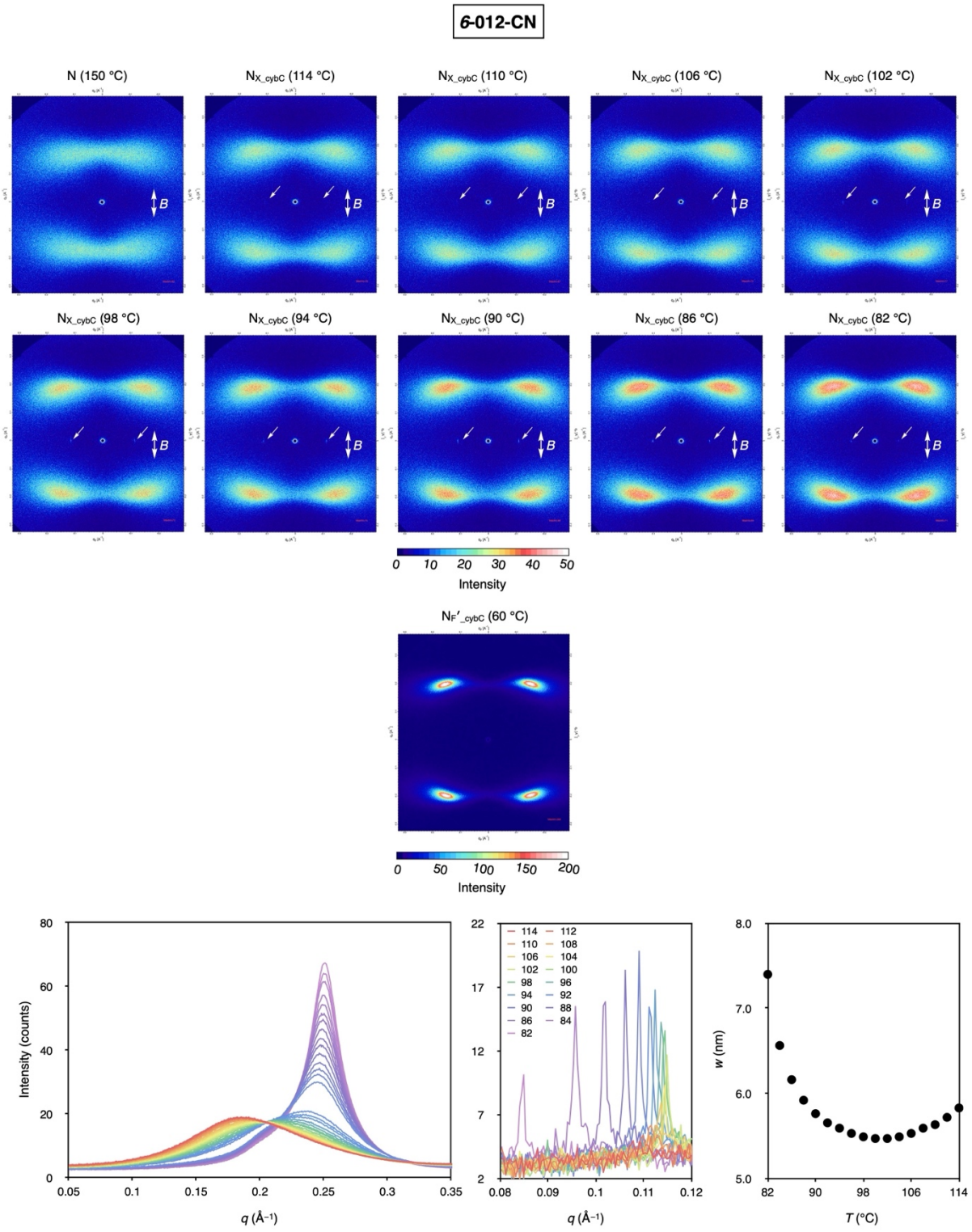

Supplementary Fig. 16 | 2D, corresponding 1D X-ray diffraction patterns and analyzed data at various temperatures under the magnetic field (~1 T, **B ∥ n**) for ***6*-012-CN**.

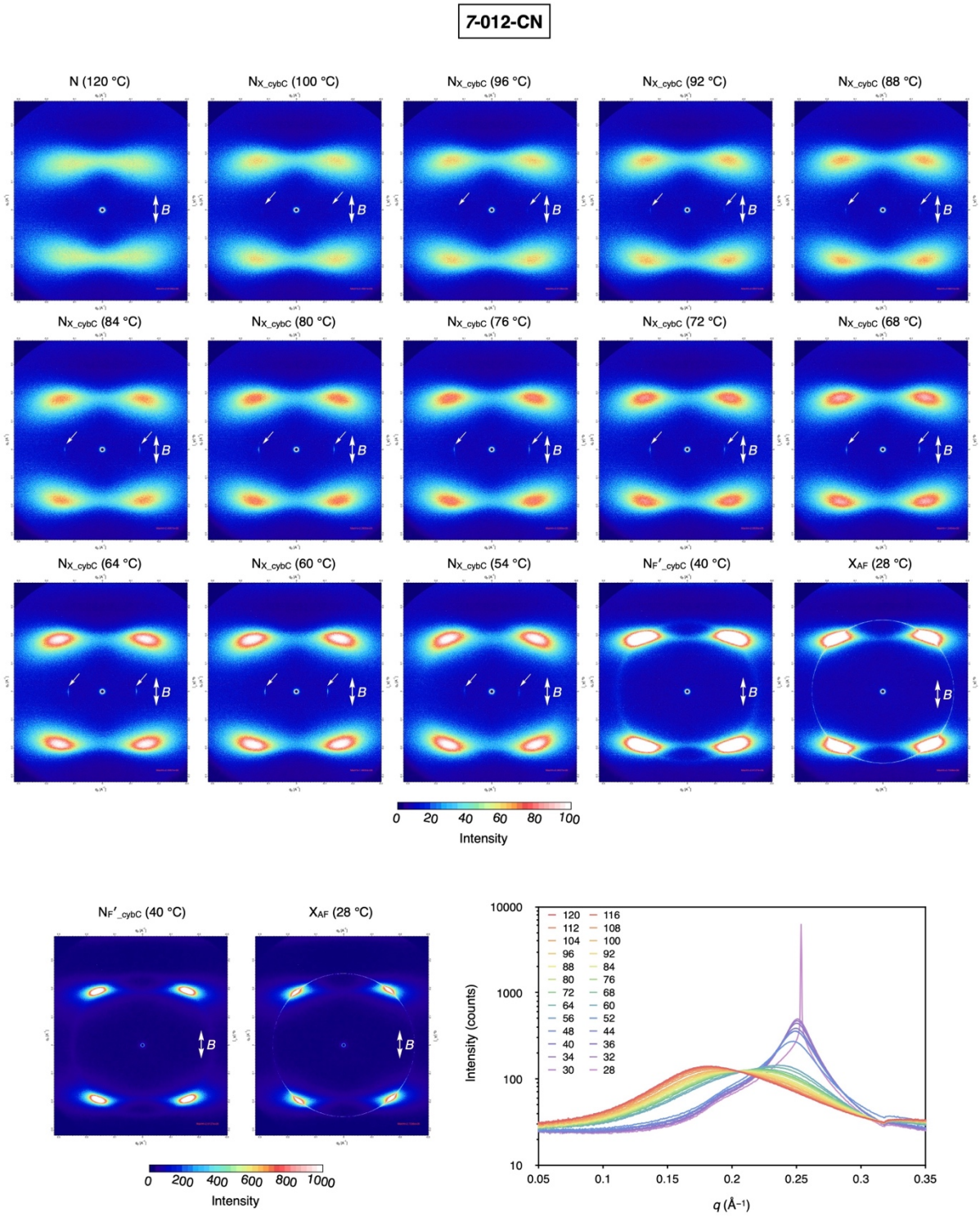

Supplementary Fig. 17 | 2D and corresponding 1D X-ray diffraction patterns and analyzed data at various temperatures under the magnetic field (~1 T, **B ∥ n**) for ***7*-012-CN**.

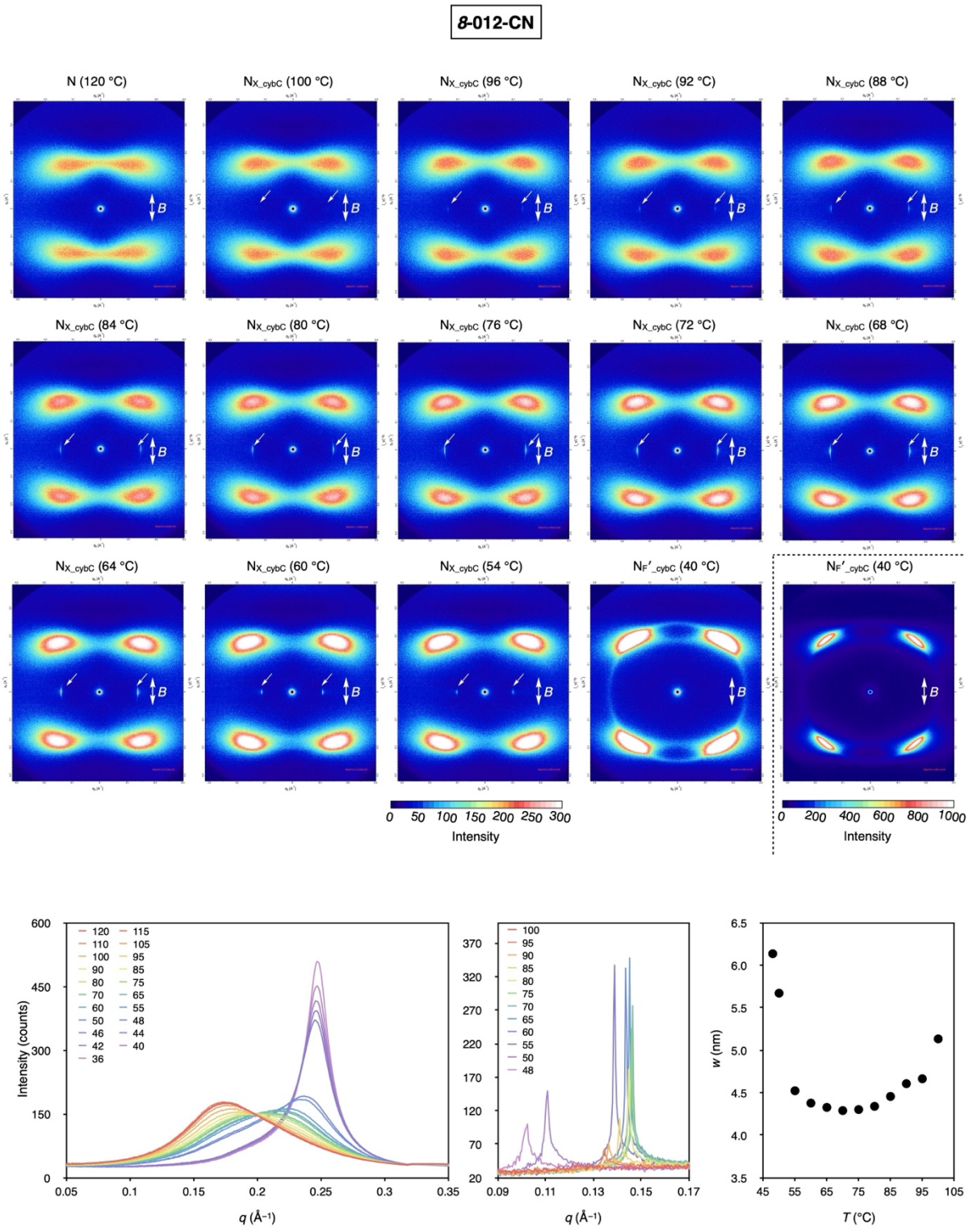

Supplementary Fig. 18 | 2D, corresponding 1D X-ray diffraction patterns and analyzed data at various temperatures under the magnetic field (~1 T, **B** ∥ **n**) for ***8*-012-CN**.

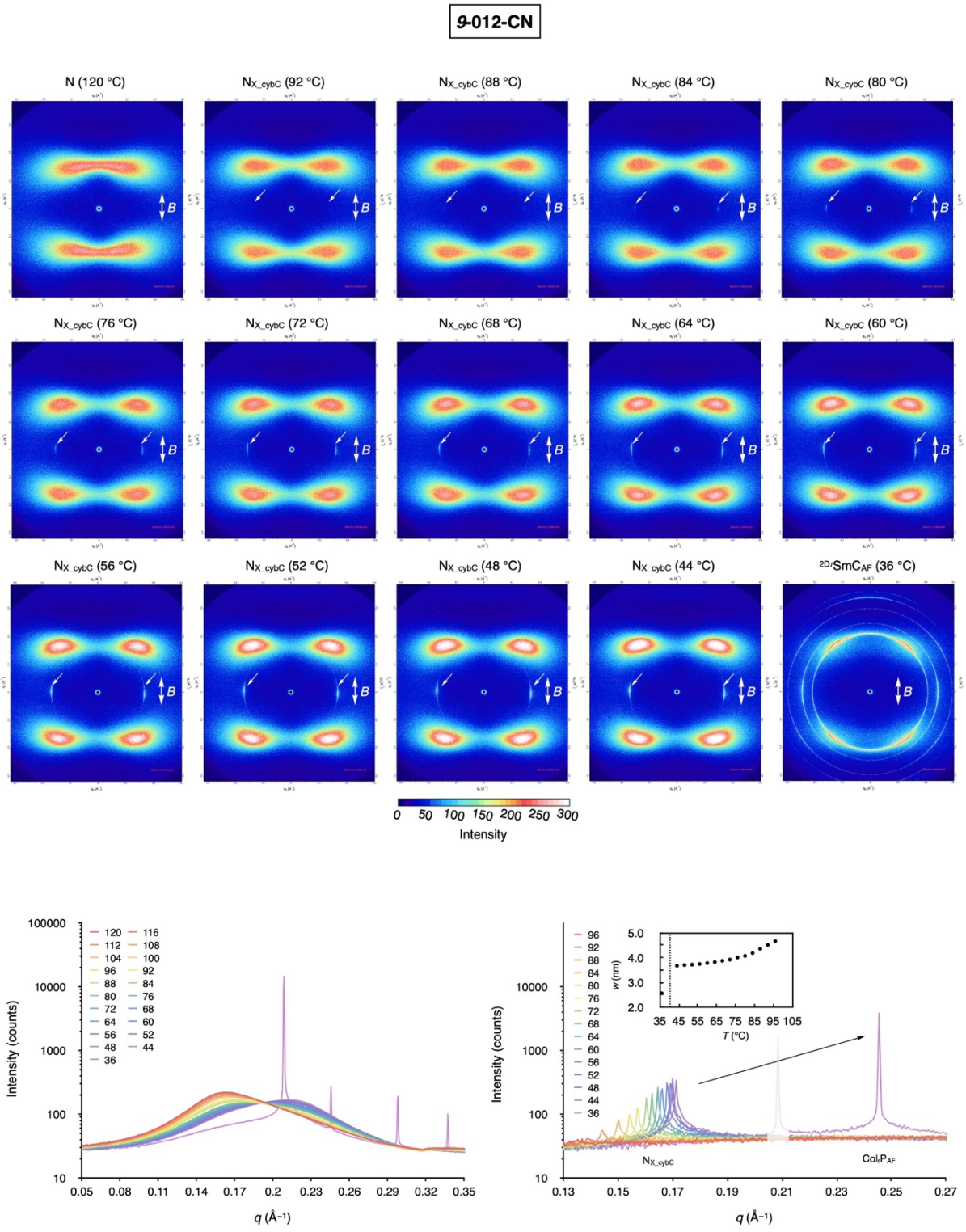

Supplementary Fig. 19 | 2D, corresponding 1D X-ray diffraction patterns and analyzed data at various temperatures under the magnetic field (~1 T, **B ∥ n**) for ***9*-012-CN**.

9-012-CN

a **b**

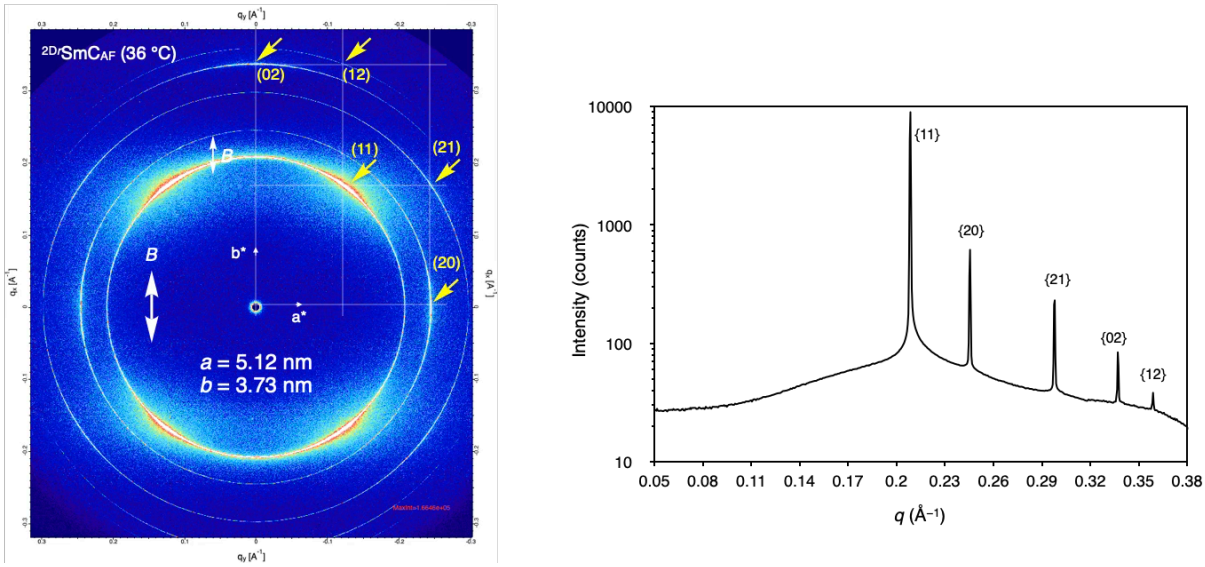

Supplementary Fig. 20 | XRD data at various temperatures under the magnetic field (~1 T, **B ∥ n**) for ***9*-012-CN**: 2D (a) and corresponding 1D (b) X-ray diffraction patterns.

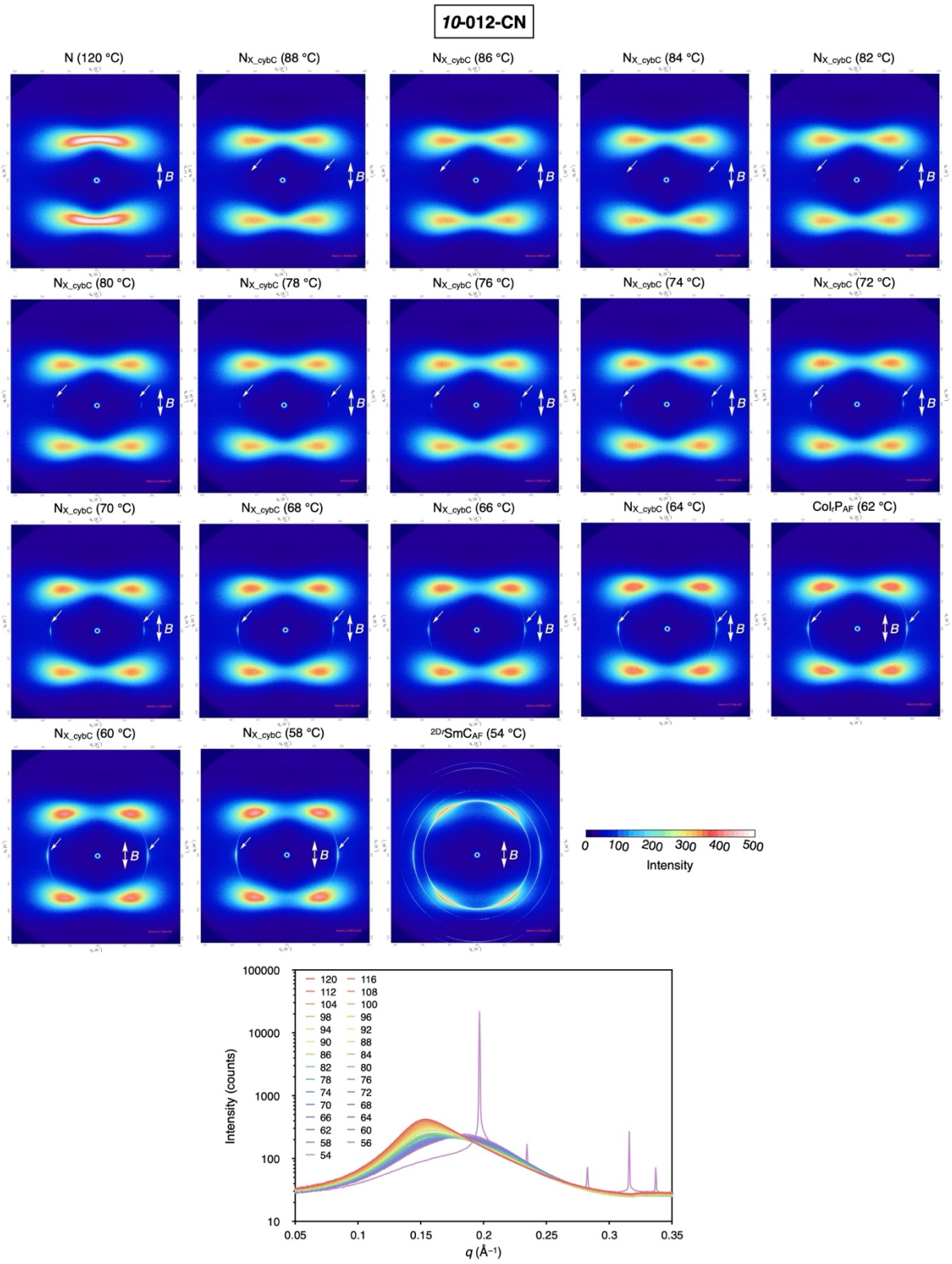

Supplementary Fig. 21 | 2D and corresponding 1D X-ray diffraction patterns at various temperatures under the magnetic field (~1 T, **B ∥ n**) for ***10*-012-CN**.

***10*-012-CN**

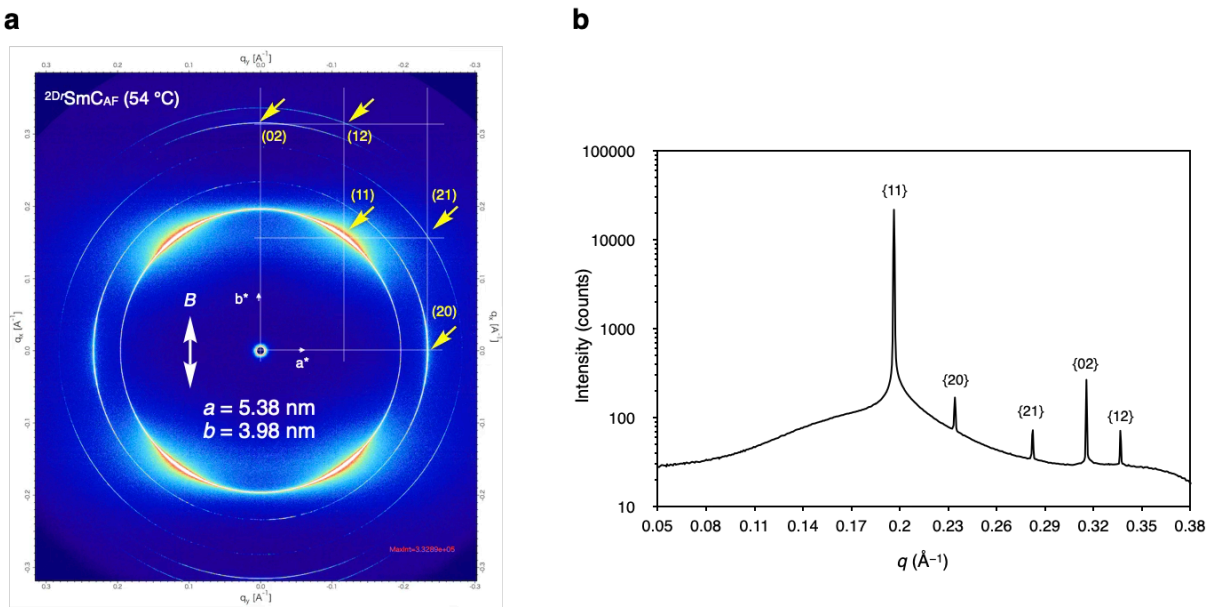

Supplementary Fig. 22 | XRD data at various temperatures under the magnetic field (~1 T, **B ∥ n**) for ***10*-012-CN**: 2D (a) and corresponding 1D (b) X-ray diffraction patterns.

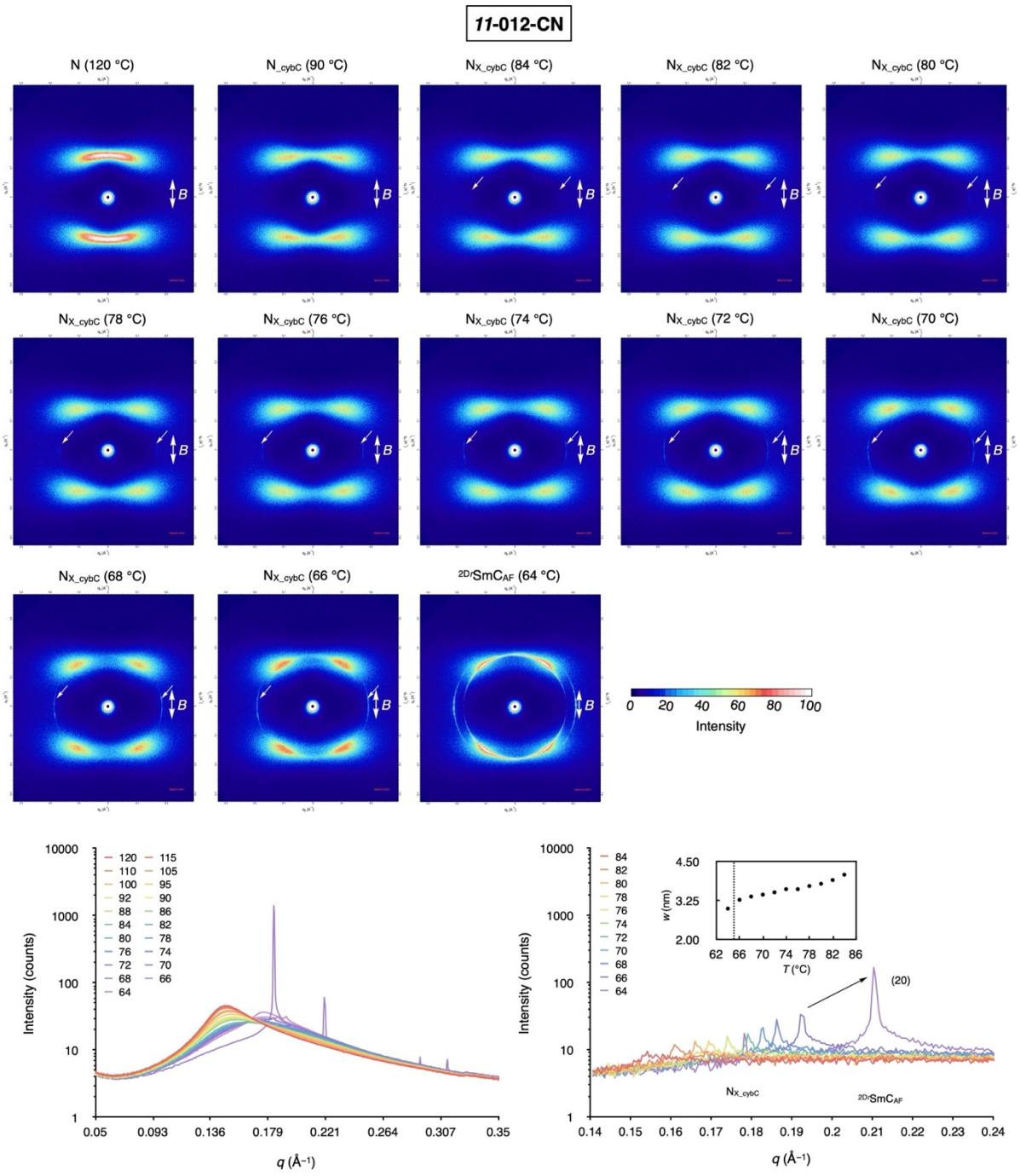

Supplementary Fig. 23 | 2D, corresponding 1D X-ray diffraction patterns and analyzed data at various temperatures under the magnetic field (~1 T, **B** ∥ **n**) for ***11*-012-CN**.

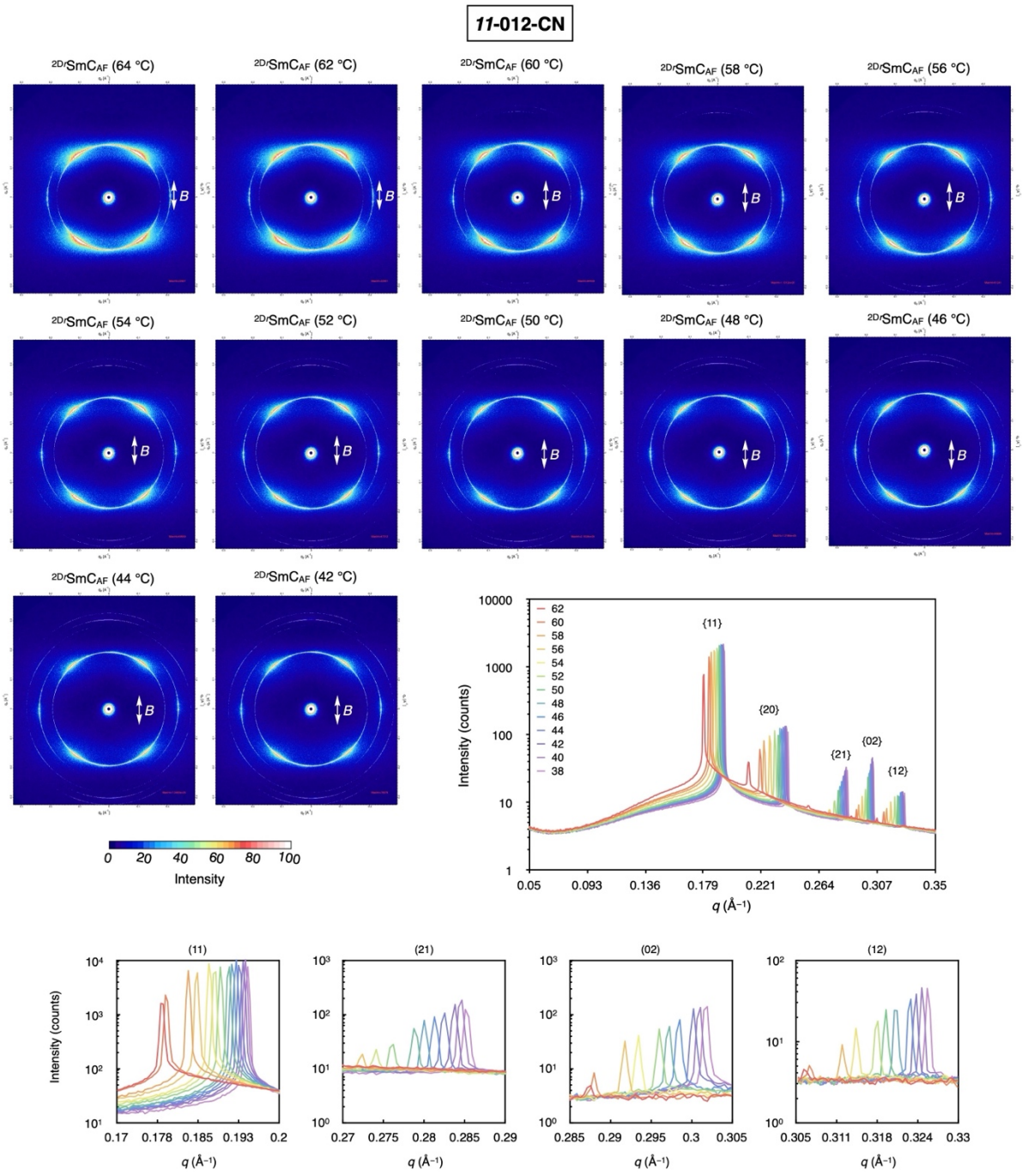

Supplementary Fig. 24 | 2D, corresponding 1D X-ray diffraction patterns and analyzed data at various temperatures under the magnetic field (~1 T, **B ∥ n**) for ***11*-012-CN**.

***11*-012-CN**

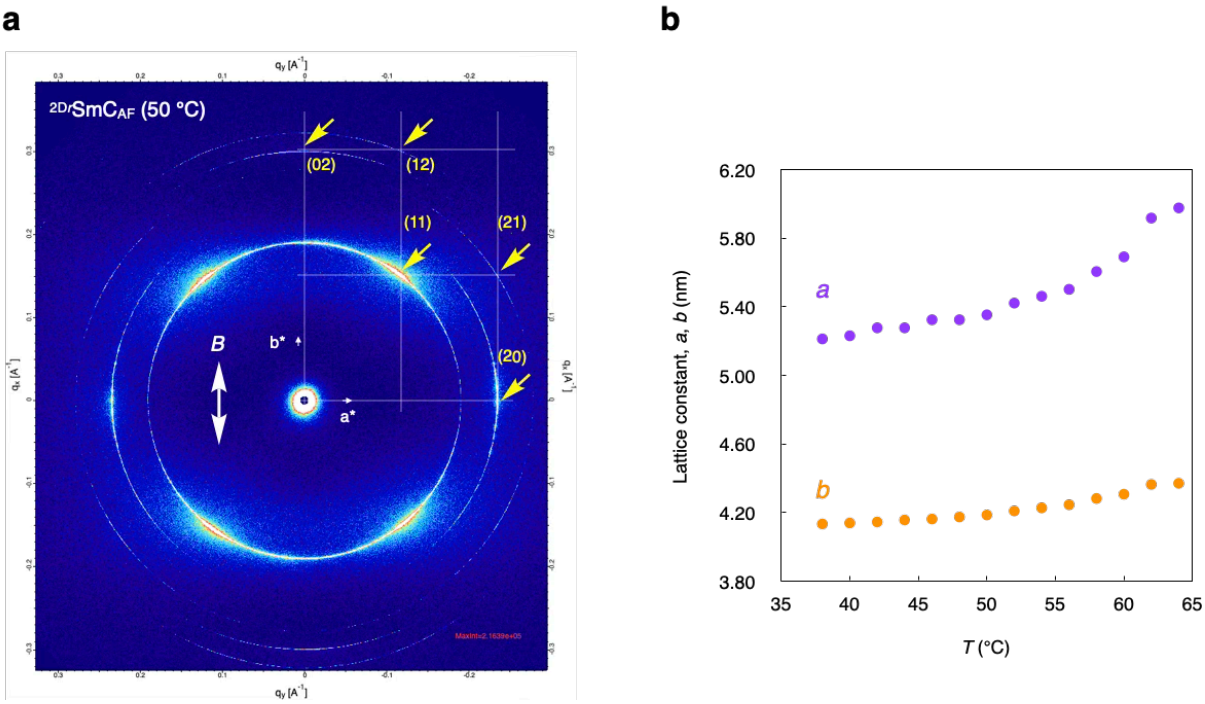

Supplementary Fig. 25 | XRD data at various temperatures under the magnetic field (~1 T, **B ∥ n**) for ***11*-012-CN**.

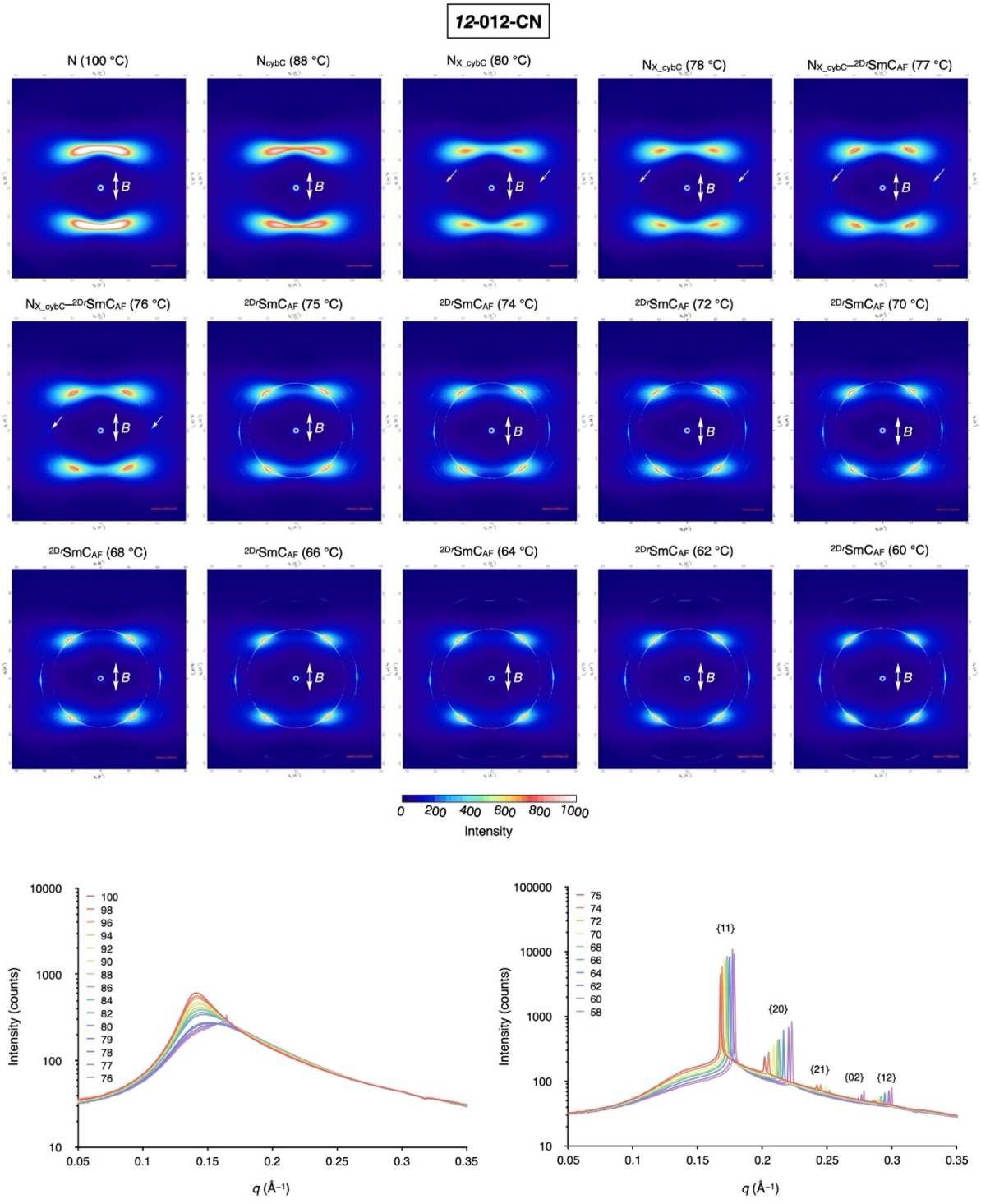

Supplementary Fig. 26 | 2D and corresponding 1D X-ray diffraction patterns at various temperatures under the magnetic field (~1 T, **B ∥ n**) for ***12*-012-CN**.

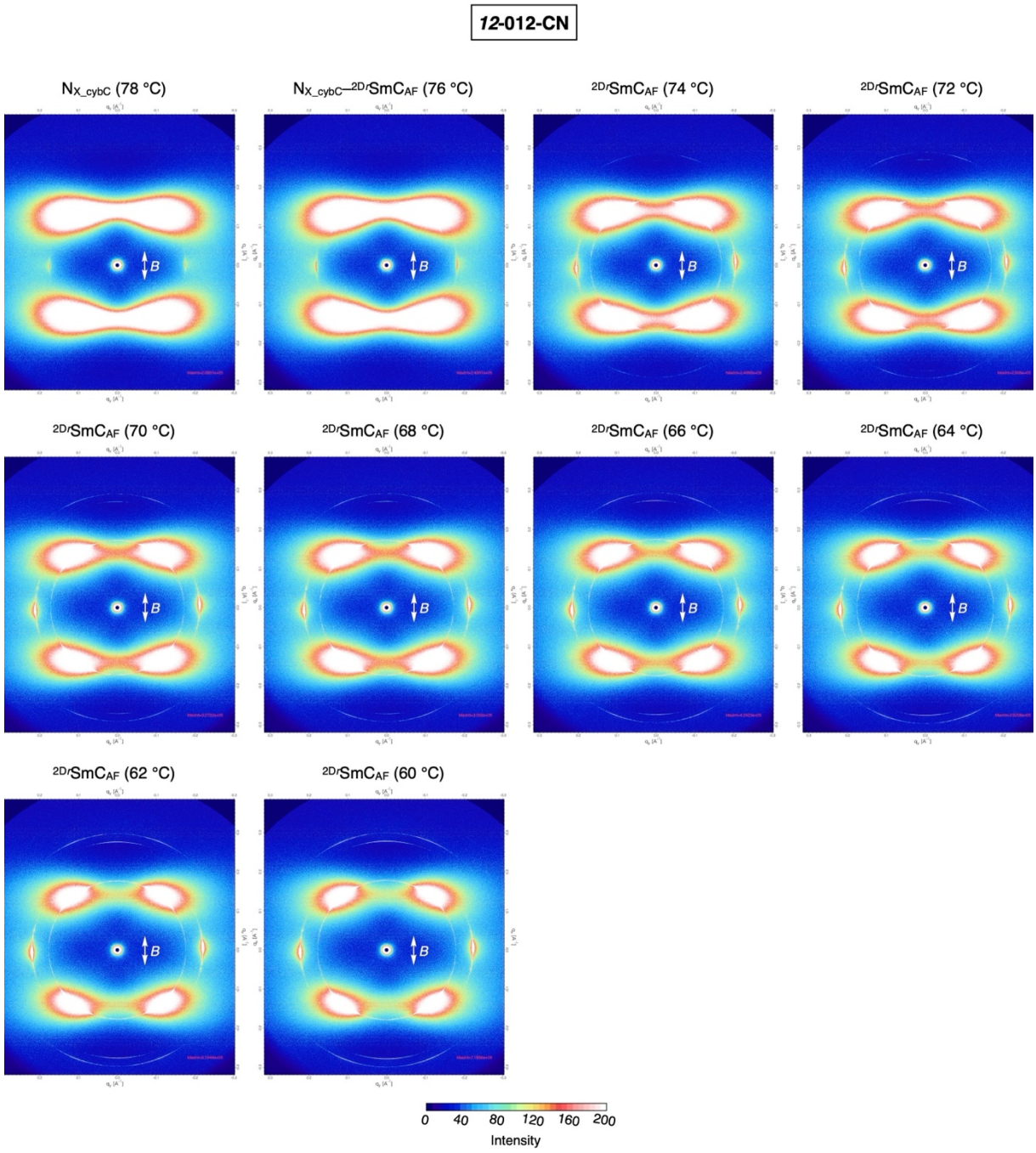

Supplementary Fig. 27 | 2D SAXS patterns at various temperatures under the magnetic field (~1 T, **B ∥ n**) for ***12*-012-CN**.

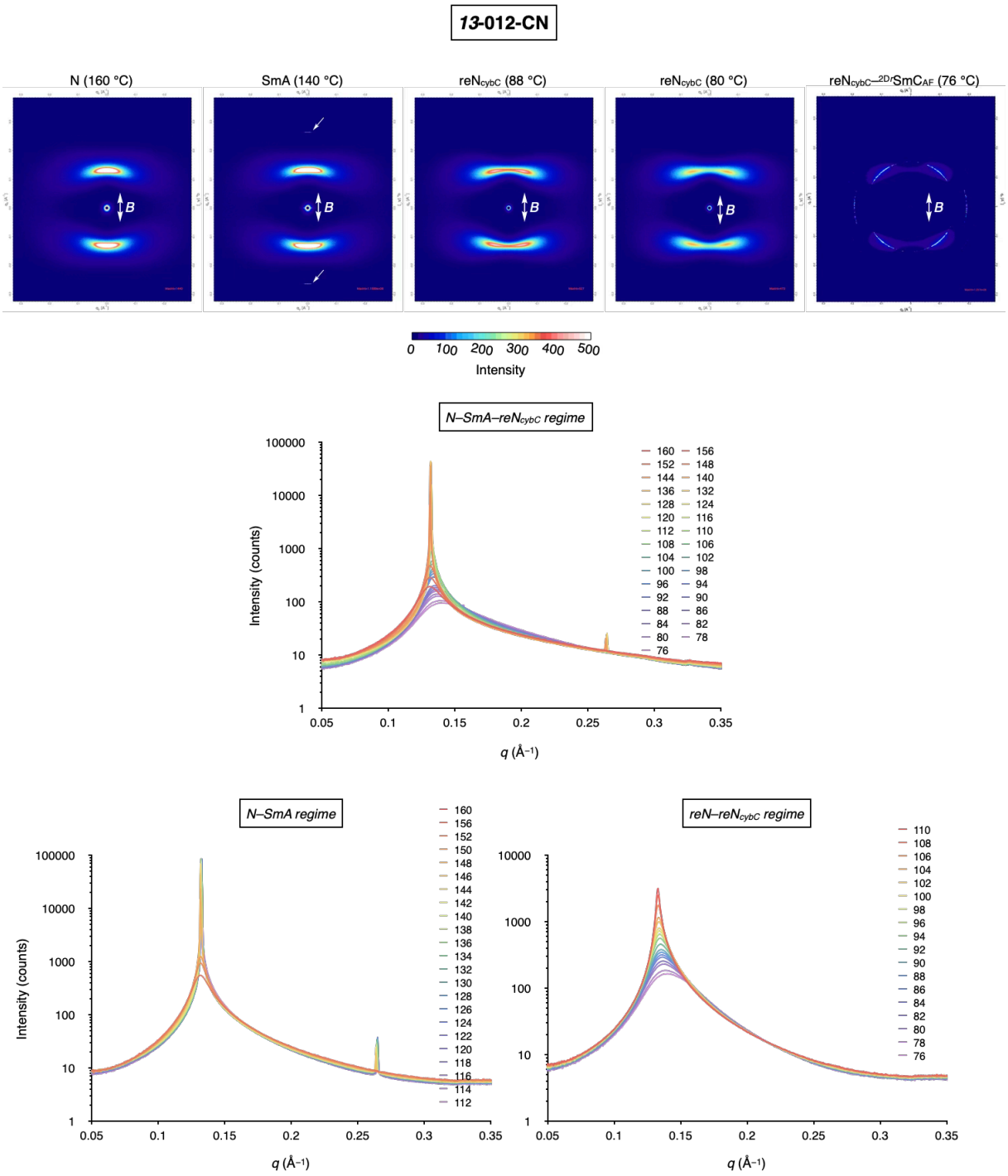

Supplementary Fig. 28 | 2D and corresponding 1D X-ray diffraction patterns at various temperatures under the magnetic field (~1 T, **B** ∥ **n**) for ***13*-012-CN**. In the SmA phase, white arrows indicate overtone peaks.

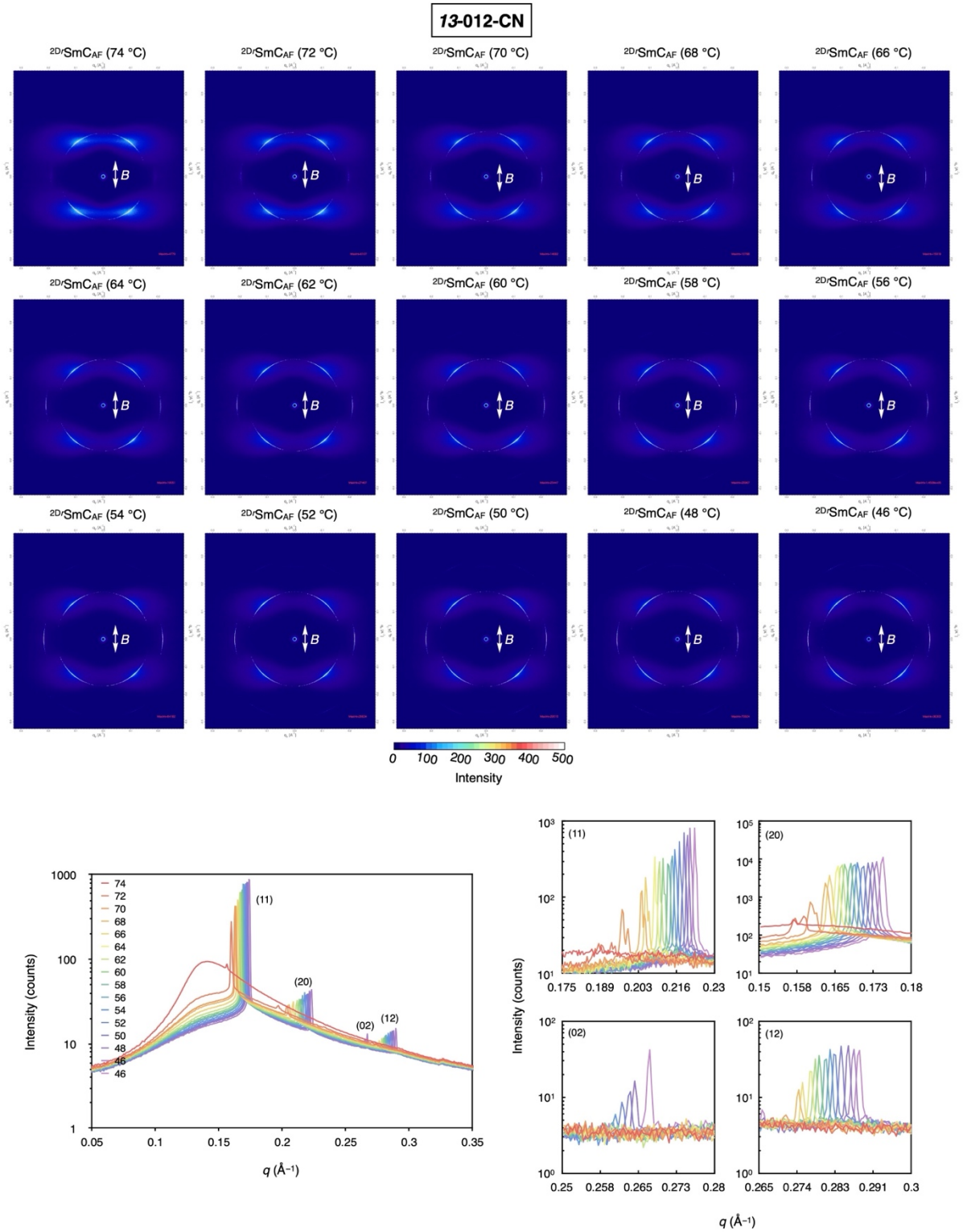

Supplementary Fig. 29 | 2D and corresponding 1D X-ray diffraction patterns at various temperatures under the magnetic field (~1 T, **B ∥ n**) for ***13*-012-CN**.

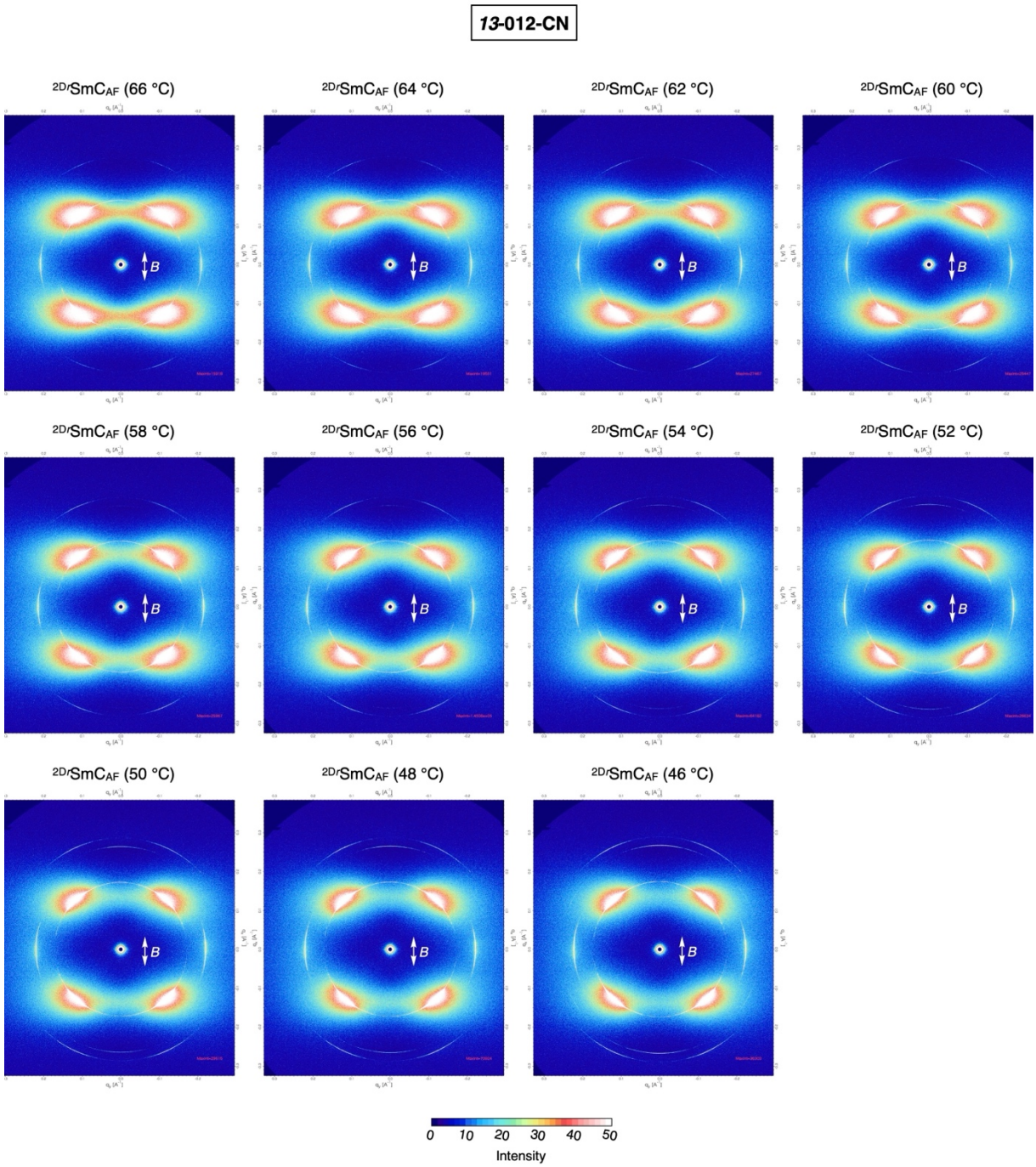

Supplementary Fig. 30 | 2D SAXS patterns at various temperatures under the magnetic field (~1 T, **B ∥ n**) for ***13*-012-CN**.

***13*-012-CN**

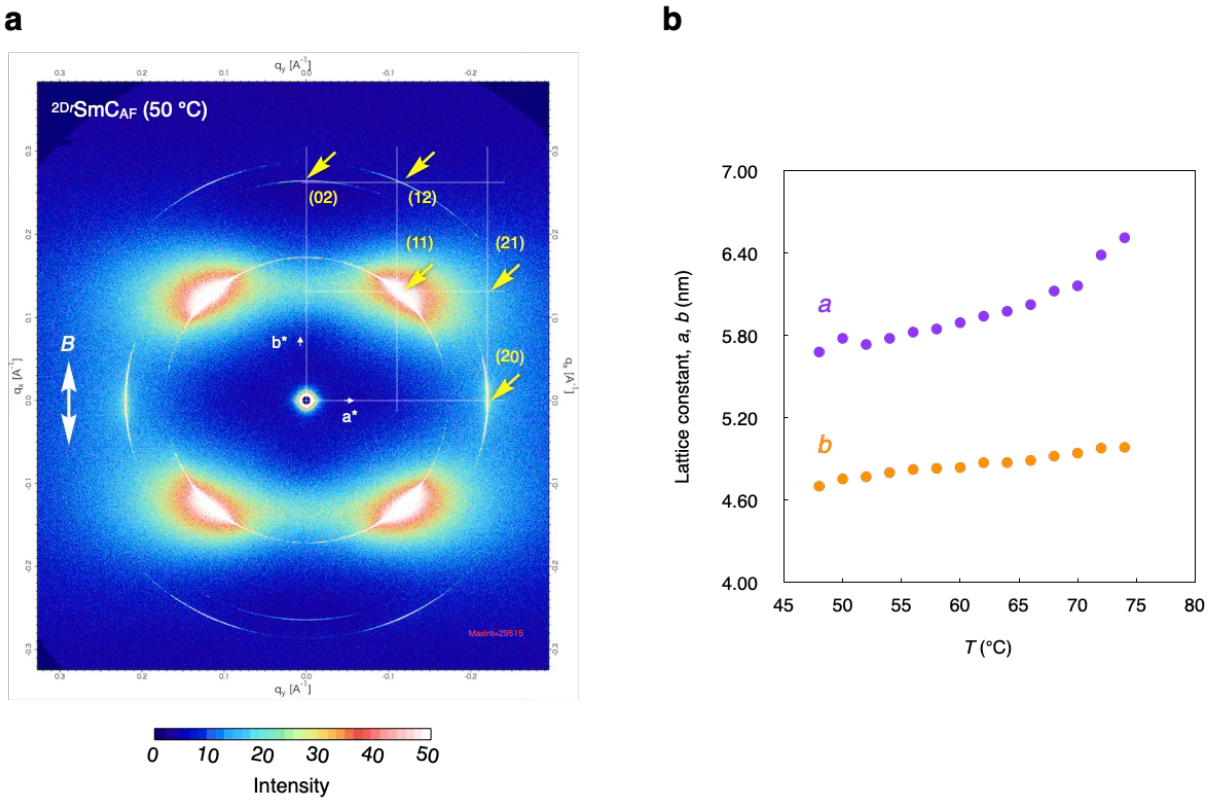

Supplementary Fig. 31 | XRD data at various temperatures under the magnetic field (~1 T, **B ‖ n**) for ***13*-012-CN**. (a) 2D SAXS patterns and (b) lattice constants *a*, *b* vs *T*.

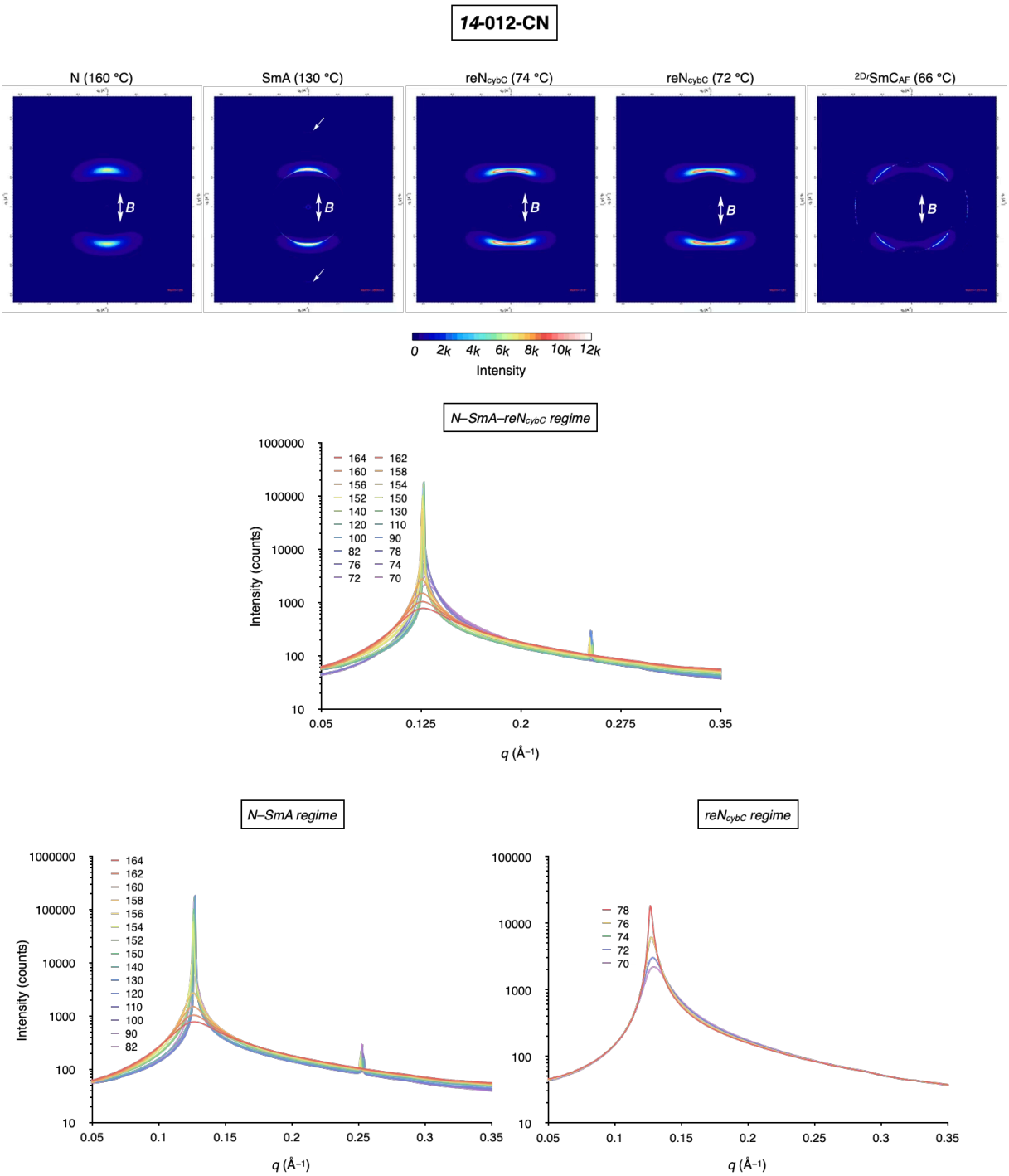

Supplementary Fig. 32 | 2D and corresponding 1D X-ray diffraction patterns at various temperatures under the magnetic field (~1 T, **B** ∥ **n**) for ***14*-012-CN**. In the SmA phase, white arrows indicate overtone peaks.

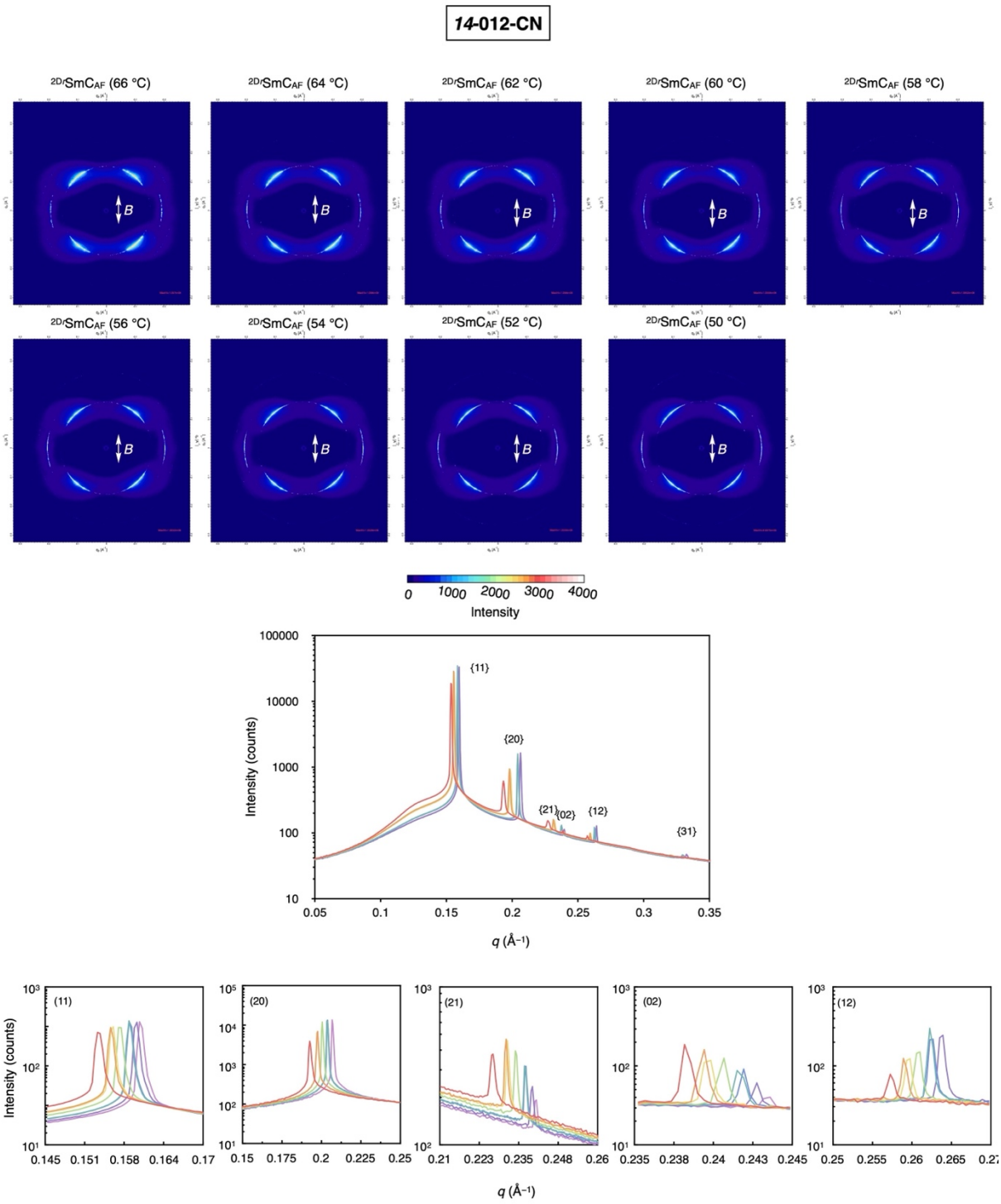

Supplementary Fig. 33 | 2D and corresponding 1D X-ray diffraction patterns at various temperatures under the magnetic field (~1 T, **B ‖ n**) for ***14*-012-CN**.

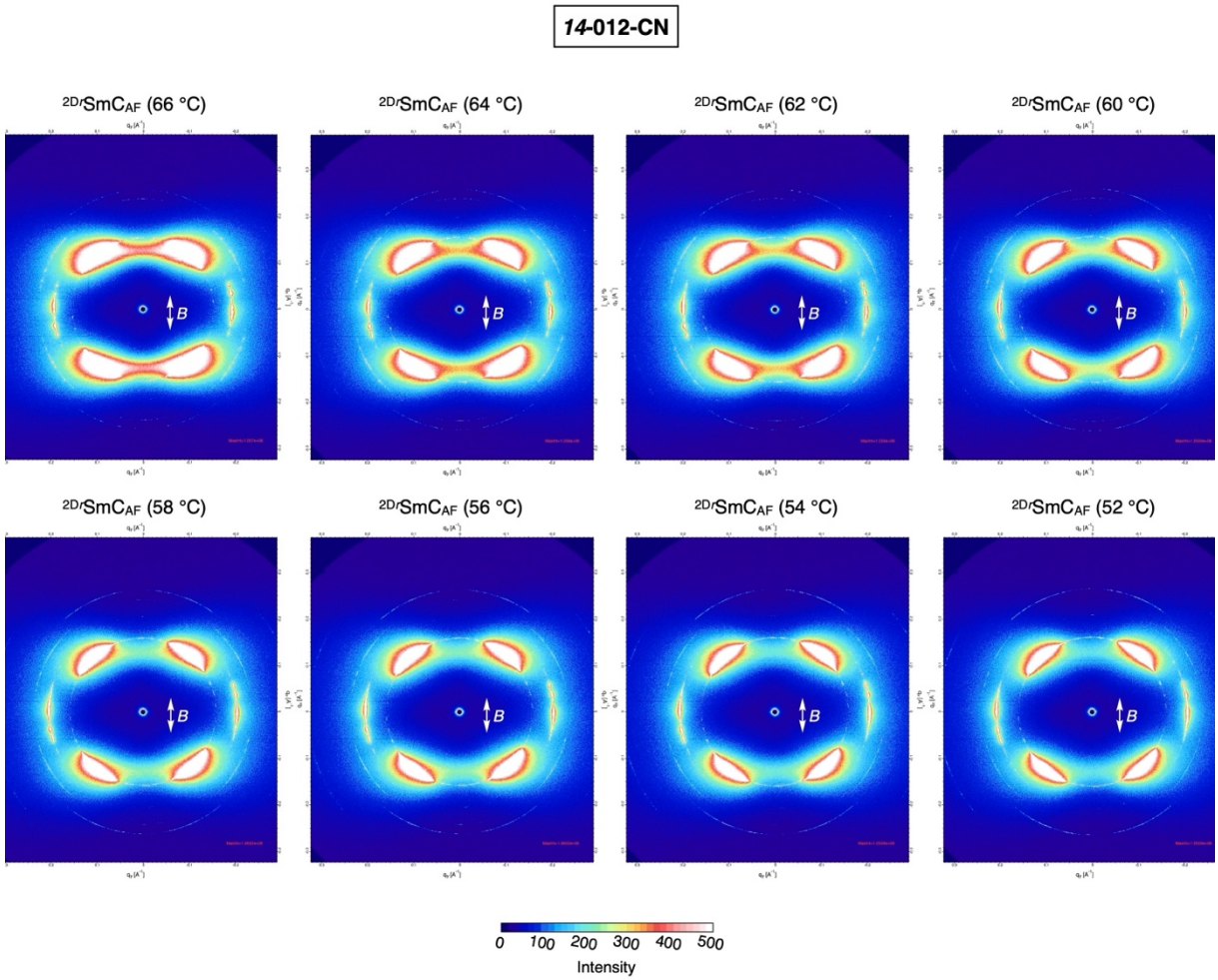

Supplementary Fig. 34 | XRD data at various temperatures under the magnetic field (~1 T, **B ‖ n**) for ***14*-012-CN**.

14-012-CN

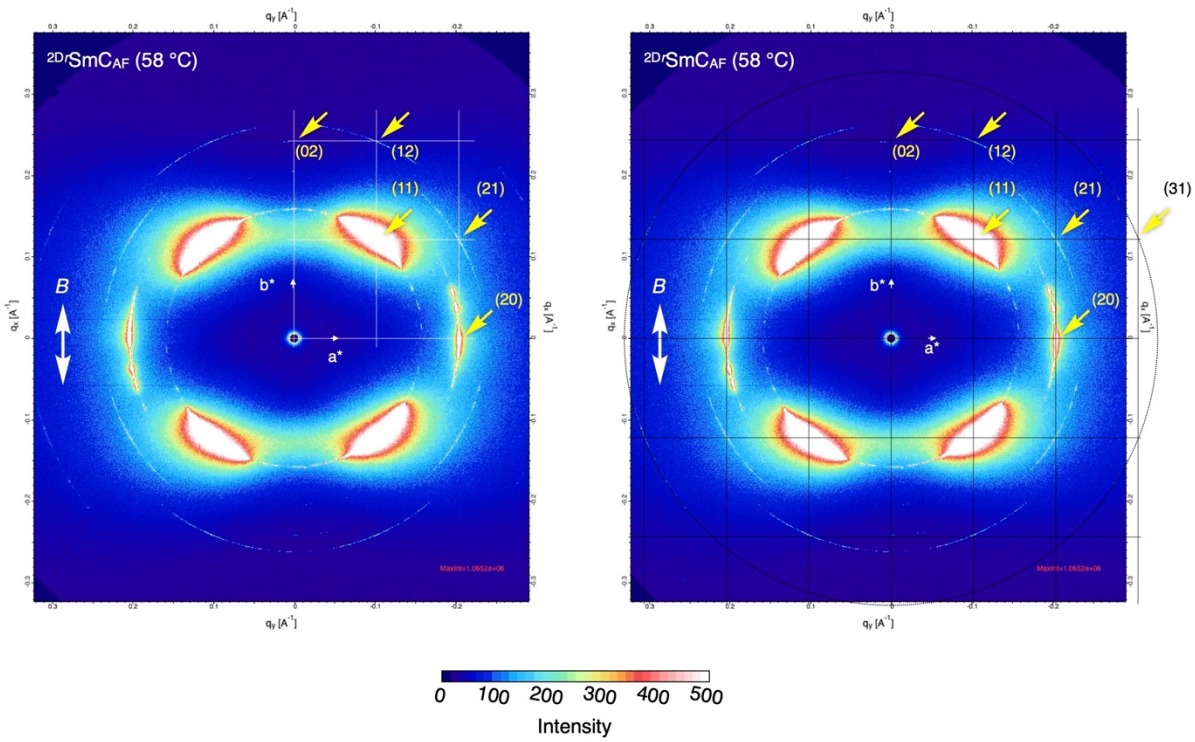

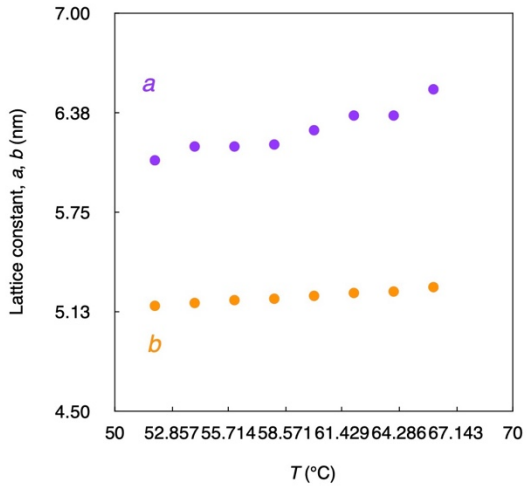

Supplementary Fig. 35 | (Upper) 2D SAXS patterns under the magnetic field (~1 T, **B ∥ n**) for ***14*-012-CN**. (Bottom) lattice constants *a*, *b* vs. *T*.

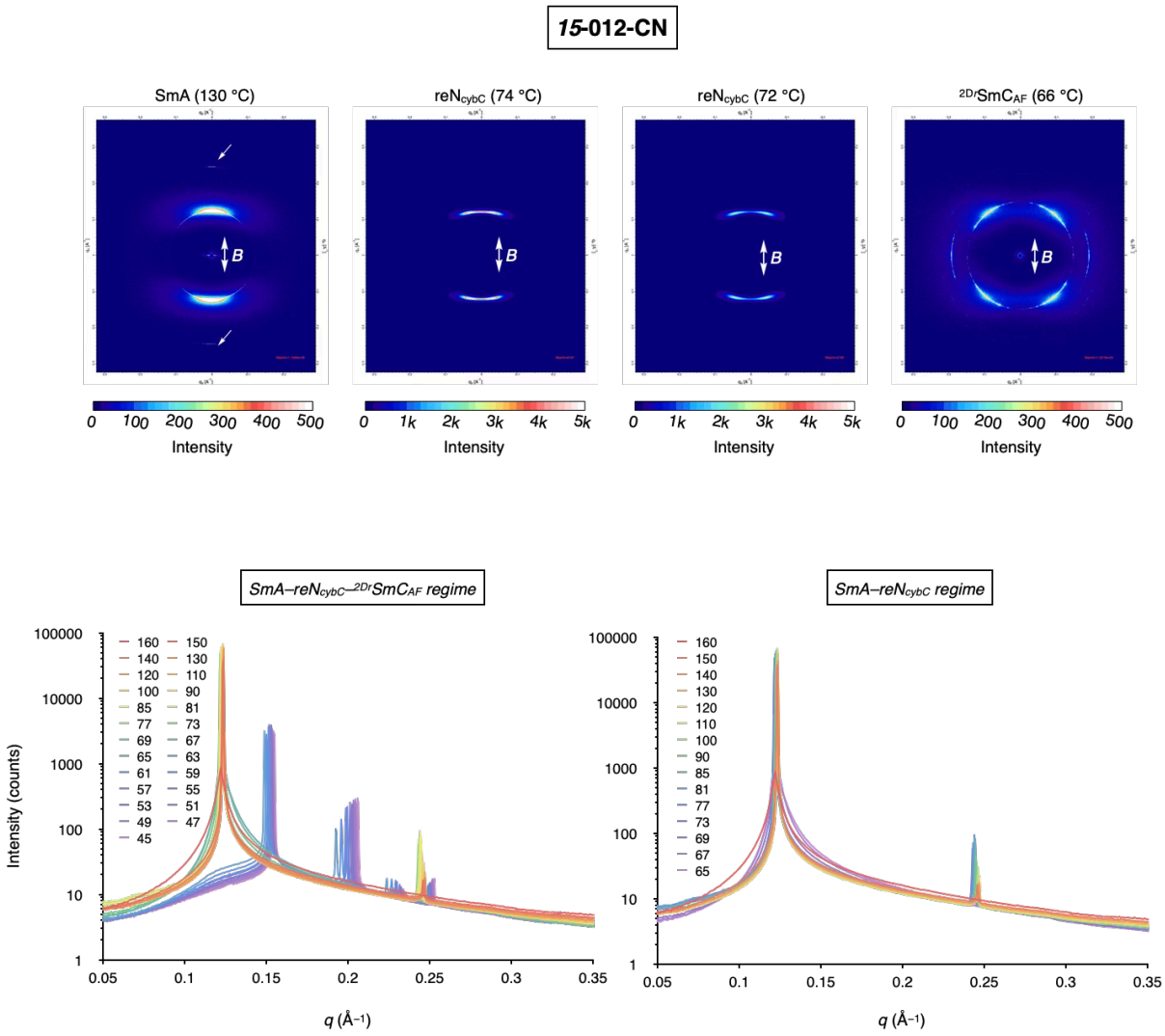

Supplementary Fig. 36 | 2D and corresponding 1D X-ray diffraction patterns at various temperatures under the magnetic field (~1 T, **B** ∥ **n**) for ***15*-012-CN**. In the SmA phase, white arrows indicate overtone peaks.

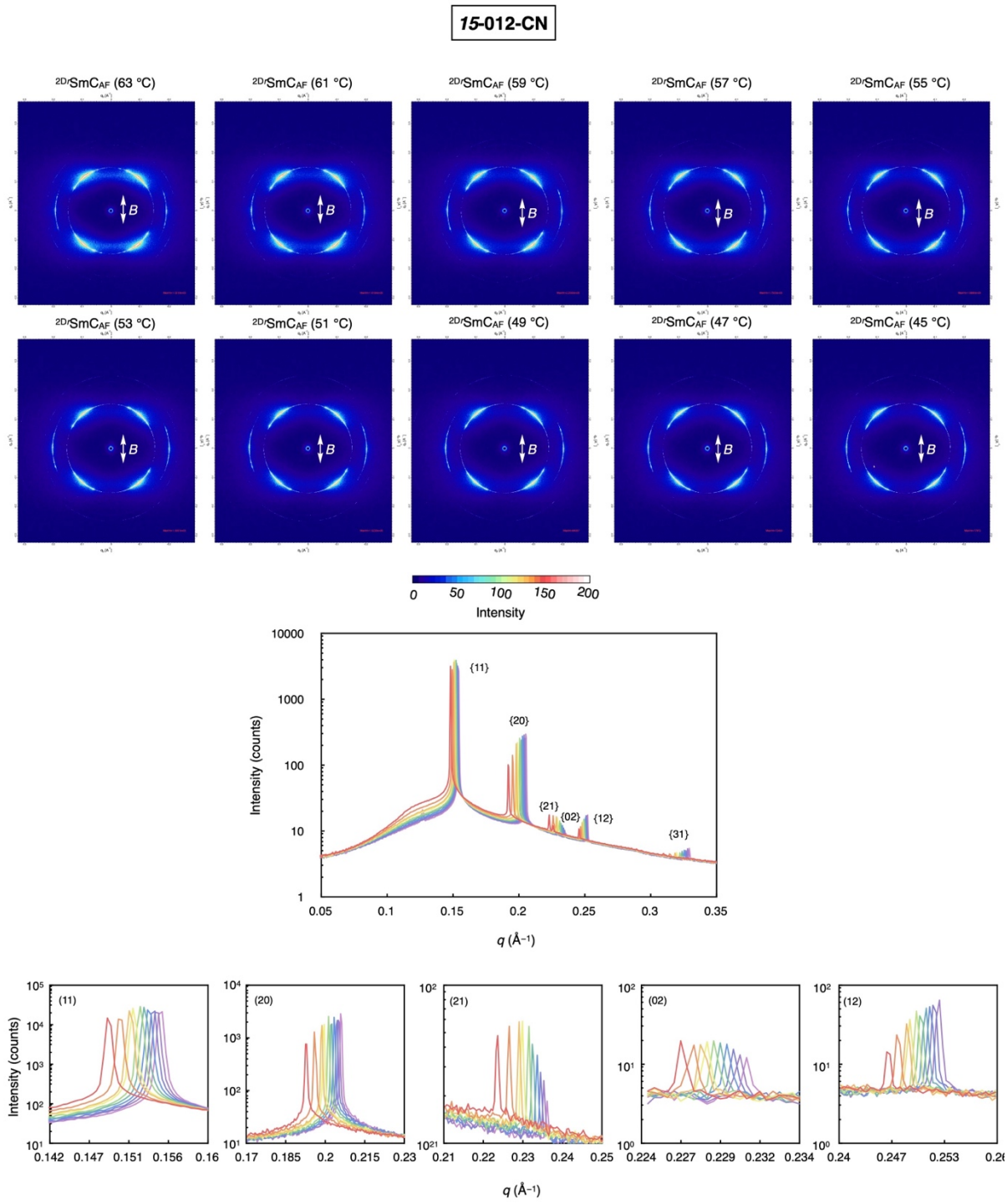

Supplementary Fig. 37 | 2D and corresponding 1D X-ray diffraction patterns at various temperatures under the magnetic field (~1 T, **B ‖ n**) for ***15*-012-CN**.

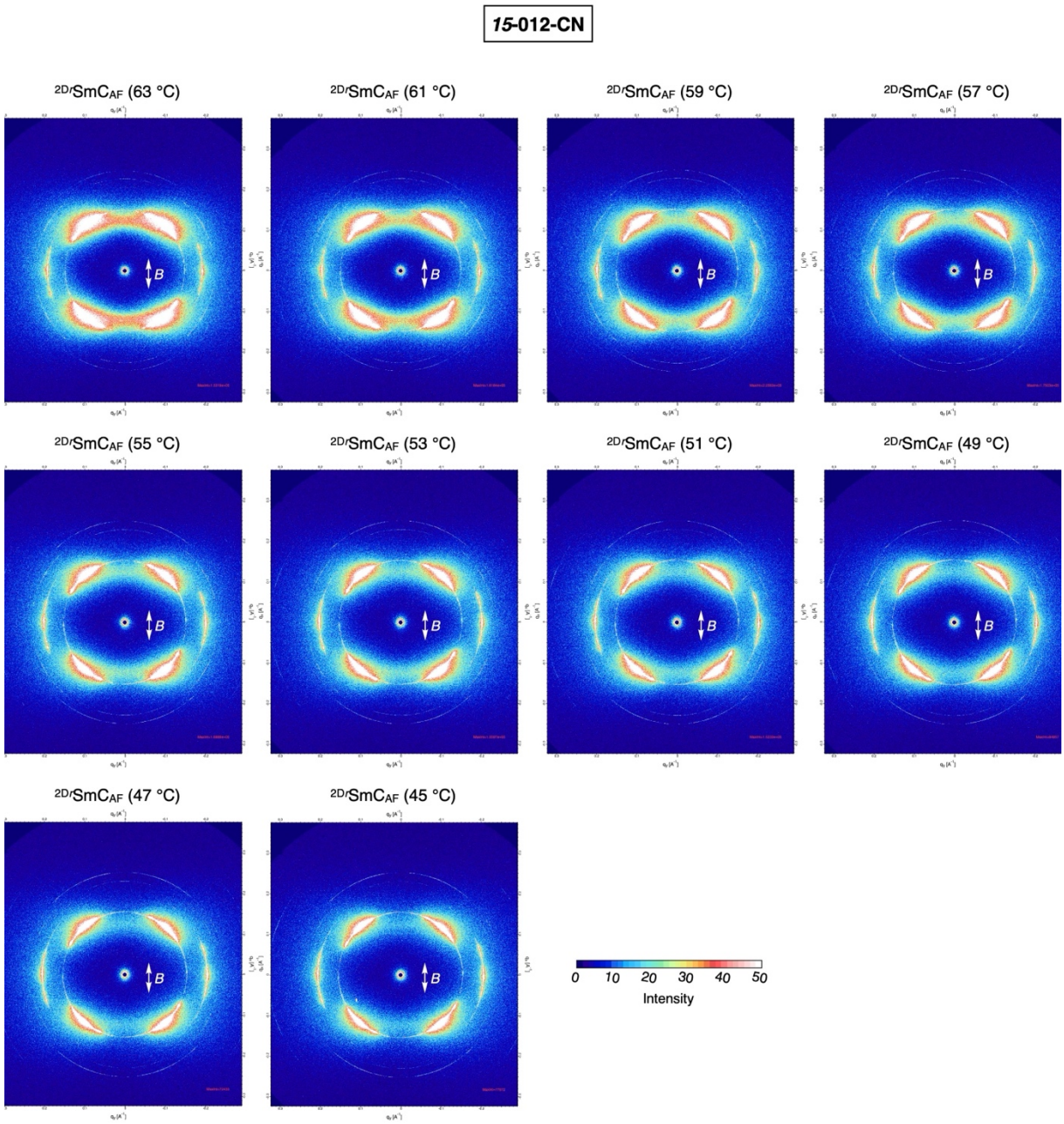

Supplementary Fig. 38 | 2D SAXS patterns at various temperatures under the magnetic field (~1 T, **B ‖ n**) for ***15*-012-CN**.

15-012-CN

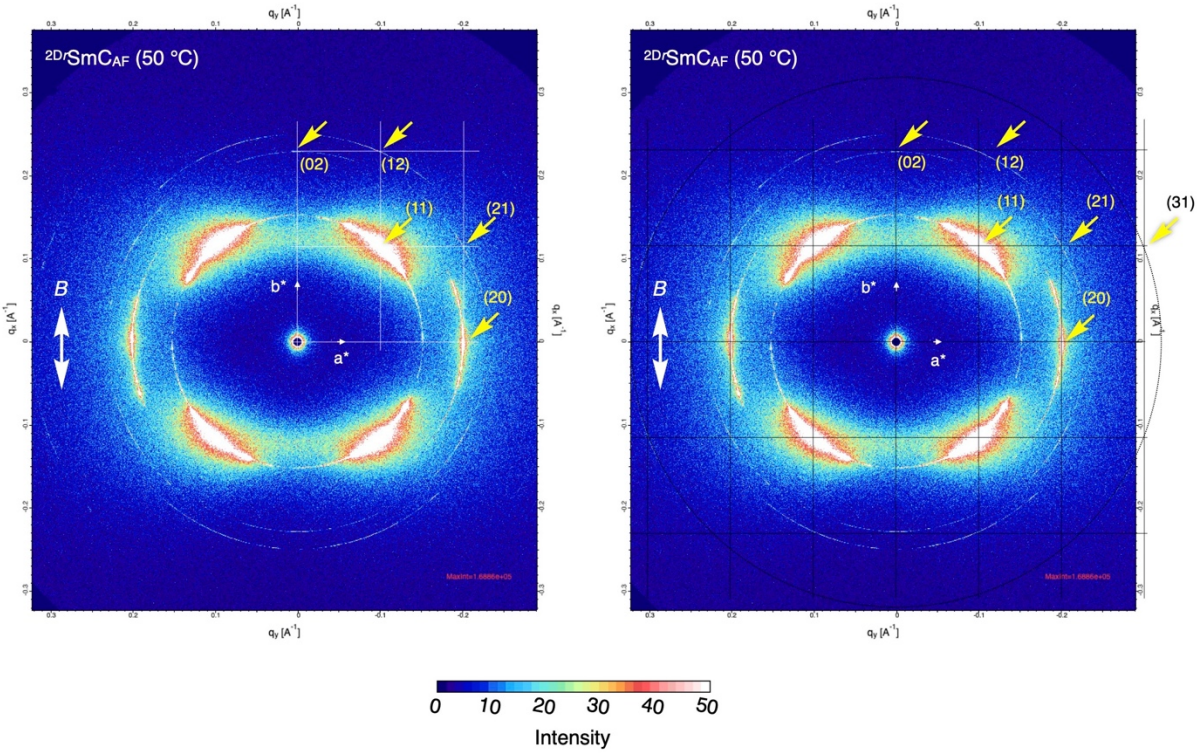

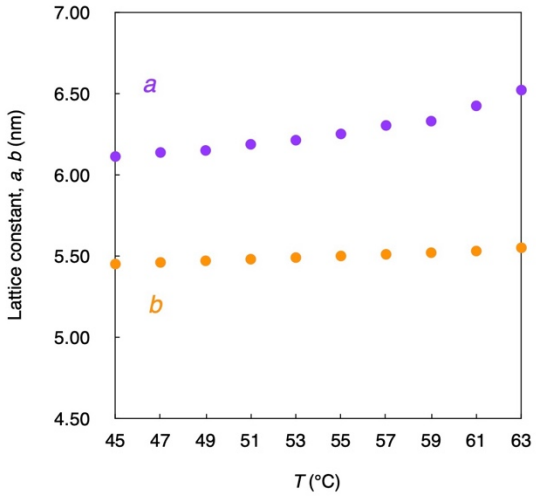

Supplementary Fig. 39 | (Upper) 2D SAXS patterns at various temperatures under the magnetic field (~1 T, **B ∥ n**) for ***15*-012-CN**. (Bottom) lattice constants *a*, *b* vs. *T*.

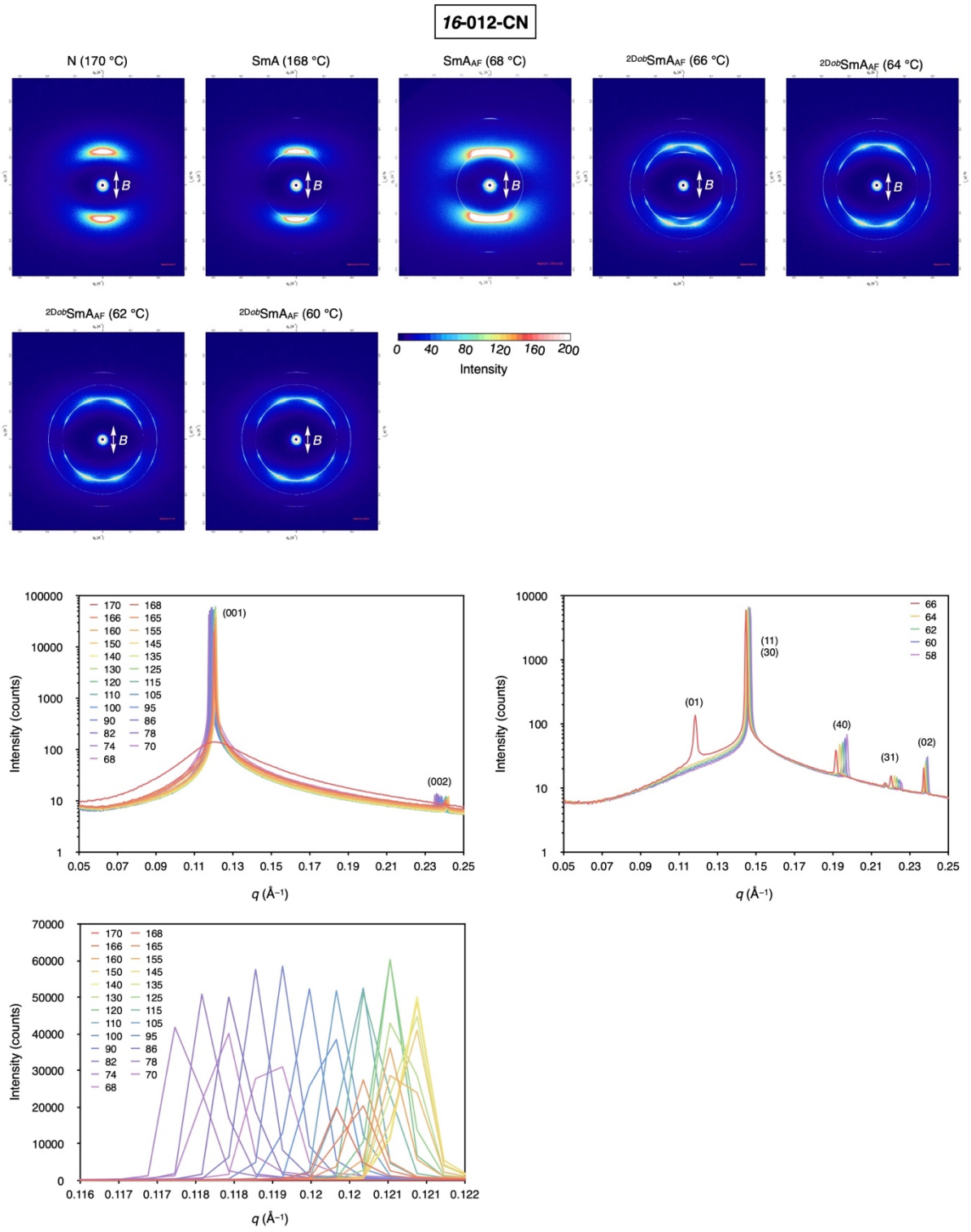

Supplementary Fig. 40 | 2D and corresponding 1D X-ray diffraction patterns at various temperatures under the magnetic field (~1 T, **B ‖ n**) for ***16*-012-CN**.

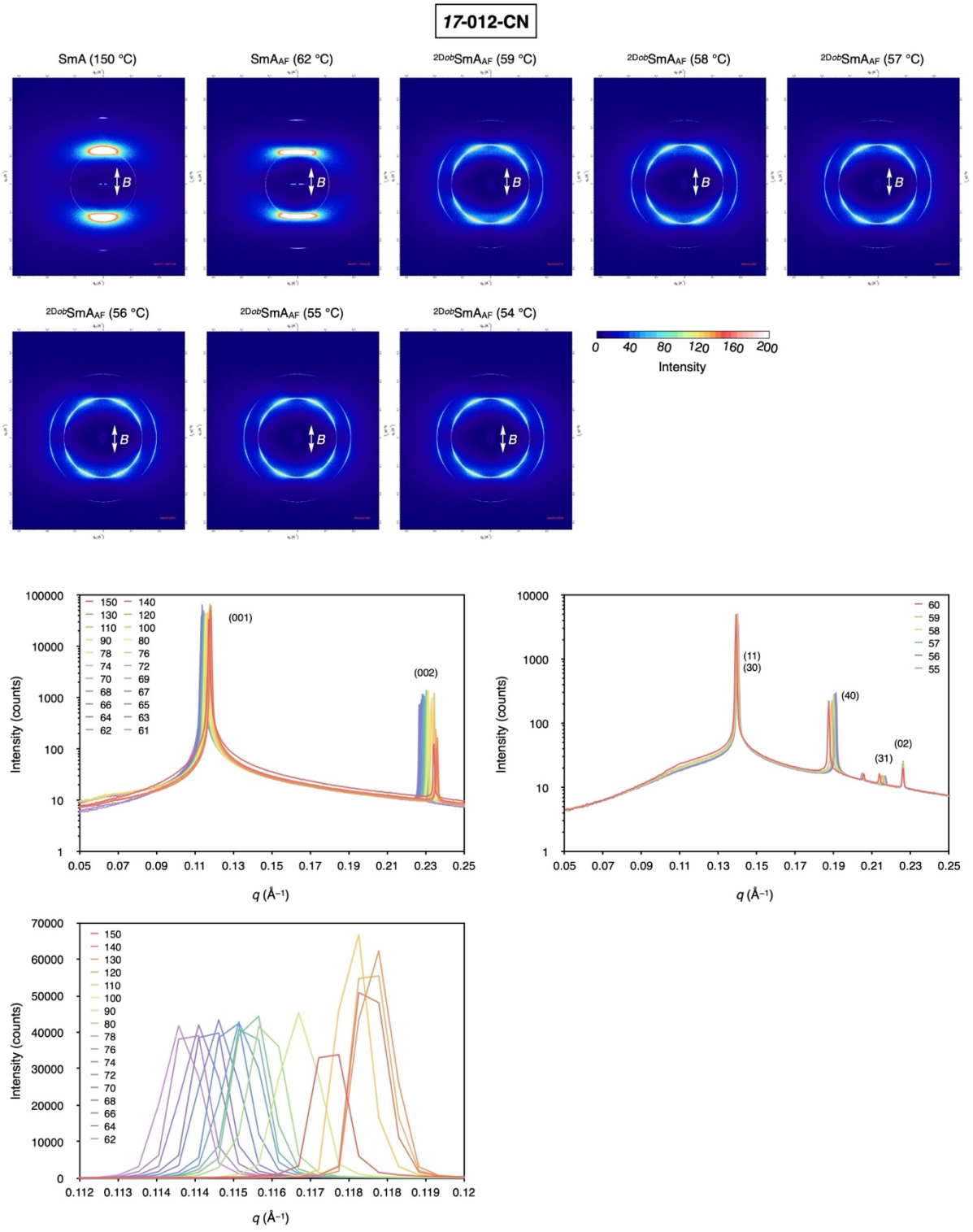

Supplementary Fig. 41 | 2D and corresponding 1D X-ray diffraction patterns at various temperatures under the magnetic field (~1 T, **B ‖ n**) for ***17*-012-CN**.

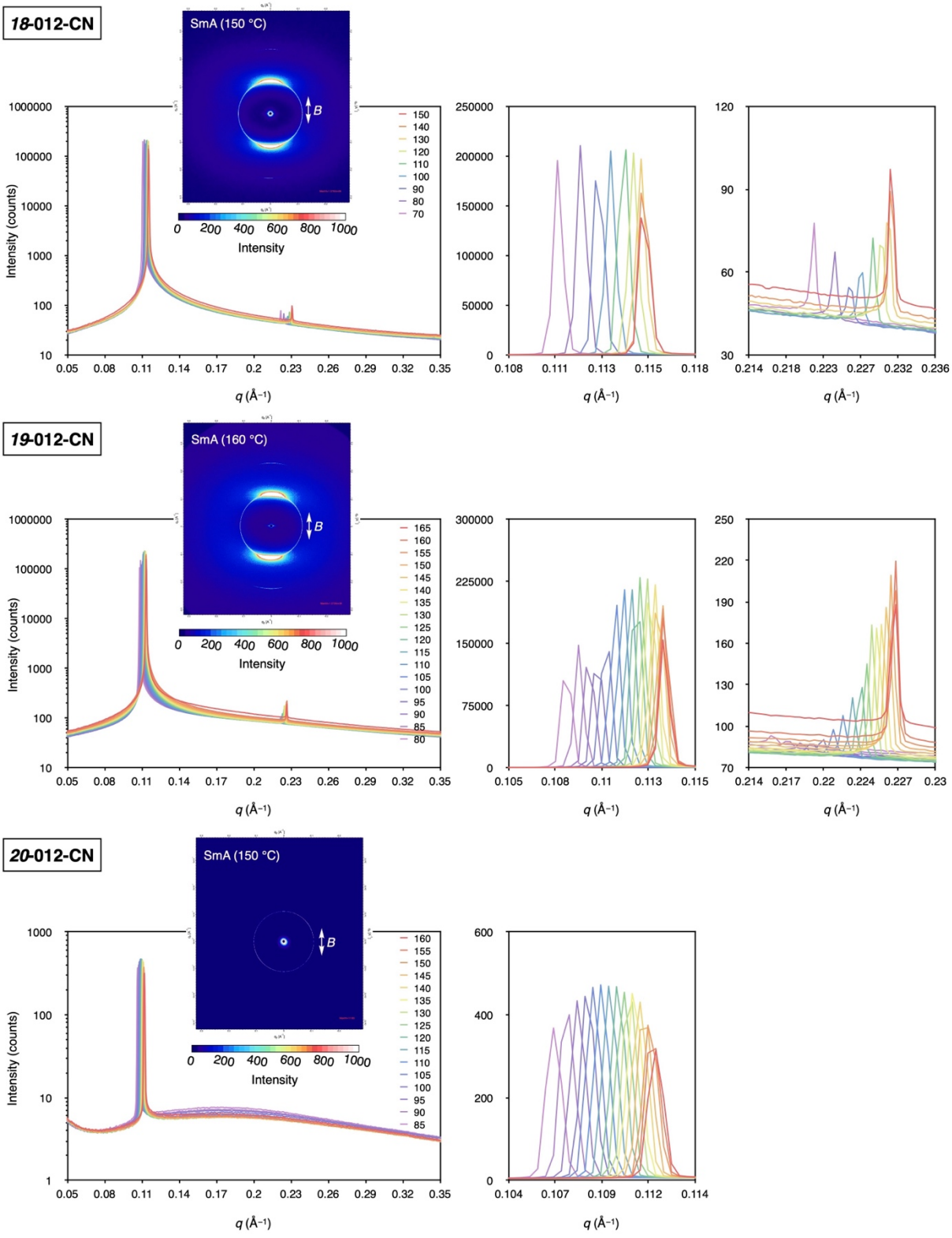

Supplementary Fig. 42 | XRD data at various temperatures under the magnetic field (~1 T, **B ∥ n**) for ***18*-012-CN** (upper), ***19*-012-CN** (middle) and ***20*-012-CN** (bottom). For ***20*-012-CN**, sufficient alignment could not be achieved under the magnetic field.

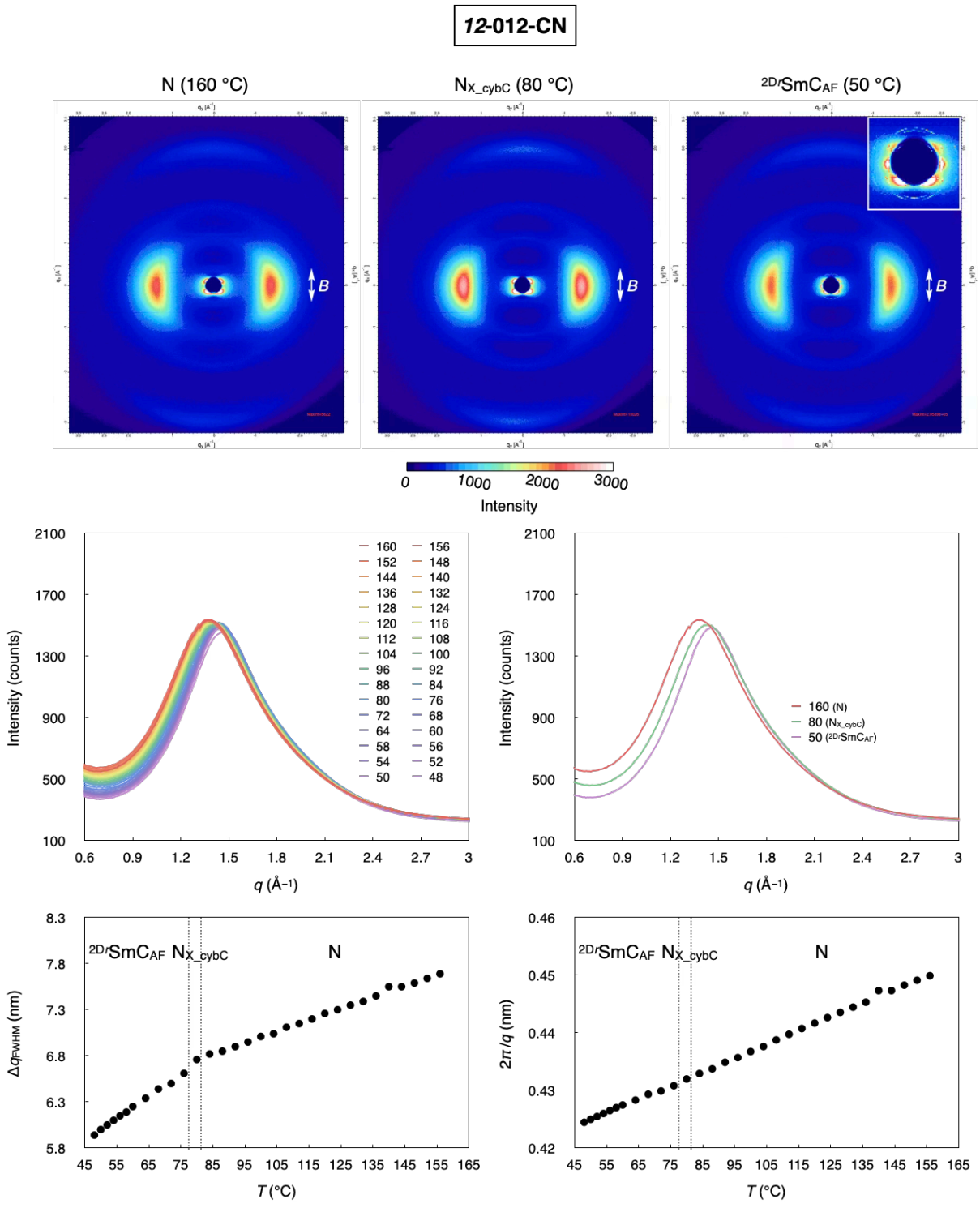

Supplementary Fig. 43 | WAXD data at various temperatures under the magnetic field (~1 T, **B ∥ n**) for ***12*-012-CN**.

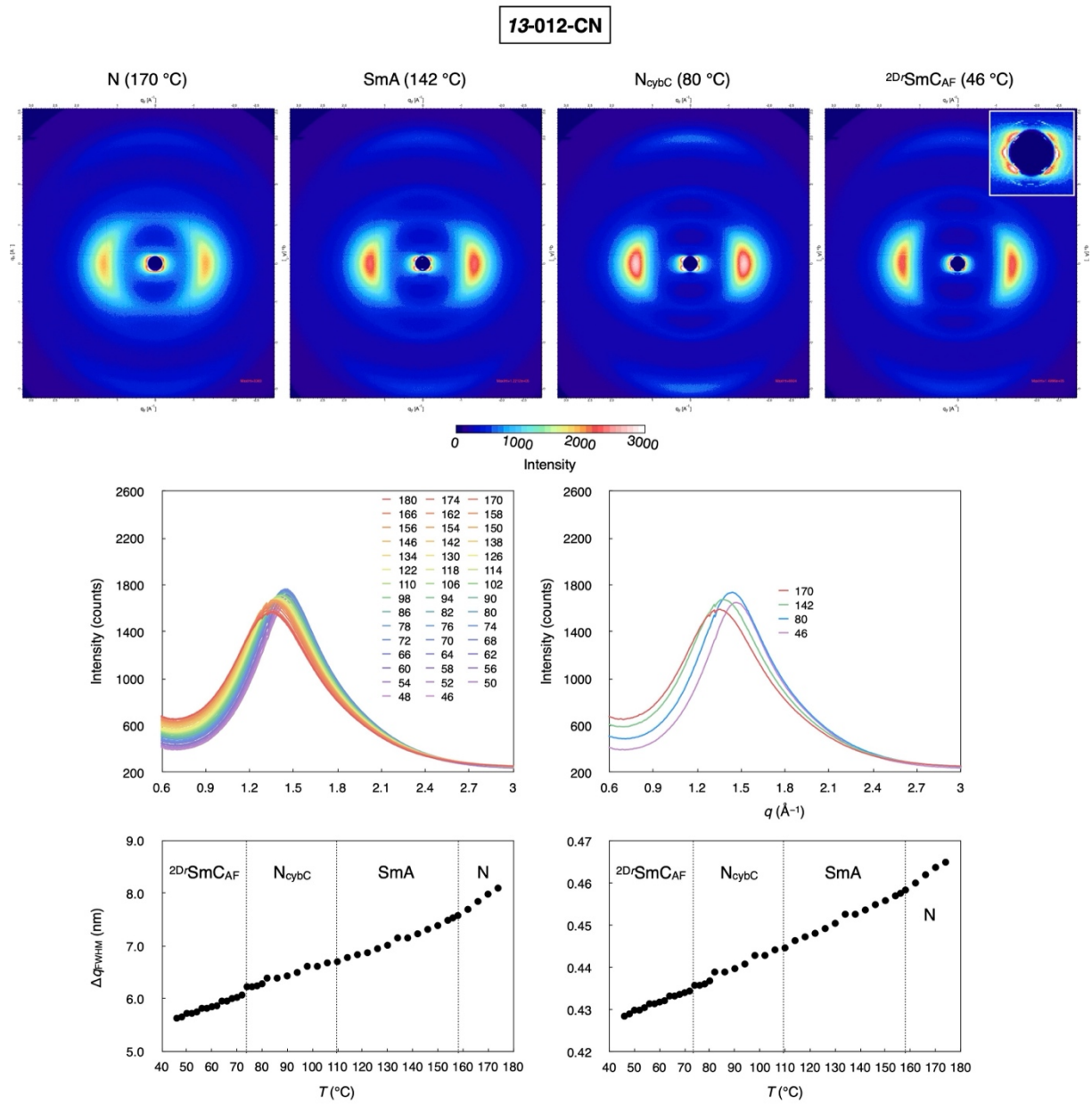

Supplementary Fig. 44 | WAXD data at various temperatures under the magnetic field (~1 T, **B ‖ n**) for ***13*-012-CN**.

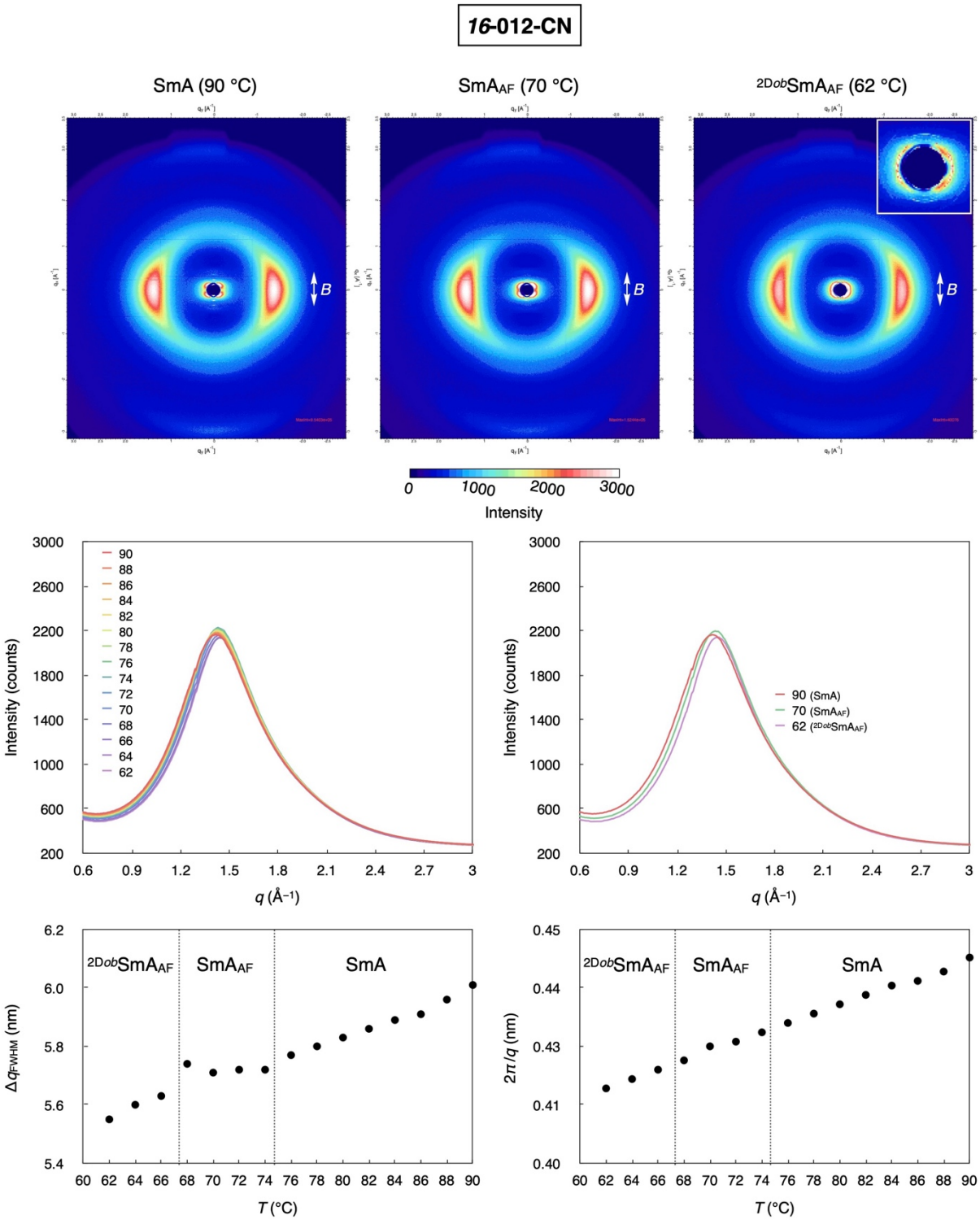

Supplementary Fig. 45 | WAXD data at various temperatures under the magnetic field (~1 T, **B ‖ n**) for ***16*-012-CN**.

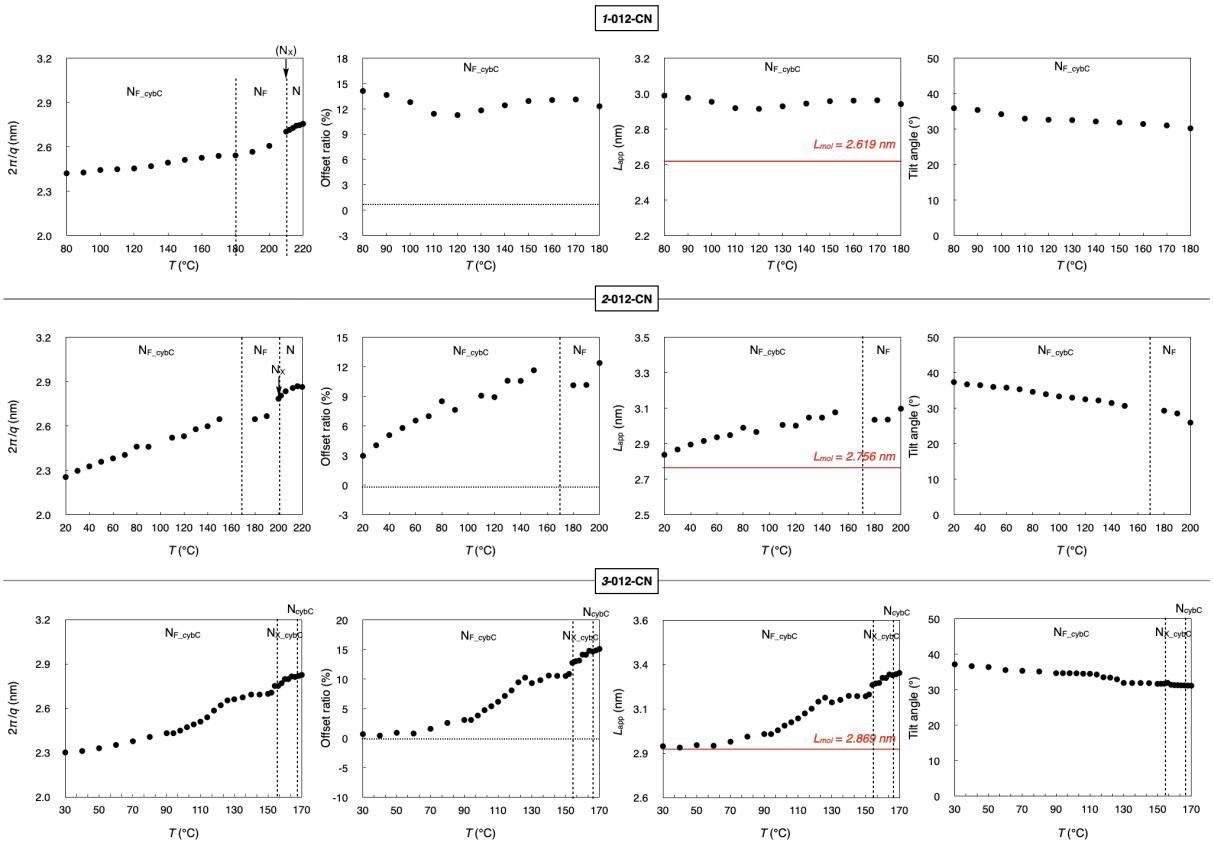

Supplementary Fig. 46 | XRD data set for ***n*-012-CN** (n = 1–3).

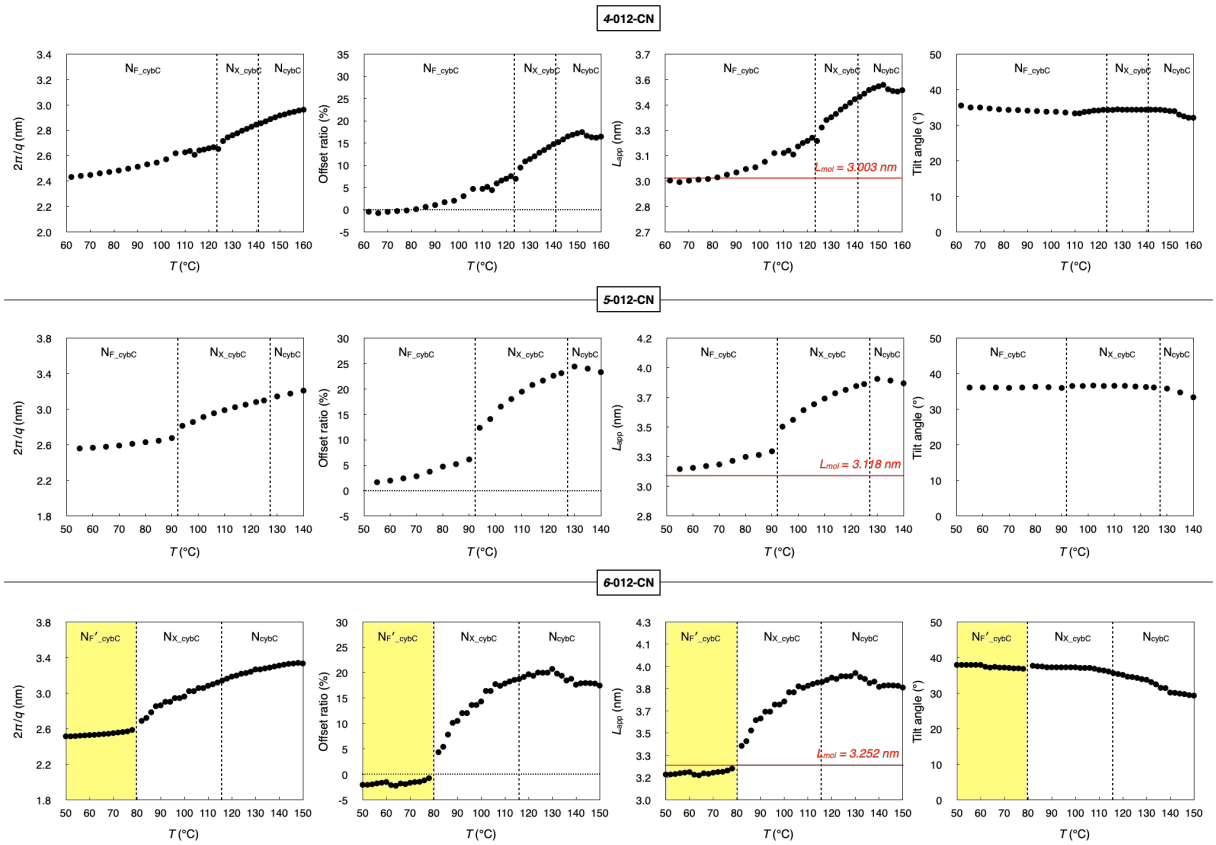

Supplementary Fig. 47 | XRD data set for ***4*-012-CN** (top), ***5*-012-CN** (middle) and ***6*-012-CN** (bottom).

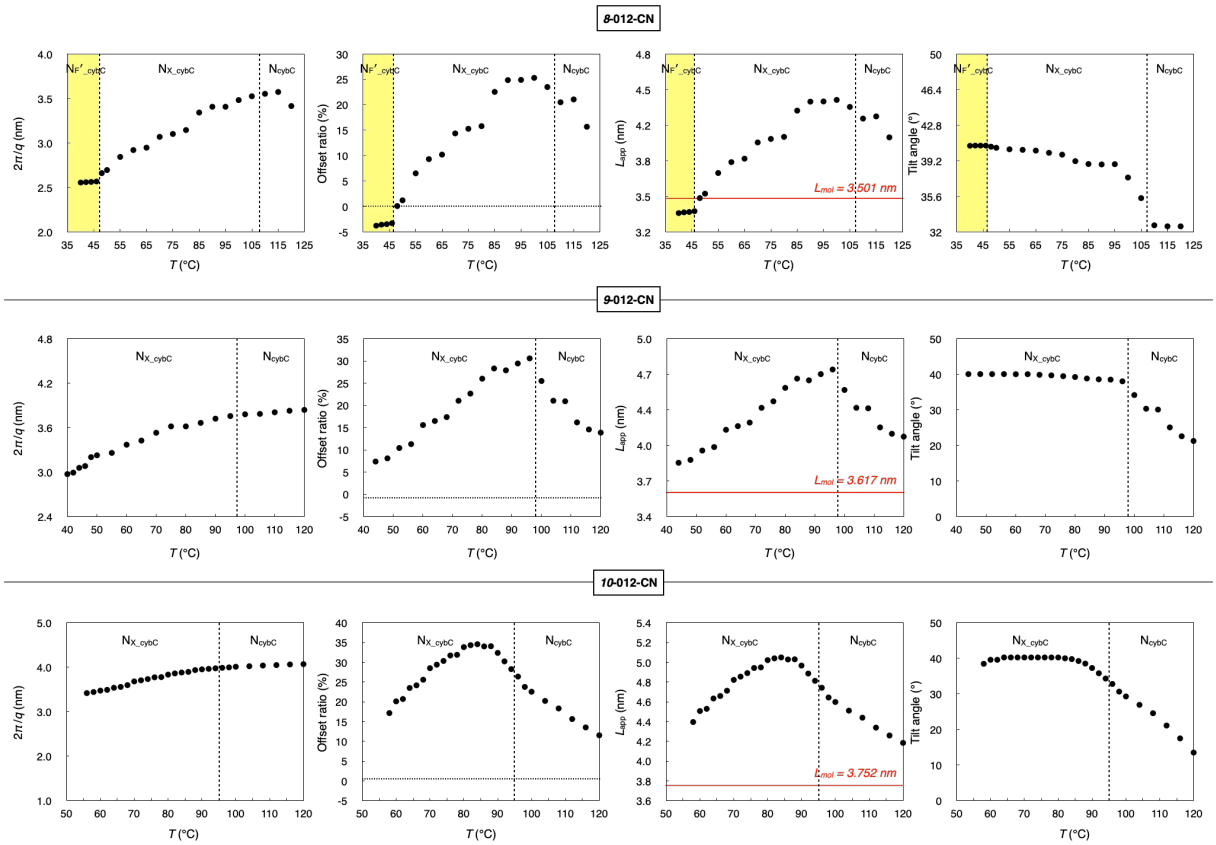

Supplementary Fig. 48 | XRD data set for ***8*-012-CN** (top), ***9*-012-CN** (middle) and ***10*-012-CN** (bottom).

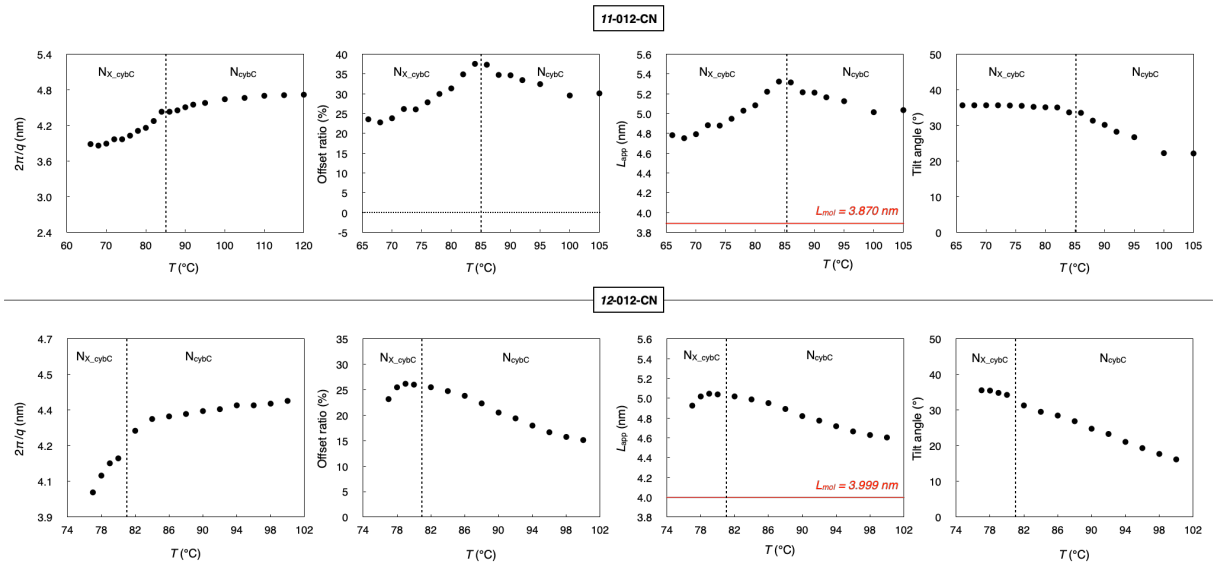

Supplementary Fig. 49 | XRD data set for ***11*-012-CN** (top) and ***12*-012-CN** (bottom).

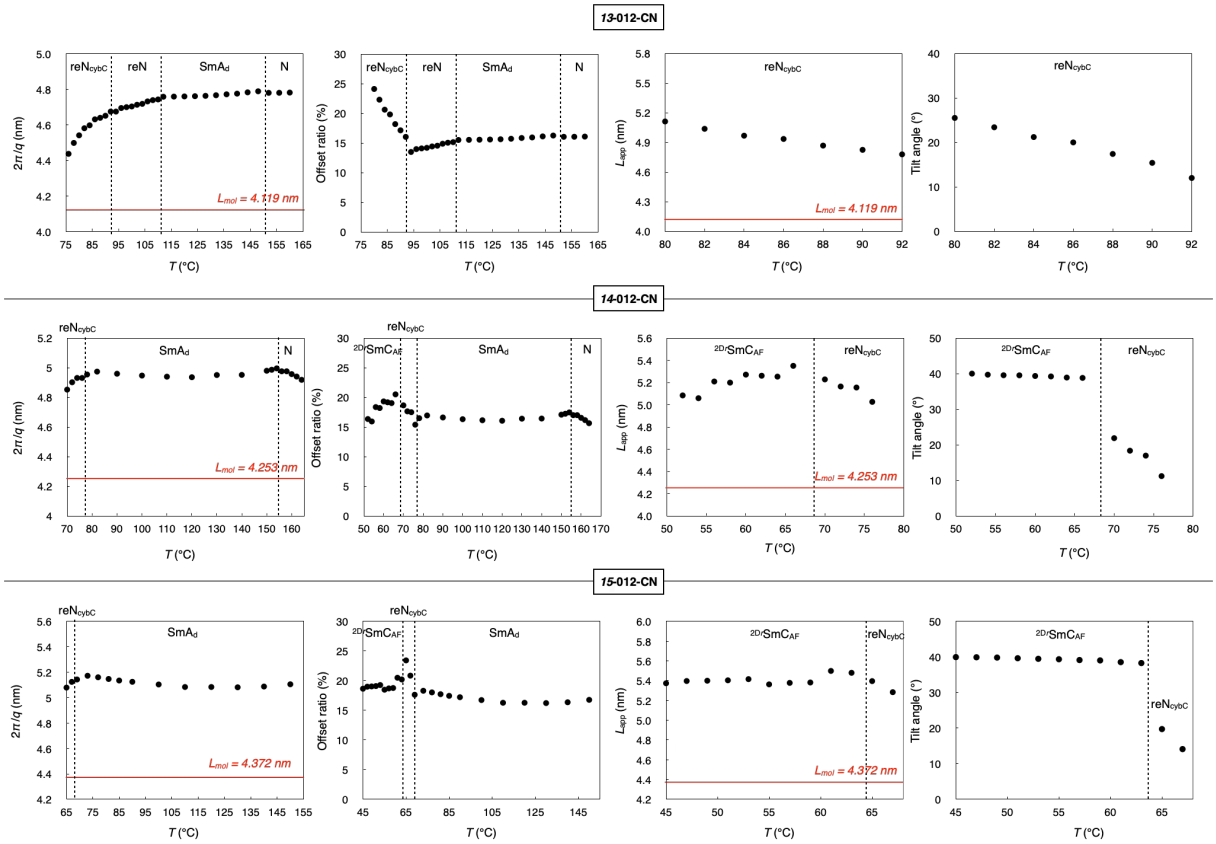

Supplementary Fig. 50 | XRD data set for ***13*-012-CN** (top), ***14*-012-CN** (middle) and ***15*-012-CN** (bottom).

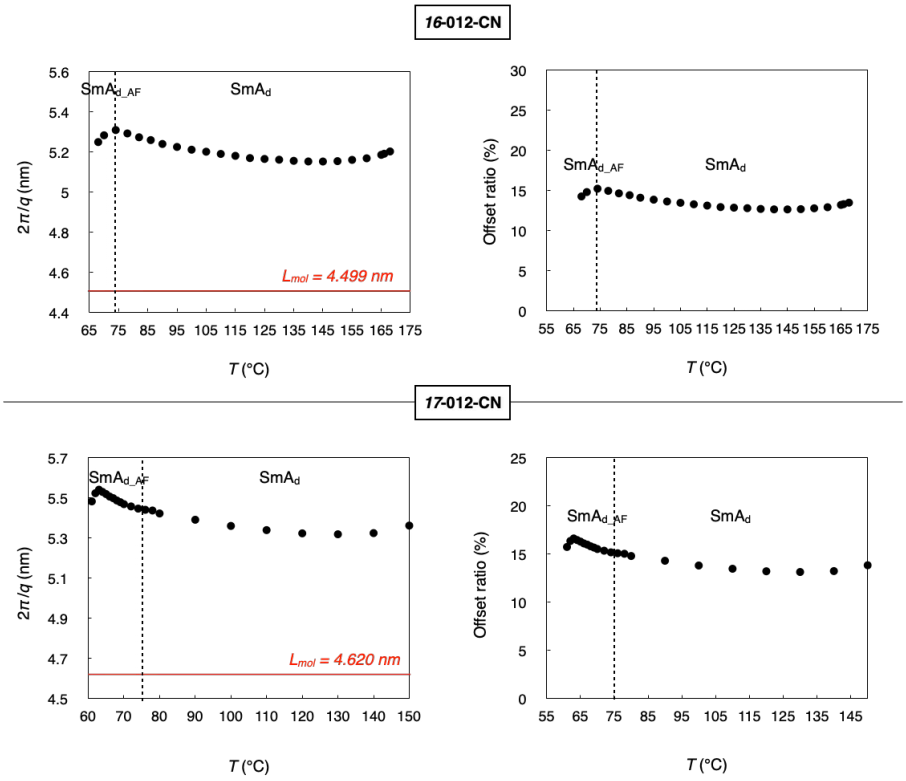

Supplementary Fig. 51 | XRD data set for ***16*-012-CN** (top) and ***17*-012-CN** (bottom).

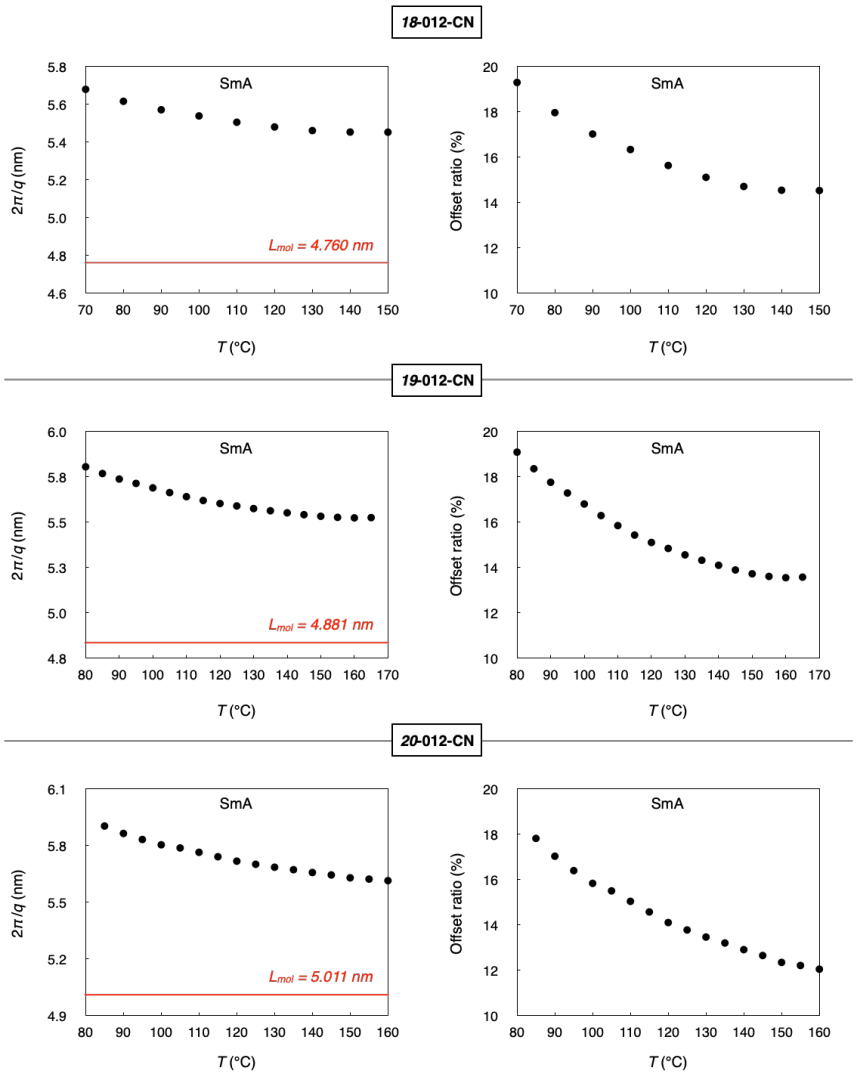

Supplementary Fig. 52 | XRD data set for ***18*-012-CN** (top), ***19*-012-CN** (middle) and ***20*-012-CN** (bottom).

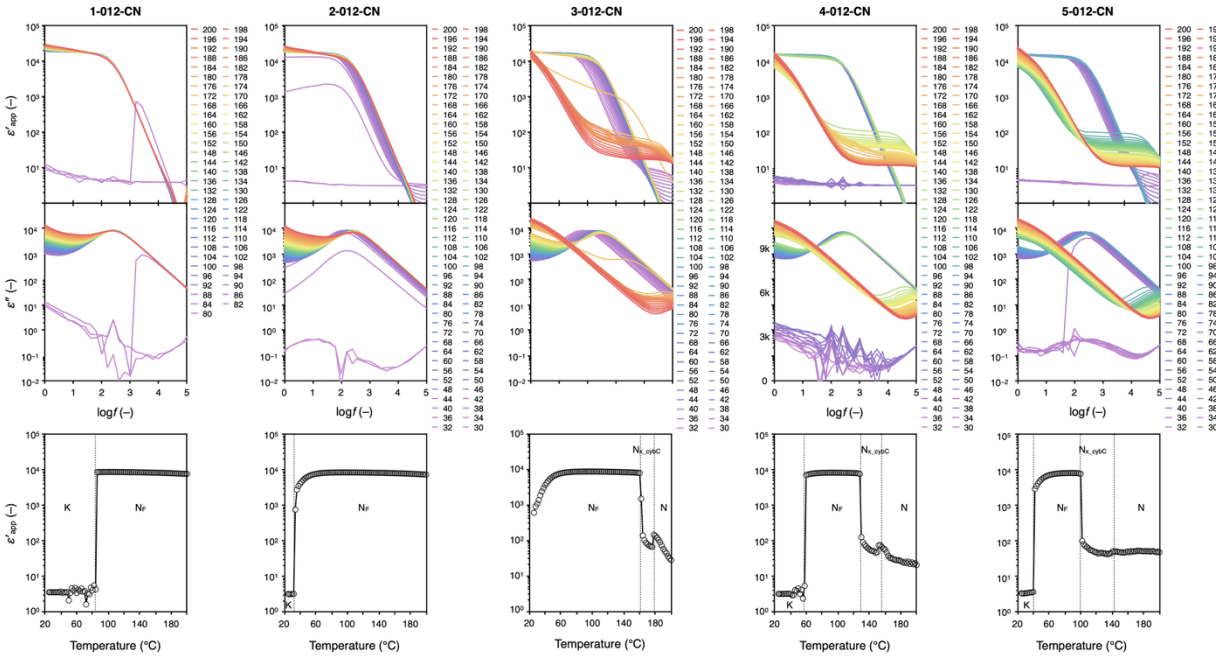

Supplementary Fig. 53 | BDS spectra and relative dielectric permittivity (ε'_{app}) vs. T (f = 400 Hz) for ***n*-012-CN** (n = 1–5).

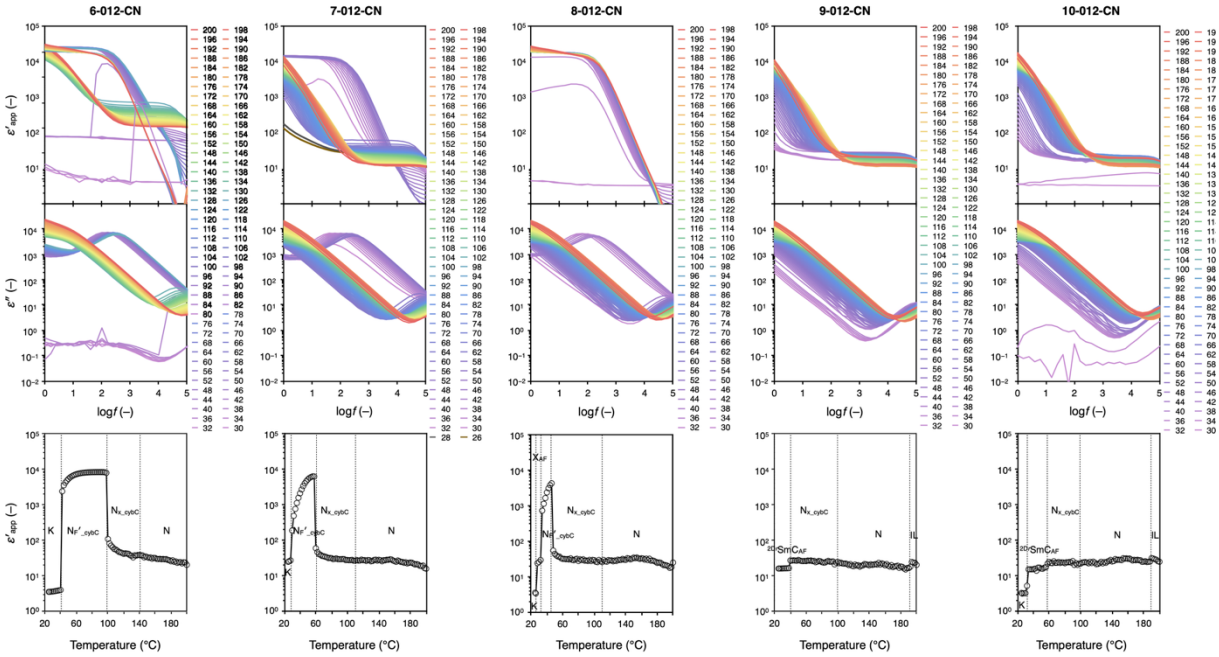

Supplementary Fig. 54 | BDS spectra and relative dielectric permittivity (ε'_{app}) vs. T (f = 400 Hz) for ***n*-012-CN** (n = 6–10).

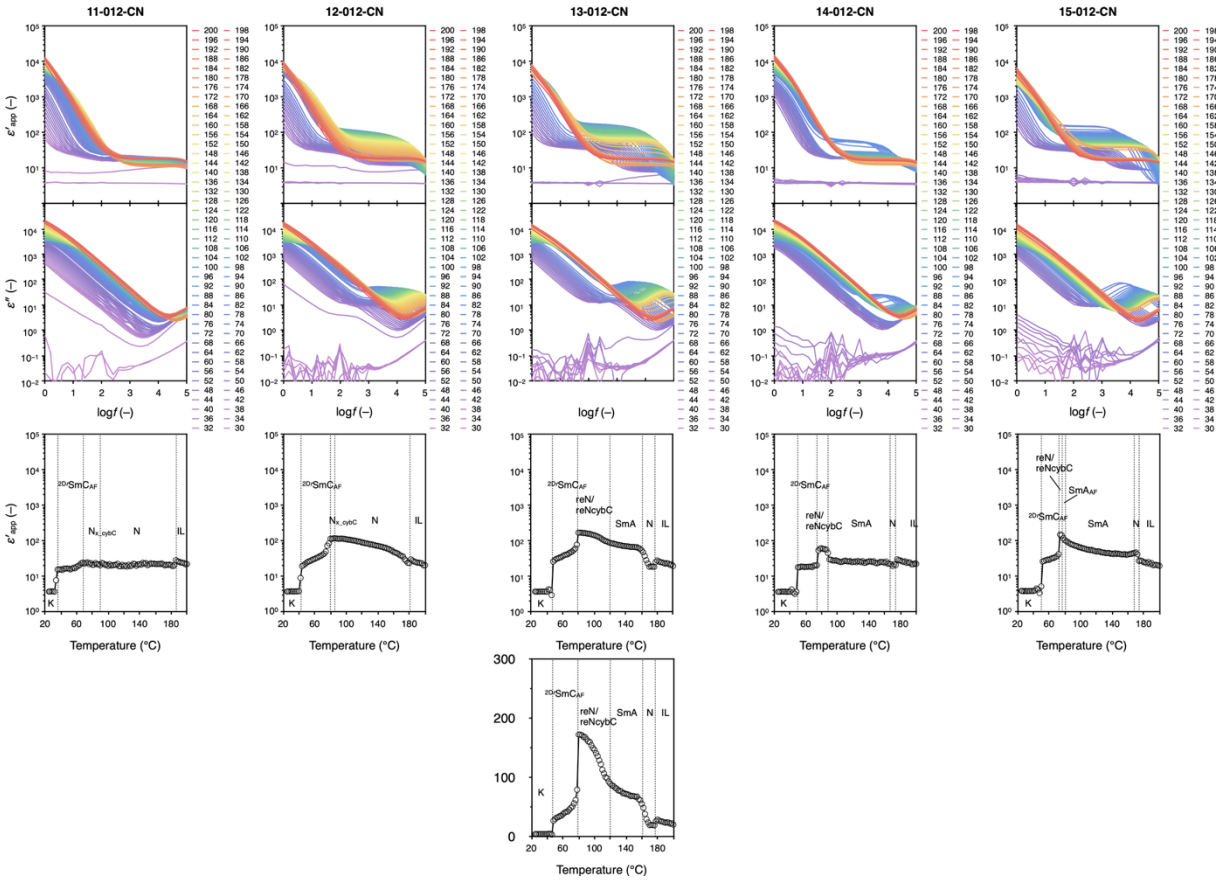

Supplementary Fig. 55 | BDS spectra and relative dielectric permittivity (ε'_{app}) vs. T (f = 400 Hz) for ***n*-012-CN** (n = 11–15).

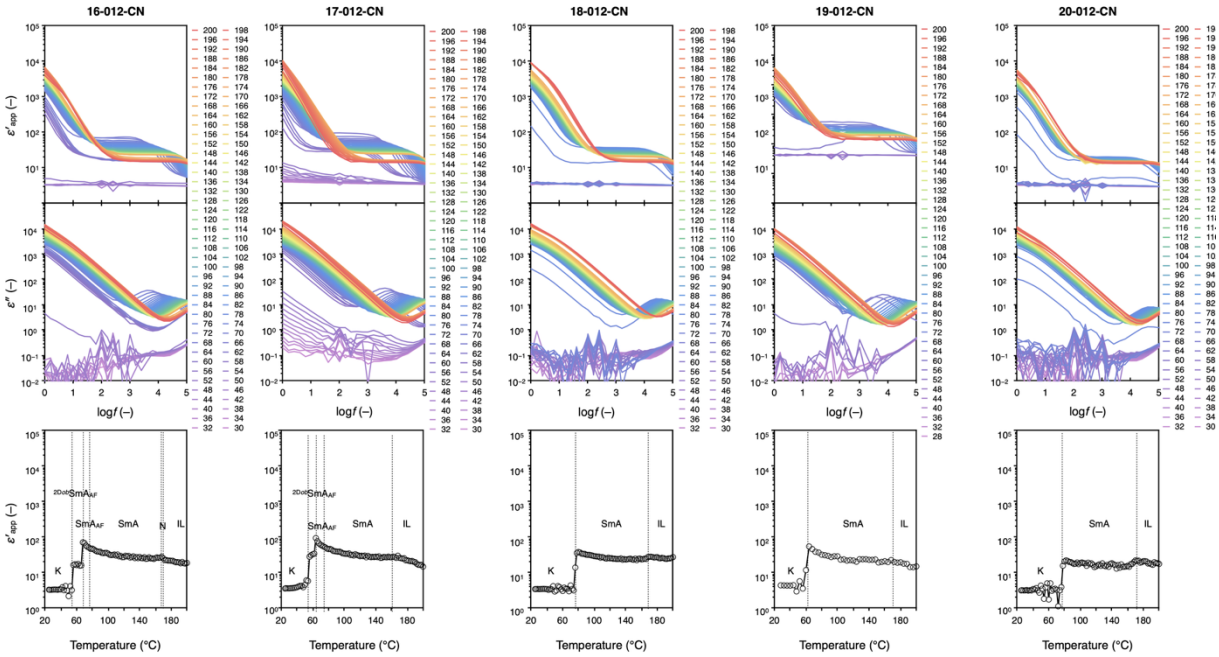

Supplementary Fig. 56 | BDS spectra and relative dielectric permittivity (ε'_{app}) vs. T (f = 400 Hz) for ***n*-012-CN** (n = 16–20).

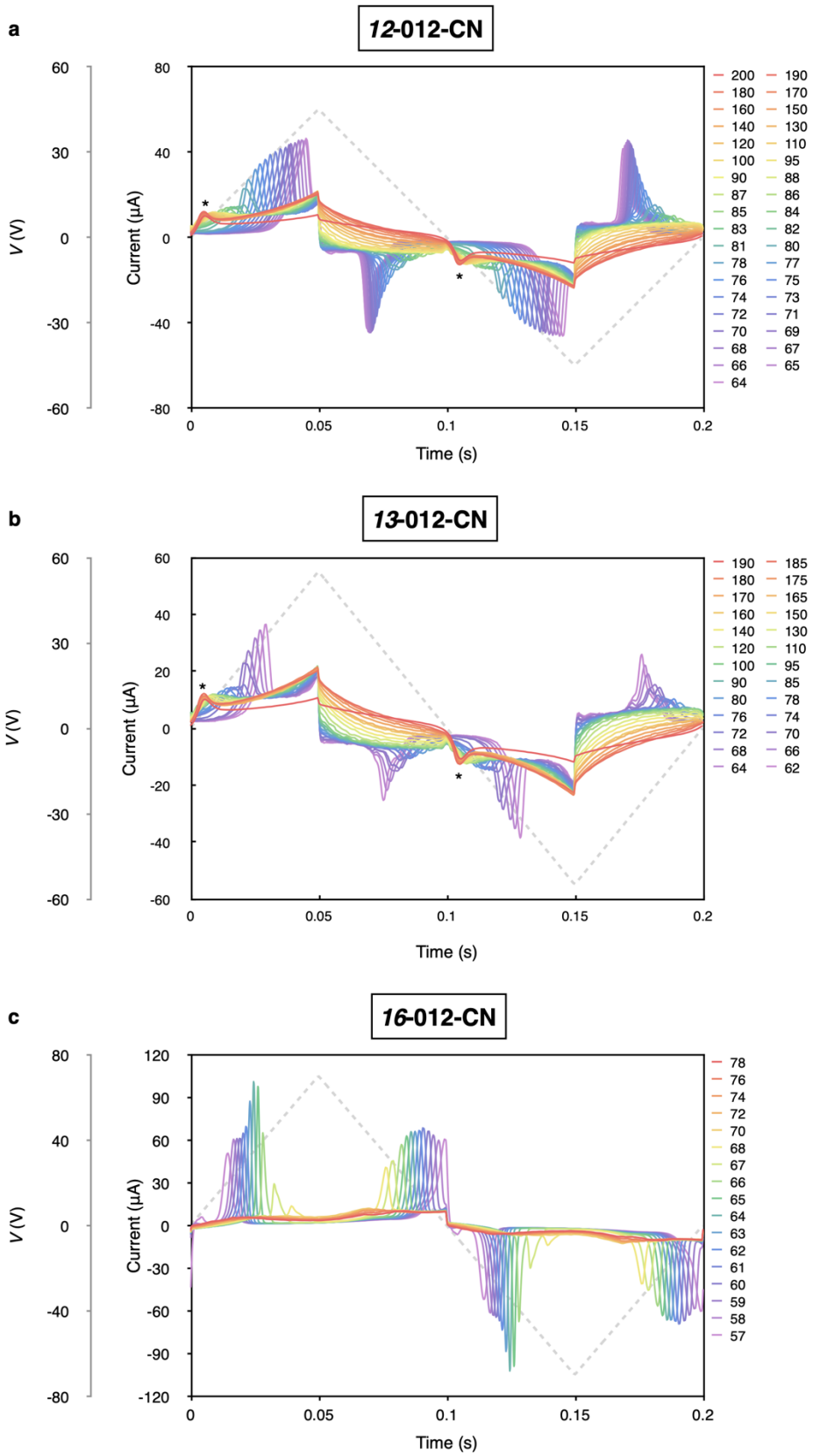

Supplementary Fig. 57 | PRC data for ***12*-012-CN** (a) and ***13*-012-CN** (b) and ***16*-012-CN** (c). Note: The peaks marked by asterisk symbols may be due to the ionic migration because it appeared from the isotropic state and then remained to the reN_{cybC} phase.

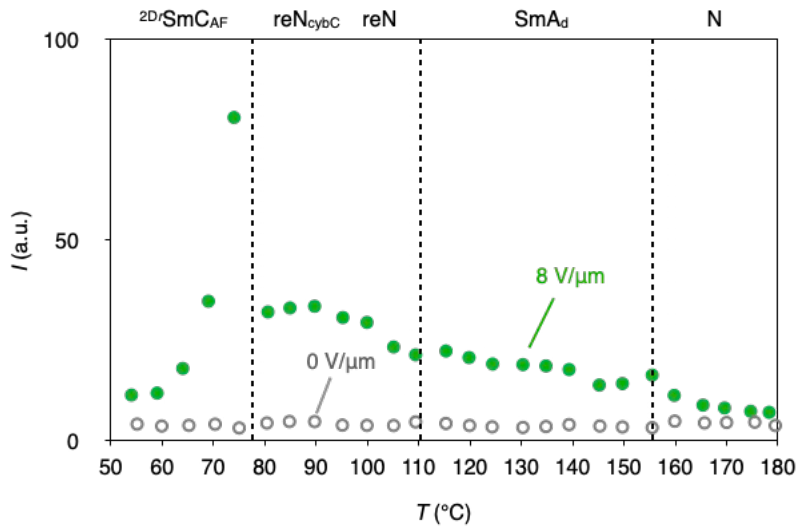

Supplementary Fig. 58 | Temperature-dependent SHG under zero and *E*-field (8.0 V µm^{-1}) for ***13*-012-CN**. The field-induced SHG signal decreased in the ^{2D}rSmC$_{AF}$ region because the applied field was insufficient to induce effective polarization switching at low temperatures. Because higher fields caused sample breakdown, the field strength was fixed at 8 V µm^{-1} (176 V / 22 µm).

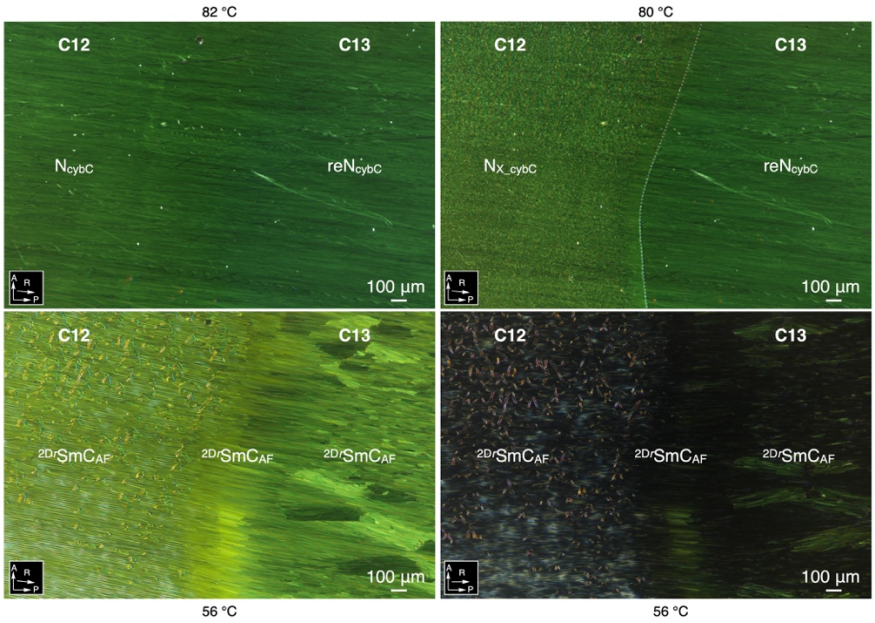

Supplementary Fig. 59 | Contact test in the LC cell between ***12*-012-CN** and ***13*-012-CN**.

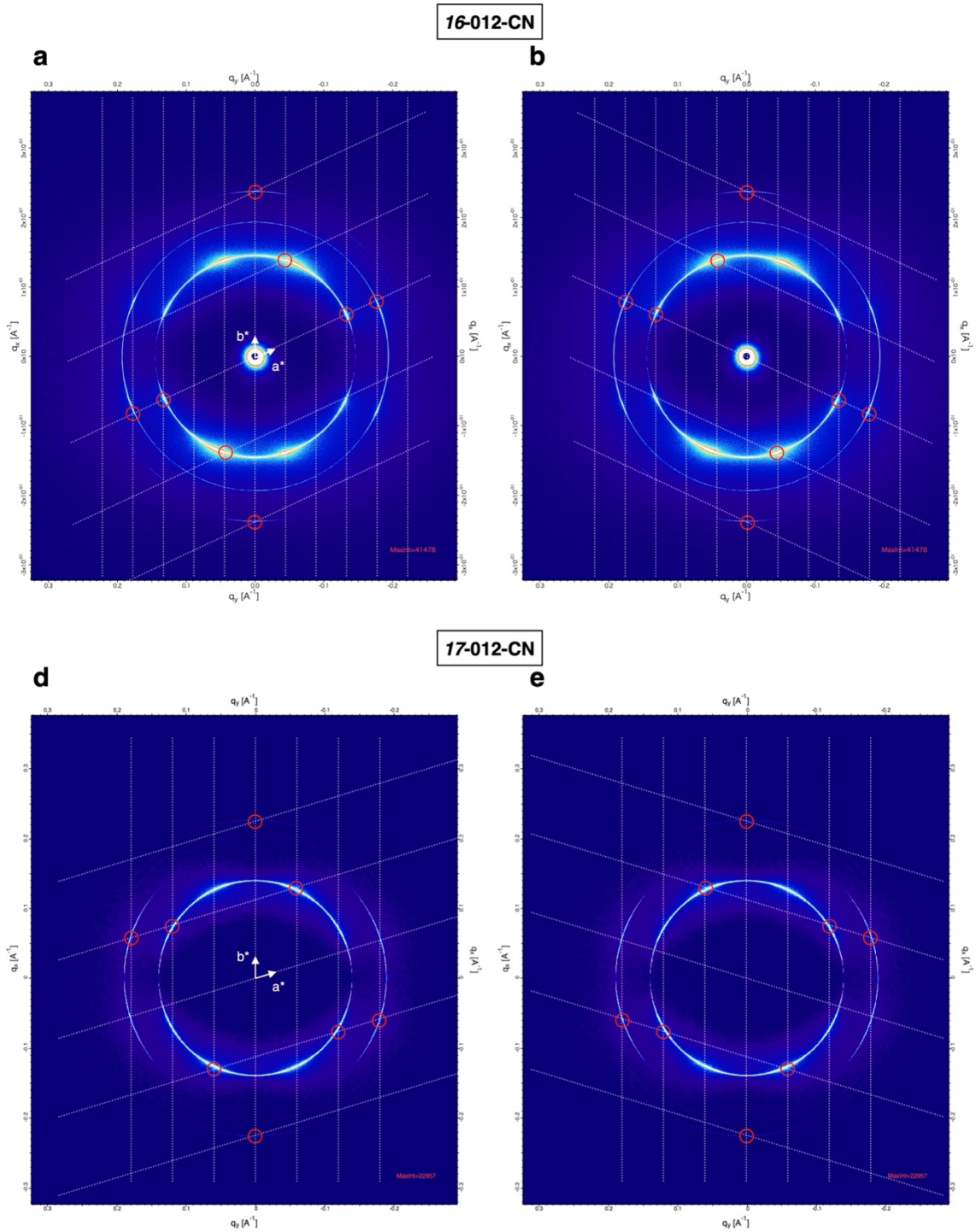

Supplementary Fig. 60 | Domain-resolved indexing of mirror-related oblique 2D lattices in ***16*-012-CN** and ***17*-012-CN**. (a,b) Magnetically aligned 2D SAXS patterns of ***16*-012-CN** at 64 °C, showing the reciprocal lattices associated with two mirror-related orientation domains. (d,e) Corresponding analysis for ***17*-012-CN** at 59 °C. The same diffraction pattern is displayed for each pair of panels, with the indexed reflections and reciprocal-lattice guides shown separately for each domain. Reflections from the two orientation domains were treated independently to avoid mixing their indices within a single lattice.

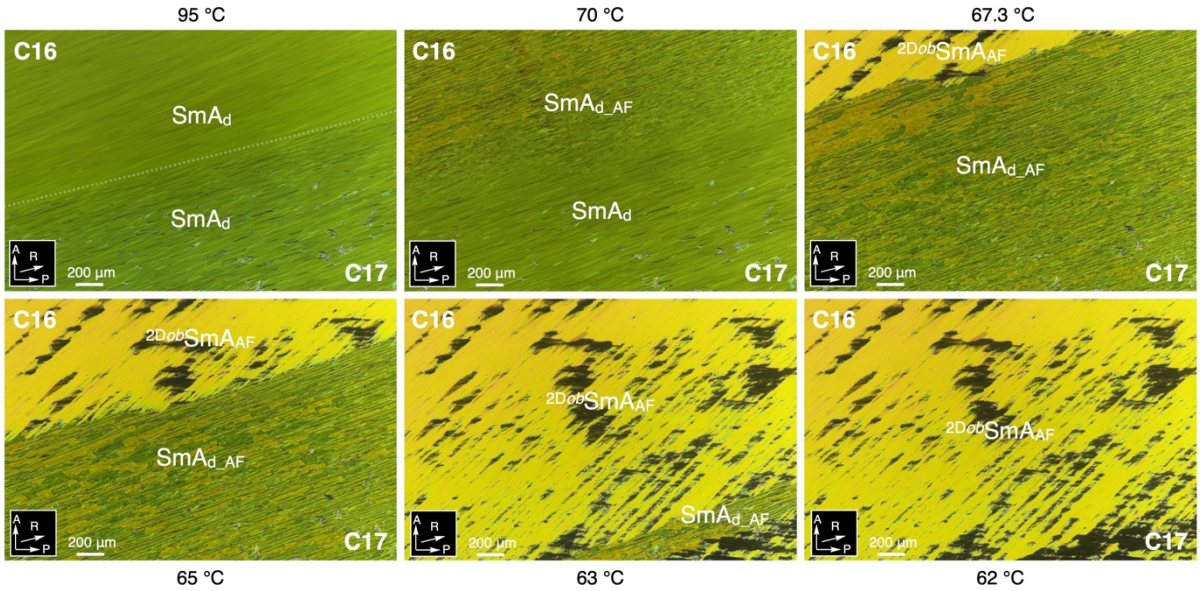

Supplementary Fig. 61 | Contact test in the LC cell between ***16*-012-CN** and ***17*-012-CN**.

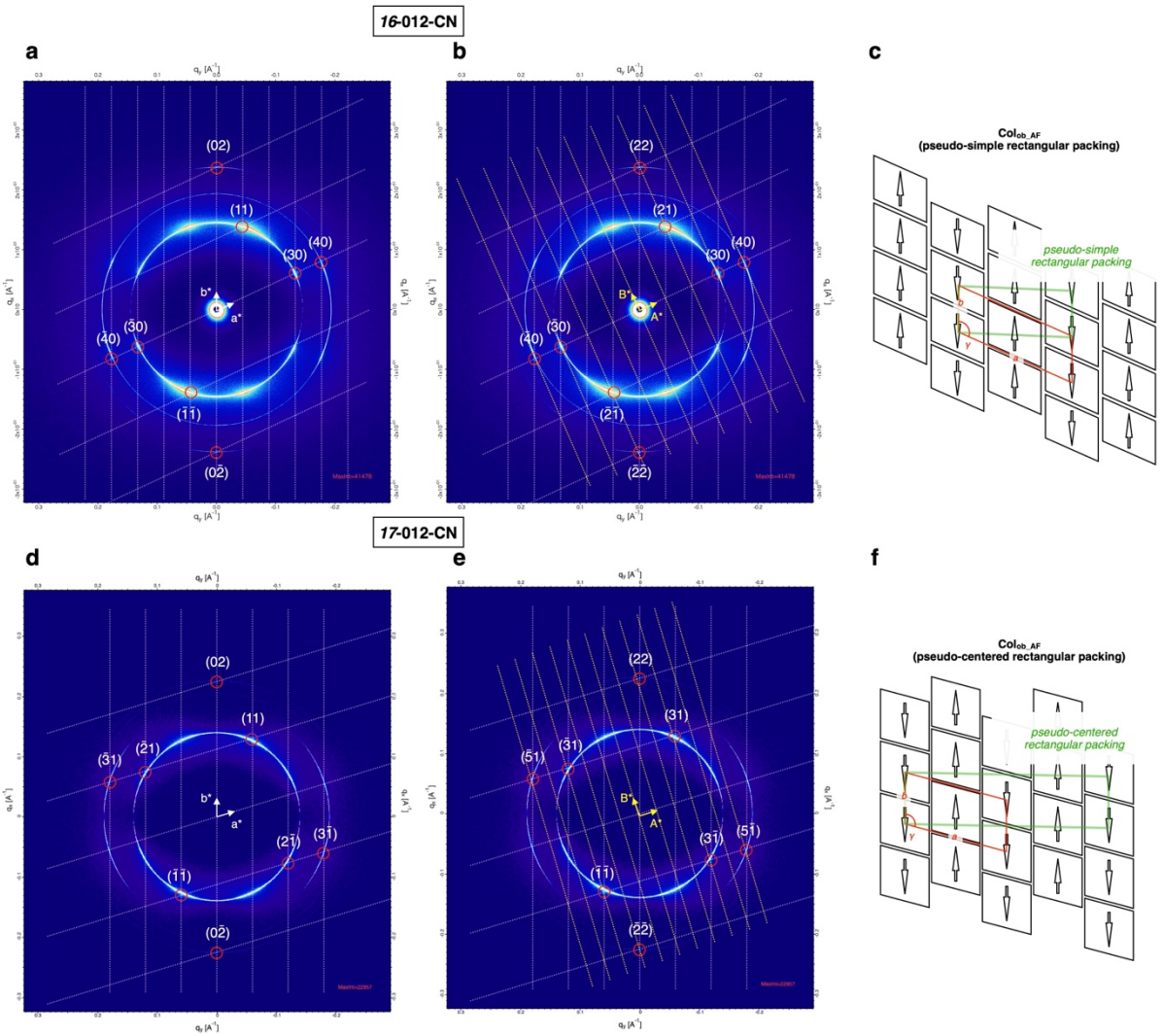

Supplementary Fig. 62 | Pseudo-rectangular representations of the oblique Col_{ob_AF} lattices in ***16*-012-CN** and ***17*-012-CN.** (a,d) Magnetically aligned 2D SAXS patterns indexed using the original oblique unit cells for ***16*-012-CN** at 64 °C and ***17*-012-CN** at 59 °C, respectively. (b,e) Corresponding patterns reindexed using nearly orthogonal unit-cell representations obtained through basis transformations. The transformed lattice angles are $\Gamma \approx 90.0°$ for ***16*-012-CN** and $\Gamma \approx 90.0°$ for ***17*-012-CN**, corresponding to pseudo-simple rectangular and pseudo-centered rectangular representations, respectively. (c,f) Proposed polar-column packing models illustrating the two lattice representations. The transformation equations, lattice parameters, and reflection-index correspondences are provided in Supplementary Note 2.

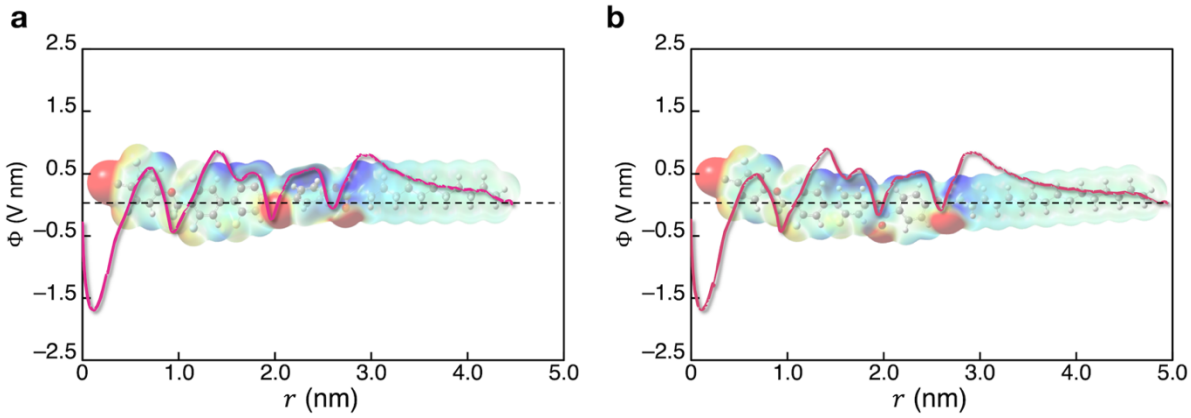

Supplementary Fig. 63 | 3D ESP surface and resulting 1D longitudinal ESP profile for ***12*-012-CN** (a) and ***16*-012-CN** (b).

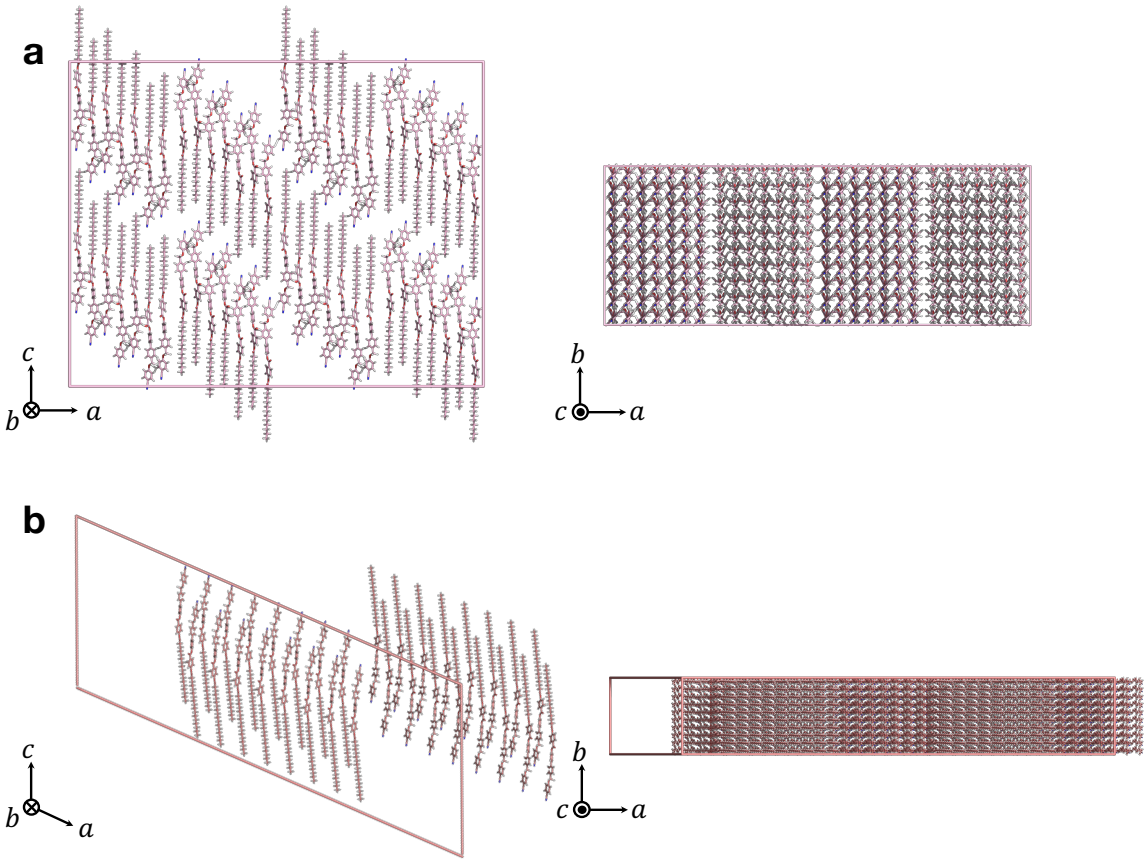

Supplementary Fig. 64 | Initial configurations for the all-atom MD simulations of ***12*-012-CN** (a) and ***16*-012-CN** (b). The initial polar columns with initial SmC-type packing contain 7 molecules per column segment with β = 38° for ***12*-012-CN** and 16 molecules per column segment with β = 19° for ***16*-012-CN**.

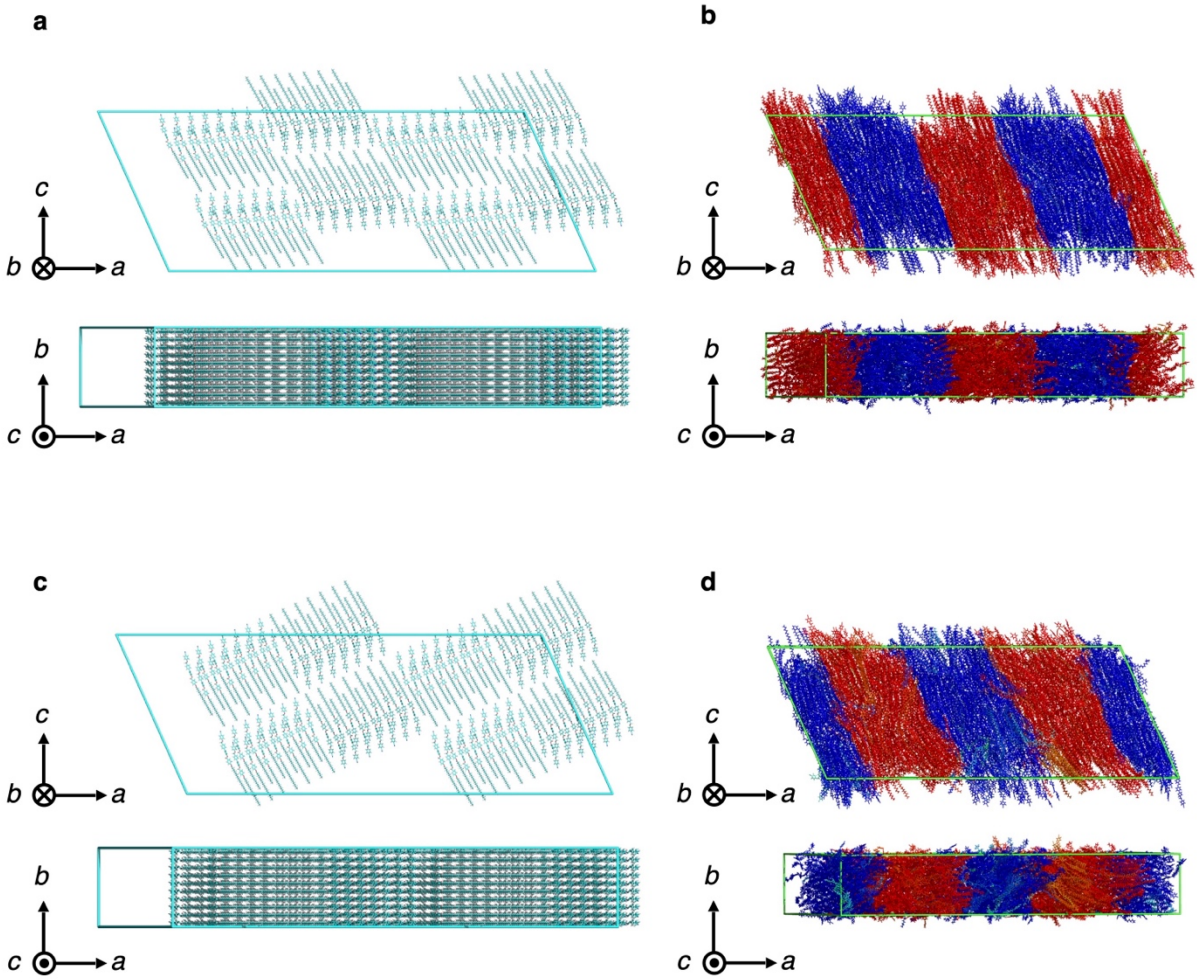

Supplementary Fig. 65 | Effect of initial molecular packing on the relaxed polar-column arrangements of ***16*-012-CN**. Initial configurations containing 14 molecules per column segment, with SmC-type (β = 19°) (a) and SmA-type (β = 0°) (c) packing, respectively. (b,d) Corresponding MD snapshots after 100 ns of equilibration at 335 K. Red and blue indicate oppositely polarized columns.

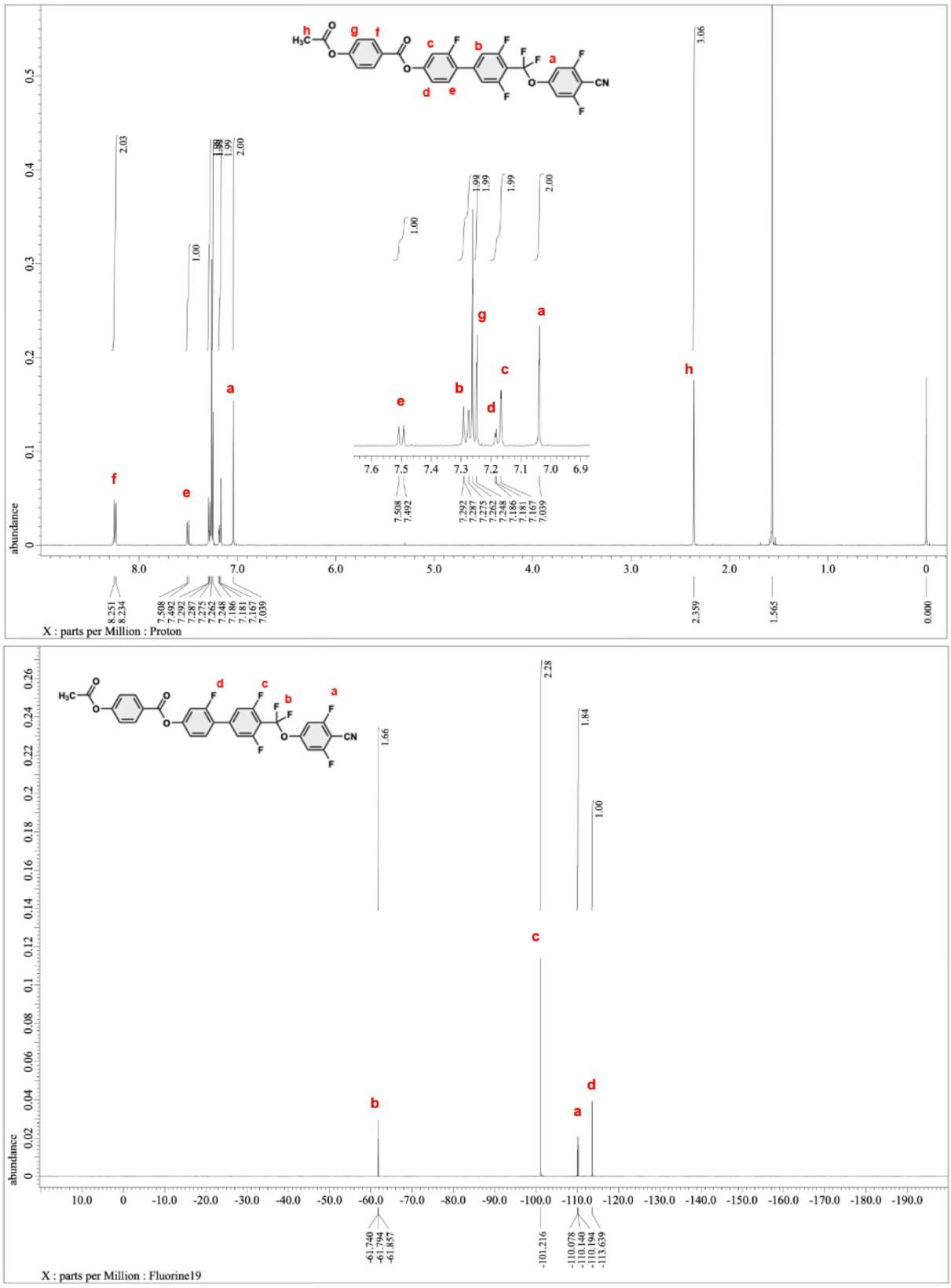

Supplementary Fig. 66 | $^{1}H\{^{19}F\}$ (upper) and $^{19}F\{^{1}H\}$ (bottom) NMR spectra for ***1*-012-CN**.

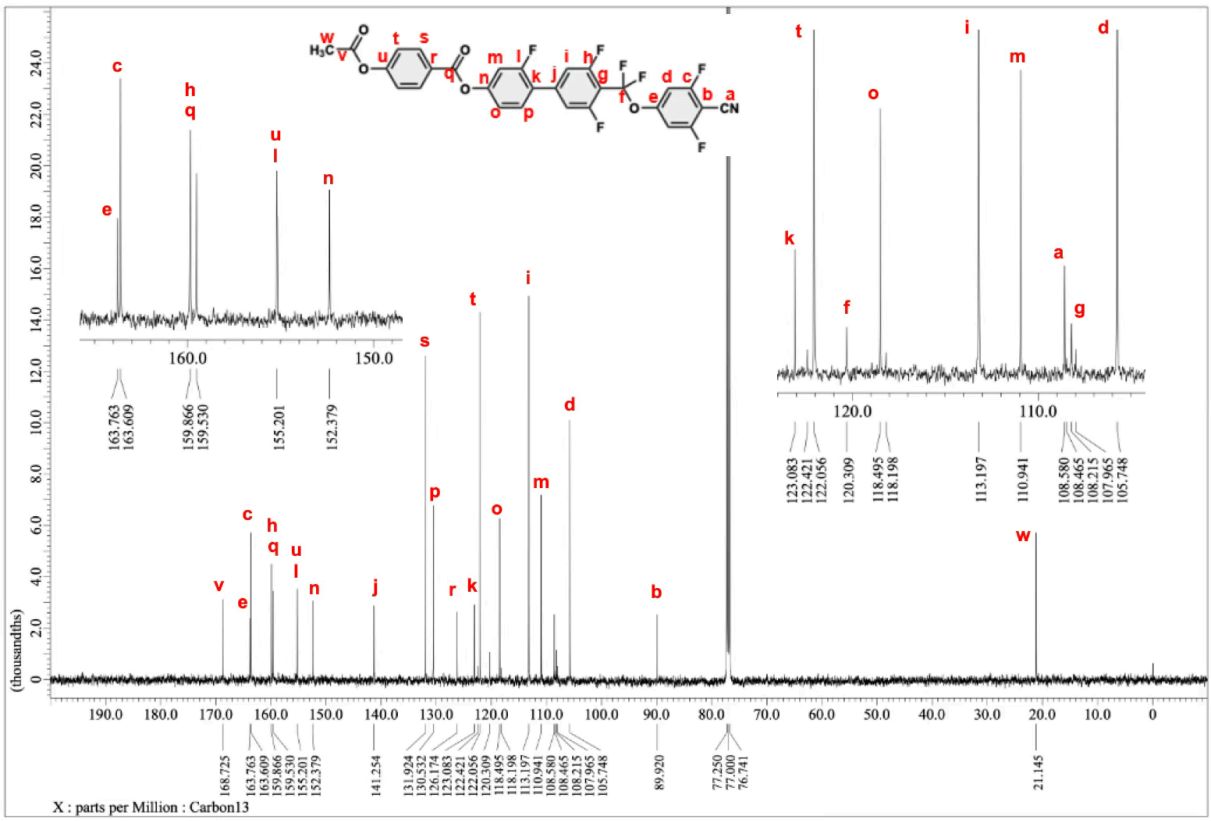

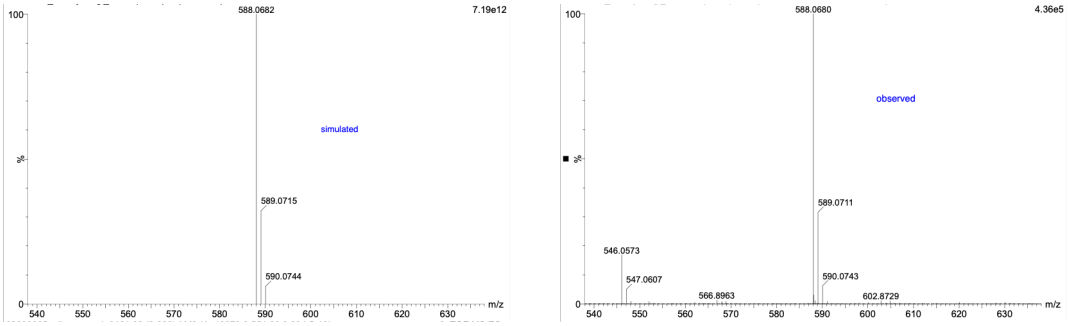

Supplementary Fig. 67 | $^{13}C\{^{1}H,^{19}F\}$NMR (upper) and HR-ESI-TOF-MS spectra (bottom) for ***1*-012-CN**.

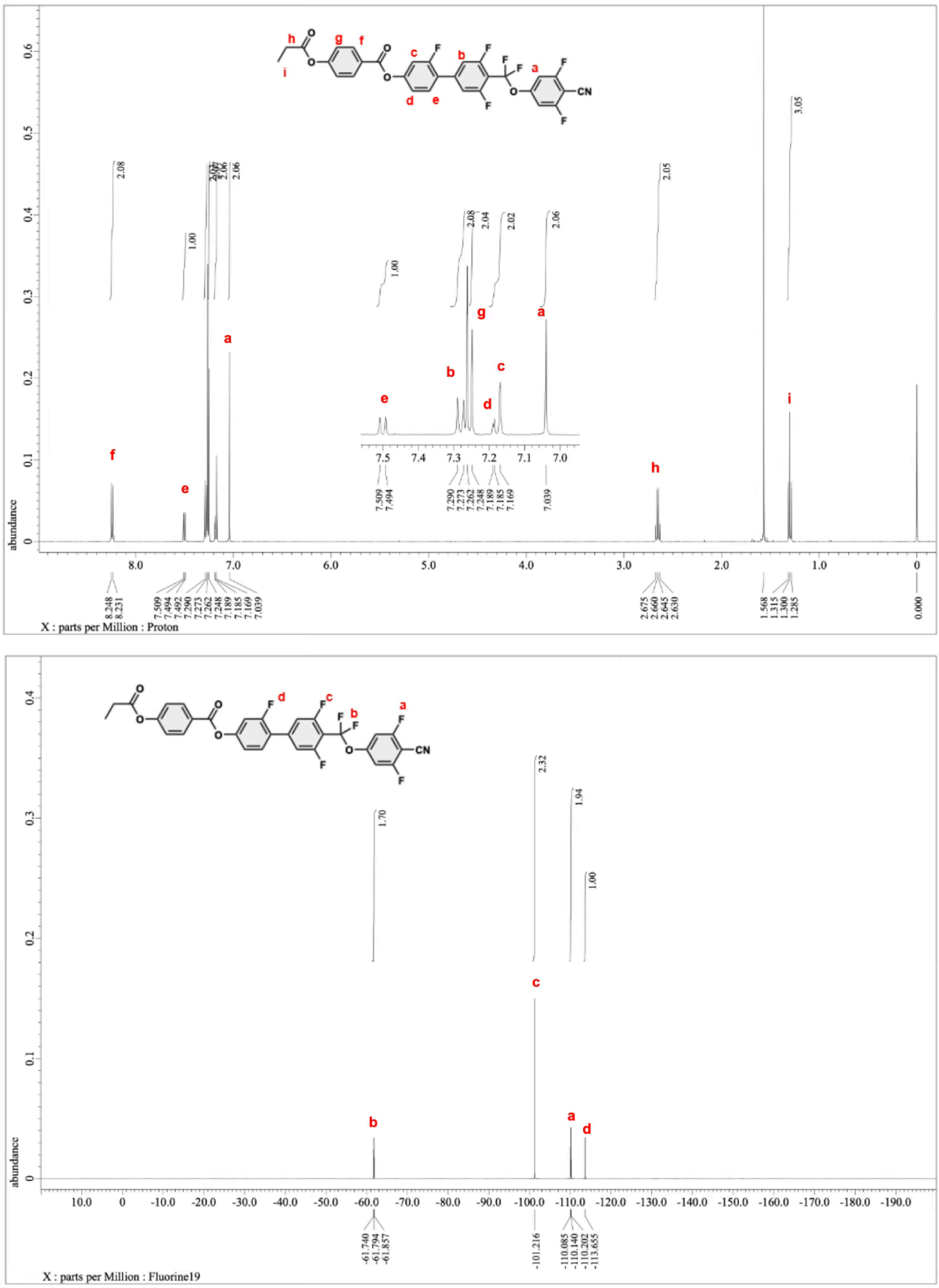

Supplementary Fig. 68 | $^{1}H\{^{19}F\}$ (upper) and $^{19}F\{^{1}H\}$ (bottom) NMR spectra for ***2*-012-CN**.

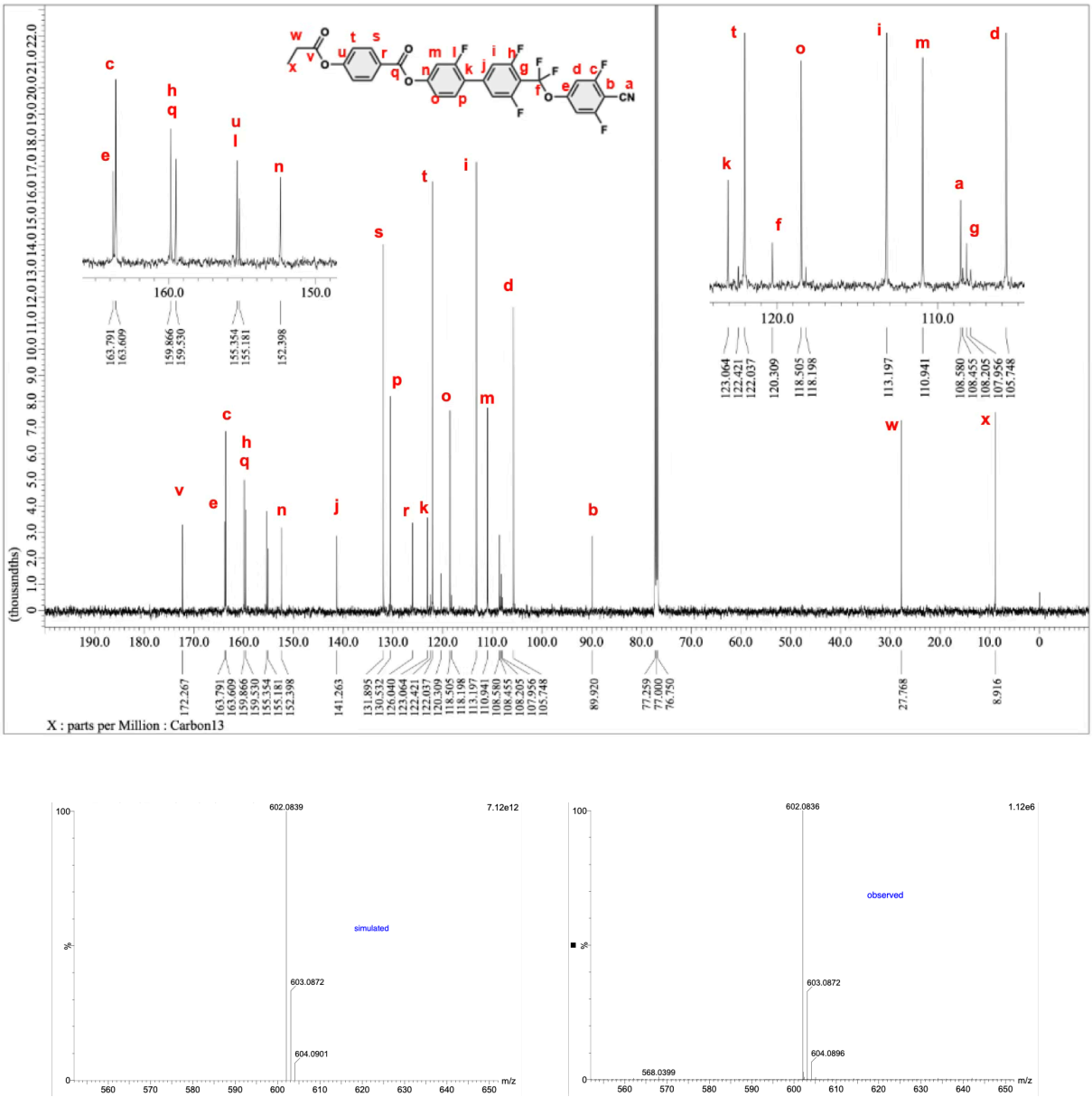

Supplementary Fig. 69 | $^{13}C\{^{1}H,^{19}F\}$NMR (upper) and HR-ESI-TOF-MS spectra (bottom) for ***2*-012-CN**.

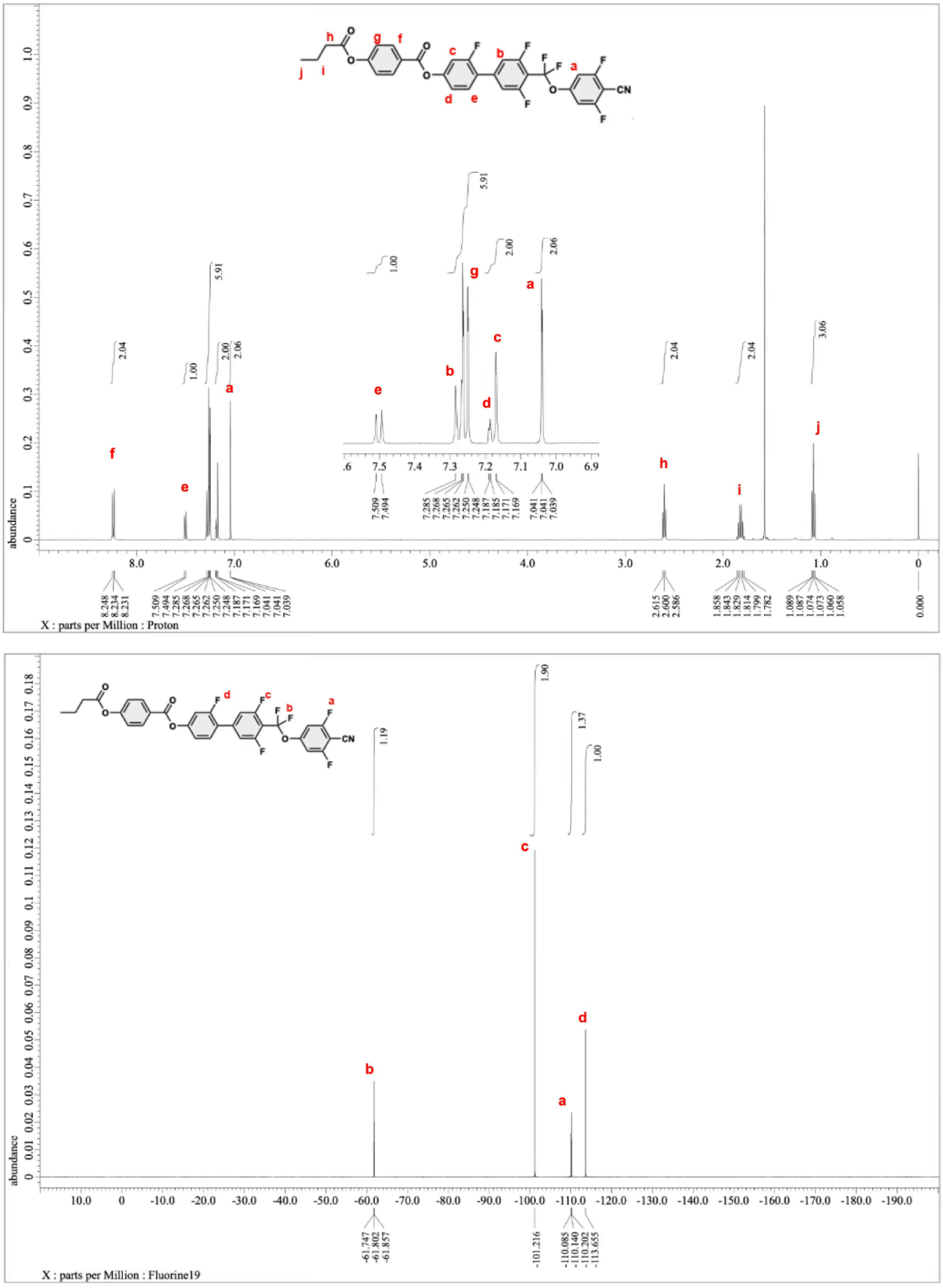

Supplementary Fig. 70 | $^{1}H\{^{19}F\}$ (upper) and $^{19}F\{^{1}H\}$ (bottom) NMR spectra for ***3*-012-CN**.

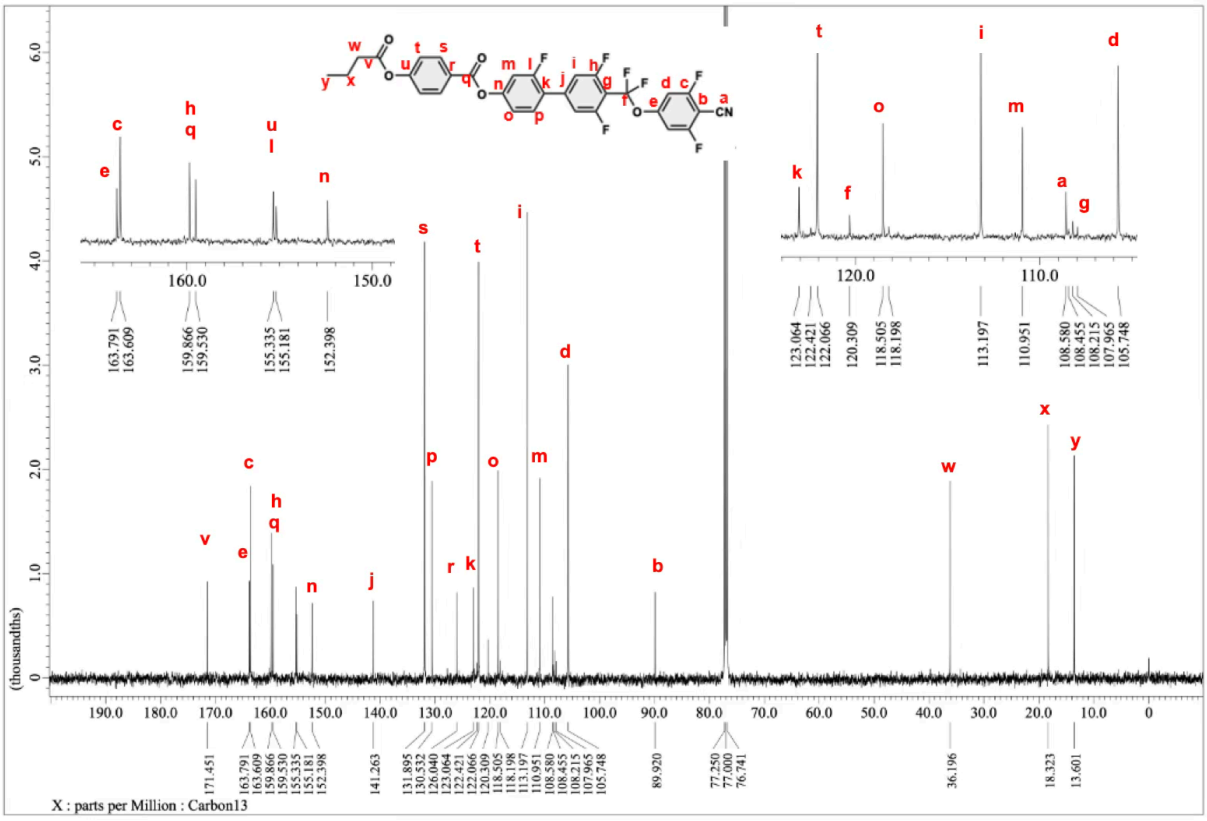

Supplementary Fig. 71 | $^{13}C\{^{1}H,^{19}F\}$NMR (upper) and HR-ESI-TOF-MS spectra (bottom) for ***3*-012-CN**.

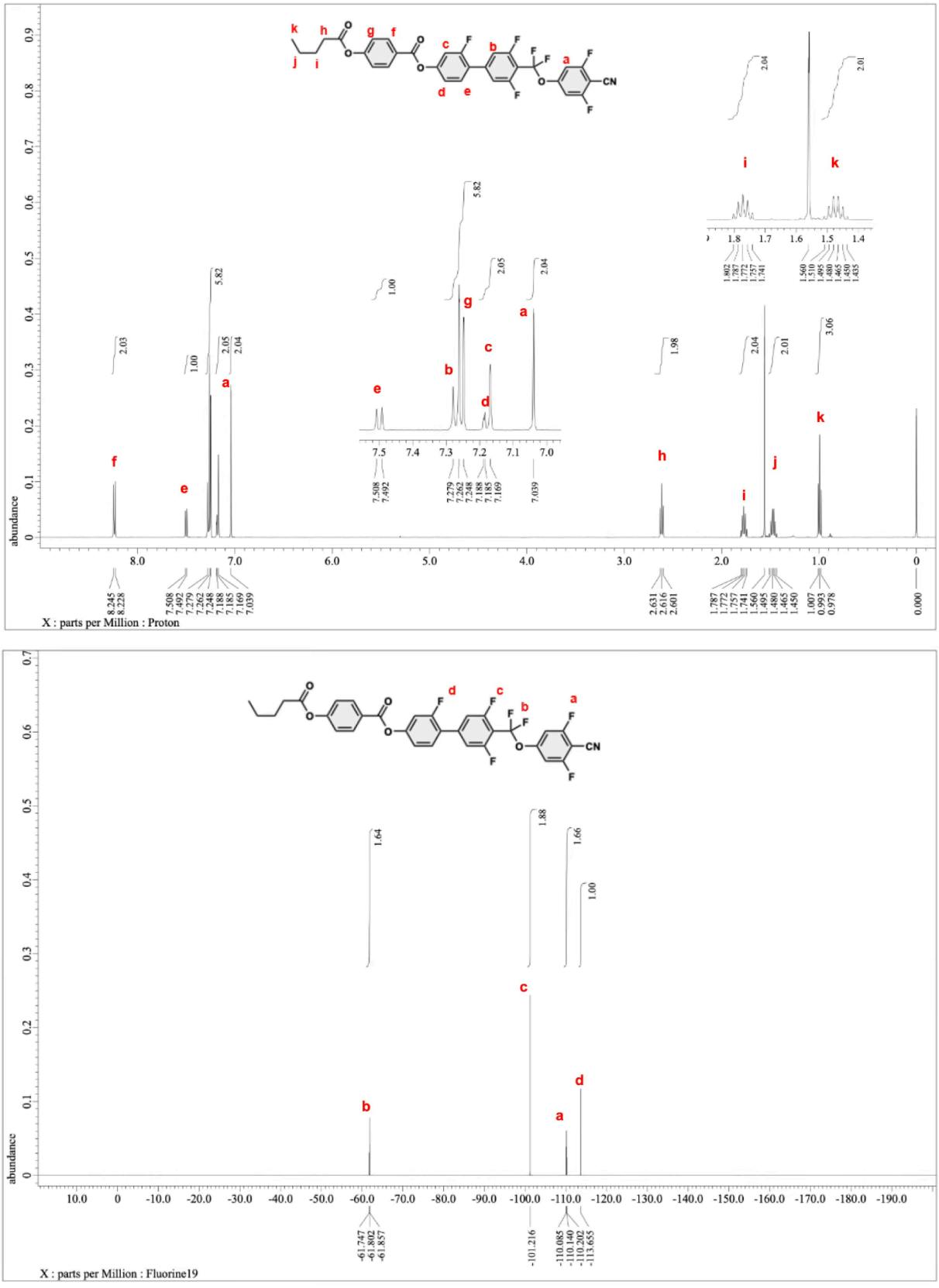

Supplementary Fig. 72 | $^{1}H\{^{19}F\}$ (upper) and $^{19}F\{^{1}H\}$ (bottom) NMR spectra for ***4*-012-CN**.

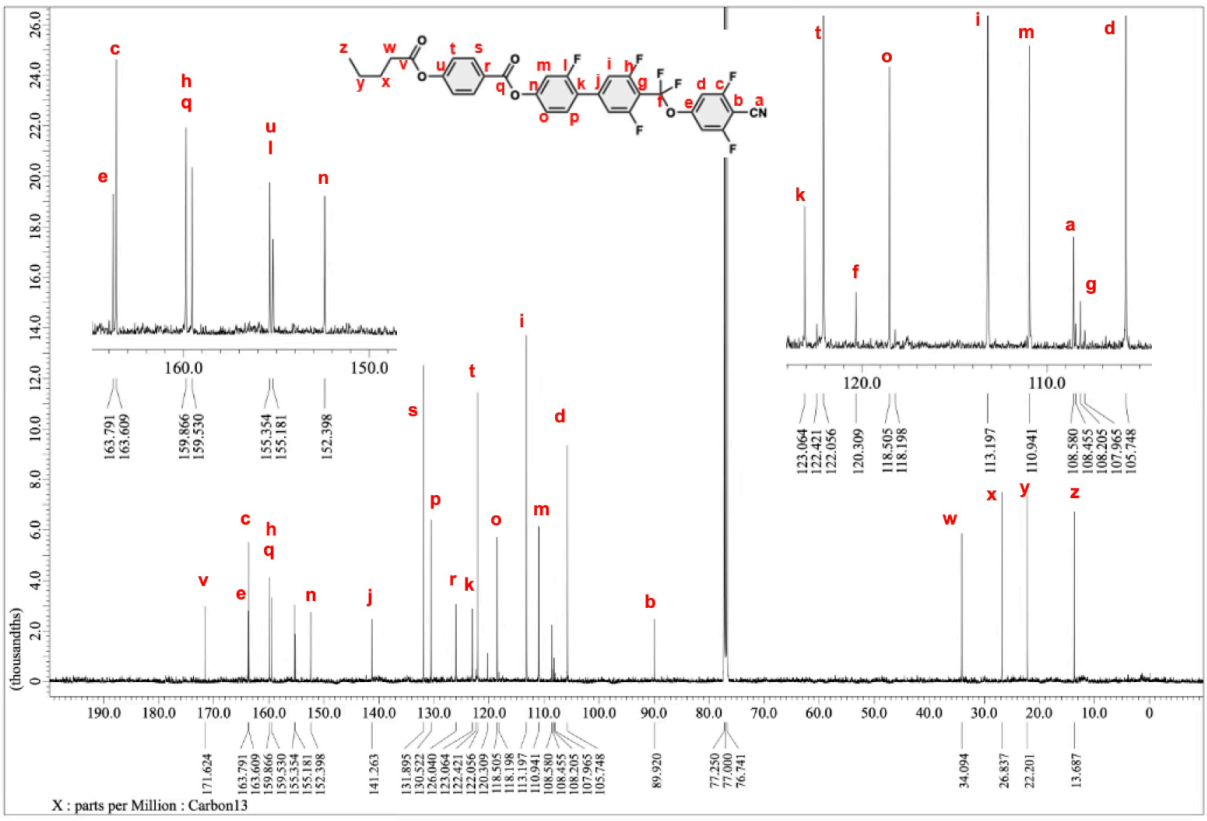

Supplementary Fig. 73 | $^{13}C\{^{1}H,^{19}F\}$NMR (upper) and HR-ESI-TOF-MS spectra (bottom) for ***4*-012-CN**.

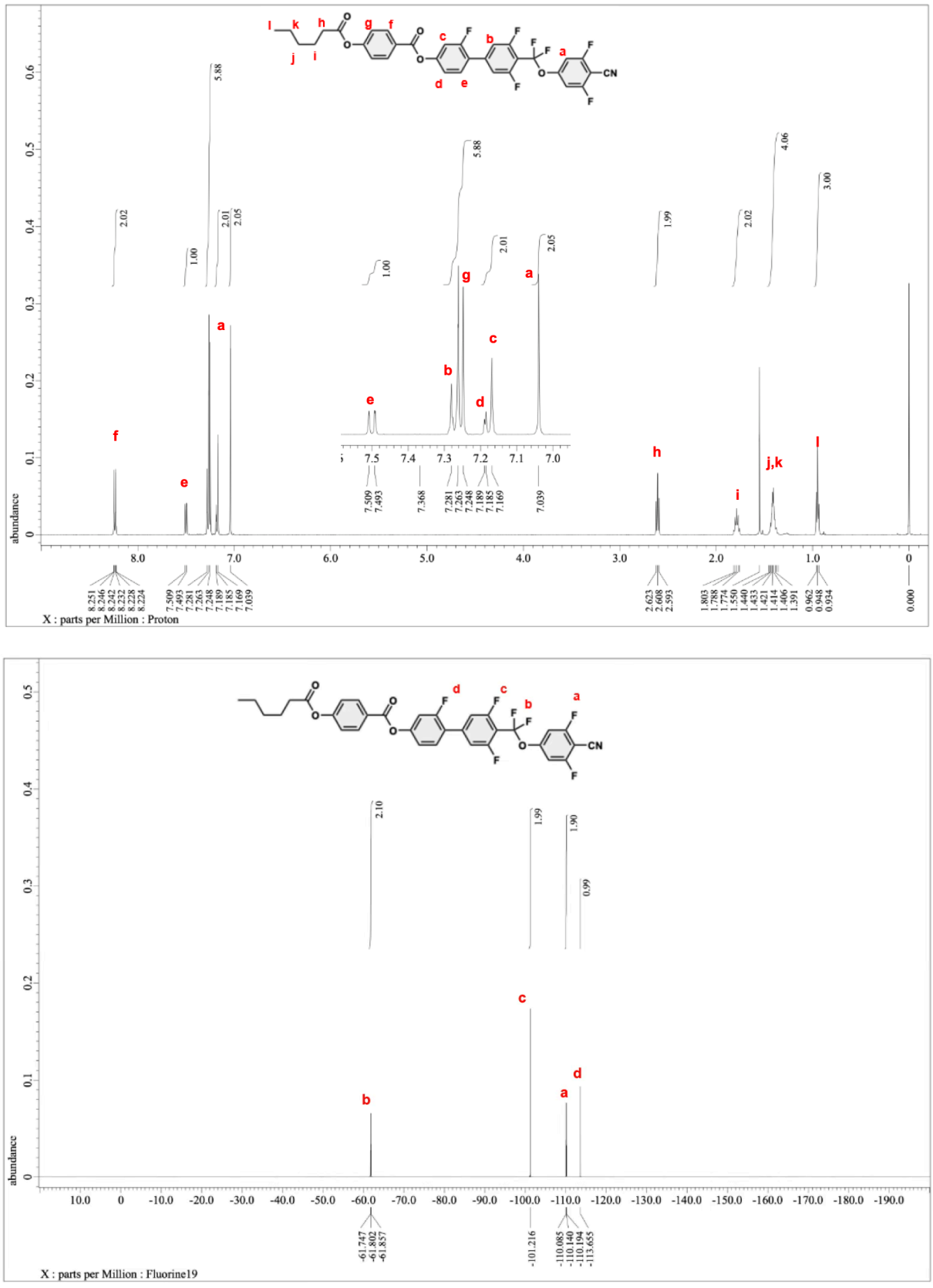

Supplementary Fig. 74 | $^{1}H\{^{19}F\}$ (upper) and $^{19}F\{^{1}H\}$ (bottom) NMR spectra for **5-012-CN**.

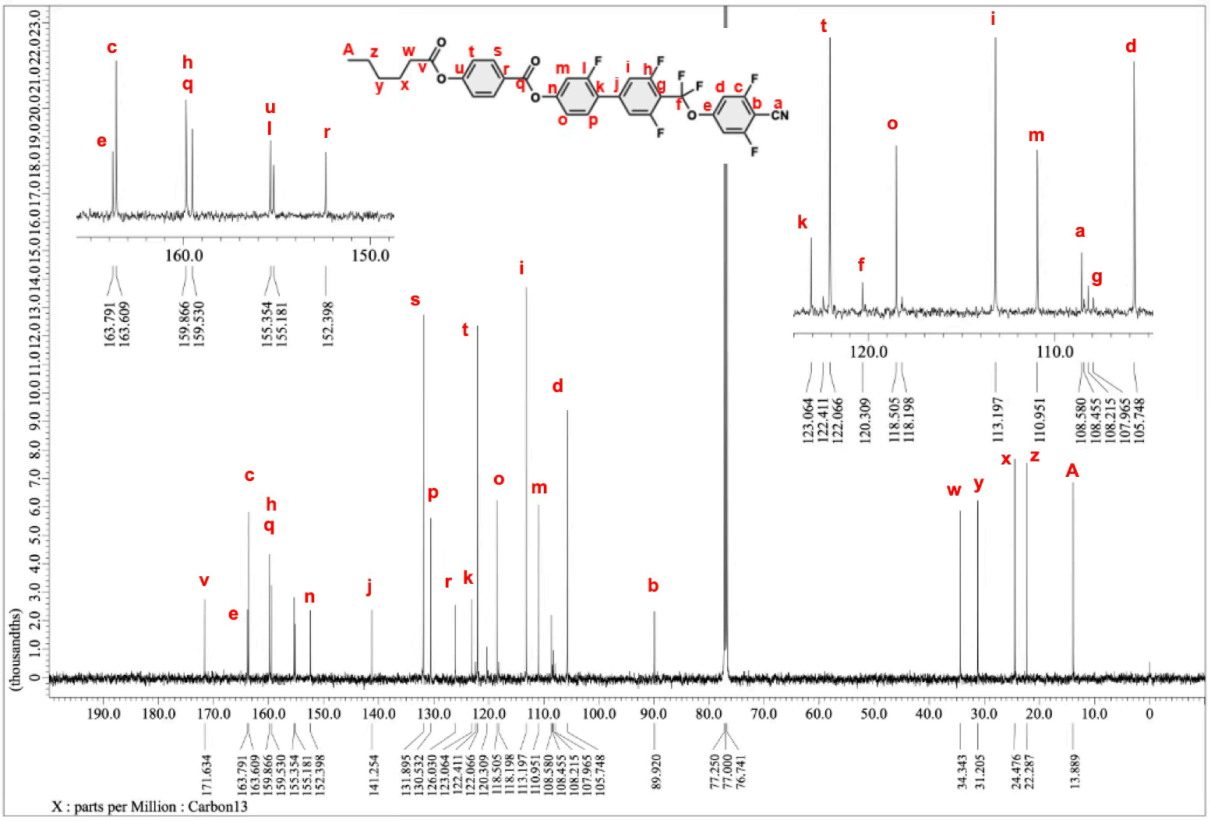

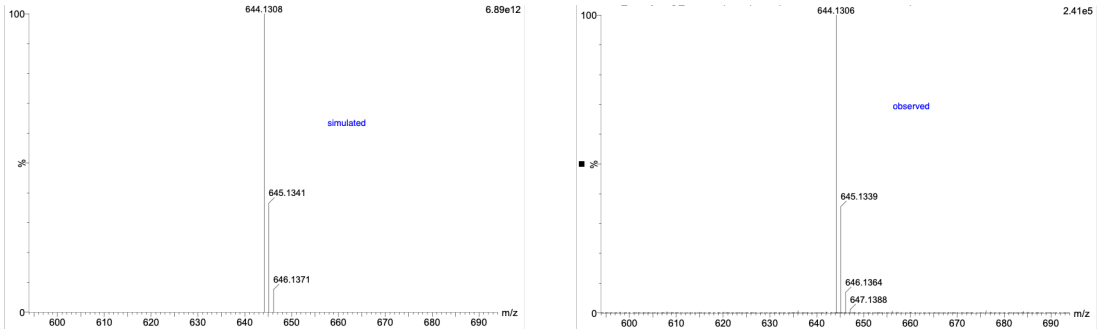

Supplementary Fig. 75 | $^{13}C\{^{1}H,^{19}F\}$NMR (upper) and HR-ESI-TOF-MS spectra (bottom) for ***5*-012-CN**.

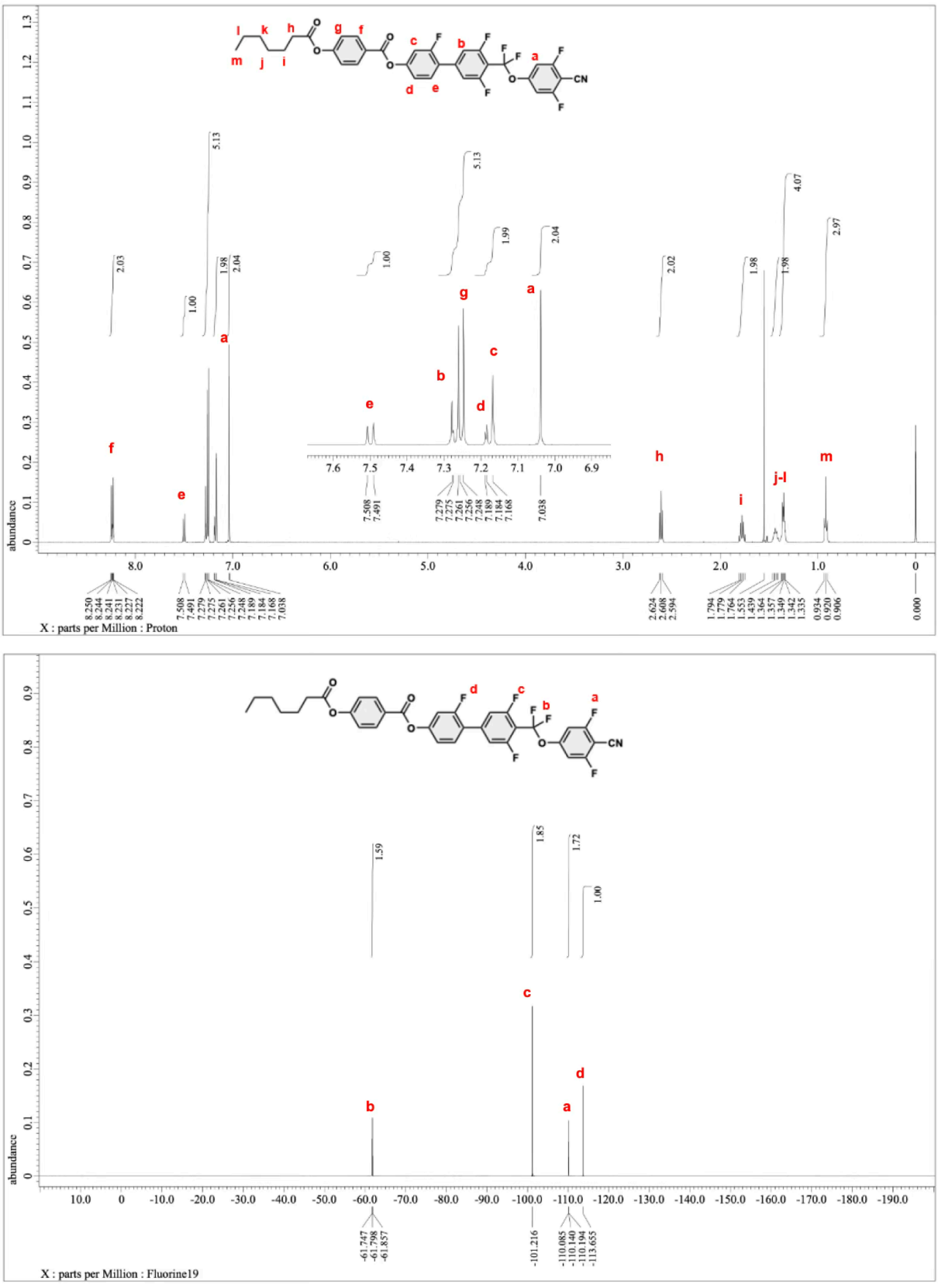

Supplementary Fig. 76 | $^{1}H\{^{19}F\}$ (upper) and $^{19}F\{^{1}H\}$ (bottom) NMR spectra for ***6*-012-CN**.

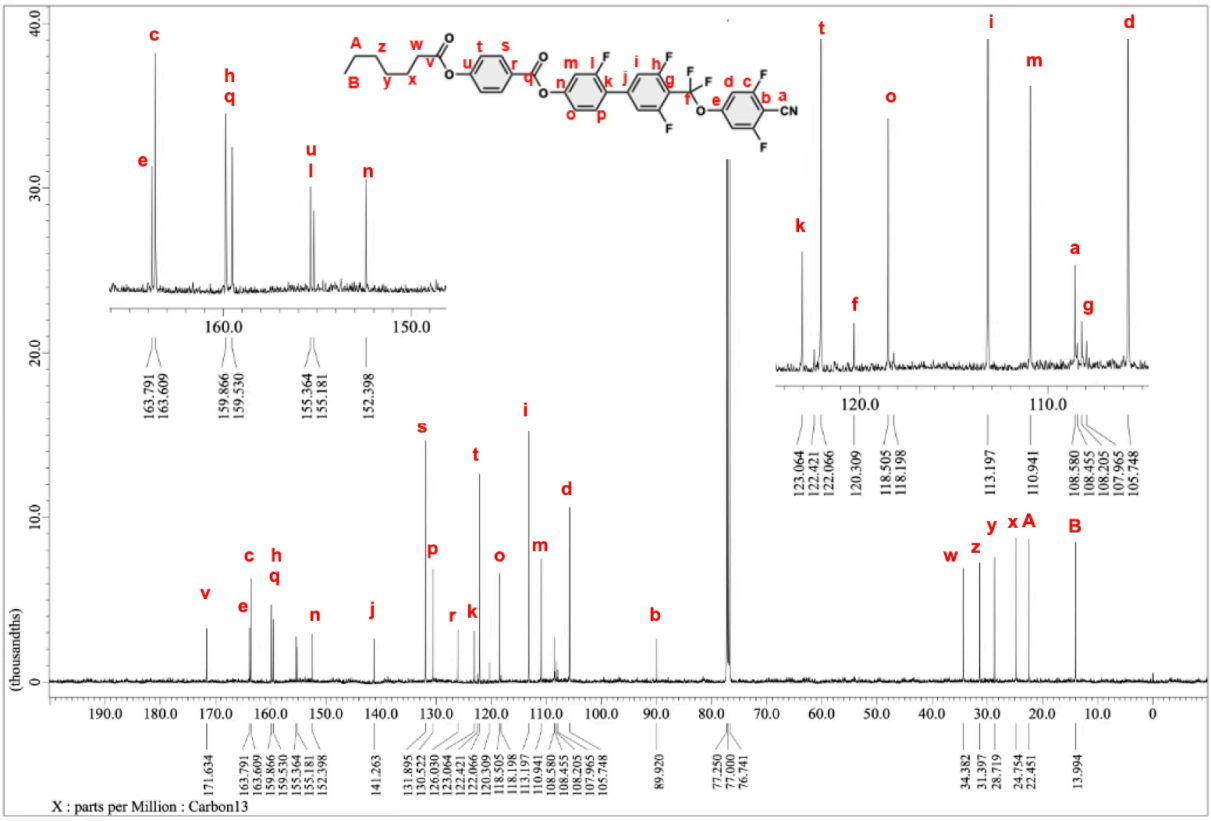

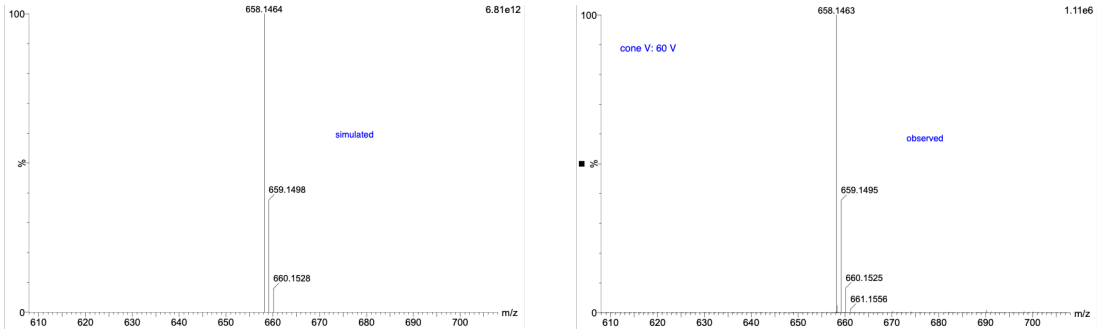

Supplementary Fig. 77 | $^{13}C\{1H,^{19}F\}$NMR (upper) and HR-ESI-TOF-MS spectra (bottom) for ***6*-012-CN**.

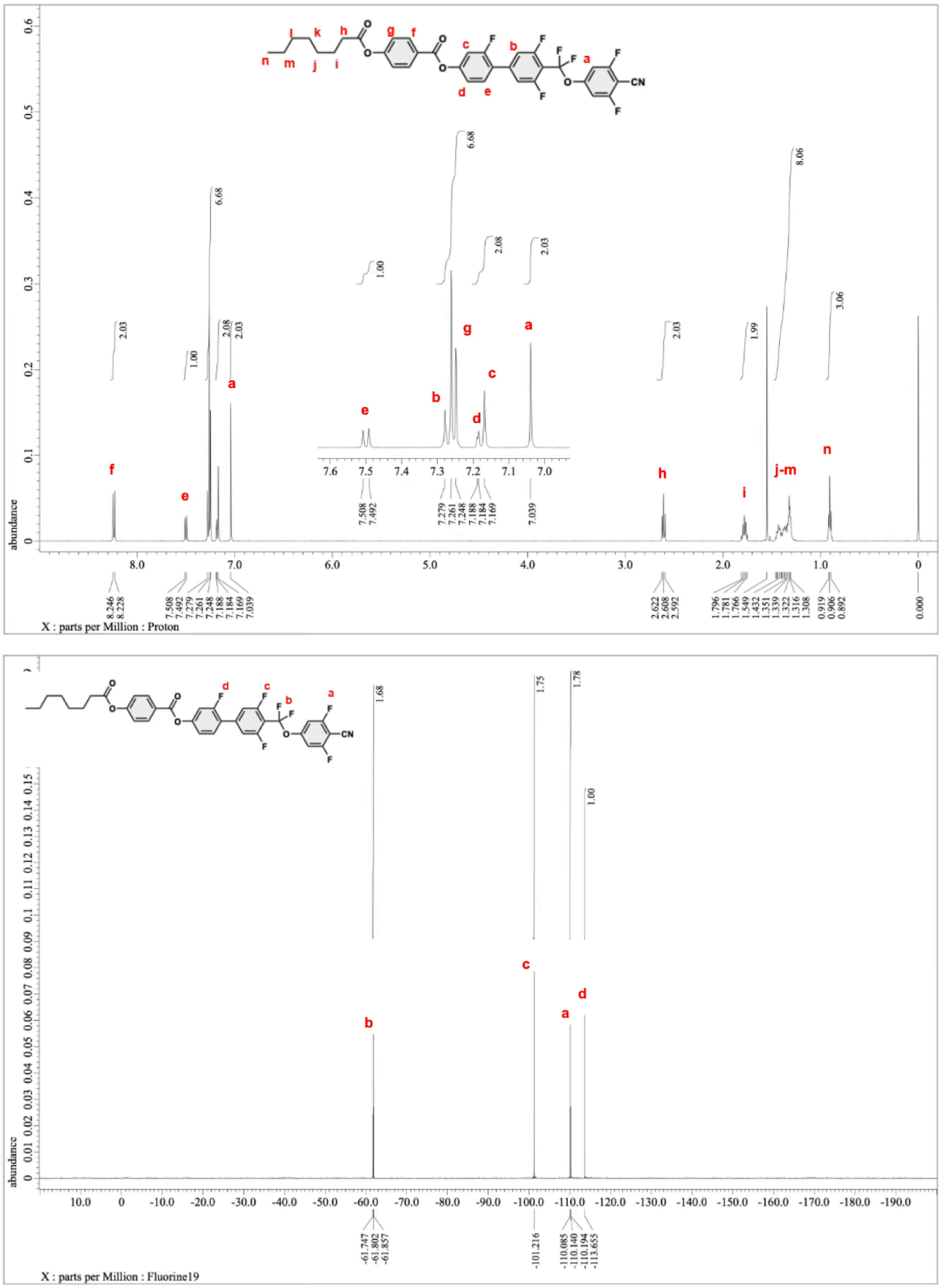

Supplementary Fig. 78 | $^{1}H\{^{19}F\}$ (upper) and $^{19}F\{^{1}H\}$ (bottom) NMR spectra for ***7*-012-CN**.

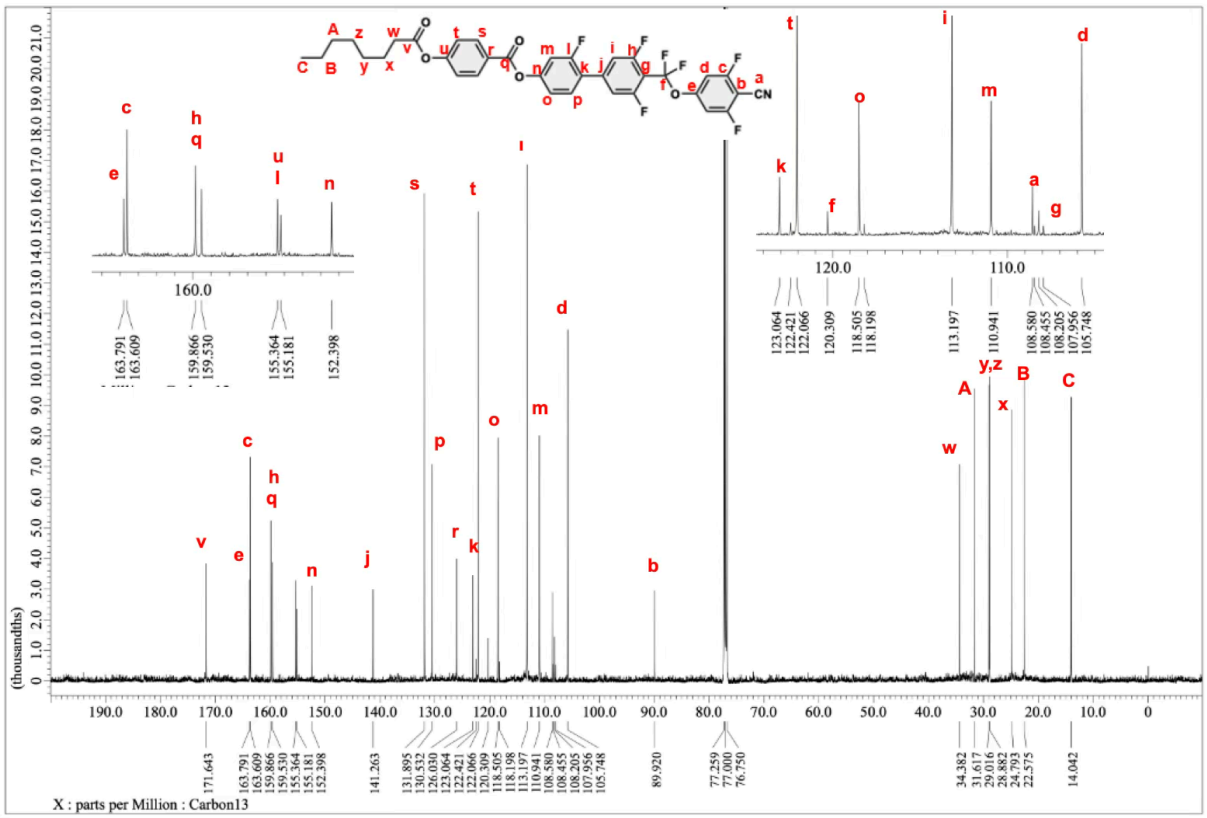

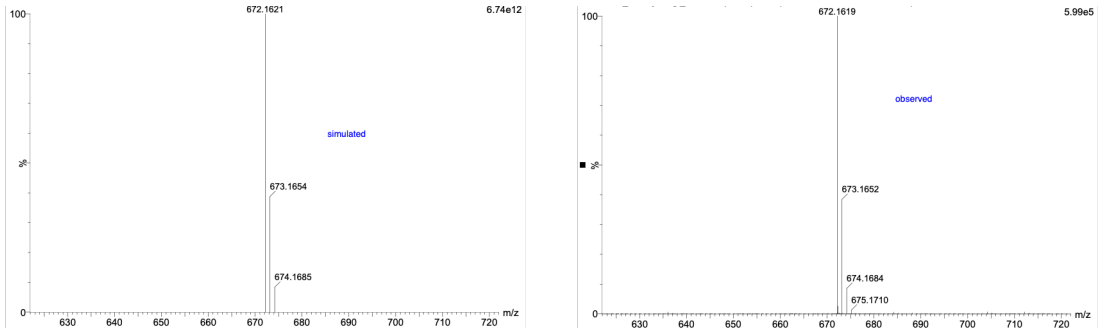

Supplementary Fig. 79 | $^{13}C\{^{1}H,^{19}F\}$NMR (upper) and HR-ESI-TOF-MS spectra (bottom) for ***7*-012-CN**.

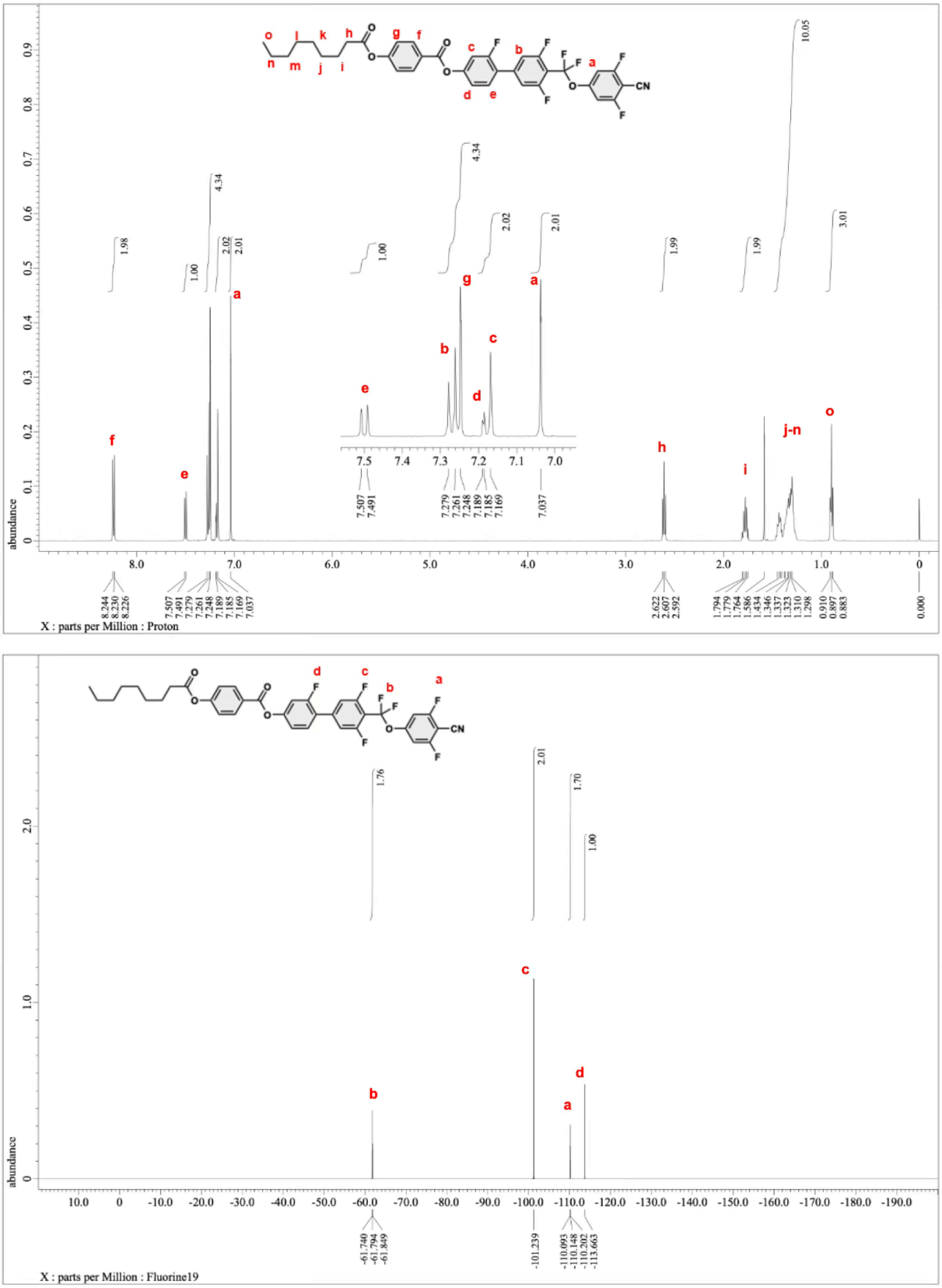

Supplementary Fig. 80 | $^{1}H\{^{19}F\}$ (upper) and $^{19}F\{^{1}H\}$ (bottom) NMR spectra for ***8*-012-CN**.

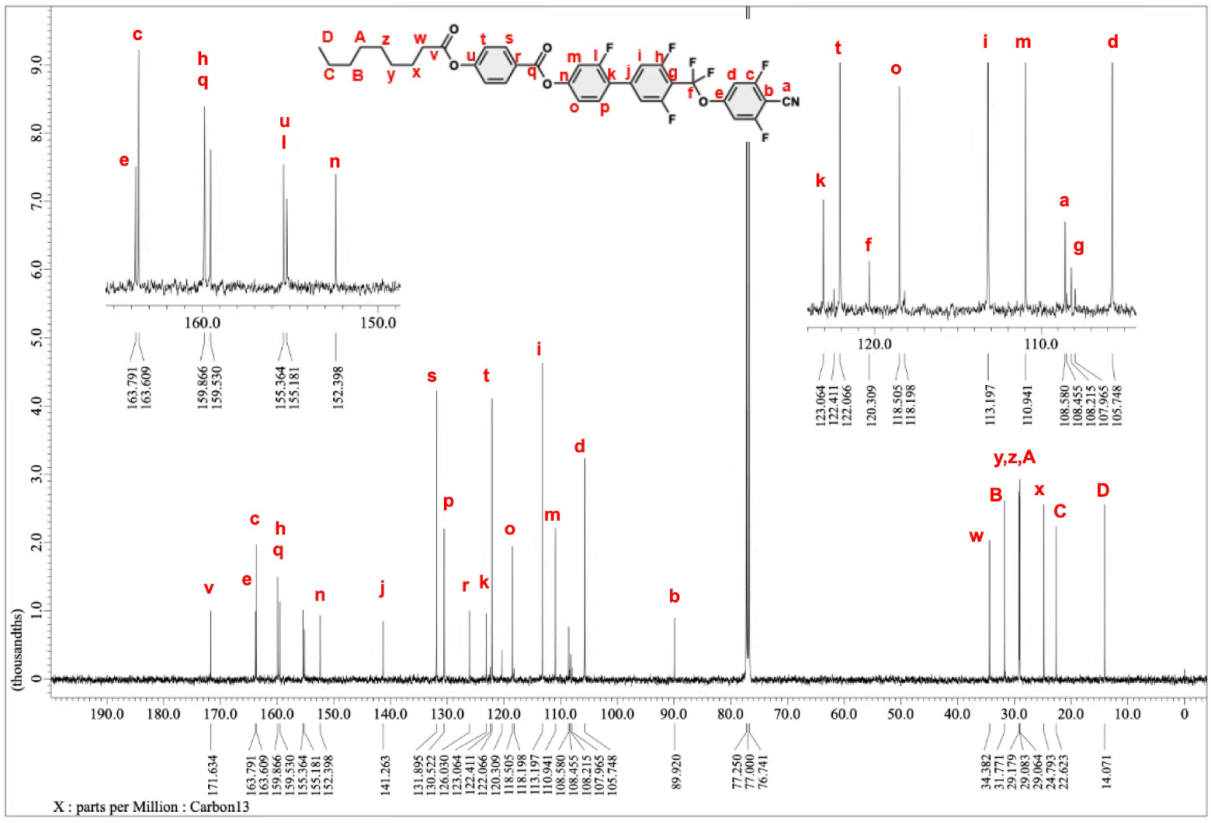

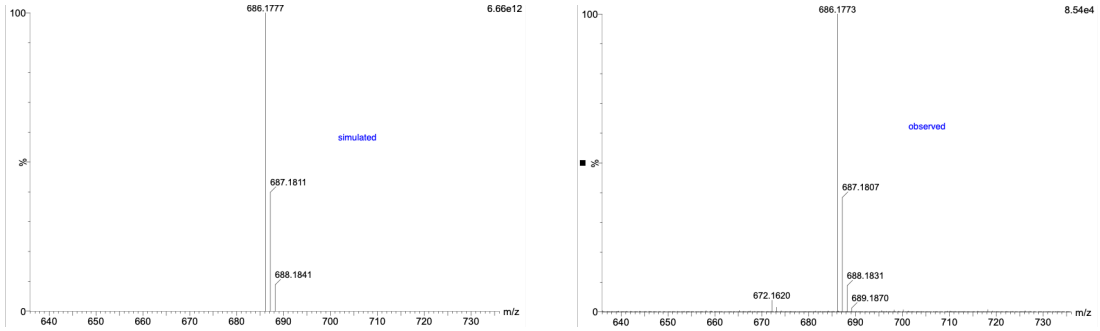

Supplementary Fig. 81 | $^{13}C\{^{1}H,^{19}F\}$NMR (upper) and HR-ESI-TOF-MS spectra (bottom) for ***8*-012-CN**.

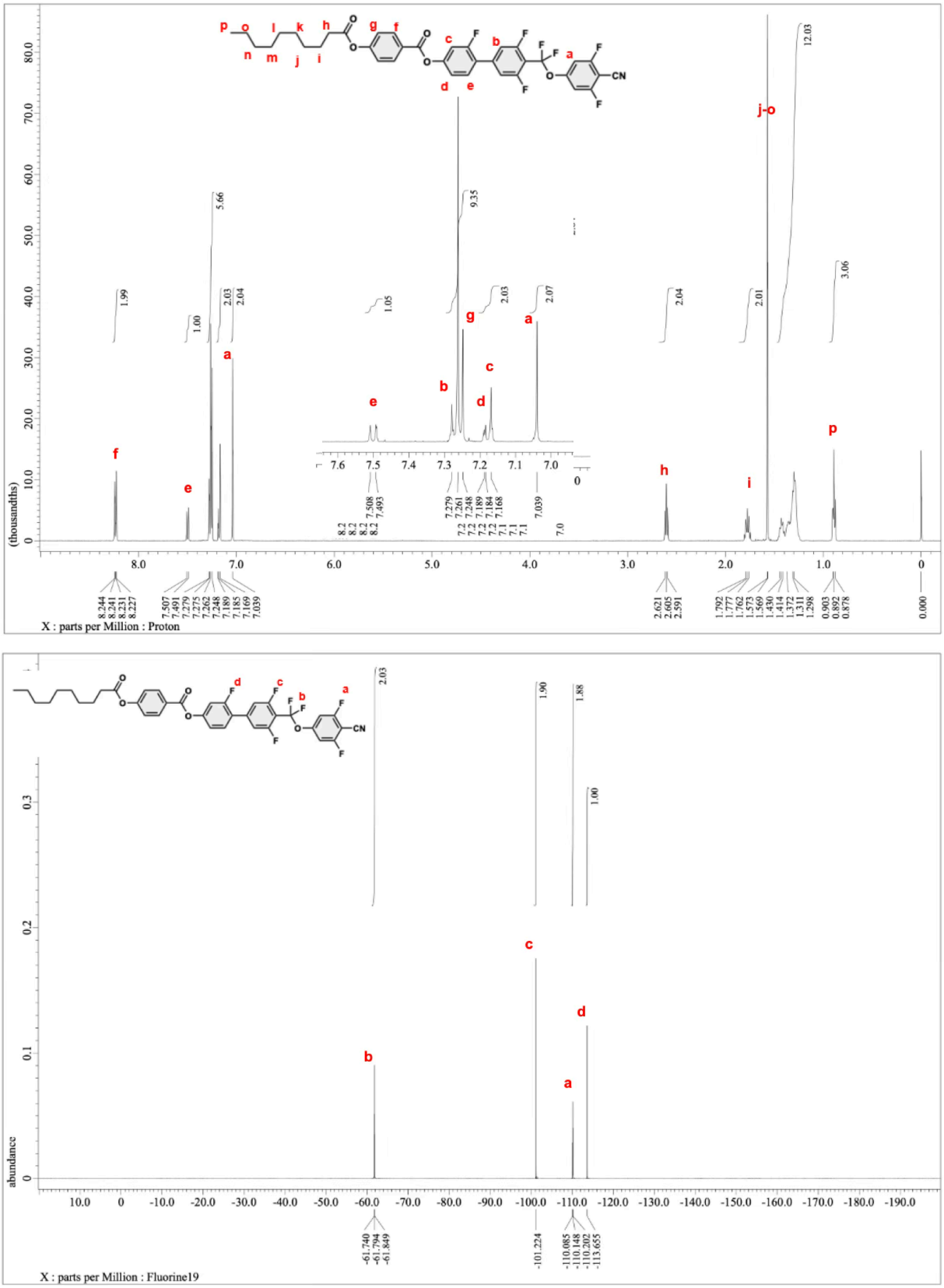

Supplementary Fig. 82 | $^{1}H\{^{19}F\}$ (upper) and $^{19}F\{^{1}H\}$ (bottom) NMR spectra for ***9*-012-CN**.

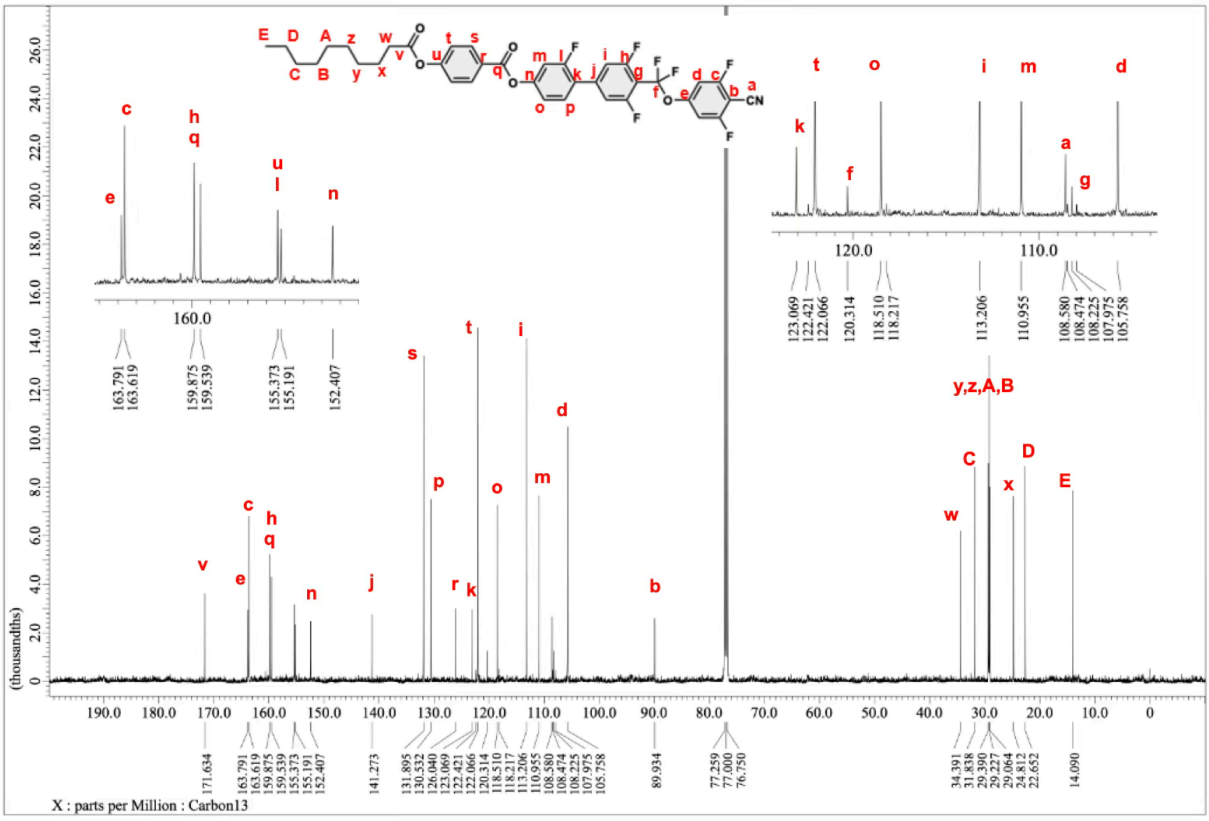

Supplementary Fig. 83 | $^{13}C\{^{1}H,^{19}F\}$NMR (upper) and HR-ESI-TOF-MS spectra (bottom) for ***9*-012-CN**.

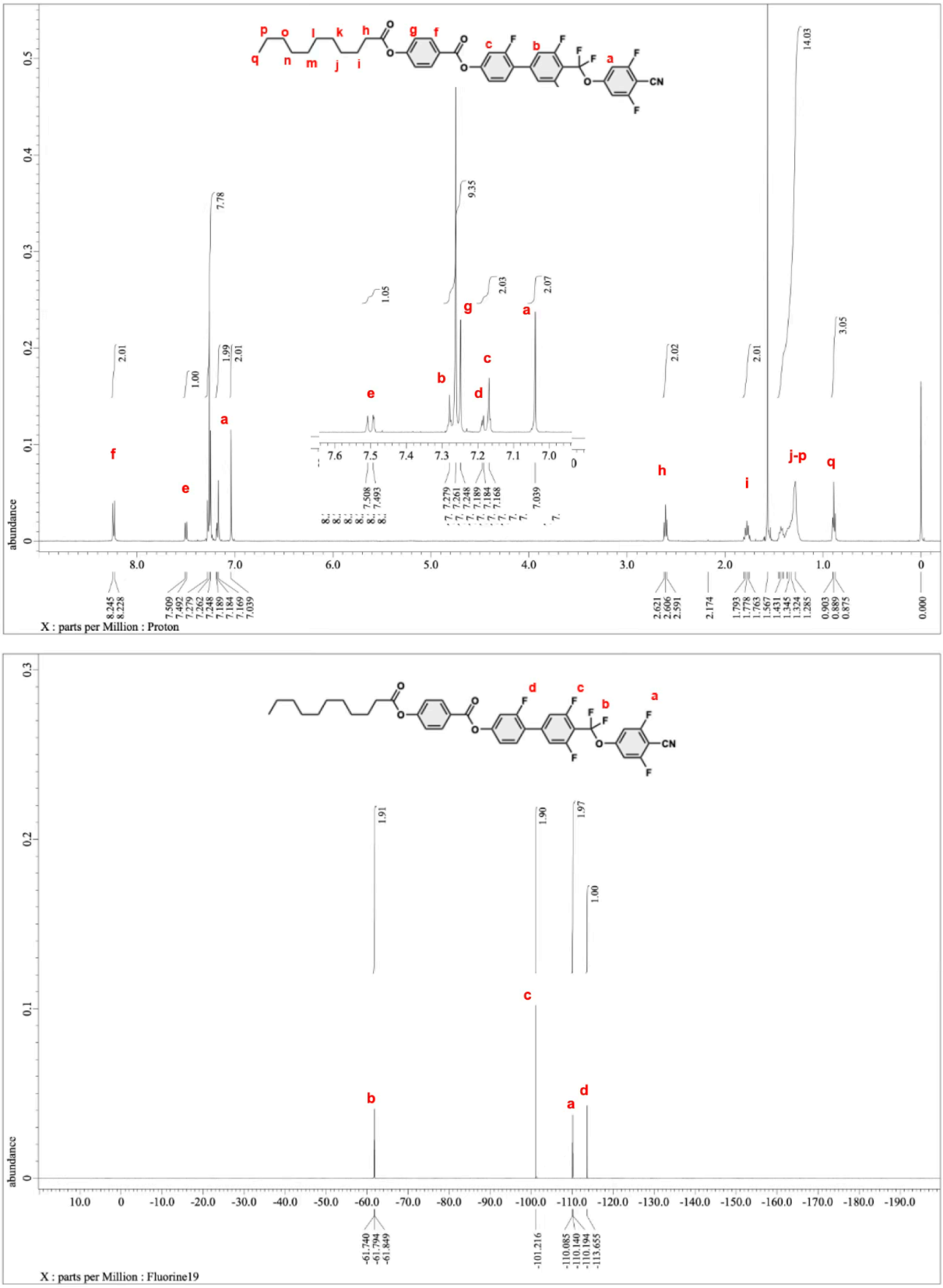

Supplementary Fig. 84 | $^{1}H\{^{19}F\}$ (upper) and $^{19}F\{^{1}H\}$ (bottom) NMR spectra for ***10*-012-CN**.

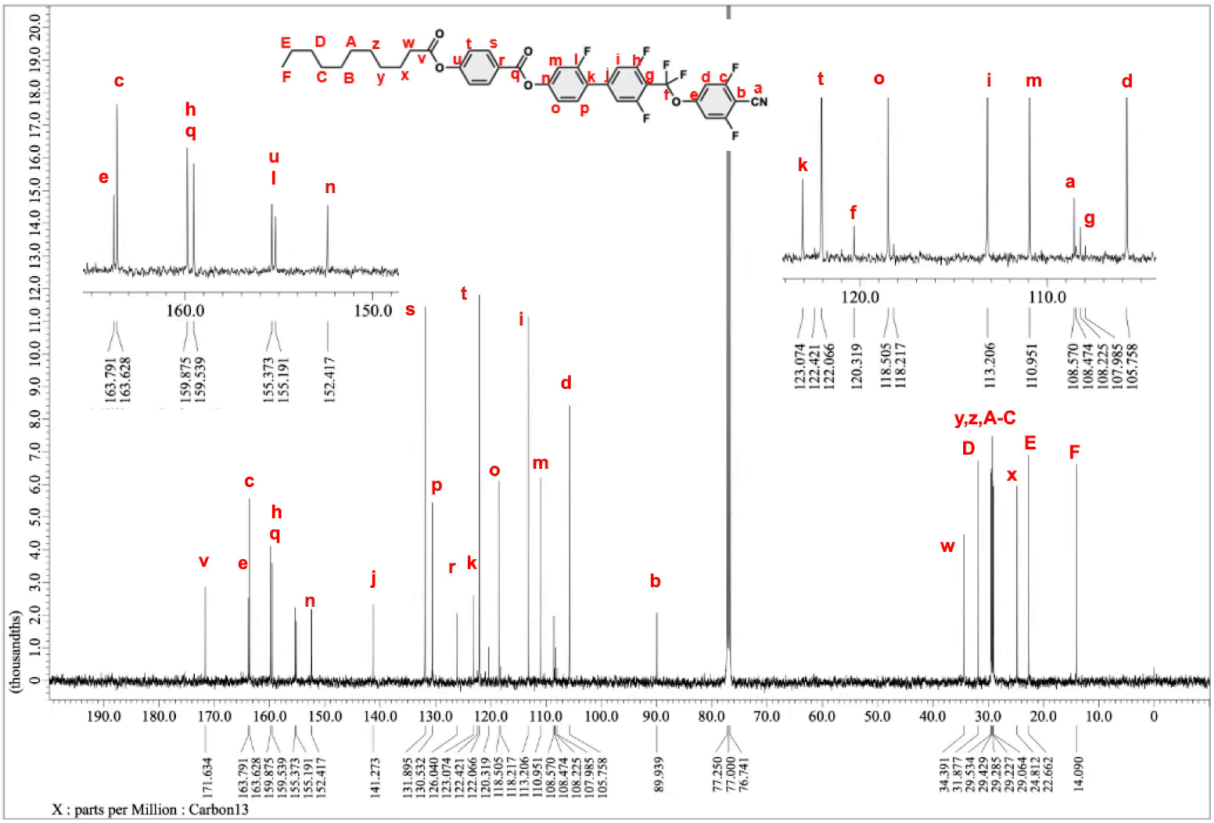

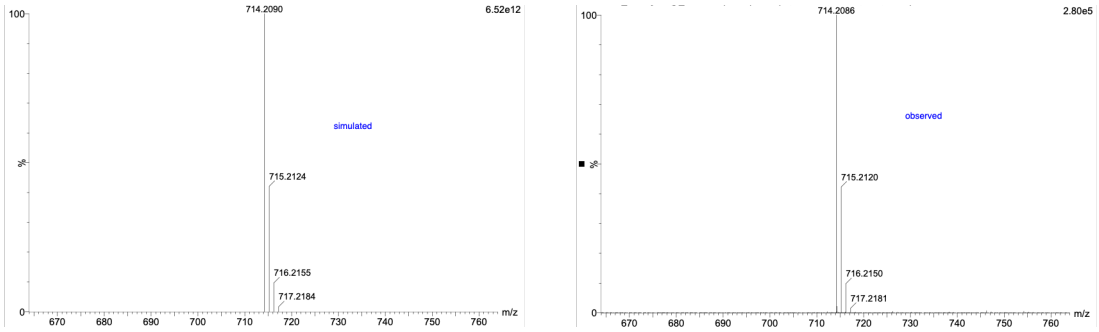

Supplementary Fig. 85 | $^{13}C\{^{1}H,^{19}F\}$NMR (upper) and HR-ESI-TOF-MS spectra (bottom) for ***10*-012-CN**.

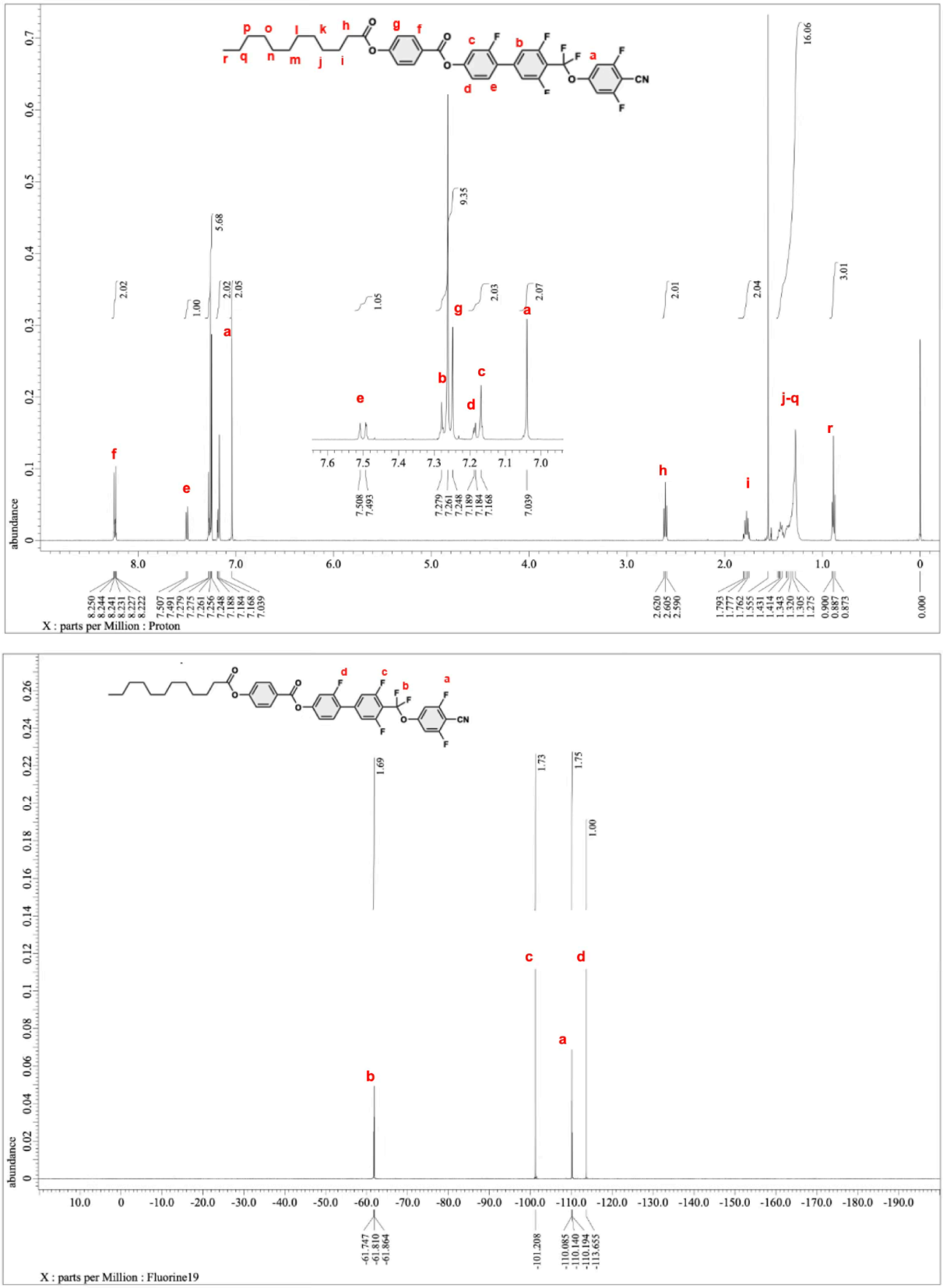

Supplementary Fig. 86 | $^{1}H\{^{19}F\}$ (upper) and $^{19}F\{^{1}H\}$ (bottom) NMR spectra for ***11*-012-CN**.

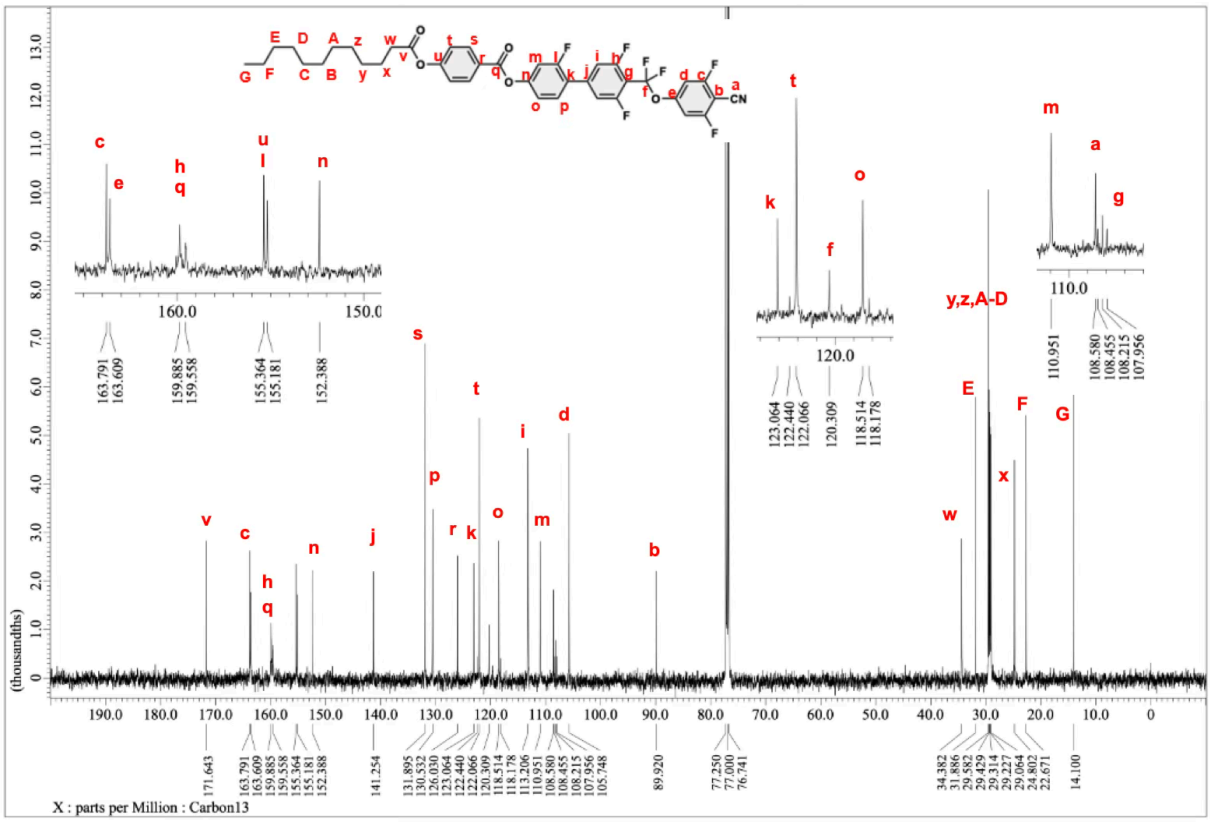

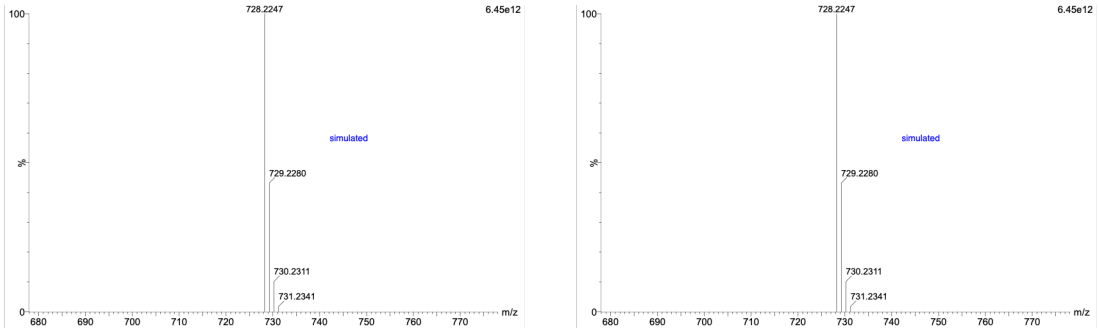

Supplementary Fig. 87 | $^{13}C\{^{1}H,^{19}F\}$NMR (upper) and HR-ESI-TOF-MS spectra (bottom) for ***11*-012-CN**.

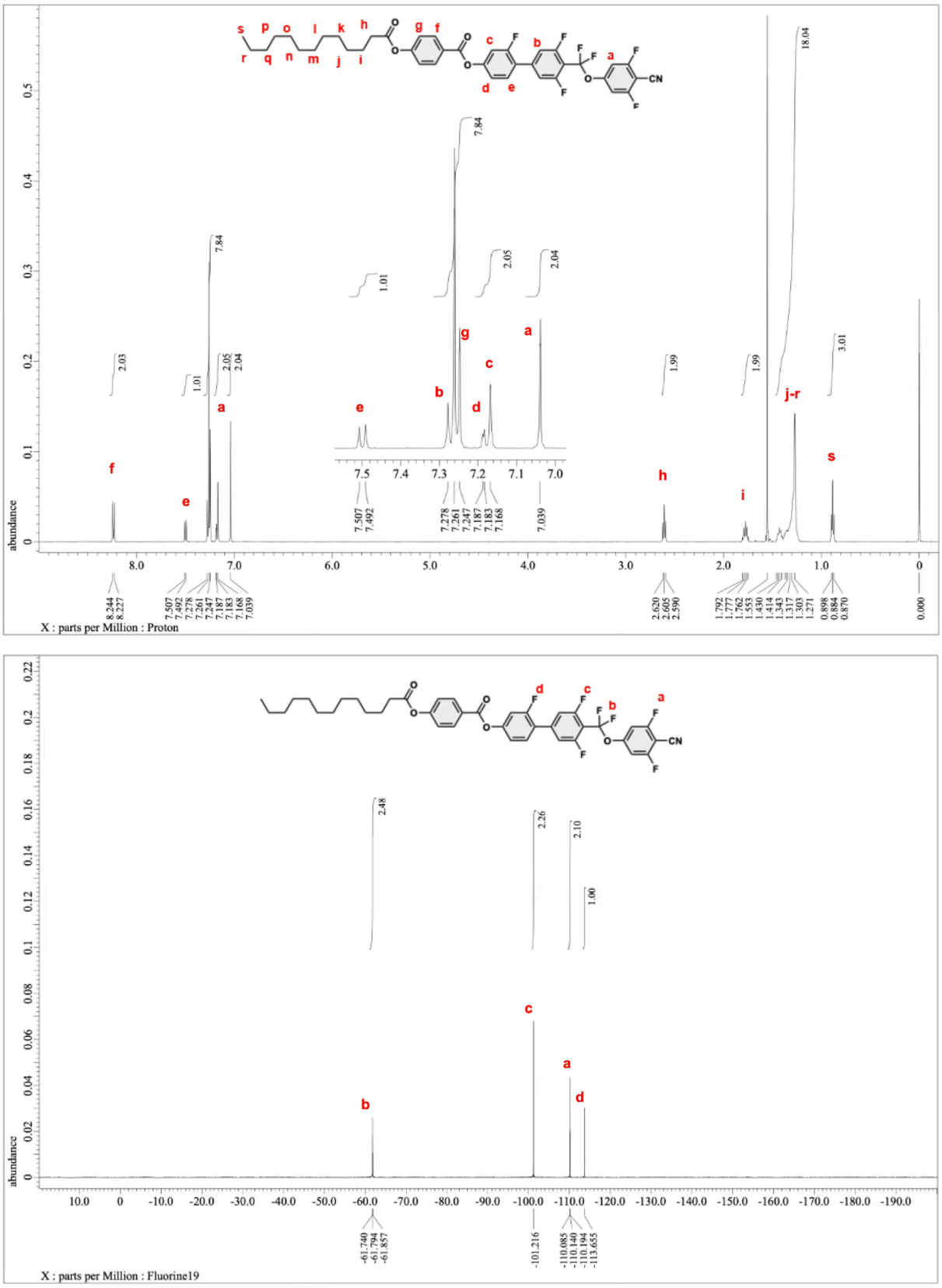

Supplementary Fig. 88 | $^{1}H\{^{19}F\}$ (upper) and $^{19}F\{^{1}H\}$ (bottom) NMR spectra for ***12*-012-CN**.

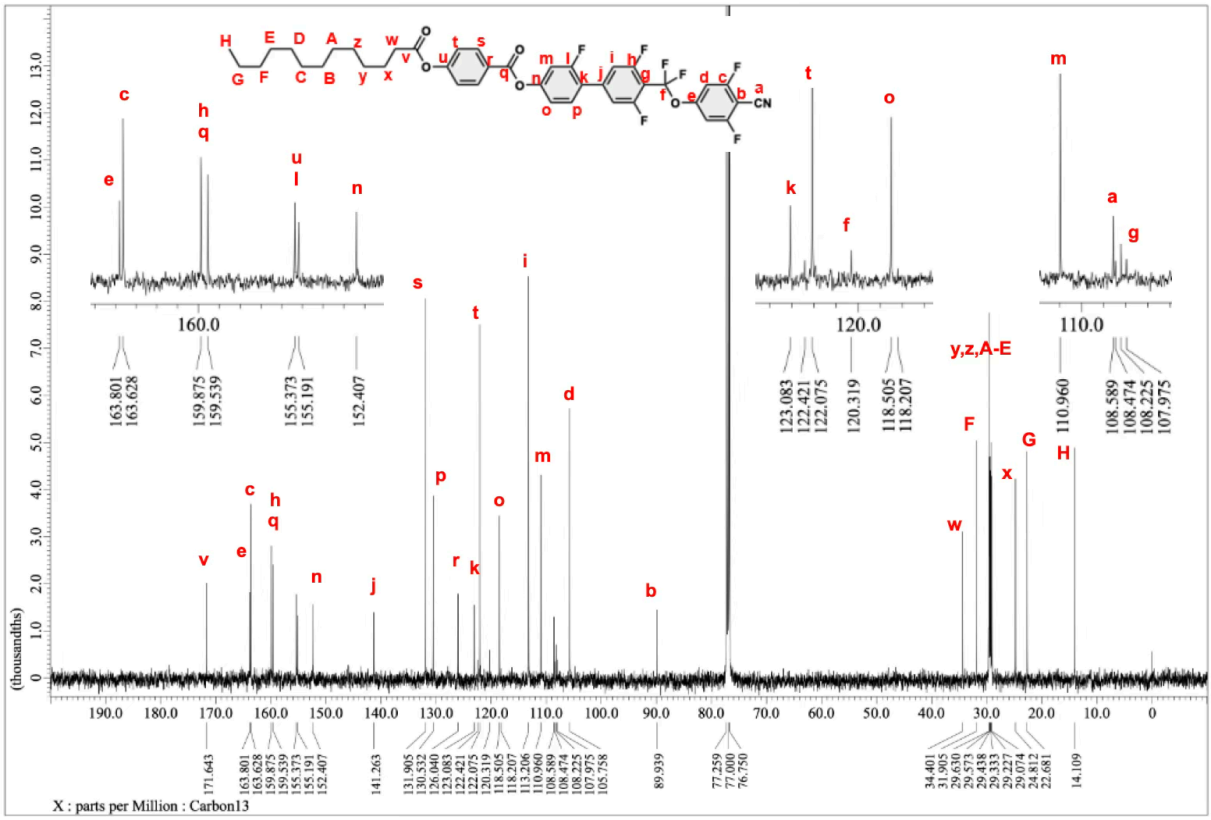

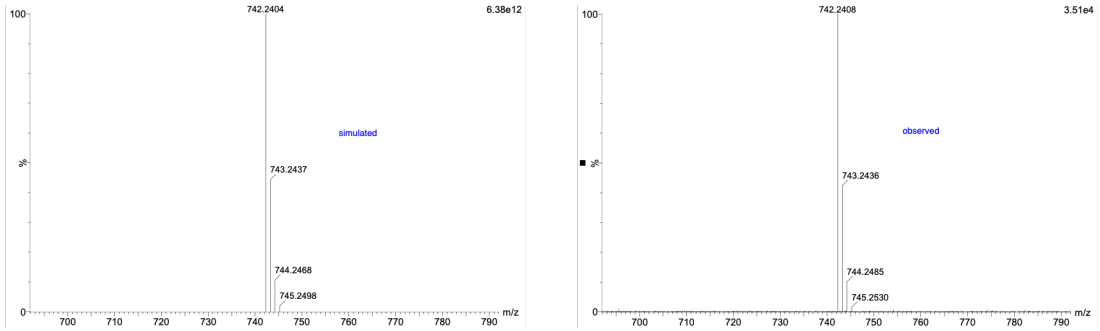

Supplementary Fig. 89 | $^{13}C\{^{1}H,^{19}F\}$NMR (upper) and HR-ESI-TOF-MS spectra (bottom) for ***12*-012-CN**.

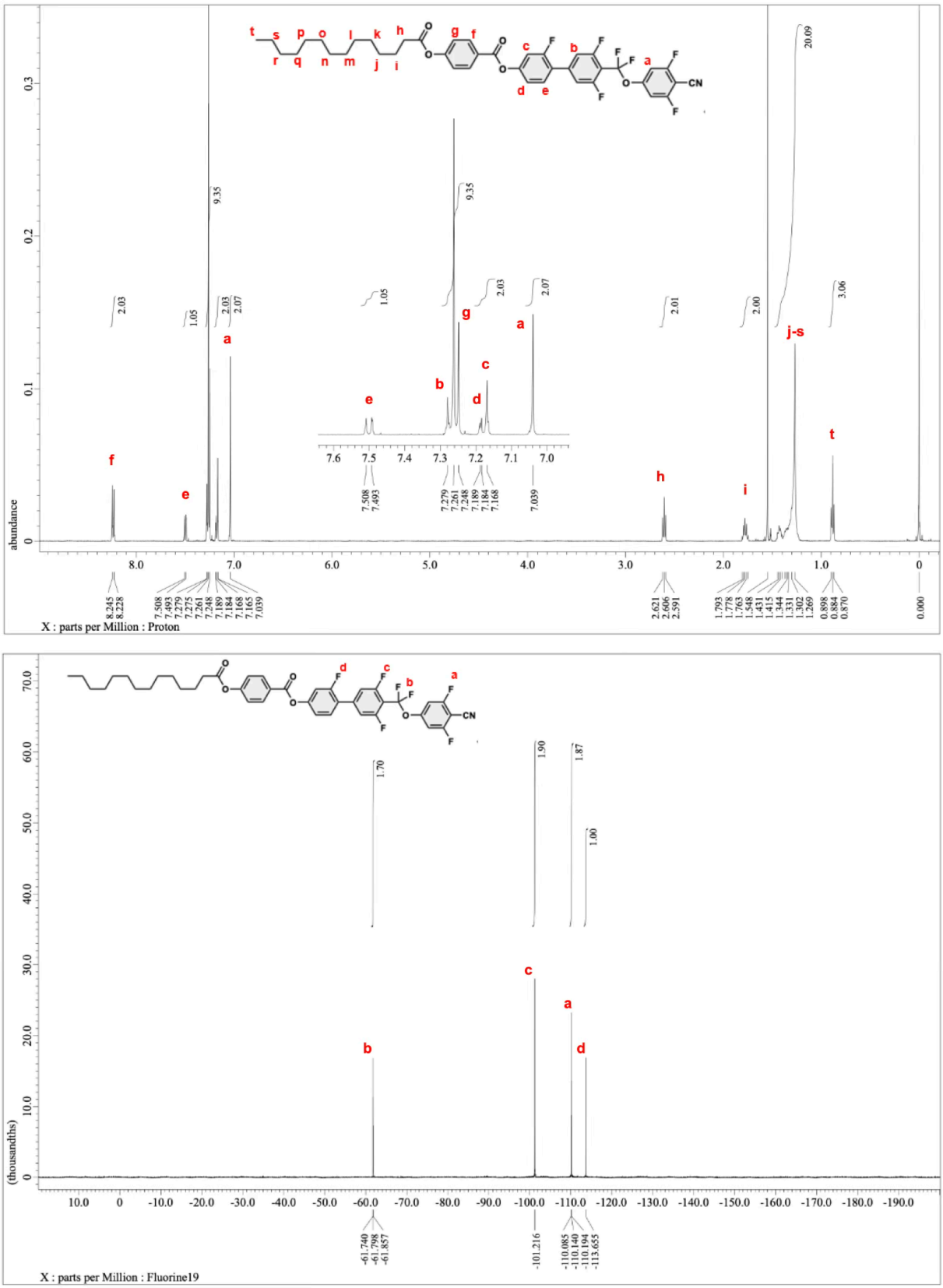

Supplementary Fig. 90 | $^{1}H\{^{19}F\}$ (upper) and $^{19}F\{^{1}H\}$ (bottom) NMR spectra for ***13*-012-CN**.

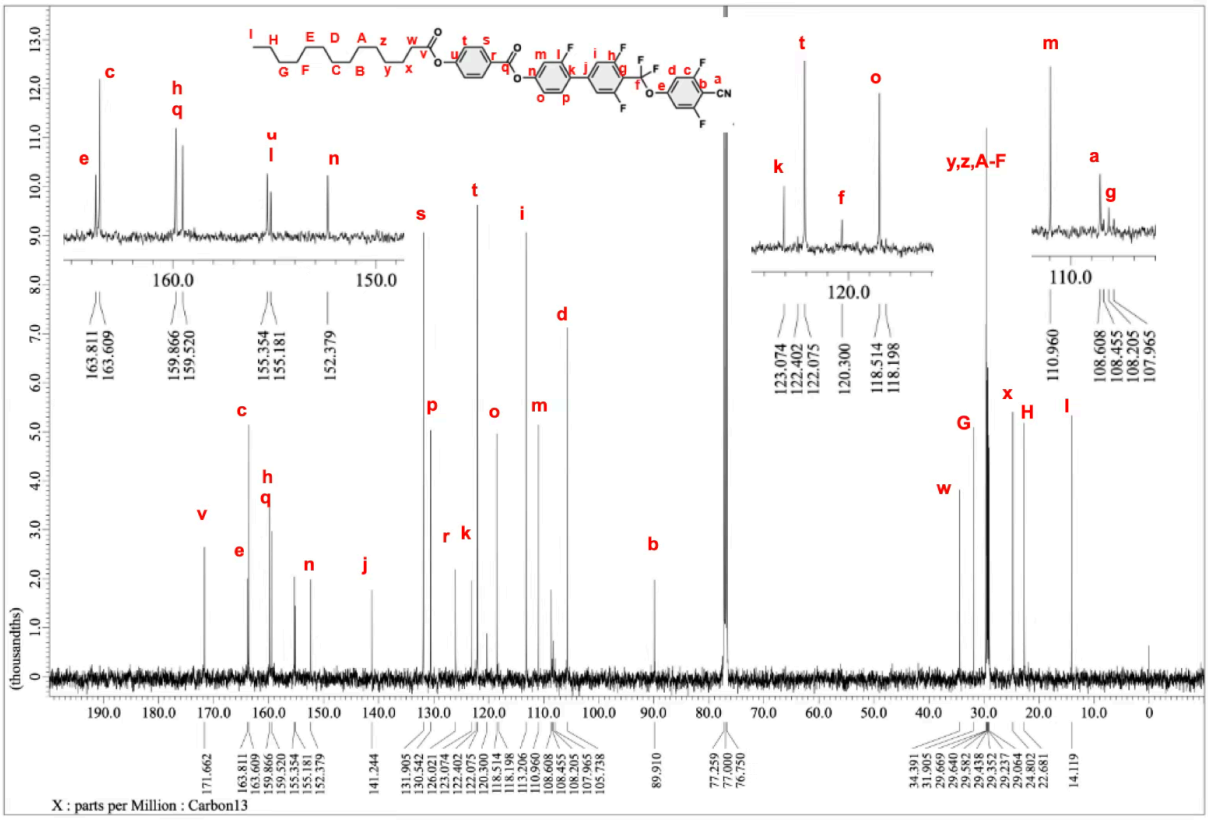

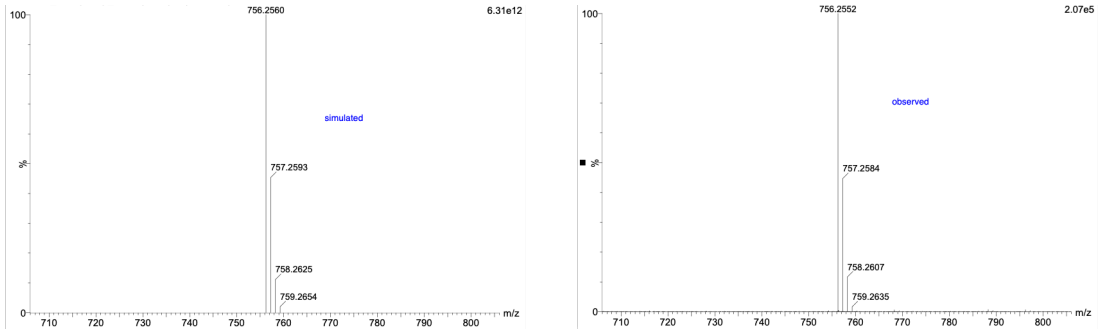

Supplementary Fig. 91 | $^{13}C\{1H,^{19}F\}$NMR (upper) and HR-ESI-TOF-MS spectra (bottom) for ***13*-012-CN**.

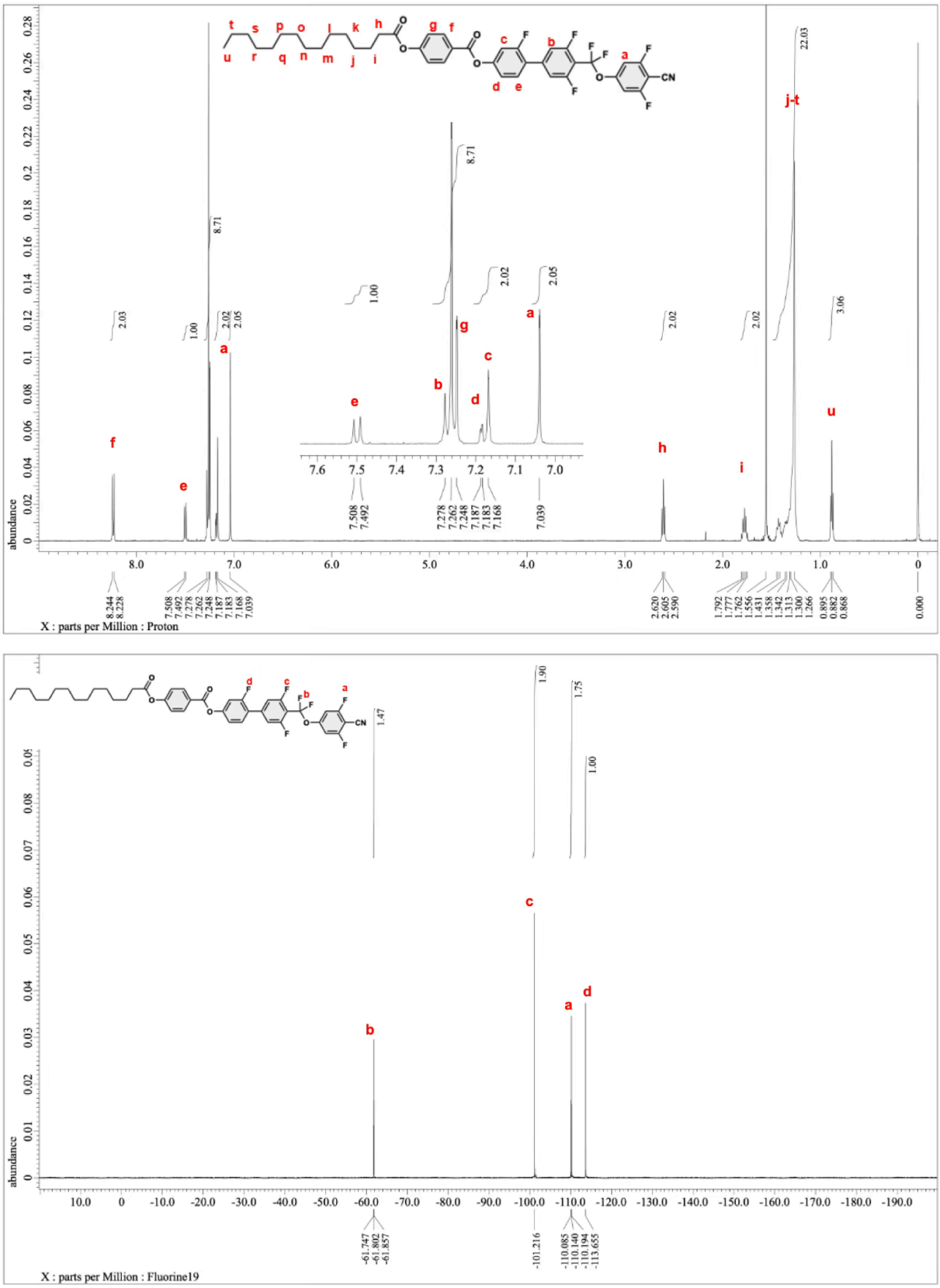

Supplementary Fig. 92 | $^{1}H\{^{19}F\}$ (upper) and $^{19}F\{^{1}H\}$ (bottom) NMR spectra for ***14*-012-CN**.

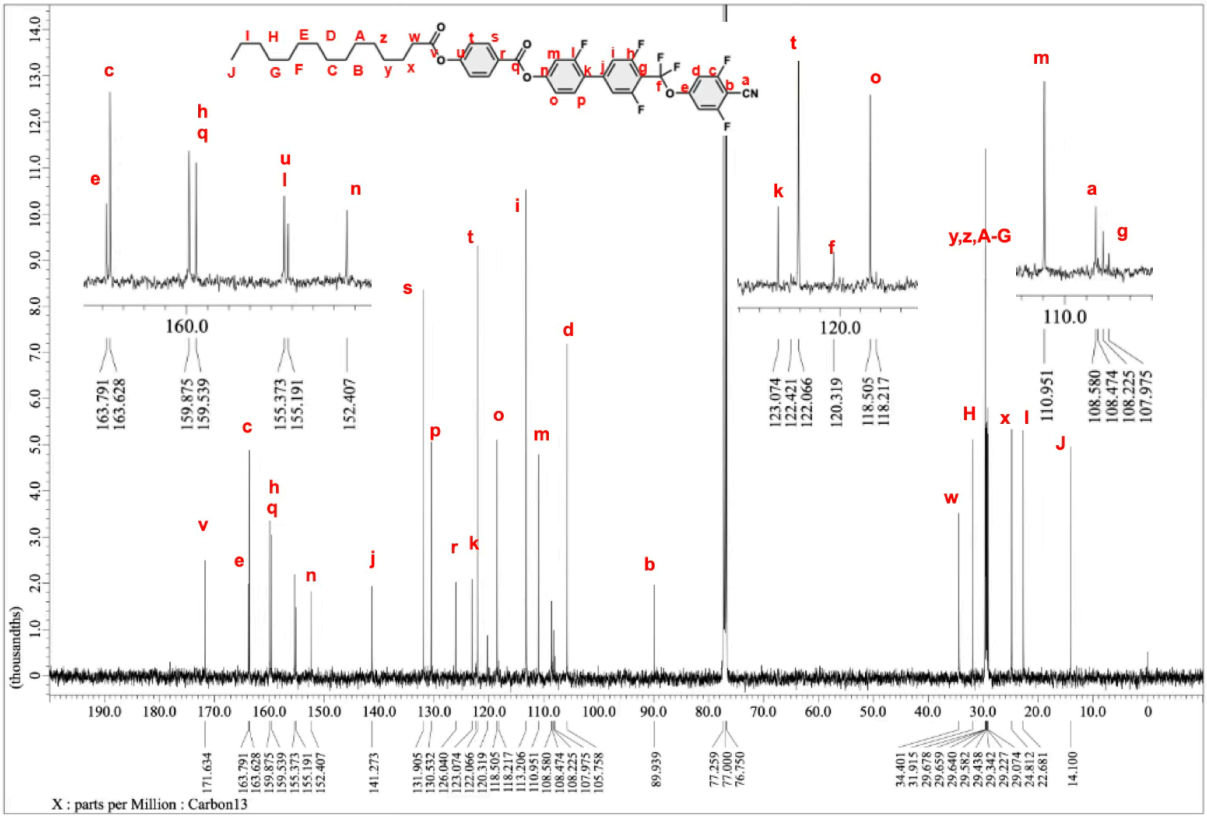

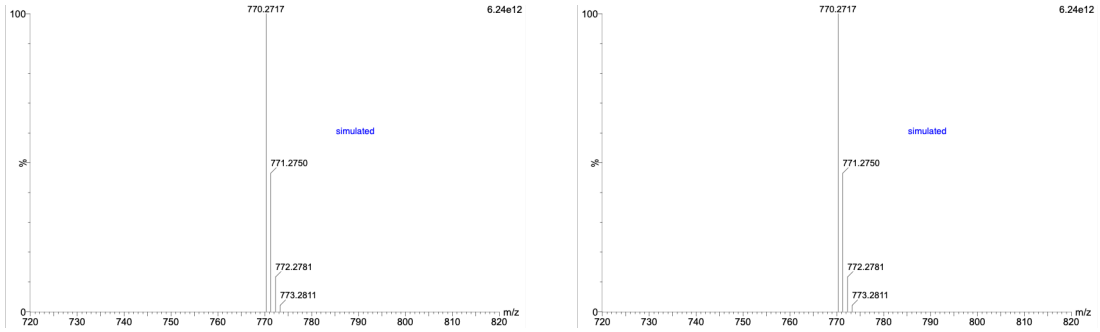

Supplementary Fig. 93 | $^{13}C\{^{1}H,^{19}F\}$NMR (upper) and HR-ESI-TOF-MS spectra (bottom) for ***14*-012-CN**.

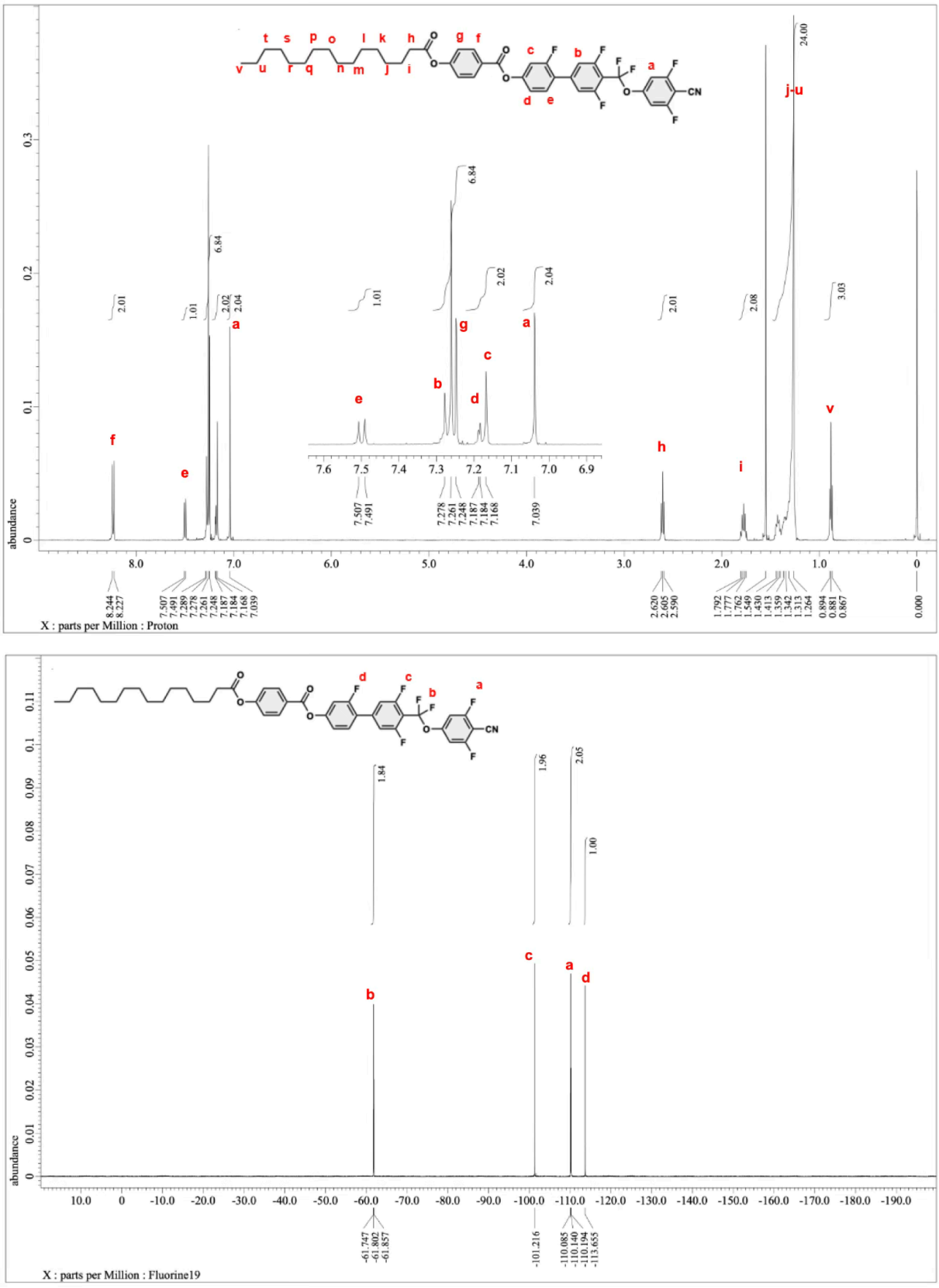

Supplementary Fig. 94 | $^{1}H\{^{19}F\}$ (upper) and $^{19}F\{^{1}H\}$ (bottom) NMR spectra for ***15*-012-CN**.

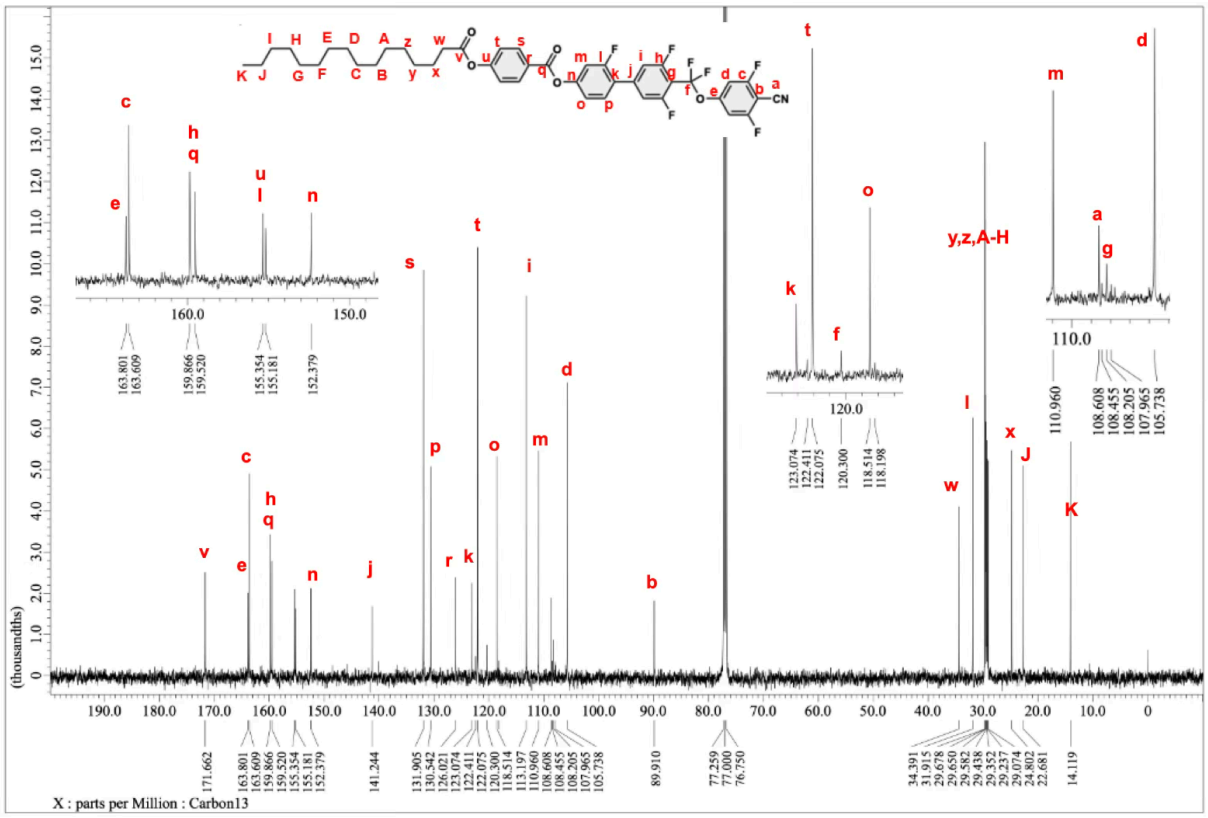

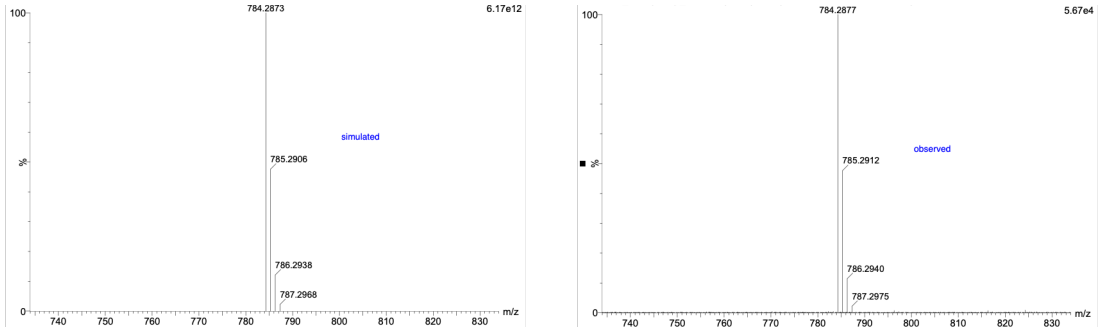

Supplementary Fig. 95 | $^{13}C\{1H,^{19}F\}$NMR (upper) and HR-ESI-TOF-MS spectra (bottom) for ***15*-012-CN**.

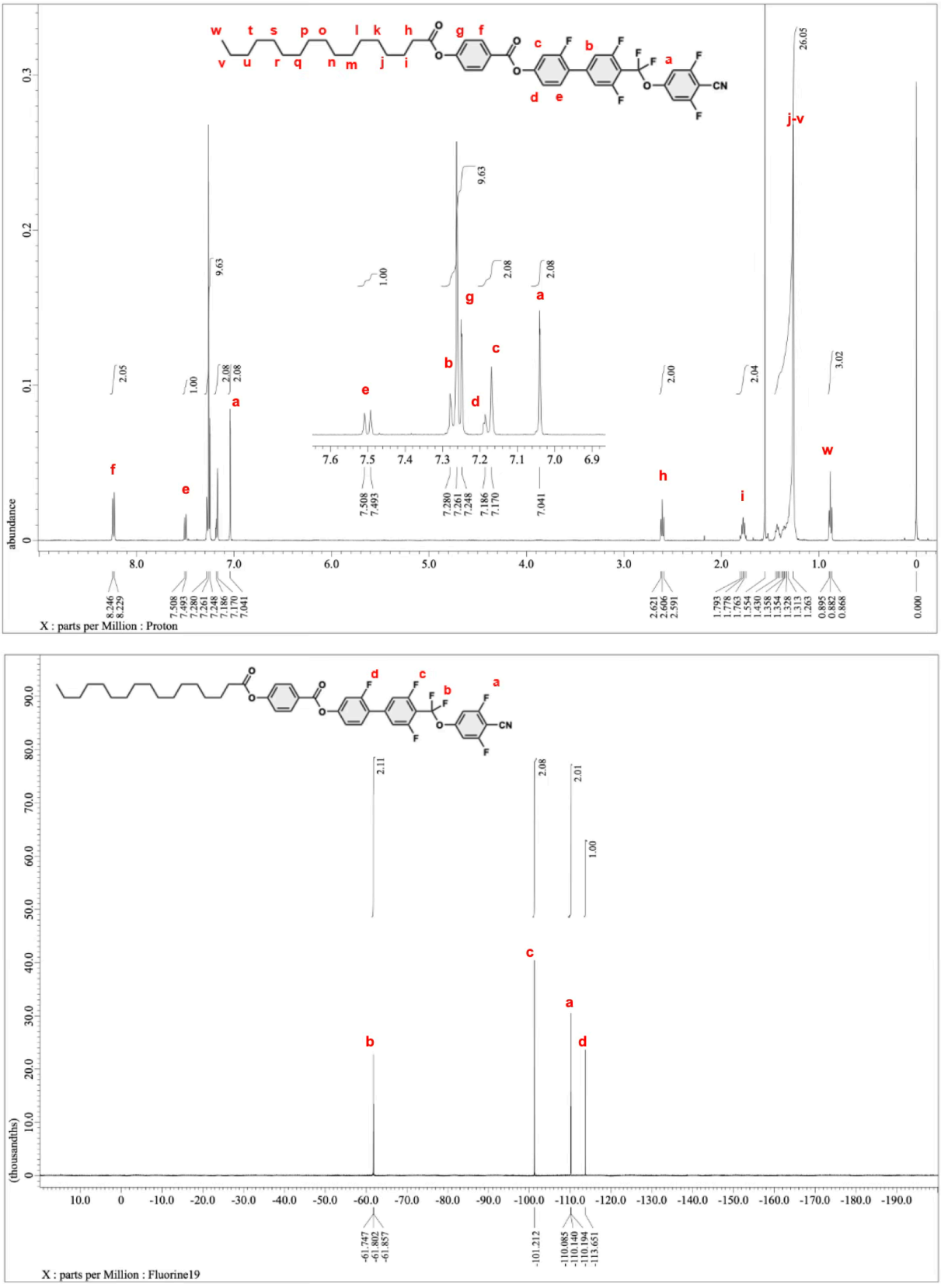

Supplementary Fig. 96 | $^{1}H\{^{19}F\}$ (upper) and $^{19}F\{^{1}H\}$ (bottom) NMR spectra for ***16*-012-CN**.

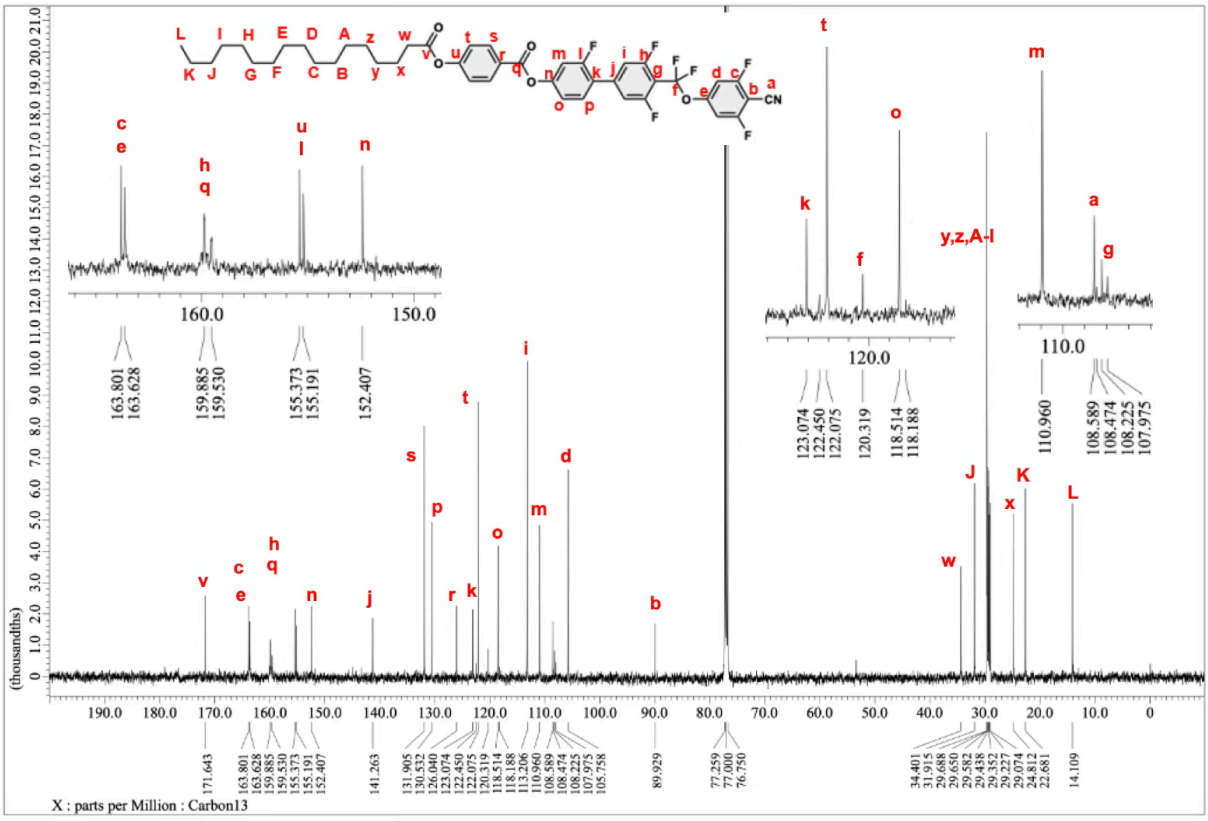

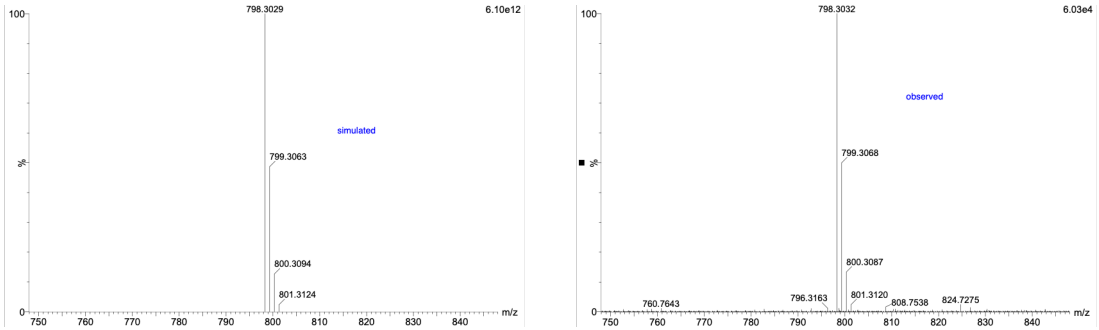

Supplementary Fig. 97 | $^{13}C\{^{1}H,^{19}F\}$NMR (upper) and HR-ESI-TOF-MS spectra (bottom) for ***16*-012-CN**.

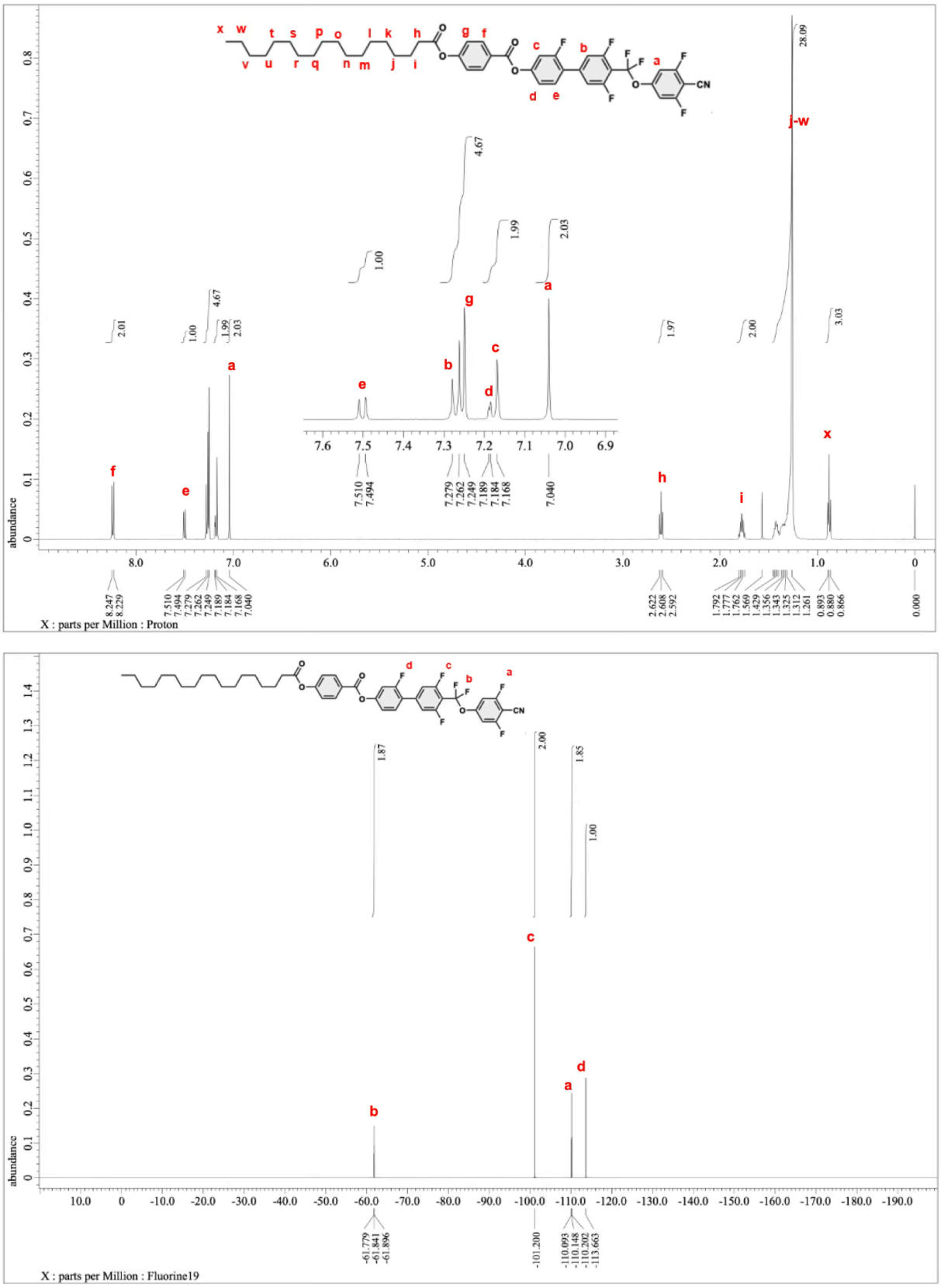

Supplementary Fig. 98 | $^{1}H\{^{19}F\}$ (upper) and $^{19}F\{^{1}H\}$ (bottom) NMR spectra for ***17*-012-CN**.

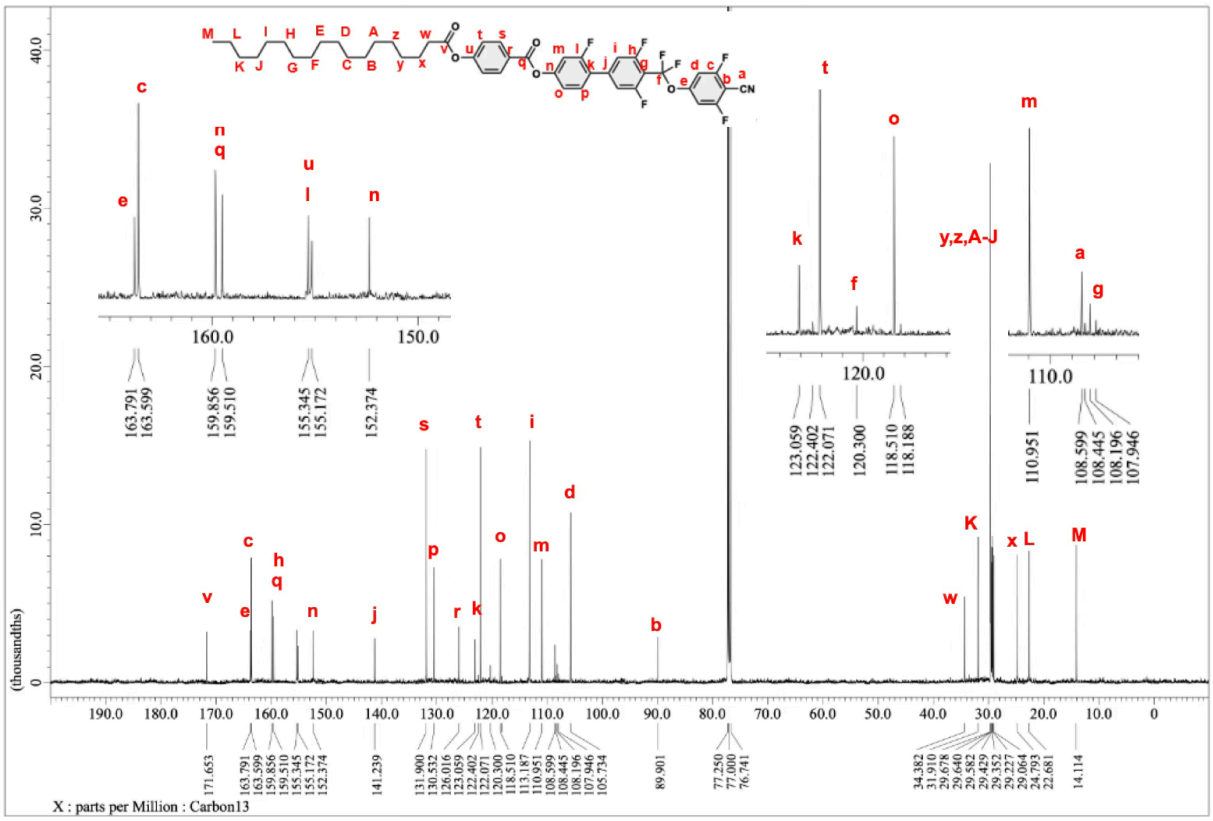

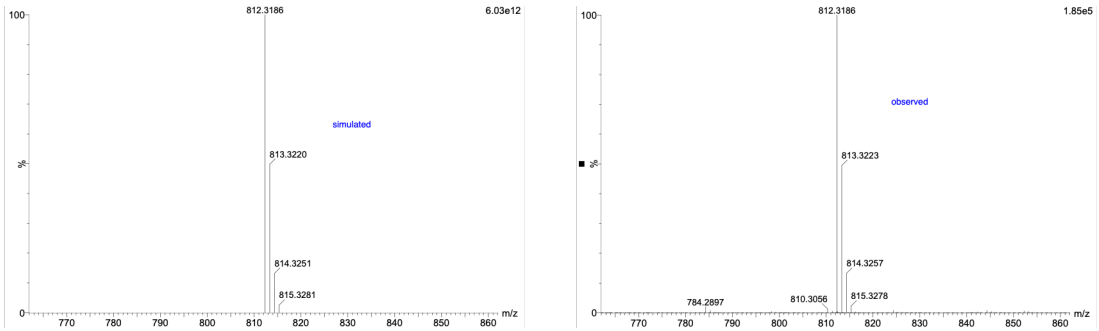

Supplementary Fig. 99 | $^{13}C\{1H,^{19}F\}$NMR (upper) and HR-ESI-TOF-MS spectra (bottom) for ***17*-012-CN**.

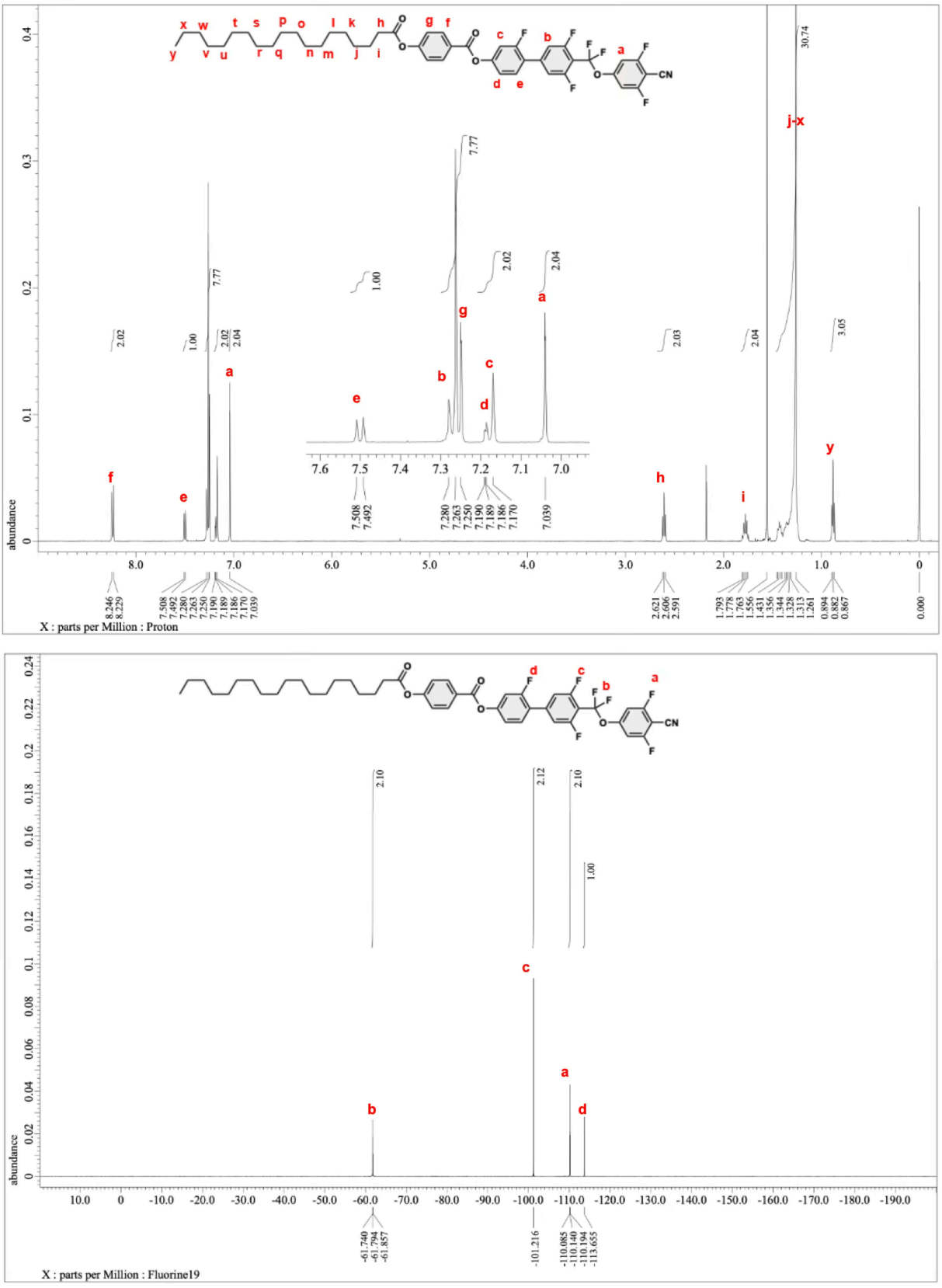

Supplementary Fig. 100 | $^{1}H\{^{19}F\}$ (upper) and $^{19}F\{^{1}H\}$ (bottom) NMR spectra for ***18*-012-CN**.

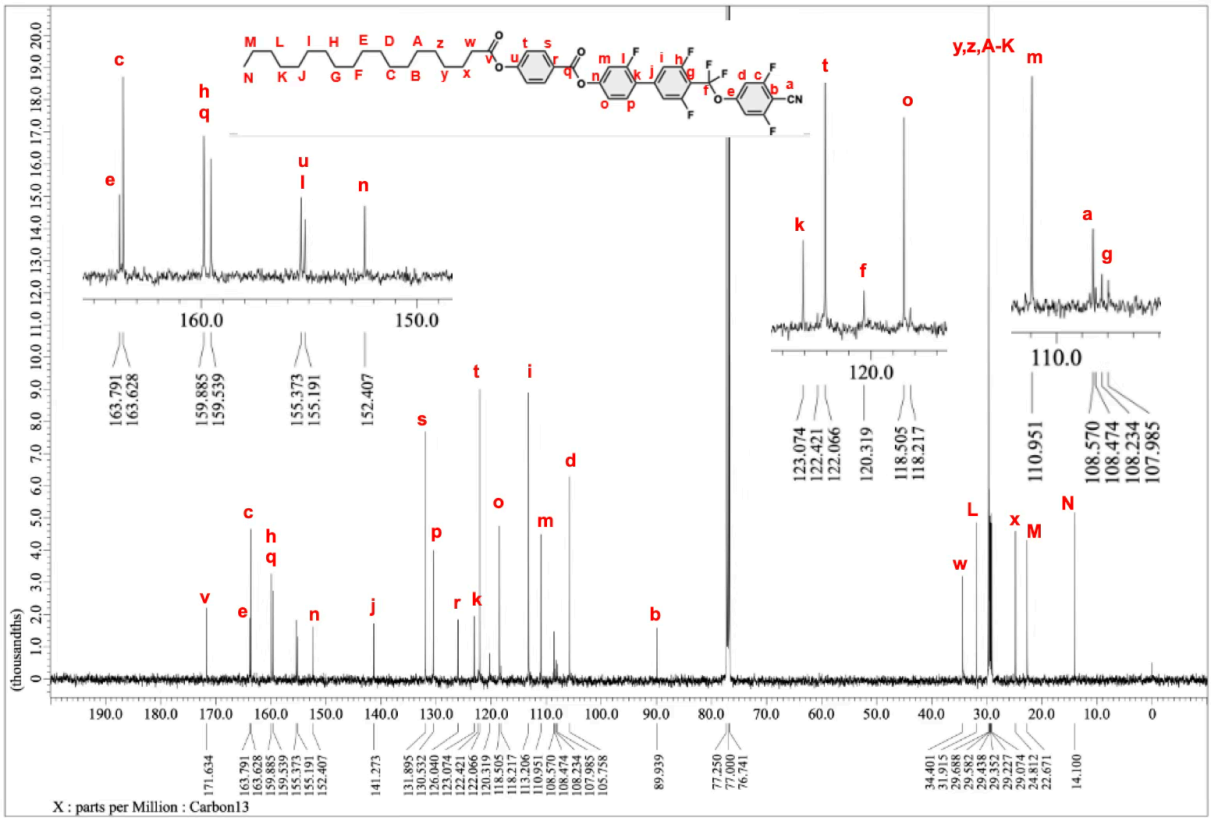

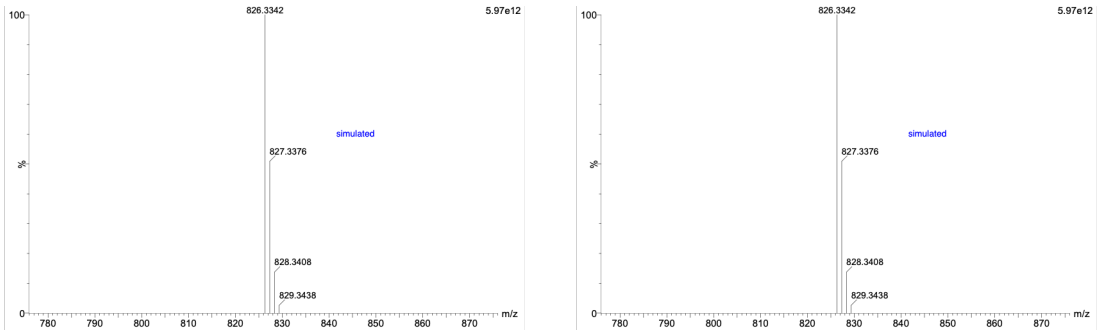

Supplementary Fig. 101 | $^{13}C\{^{1}H,^{19}F\}$NMR (upper) and HR-ESI-TOF-MS spectra (bottom) for ***18*-012-CN**.

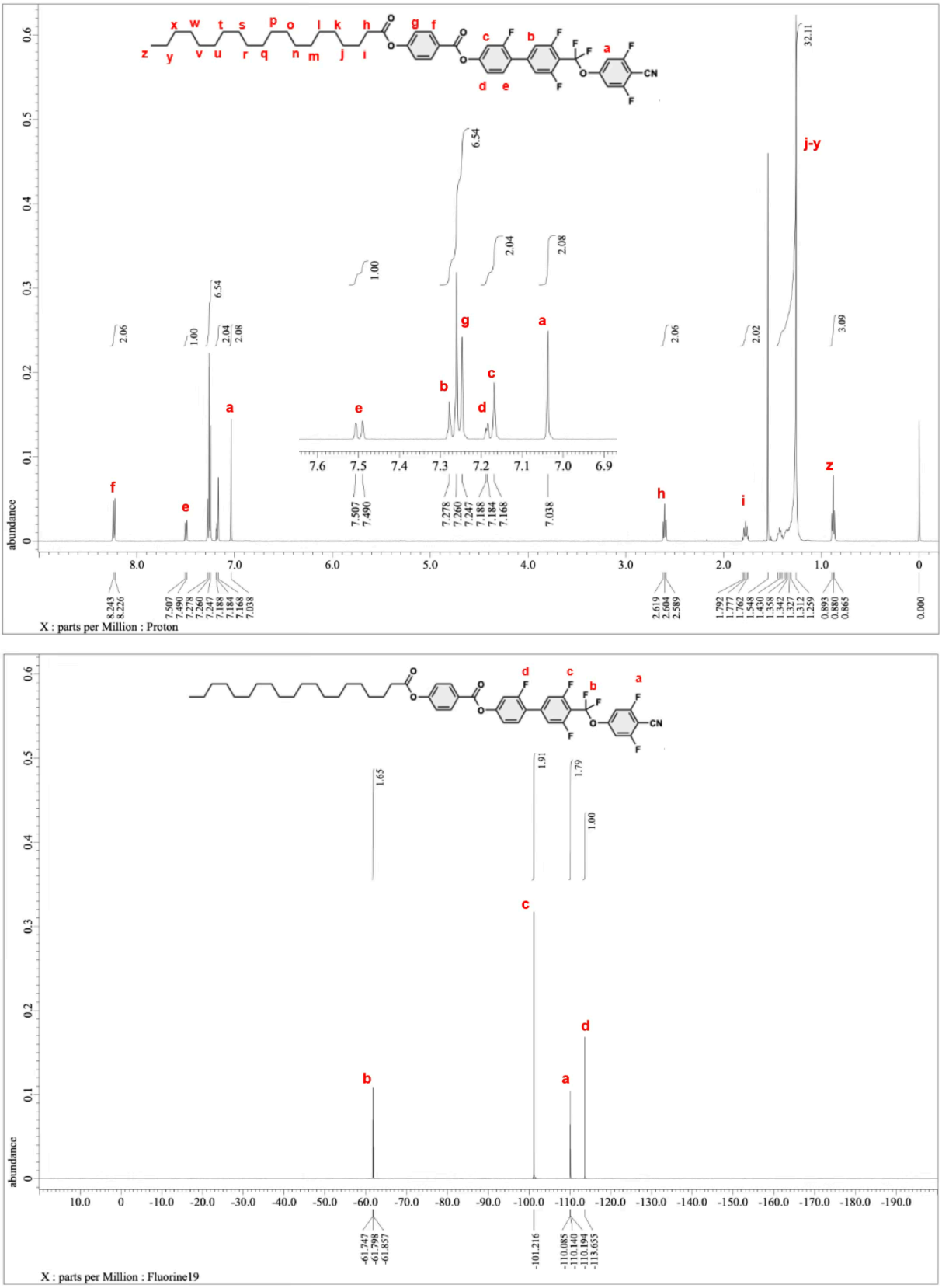

Supplementary Fig. 102 | $^{1}H\{^{19}F\}$ (upper) and $^{19}F\{^{1}H\}$ (bottom) NMR spectra for ***19*-012-CN**.

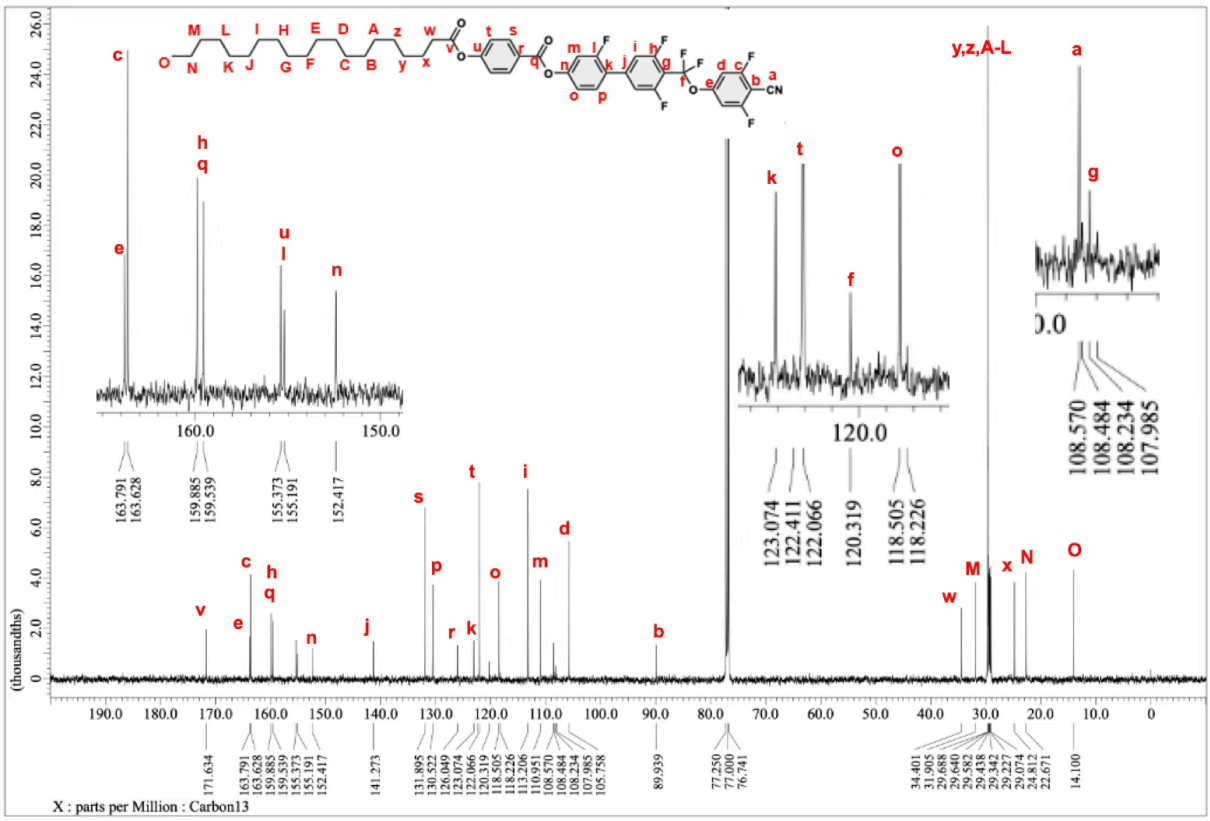

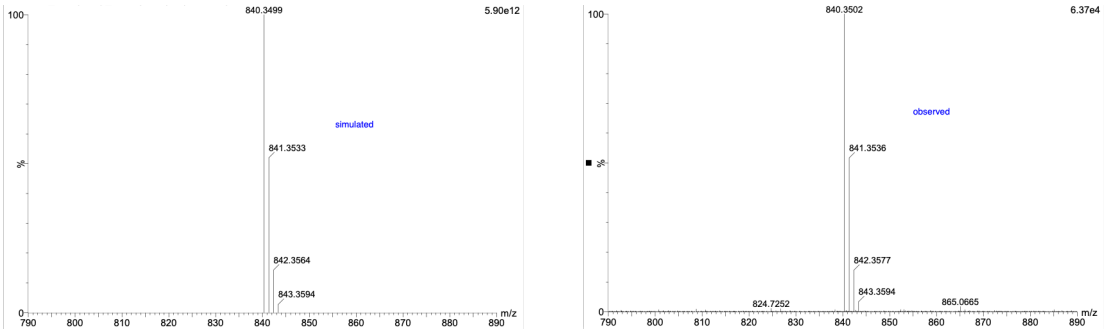

Supplementary Fig. 103 | $^{13}C\{^{1}H,^{19}F\}$NMR (upper) and HR-ESI-TOF-MS spectra (bottom) for ***19*-012-CN**.

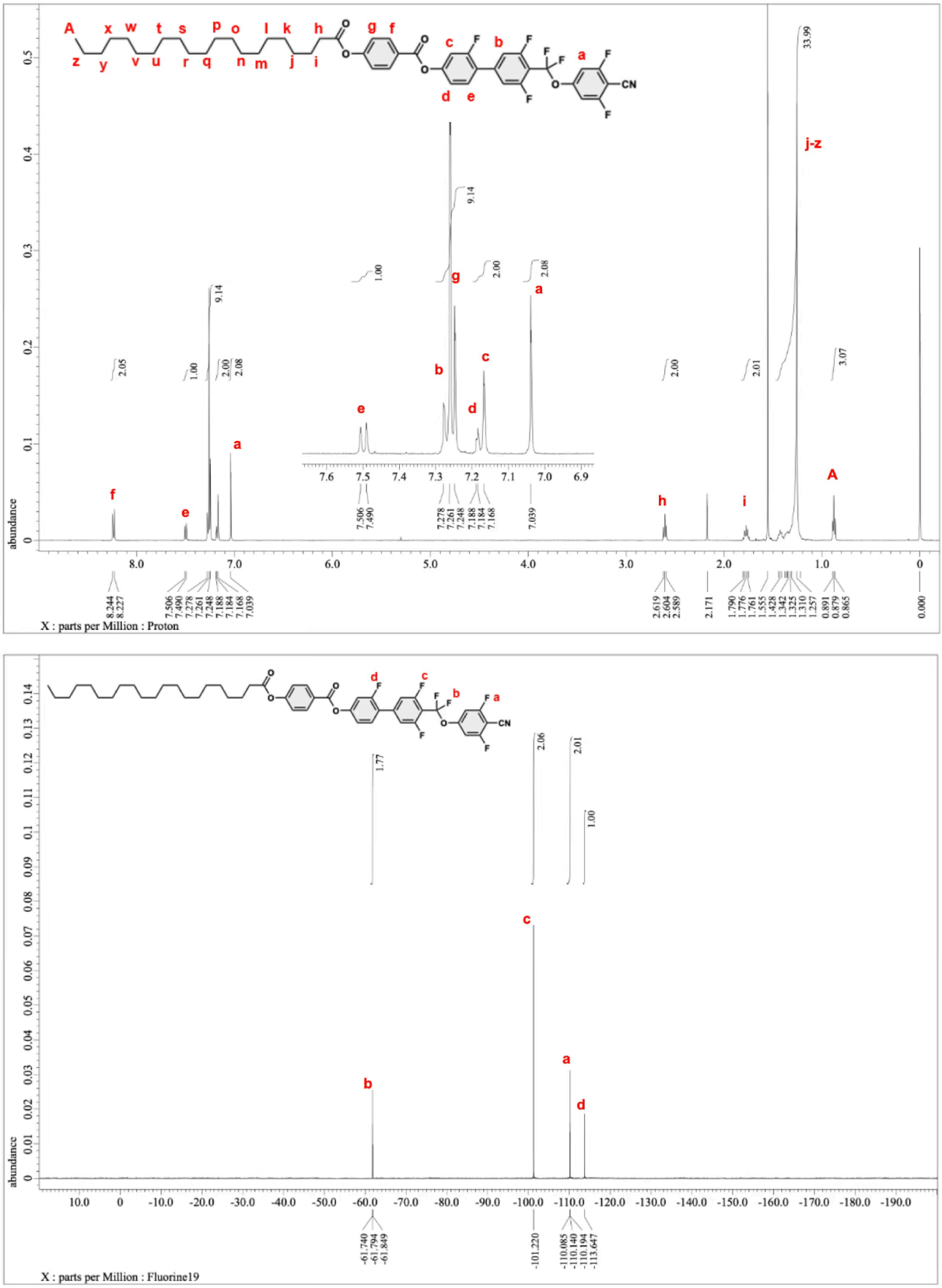

Supplementary Fig. 104 | $^{1}H\{^{19}F\}$ (upper) and $^{19}F\{^{1}H\}$ (bottom) NMR spectra for ***20*-012-CN**.

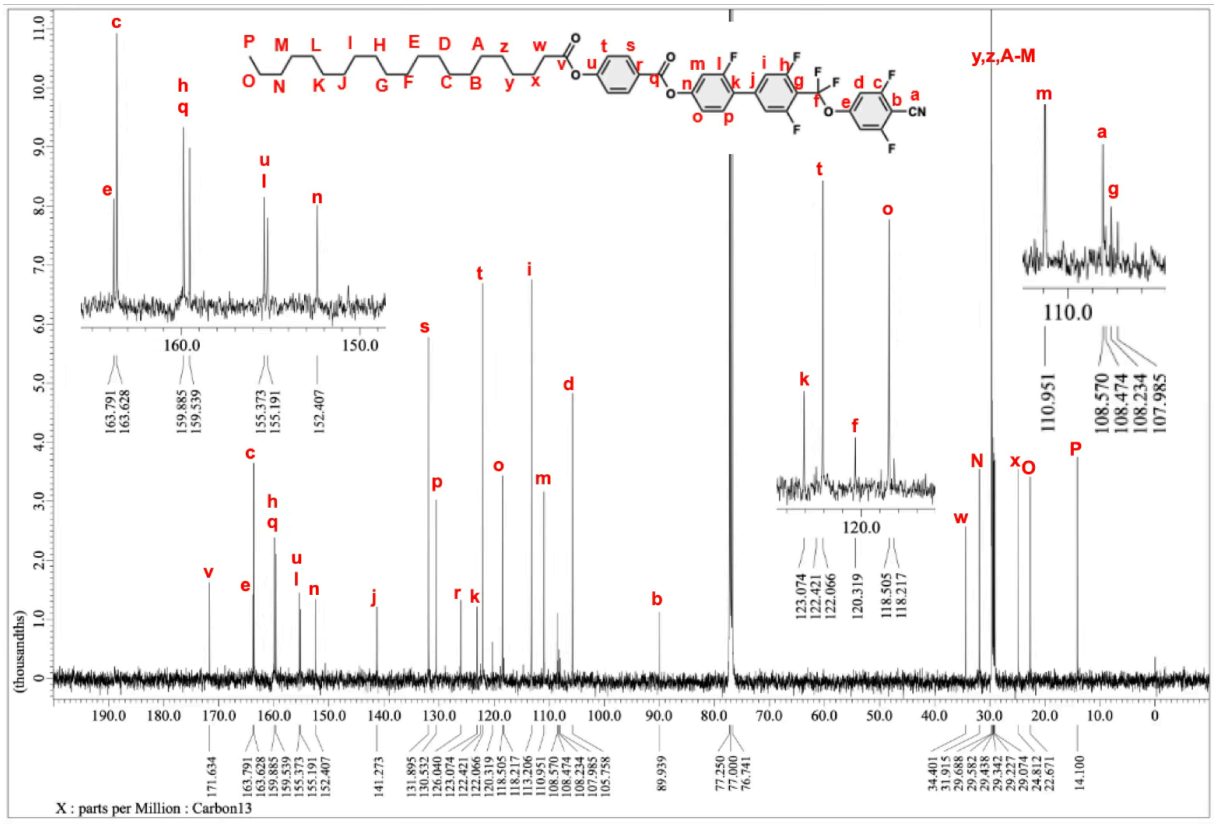

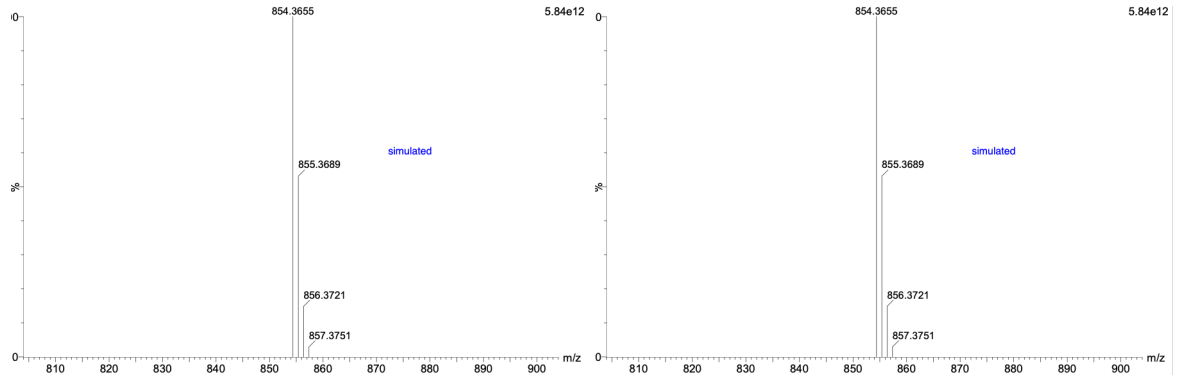

Supplementary Fig. 105 | $^{13}C\{^{1}H,^{19}F\}$NMR (upper) and HR-ESI-TOF-MS spectra (bottom) for ***20*-012-CN**.

Supplementary Tables (Table 1–11)

Supplementary Table 1 The molecular parameters of energy-minimized conformations calculated by DFT for ***n*-012-CN** (n = 1–20).

Entry	Vector X	Vector Y	Vector Z	μ (D)	β (deg)†
***1*-012-CN**	12.90393	3.8181	0.1162	13.457	16.49
***2*-012-CN**	13.113	3.7917	0.0079	13.650	16.13
***3*-012-CN**	13.2316	3.7365	0.0127	13.749	15.77
***4*-012-CN**	13.2999	3.8148	0.0547	13.836	16.01
***5*-012-CN**	13.3289	3.7706	0.0738	13.852	15.80
***6*-012-CN**	13.3591	3.8955	0.0491	13.916	16.26
***7*-012-CN**	13.3624	3.8648	0.032	13.910	16.13
***8*-012-CN**	-13.3798	-3.9846	-0.1333	13.961	16.59
***9*-012-CN**	-13.3729	-3.9353	-0.1915	13.941	16.42
***10*-012-CN**	-13.3663	-4.0544	-0.5499	13.979	17.02
***11*-012-CN**	-13.3514	-3.9696	-0.6882	13.946	16.79
***12*-012-CN**	-13.3579	-3.9565	-1.4045	14.002	17.45
***13*-012-CN**	13.3402	-3.8523	1.5402	13.970	17.28
***14*-012-CN**	13.3277	-3.8703	1.9278	14.012	17.97
***15*-012-CN**	13.31	-3.6992	2.112	13.975	17.75
***16*-012-CN**	13.3056	-3.5398	2.5441	14.001	18.14
***17*-012-CN**	13.2849	-3.49	2.5629	13.973	18.05
***18*-012-CN**	13.2983	-3.6832	2.5188	14.027	18.55
***19*-012-CN**	13.2819	-3.6086	2.5629	14.000	18.43
***20*-012-CN**	-13.2614	3.7443	2.6528	14.033	19.09

† An angle between the permanent dipole moment (μ) and long molecular axis.

Supplementary Table 2 Observed and calculated *d*-spacings and lattice parameters at different temperatures for ***9*-012-CN**.

T (°C)	(*hk*)	$d_{obs.}$ (nm)	$d_{calc.}$ (nm)	*a* (nm)	*b* (nm)	*γ* (°)
36	(02)	1.864	1.865	5.12	3.73	90
	(12)	1.751	1.752			
	(11)	3.013	3.015			
	(21)	2.109	2.111			
	(20)	2.560	2.560			

Supplementary Table 3 Observed and calculated *d*-spacings and lattice parameters at different temperatures for ***10*-012-CN**.

T (°C)	(*hk*)	$d_{obs.}$ (nm)	$d_{calc.}$ (nm)	*a* (nm)	*b* (nm)	*γ* (°)
54	(02)	1.991	1.991	5.38	3.98	90
	(12)	1.864	1.867			
	(11)	3.200	3.200			
	(21)	2.225	2.228			
	(20)	2.688	2.688			

Supplementary Table 4 Observed and calculated *d*-spacings and lattice parameters at different temperatures for ***11*-012-CN**.

T (°C)	(*hk*)	$d_{obs.}$ (nm)	$d_{calc.}$ (nm)	*a* (nm)	*b* (nm)	*γ* (°)
64	(02)	2.185	2.185	5.98	4.37	90
	(12)	2.052	2.052			
	(11)	3.526	3.527			
	(21)	–	2.466			
	(20)	2.988	2.988			
62	(02)	2.181	2.181	5.92	4.36	90
	(12)	2.046	2.047			
	(11)	3.509	3.511			
	(21)	–	2.448			
	(20)	2.958	2.958			
60	(02)	2.153	2.153	5.69	4.31	90
	(12)	2.013	2.014			
	(11)	3.429	3.434			
	(21)	–	2.374			
	(20)	2.845	2.845			
58	(02)	2.141	2.141	5.60	4.28	90
	(12)	2.000	2.000			
	(11)	3.397	3.402			
	(21)	–	2.345			
	(20)	2.802	2.802			
56	(02)	2.122	2.122	5.50	4.24	90
	(12)	1.978	1.980			
	(11)	3.359	3.360			
	(21)	2.307	2.308			
	(20)	2.750	2.750			

Supplementary Table 4 Observed and calculated *d*-spacings and lattice parameters at different temperatures for ***11*-012-CN**. (*continued*)

T (°C)	(*hk*)	$d_{obs.}$ (nm)	$d_{calc.}$ (nm)	*a* (nm)	*b* (nm)	*γ* (°)
54	(02)	2.113	2.113	5.46	4.23	90
	(12)	1.970	1.971			
	(11)	3.336	3.342			
	(21)	2.292	2.293			
	(20)	2.730	2.730			
52	(02)	2.104	2.104	5.42	4.21	90
	(12)	1.963	1.962			
	(11)	3.321	3.324			
	(21)	2.275	2.279			
	(20)	2.710	2.710			
50	(02)	2.092	2.092	5.35	4.18	90
	(12)	1.947	1.949			
	(11)	3.292	3.297			
	(21)	2.254	2.255			
	(20)	2.676	2.676			
48	(02)	2.087	2.087	5.32	4.17	90
	(12)	1.942	1.943			
	(11)	3.285	3.284			
	(21)	2.244	2.244			
	(20)	2.662	2.662			
46	(02)	2.081	2.081	5.32	4.16	90
	(12)	1.937	1.938			
	(11)	3.270	3.279			
	(21)	2.234	2.242			
	(20)	2.662	2.662			
44	(02)	2.078	2.078	5.28	4.16	90
	(12)	1.932	1.933			
	(11)	3.263	3.265			
	(21)	2.224	2.227			
	(20)	2.638	2.638			
42	(02)	2.072	2.072	5.28	4.14	90
	(12)	1.925	1.929			
	(11)	3.249	3.259			
	(21)	2.214	2.225			
	(20)	2.638	2.638			
40	(02)	2.069	2.069	5.23	4.14	90
	(12)	1.922	1.924			
	(11)	3.242	3.245			
	(21)	2.207	2.211			
	(20)	2.615	2.615			
38	(02)	2.066	2.066	5.21	4.13	90
	(12)	1.920	1.921			
	(11)	3.235	3.238			
	(21)	2.204	2.204			
	(20)	2.606	2.606			

Supplementary Table 5 Observed and calculated *d*-spacings and lattice parameters at different temperatures for ***12*-012-CN**.

T (°C)	(*hk*)	$d_{obs.}$ (nm)	$d_{calc.}$ (nm)	*a* (nm)	*b* (nm)	*γ* (°)
76	(02)	2.362	2.362	6.93	4.72	90
	(12)	2.235	2.236			
	(11)	–	3.903			
	(21)	2.847	2.795			
	(20)	3.466	3.466			
75	(02)	2.407	2.407	6.24	4.81	90
	(12)	2.189	2.246			
	(11)	3.753	3.812			
	(21)	2.595	2.618			
	(20)	3.120	3.120			
74	(02)	2.343	2.343	6.14	4.69	90
	(12)	2.189	2.189			
	(11)	3.725	3.725			
	(21)	2.568	2.567			
	(20)	3.069	3.069			
72	(02)	2.332	2.332	6.03	4.66	90
	(12)	2.173	2.175			
	(11)	3.679	3.689			
	(21)	2.529	2.531			
	(20)	3.013	3.013			
70	(02)	2.318	2.318	5.94	4.64	90
	(12)	2.161	2.159			
	(11)	3.652	3.655			
	(21)	2.500	2.501			
	(20)	2.971	2.971			
68	(02)	2.314	2.314	5.91	4.63	90
	(12)	2.154	2.155			
	(11)	3.635	3.643			
	(21)	2.487	2.490			
	(20)	2.953	2.953			
66	(02)	2.296	2.296	5.82	4.59	90
	(12)	2.136	2.136			
	(11)	3.600	3.604			
	(21)	2.455	2.457			
	(20)	2.908	2.908			
64	(02)	2.282	2.282	5.74	4.56	90
	(12)	2.121	2.121			
	(11)	3.565	3.572			
	(21)	–	2.429			
	(20)	2.869	2.869			
62	(02)	2.275	2.275	5.72	4.55	90
	(12)	2.112	2.114			
	(11)	3.557	3.560			
	(21)	–	2.420			
	(20)	2.858	2.858			

Supplementary Table 5 Observed and calculated *d*-spacings and lattice parameters at different temperatures for ***12*-012-CN**. (*Continued*)

T (°C)	(*hk*)	$d_{obs.}$ (nm)	$d_{calc.}$ (nm)	*a* (nm)	*b* (nm)	*γ* (°)
60	(02)	2.258	2.258	5.65	4.52	90
	(12)	2.097	2.097			
	(11)	3.523	3.528			
	(21)	–	2.395			
	(20)	2.825	2.825			

Supplementary Table 6 Observed and calculated *d*-spacings and lattice parameters at different temperatures for ***13*-012-CN**.

T (°C)	(*hk*)	$d_{obs.}$ (nm)	$d_{calc.}$ (nm)	*a* (nm)	*b* (nm)	*γ* (°)
74	(02)	3.256	3.256	4.98	6.51	90
	(12)	–	2.726			
	(11)	3.958	3.958			
	(21)	–	2.327			
	(20)	–	2.492			
72	(02)	3.193	3.193	4.98	6.39	90
	(12)	–	2.688			
	(11)	3.926	3.926			
	(21)	–	2.319			
	(20)	–	2.489			
70	(02)	3.081	3.081	4.94	6.16	90
	(12)	2.615	2.614			
	(11)	3.855	3.855			
	(21)	2.292	2.293			
	(20)	–	2.471			
68	(02)	3.062	3.062	4.92	6.12	90
	(12)	2.601	2.599			
	(11)	3.835	3.835			
	(21)	2.285	2.283			
	(20)	–	2.460			
66	(02)	3.012	3.012	4.89	6.02	90
	(12)	2.565	2.564			
	(11)	3.796	3.796			
	(21)	2.271	2.265			
	(20)	–	2.444			
64	(02)	2.988	2.988	4.87	5.98	90
	(12)	2.552	2.547			
	(11)	3.777	3.777			
	(21)	2.261	2.256			
	(20)	–	2.437			
62	(02)	2.970	2.970	4.87	5.94	90
	(12)	2.539	2.536			
	(11)	3.767	3.767			
	(21)	2.254	2.254			
	(20)	–	2.436			
60	(02)	2.946	2.946	4.84	5.89	90
	(12)	2.518	2.516			
	(11)	3.739	3.739			
	(21)	2.241	2.237			
	(20)	2.431	2.418			
58	(02)	2.923	2.923	4.83	5.85	90
	(12)	–	2.501			
	(11)	3.720	3.724			
	(21)	2.234	2.232			
	(20)	2.415	2.415			

Supplementary Table 6 Observed and calculated *d*-spacings and lattice parameters at different temperatures for ***13*-012-CN** (*Continued*).

T (°C)	(*hk*)	$d_{obs.}$ (nm)	$d_{calc.}$ (nm)	*a* (nm)	*b* (nm)	*γ* (°)
56	(02)	2.912	2.912	4.82	5.82	90
	(12)	–	2.493			
	(11)	3.711	3.714			
	(21)	2.227	2.228			
	(20)	2.411	2.411			
54	(02)	2.889	2.889	4.80	5.78	90
	(12)	–	2.475			
	(11)	3.683	3.692			
	(21)	2.214	2.216			
	(20)	2.400	2.400			
52	(02)	2.867	2.867	4.77	5.73	90
	(12)	–	2.457			
	(11)	3.665	3.666			
	(21)	2.201	2.202			
	(20)	2.384	2.384			
50	(02)	2.889	2.889	4.75	5.78	90
	(12)	–	2.469			
	(11)	3.647	3.671			
	(21)	2.191	2.198			
	(20)	2.377	2.377			
48	(02)	2.840	2.840	4.70	5.68	90
	(12)	–	2.431			
	(11)	3.629	3.621			
	(21)	2.181	2.172			
	(20)	2.350	2.350			

Supplementary Table 7 Observed and calculated *d*-spacings and lattice parameters at different temperatures for ***14*-012-CN**.

T (°C)	(*hk*)	$d_{obs.}$ (nm)	$d_{calc.}$ (nm)	*a* (nm)	*b* (nm)	*γ* (°)
66	(02)	2.638	2.638	6.52	5.28	90
	(12)	2.442	2.446			
	(11)	4.101	4.102			
	(21)	2.769	2.773			
	(20)	3.260	3.260			
64	(02)	2.625	2.625	6.35	5.25	90
	(12)	2.426	2.426			
	(11)	4.046	4.047			
	(21)	2.719	2.718			
	(20)	3.177	3.177			
62	(02)	2.620	2.620	6.35	5.24	90
	(12)	2.418	2.422			
	(11)	4.036	4.043			
	(21)	2.714	2.717			
	(20)	3.177	3.177			
60	(02)	2.611	2.611	6.26	5.22	90
	(12)	2.407	2.410			
	(11)	4.014	4.011			
	(21)	2.685	2.685			
	(20)	3.131	3.131			
58	(02)	2.602	2.602	6.17	5.20	90
	(12)	2.395	2.398			
	(11)	3.972	3.979			
	(21)	2.652	2.655			
	(20)	3.086	3.086			
56	(02)	2.598	2.598	6.16	5.20	90
	(12)	2.392	2.393			
	(11)	3.972	3.971			
	(21)	2.648	2.649			
	(20)	3.080	3.080			
54	(02)	2.589	2.589	6.16	5.18	90
	(12)	2.380	2.386			
	(11)	3.941	3.963			
	(21)	2.625	2.647			
	(20)	3.080	3.080			
52	(02)	2.580	2.580	6.07	5.16	90
	(12)	2.373	2.374			
	(11)	3.931	3.932			
	(21)	2.611	2.617			
	(20)	3.037	3.037			

Supplementary Table 8 Observed and calculated *d*-spacings and lattice parameters at different temperatures for ***15*-012-CN**.

T (°C)	(*hk*)	$d_{obs.}$ (nm)	$d_{calc.}$ (nm)	*a* (nm)	*b* (nm)	*γ* (°)
63	(02)	2.774	2.774	6.52	5.55	90
	(12)	2.554	2.553			
	(11)	4.228	4.225			
	(21)	2.810	2.811			
	(20)	3.260	3.260			
61	(02)	2.764	2.764	6.42	5.53	90
	(12)	2.541	2.539			
	(11)	4.193	4.190			
	(21)	2.774	2.777			
	(20)	3.211	3.211			
59	(02)	2.759	2.759	6.33	5.52	90
	(12)	2.528	2.529			
	(11)	4.158	4.159			
	(21)	2.744	2.745			
	(20)	3.164	3.164			
57	(02)	2.754	2.754	6.30	5.51	90
	(12)	2.524	2.524			
	(11)	4.147	4.147			
	(21)	2.734	2.735			
	(20)	3.151	3.151			
55	(02)	2.749	2.749	6.25	5.50	90
	(12)	2.515	2.516			
	(11)	4.124	4.128			
	(21)	2.714	2.717			
	(20)	3.125	3.125			
53	(02)	2.744	2.744	6.21	5.49	90
	(12)	2.511	2.510			
	(11)	4.113	4.113			
	(21)	2.705	2.703			
	(20)	3.105	3.105			
51	(02)	2.739	2.739	6.19	5.48	90
	(12)	2.503	2.504			
	(11)	4.101	4.101			
	(21)	2.690	2.693			
	(20)	3.093	3.093			
49	(02)	2.734	2.734	6.15	5.47	90
	(12)	2.499	2.498			
	(11)	4.079	4.086			
	(21)	2.681	2.679			
	(20)	3.074	3.074			
47	(02)	2.729	2.729	6.14	5.46	90
	(12)	2.494	2.494			
	(11)	4.079	4.078			
	(21)	2.671	2.674			
	(20)	3.068	3.068			

Supplementary Table 8 Observed and calculated *d*-spacings and lattice parameters at different temperatures for ***15*-012-CN** (*Continued*).

T (°C)	(*hk*)	$d_{obs.}$ (nm)	$d_{calc.}$ (nm)	*a* (nm)	*b* (nm)	*γ* (°)
45	(02)	2.724	2.724	6.11	5.45	90
	(12)	2.486	2.488			
	(11)	4.057	4.067			
	(21)	2.662	2.665			
	(20)	3.055	3.055			

Supplementary Table 9 Observed and calculated *d*-spacings and lattice parameters at different temperatures for ***16*-012-CN**.

T (°C)	(*hk*)	$d_{obs.}$ (nm)	$d_{calc.}$ (nm)	*a* (nm)	*b* (nm)	*γ* (°)
66	(02)	2.650	2.650	14.21	5.78	113.56
	(01)	5.311	5.300			
	(11)	4.341	4.341			
	(31)	2.896	2.847			
	(30)	4.341	4.341			
	(40)	3.277	3.256			
64	(02)	2.641	2.641	14.17	5.78	113.96
	(11)	4.316	4.316			
	(31)	2.891	2.826			
	(30)	4.316	4.316			
	(40)	3.241	3.237			
62	(02)	2.636	2.636	14.09	5.77	114.02
	(11)	4.303	4.303			
	(31)	2.885	2.814			
	(30)	4.291	4.291			
	(40)	3.213	3.218			
60	(02)	2.632	2.632	14.15	5.80	114.88
	(11)	4.279	4.279			
	(31)	2.885	2.794			
	(30)	4.279	4.279			
	(40)	3.193	3.209			
58	(02)	2.627	2.627	14.13	5.80	115.08
	(11)	4.266	4.266			
	(31)	2.885	2.784			
	(30)	4.266	4.266			
	(40)	3.179	3.200			

Supplementary Table 10 Observed and calculated *d*-spacings and lattice parameters at different temperatures for ***17*-012-CN**.

T (°C)	(*hk*)	$d_{obs.}$ (nm)	$d_{calc.}$ (nm)	*a* (nm)	*b* (nm)	*γ* (°)
60	(02)	2.790	2.790	11.36	5.77	104.70
	(11)	4.533	4.533			
	(2$\bar{1}$)	4.533	4.533			
	(3$\bar{1}$)	3.354	3.497			
59	(02)	2.790	2.790	11.27	5.77	104.83
	(11)	4.519	4.519			
	(2$\bar{1}$)	4.506	4.519			
	(3$\bar{1}$)	3.332	3.478			
58	(02)	2.785	2.785	11.22	5.76	104.88
	(11)	4.506	4.506			
	(2$\bar{1}$)	4.506	4.506			
	(3$\bar{1}$)	3.310	3.465			
57	(02)	2.785	2.785	11.22	5.76	104.88
	(11)	4.506	4.506			
	(2$\bar{1}$)	4.506	4.506			
	(3$\bar{1}$)	3.303	3.465			
56	(02)	2.790	2.790	11.18	5.78	104.96
	(11)	4.506	4.506			
	(2$\bar{1}$)	4.492	4.506			
	(3$\bar{1}$)	3.295	3.460			
55	(02)	2.790	2.790	11.18	5.78	104.96
	(11)	4.506	4.506			
	(2$\bar{1}$)	4.492	4.506			
	(3$\bar{1}$)	3.288	3.460			

Supplementary Table 11 The total number of molecules in the MD simulation box and the initial sizes of the MD simulation box for ***12*-012-CN** and ***16*-012-CN**.

Entry	Number of molecules	Size of MD simulation box					
		a (nm)	*b* (nm)	*c* (nm)	*α* (deg)	*β* (deg)	*γ* (deg)
***12*-012-CN**	560	11.82	4.40	9.26	90	90	90
***16*-012-CN**	1280	28.20	5.00	11.54	90	66	90

Supplementary References

1. Frisch, M. J. *et al.* Gaussian 09, Revision E.01. Gaussian, Inc. (2009).
2. Nishikawa, H. *et al.* Electrically Tunable Heliconical Smectic Superstructure in Polar Fluids. *Advanced Materials* e74025 (2026) doi:10.1002/adma.74025.
3. Fluorine-containing ferroelectric liquid crystal molecules containing heteroatom hexatomic alicyclic ring and synthesis method thereof. (2023).
4. Hess, B., Bekker, H., Berendsen, H. J. C. & Fraaije, J. G. E. M. LINCS: A linear constraint solver for molecular simulations. *J. Comput. Chem.* **18**, 1463–1472 (1997).
5. Godbert, N. *et al. LCDiXRay* : a user-friendly program for powder diffraction indexing of columnar liquid crystals. *J Appl Crystallogr* **47**, 668–679 (2014).
6. Hobbs, J., Gibb, C. J. & Mandle, R. J. Emergent Antiferroelectric Ordering and the Coupling of Liquid Crystalline and Polar Order. *Small Science* 2400189 (2024) doi:10.1002/smsc.202400189.
7. Wang, J., Wolf, R. M., Caldwell, J. W., Kollman, P. A. & Case, D. A. Development and testing of a general amber force field. *J Comput Chem* **25**, 1157–1174 (2004).
8. Nishikawa, H. *et al.* Nano-clustering mediates phase transitions in a diastereomerically-stabilized ferroelectric nematic system. *Commun Mater* **3**, 89 (2022).
9. Bayly, C. I., Cieplak, P., Cornell, W. & Kollman, P. A. A well-behaved electrostatic potential based method using charge restraints for deriving atomic charges: the RESP model. *J. Phys. Chem.* **97**, 10269–10280 (1993).
10. Berendsen, H. J. C., Postma, J. P. M., Van Gunsteren, W. F., DiNola, A. & Haak, J. R. Molecular dynamics with coupling to an external bath. *The Journal of Chemical Physics* **81**, 3684–3690 (1984).
11. Bussi, G., Donadio, D. & Parrinello, M. Canonical sampling through velocity rescaling. *The Journal of Chemical Physics* **126**, 014101 (2007).

12. Parrinello, M. & Rahman, A. Polymorphic transitions in single crystals: A new molecular dynamics method. *Journal of Applied Physics* **52**, 7182–7190 (1981).

13. Nosé, S. A molecular dynamics method for simulations in the canonical ensemble. *Molecular Physics* **52**, 255–268 (1984).

14. Nosé, S. A unified formulation of the constant temperature molecular dynamics methods. *The Journal of Chemical Physics* **81**, 511–519 (1984).

15. Hoover, W. G. Canonical dynamics: Equilibrium phase-space distributions. *Phys. Rev. A* **31**, 1695–1697 (1985).

16. Essmann, U. *et al.* A smooth particle mesh Ewald method. *The Journal of Chemical Physics* **103**, 8577–8593 (1995).

17. Delshad, Y., Azizi, K., Fogolari, F. & Ganjali Koli, M. Structural characterization and thermodynamic behavior of melittin-derived peptide interactions with gram-positive bacterial cell membranes using molecular dynamics simulation. *RSC Adv.* **16**, 11562–11579 (2026).

18. Takegawa, S. *et al.* Lithium-ion batteries with fluorinated mesogen-based liquid-crystalline electrolytes: molecular design towards enhancing oxidation stability. *Nanoscale* **16**, 21118–21127 (2024).

19. Mandle, R. J. Implementation of a cylindrical distribution function for the analysis of anisotropic molecular dynamics simulations. *PLoS ONE* **17**, e0279679 (2022).

20. Patra, A. & Kumar, S. Shape-directed self-assembly into columnar phases: beyond the discotic paradigm. *J. Mater. Chem. C* **14**, 9350–9384 (2026).

21. Nguyen, H., Destrade, C. & Malthécte, J. Phasmids and Polycatenar Mesogens. *Advanced Materials* **9**, 375–388 (1997).

22. Parton-Barr, C., Gleeson, H. F. & Mandle, R. J. Room-temperature ferroelectric nematic liquid crystal showing a large and diverging density. *Soft Matter* **20**, 672–680 (2024).

23. Guragain, P. *et al.* Ferroelectric nematic and smectic liquid crystals with sub-molecular spatial correlations. *Mater. Horiz.* **12**, 8153–8164 (2025).